AVERTISSEMENT

Ce document est le fruit d'un long travail approuvé par le jury de soutenance et mis à disposition de l'ensemble de la communauté universitaire élargie.

Il est soumis à la propriété intellectuelle de l'auteur. Ceci implique une obligation de citation et de référencement lors de l'utilisation de ce document.

D'autre part, toute contrefaçon, plagiat, reproduction illicite encourt une poursuite pénale.

Contact : ddoc-theses-contact@univ-lorraine.fr

LIENS

Code de la Propriété Intellectuelle. articles L 122. 4
Code de la Propriété Intellectuelle. articles L 335.2- L 335.10
http://www.cfcopies.com/V2/leg/leg_droi.php
http://www.culture.gouv.fr/culture/infos-pratiques/droits/protection.htm

Nancy-Université
Université Henri Poincaré

cnrs

DOCTORAL SCHOOL SESAMES

Formation of mixed Fe^{II}-Fe^{III} oxides and their reactivity to catalyze chemical oxidation: Remediation of hydrocarbon contaminated soils

Ph.D. Thesis

presented and defended publicly on November 17, 2011
in partial fulfillment of the requirements for the degree of
Doctor of Philosophy
Nancy Université

By

Muhammad USMAN

Jury

Reviewers:	Jean-François BOILY	Professor	Umeå University (Sweden)
	Stefan HADERLEIN	Professor	Universität Tübingen (Germany)
Examiner:	Gilles MAILHOT	Research Director CNRS	LPMM. Clermont Ferrand (France)
Advisors:	Pierre FAURE	Research Associate CNRS	G2R, Nancy (France)
	Khalil HANNA	Professor	ENSC de Rennes (France)
	Christian RUBY	Professor	Nancy Université (France)
Invited:	Georg WALDNER	Research Scientist	Austrian Inst. of Technol. (Austria)

LCPME

G2R

Nancy-Université
Université Henri Poincaré

cnrs

DOCTORAL SCHOOL SESAMES

Formation of mixed Fe^{II}-Fe^{III} oxides and their reactivity to catalyze chemical oxidation: Remediation of hydrocarbon contaminated soils

Ph.D. Thesis

presented and defended publicly on November 17, 2011
in partial fulfillment of the requirements for the degree of
Doctor of Philosophy
Nancy Université

By

Muhammad USMAN

Jury

Reviewers:	Jean-François BOILY	Professor	Umeå University (Sweden)
	Stefan HADERLEIN	Professor	Universität Tübingen (Germany)
Examiner:	Gilles MAILHOT	Research Director CNRS	LPMM. Clermont Ferrand (France)
Advisors:	Pierre FAURE	Research Associate CNRS	G2R, Nancy (France)
	Khalil HANNA	Professor	ENSC de Rennes (France)
	Christian RUBY	Professor	Nancy Université (France)
Invited:	Georg WALDNER	Research Scientist	Austrian Inst. of Technol. (Austria)

LCPME

G2R

Abstract

The main theme of this research is the use of reactive iron minerals in the remediation of hydrocarbon contaminated soils *via* chemical oxidation treatments at circumneutral pH. The contribution of this thesis is two-fold including the abiotic **synthesis** of mixed Fe^{II}-Fe^{III} oxides considered as reactive iron minerals (magnetite and green rust) and their use to **catalyze** chemical oxidation. Oxidation methods tested in this study include Fenton-like (FL) and activated persulfate oxidation (AP). The formation of magnetite and green rust was studied by abiotic Fe^{II}-induced transformations of various ferric oxides like ferrihydrite, goethite, hematite and lepidocrocite. Then, the ability of magnetite was tested to catalyze chemical oxidation (FL and AP) for the degradation of aliphatic and polycyclic aromatic hydrocarbons (PAHs) at circumneutral pH. Significant degradation of oil hydrocarbons occurring in weathered as well as in crude oil was obtained by both oxidants. Magnetite catalyzed oxidation was also effective for remediation of two PAHs contaminated soils from ancient coking plant sites. No by-products were observed in all batch slurry oxidation systems. Very low hydrocarbon degradation was observed when soluble Fe^{II} was used as catalyst under the same experimental conditions. Magnetite also exhibited high reactivity to catalyze chemical oxidation in column experiments under flow through conditions. Oxidation studies revealed the importance of catalyst type for oxidation, PAHs availability in soils and the soil matrix effect. Results of this study suggest that magnetite can be used as iron source to activate both Fenton-like and persulfate oxidation at circumneutral pH. This study has important implications in the remediation of hydrocarbon polluted soils through *in-situ* chemical oxidation.

***Keywords*:** Abiotic transformation; Green rust; Magnetite; Soil remediation; Hydrocarbons; Chemical oxidation; Fenton-like; Persulfate; Circumneutral pH.

Résumé

Le thème principal de cette recherche est la remédiation des sols contaminés par des hydrocarbures en utilisant des traitements d'oxydation chimique à pH neutre. Les minéraux à base de fer sont susceptibles de catalyser cette réaction d'oxydation. L'étude concerne donc dans un premier temps la synthèse des minéraux réactifs contenant des espèces Fe^{II} et Fe^{III} (la magnétite et la rouille verte) et, dans un second temps, leur utilisation pour catalyser l'oxydation chimique. Les procédés d'oxydation testés incluent l'oxydation de type « Fenton-like (FL) » et de type persulfate activé (AP). La formation de la magnétite et de la rouille verte a été étudiée par des transformations abiotiques de différents oxydes ferriques (ferrihydrite, goethite, hématite et lépidocrocite) mis en présence de cations Fe^{II}. La magnétite a été utilisée pour catalyser les oxydations (FL et AP) dans la dégradation des hydrocarbures aliphatiques et aromatiques polycycliques (HAP) à pH neutre. Une dégradation importante des hydrocarbures aliphatiques a été obtenue par ces deux oxydants, aussi bien pour des pétroles dégradés naturellement que pour un pétrole brut. L'oxydation catalysée par la magnétite a également été efficace pour la remédiation de deux sols contaminés par HAP provenant d'anciens sites de cokerie. Aucun sous-produit n'a été observé dans nos expériences d'oxydation. En revanche, une très faible dégradation des hydrocarbures a été observée lorsque les espèces Fe^{II} solubles ont été utilisées comme catalyseur. Des expériences d'oxydation ont également été réalisées en colonne. Ces études d'oxydation ont révélé l'importance du type de catalyseur utilisé pour l'oxydation, la disponibilité des HAP dans les sols et l'effet de la matrice du sol. Les résultats suggèrent que la magnétite peut être utilisée comme source de fer pour activer les deux oxydations par Fenton-like et persulfate à pH neutre. Ce travail a de fortes implications sur la remédiation par oxydation chimique ***in situ*** des sols pollués par des hydrocarbures.

Mots-clés: transformation abiotic; rouille verte; magnétite; remédiation de sols; hydrocarbures; oxydation chimique ; Fenton-like ; persulfate ; pH neutre.

Introduction

Ce travail de thèse porte sur la synthèse de minéraux réactifs à base de fer ainsi que sur leur rôle lors de la remédiation par oxydation chimique des sols contaminés. Les oxydes de fer forment un groupe de minéraux très répandu dans la nature. Le fer présent dans ces oxydes peut prendre deux degrés d'oxydation : le fer ferrique (Fe^{III}) ou ferreux (Fe^{II}). La forme prédominante du fer dans les sols est l'oxyde ferrique sous forme solide. Les oxydes ferriques les plus communs étant la goethite, la ferrihydrite, l'hématite et la lépidocrocite, se distinguent les uns des autres par différentes caractéristiques : la composition chimique, la cristallinité, la stabilité, la surface spécifique et la réactivité. Dans la zone anoxique du sol, il existe un autre groupe d'oxydes de fer constitué d'un mélange des espèces Fe^{II} et Fe^{III}. Il s'agit de la magnétite et de la rouille verte. En raison de la présence du Fe^{II} structural, les composés mixtes sont considérés comme plus réactifs pour la dépollution des sols. Ces minéraux sont moins abondants dans la nature et il est donc intéressant d'étudier leur formation à partir des oxydes ferriques. Bien que la transformation de la ferrihydrite (moins stable) catalysée par des espèces Fe^{II} ait été décrite dans la littérature, peu d'études traitent de la cinétique de la transformation des composés ferriques en composés mixtes Fe^{II}-Fe^{III}. De plus, la transformation des oxydes ferriques plus stables comme la goethite et l'hématite n'a pas été étudiée jusqu'à présent.

L'utilisation intense de la matière organique fossile (pétrole et charbon) depuis le $18^{ème}$ siècle à des fins industrielles (extraction de pétrole, raffineries, cokerie, industries de l'acier, ….) a conduit à la contamination de nombreux sites par les hydrocarbures aliphatiques (produits essentiellement hérités du pétrole) et aromatiques polycycliques (HAP hérités principalement de l'utilisation du charbon). Ces composés provoquent des problèmes environnementaux majeurs et également de santé pour les populations. Différentes techniques de remédiation biologique, physique et chimique ont été explorées sur des sols contaminés. En raison de leur forte rémanence dans les sols, les HAP sont des polluants très récalcitrants à la dégradation. La bioremédiation a, quant à elle, fait ses preuves dans de nombreuses applications pour la dépollution des sols contaminés par les sous-produits pétroliers. Cependant, la minéralisation des hydrocarbures pétroliers reste incomplète car les microorganismes ne semblent pas pouvoir dégrader une fraction organique complexe et résistante.

L'oxydation chimique a récemment été appliquée dans la remédiation des sols en utilisant différents oxydants comme l'oxydation Fenton, le persulfate, l'ozone, le permanganate…. Les traitements chimiques par oxydation ont un potentiel prometteur pour la dégradation des hydrocarbures présents dans les sols contaminés. Certains modes d'oxydation comme les traitements d'oxydation de type Fenton et le persulfate nécessitent une activation par les espèces Fe^{II} pour augmenter leur efficacité. Afin de garder les espèces Fe^{II} en solution, le pH optimum pour de telles réactions se situe entre 2-4. Cela se traduit alors par des impacts négatifs sur les propriétés du sol. Cependant un pH aussi acide peut être évité en utilisant des agents chélateurs ou des minéraux naturels à base de fer qui induisent une dégradation efficace même à pH neutre.

Les minéraux du fer (goethite et ferrihydrite) ont été utilisés pour catalyser les traitements Fenton et ainsi dégrader les polluants dans des sols dopés par les HAP. Récemment, il a été démontré que la magnétite est plus réactive pour catalyser l'oxydation Fenton si on la compare à d'autres oxydes ferriques. Cependant, son rôle de catalyseur dans l'oxydation chimique pour la dégradation des hydrocarbures dans les sols à pH neutre a était très peu abordé. Dans cette étude, nous avons souhaité tester l'hypothèse que l'ajout de la magnétite pourrait induire une oxydation efficace (Fenton-like et le persulfate) pour la dégradation des hydrocarbures dans les sols.

Objectifs

Ainsi, les objectifs de ce travail sont les suivants :

- Evaluation de la cinétique de formation de la magnétite ou de la rouille verte lors de la transformation minéralogique des oxydes ferriques induites par les espèces Fe^{II}. Le but était de synthétiser, soit la magnétite, soit la rouille verte en utilisant des quantités stoechiométriques de Fe^{II} et le substrat Fe^{III}.

- Utilisation de la magnétite comme source de fer pour catalyser l'oxydation chimique (Fenton-like et le persulfate) à pH neutre pour la remédiation de sols contaminés par des hydrocarbures (i) aromatiques polycycliques et (ii) aliphatiques.

Contents

Preface

The present dissertation is submitted as the partial requirement for the attainment of the Ph. D. degree of Nancy Université, France. The research was conducted in the "Laboratoire de Chimie Physique et Microbiologie pour l'Environnement" (LCPME), and in the "Géologie et Gestion des Ressources minérales et énergétiques" (G2R), unit of Nancy Université, France. The study was funded by a Ph. D. scholarship awarded by Higher Education Commission of Pakistan (http://www.hec.gov.pk) and further financed by "CNRS- Centre National de la Recherche Scientifique" (http://www.cnrs.fr/centre-est). This work has been a part of the project of GISFI-Groupement d'Intérêt Scientifique sur les Friches Industrielles (http://www.gisfi.fr/index_fr.htm). This work has been supervised by Professor Christian Ruby and Professor Khalil Hanna, both from LCPME and Dr. Pierre Faure from G2R. Pr. Khalil Hanna has joined the "Ecole Nationale Supérieure de Chimie de Rennes" since September, 2011.

The dissertation reports the synthesis of reactive iron minerals and ultimately their role in chemical oxidation-based remediation of contaminated soils. After a brief review of literature about both aspects, the results are presented for ease of understanding and for convenience, under the following two sections in the form of various articles:

***Section 1*:** entitled "Formation of mixed Fe^{II}-Fe^{III} oxides: magnetite and green rust". In this section, results are presented in three articles describing their formation by Fe^{II} induced transformations of different ferric oxides.

***Section 2*:** entitled "Reactivity of magnetite to catalyze chemical oxidation for hydrocarbon remediation in soils". In this section, reactivity of magnetite was evaluated to catalyze Fenton-like and persulfate oxidation. This section comprises four articles, first three describing oxidation in batch slurry system. Oxidation under flow through conditions is reported in last chapter of this section.

Another two articles partially related to this dissertation are presented in annexes. Among these two, first reviewed the general properties of iron-based layered double hydroxides (green rust) and second compared magnetite yielded by biotic and abiotic (Fe^{II} induced) ways.

Apart from these journal articles, the obtained results of this research have been published in the following conferences. These oral or poster communications presented in these conferences are detailed below:

Oral communications

- Abdelmoula M., **Usman M.**, Hanna K., Ruby C. Transformations minéralogiques induites par adsorption d'espèces Fe^{II} sur oxydes de fer. *Groupe Francophone de Spectrométrie Mössbauer (GFSM 2010)* May 20- 21, 2010. Lisbonne, Portugal.

- **Usman M.**, Hanna K., Abdelmoula M., Ruby C. Magnetite formation via Fe^{II} induced mineralogical transformations of ferric oxyhydroxides. *Goldschmidt 2010*. June 13-18, 2010. Knoxville, Tennessee, USA.

- **Usman M.**, Hanna K., Faure P., Ruby C. Reactivity of newly generated magnetite to promote Fenton-like oxidation of polycyclic aromatic hydrocarbons in contaminated soil matrices. *SEGH 2010, International Conference and Workshops, Environmental Quality and Human Health*, June 27- July 2, 2010. Galway, Ireland.

- **Usman M.**, Hanna K., Faure P., Abdelmoula M., Ruby C. Remediation of petroleum (biodegraded and crude) contaminated soils by chemical oxidation. *Journée Scientifique d'automne SESAMES*, 28 October 2010. Metz. France.

- Ruby C., Zegeye A., Abdelmoula M., **Usman M.**, Hanna K. Mineralogical transformations of ferric oxides into mixed Fe(II)-Fe(III) compounds : magnetite versus green rust. *6th Nassau-Argonne International Mössbauer Symposium.* January 13 - 14, 2011. New York, USA. (Invited conference)

- Hanna K., **Usman M.**, Abdelmoula M., Faure P., Ruby C. Fe^{II}-induced mineralogical transformation of goethite into magnetite. *242nd ACS National Meeting & Exposition.* August 28-September 1, 2011. Denver, Colorado, USA.

- Hanna K., **Usman M.**, Faure P., Ruby C. Degradation of polycyclic aromatic hydrocarbons by magnetite catalyzed Fenton-like oxidation. *The 17th International Conference on Advanced Oxidation Technologies for Treatment of Water, Air and Soil (AOTs-17).* November 7-10, 2011. San Diego, California, USA. (Invited conference)

Poster communications

- **Usman M.**, Hanna K., Abdelmoula M., Faure P., Ruby C. Reactivity of Ferric Oxyhydroxides with Fe^{II}: Application for Soil Remediation. *Doctoriales de Lorraine*, May 16-21, 2010. Ventron, France.

- **Usman M.**, Hanna K., Abdelmoula M., Ruby C., Faure P. Transformation of soil iron minerals under static batch and flow through conditions: application for soil remediation. *19th World Congress of Soil Science.* August 1-6, 2010. Brisbane, Australia.

- **Usman M**., Faure P., Hanna K., Ruby C. Remediation of hydrocarbon contaminated soils by modified Fenton oxidation in the presence of magnetite. *25th International Meeting on Organic Geochemistry (IMOG 2011).* September 18-23, 2011. Interlaken, Switzerland.

Introduction

The main concern of this study is the synthesis of mixed Fe^{II}-Fe^{III} oxides considered as reactive iron minerals and ultimately their use in chemical oxidation-based remediation of contaminated soils. Iron oxides are a group of minerals widespread in nature. Various states of Fe in iron oxides are observed including ferric (Fe^{III}) and ferrous (Fe^{II}) forms. The predominant form of soil iron is found in solid ferric oxides. Common ferric oxides are goethite, ferrihydrite, hematite and lepidocrocite with different characteristics such as chemical composition, crystallinity, stability, specific surface area and reactivity. Another group of iron oxides is the mixed Fe^{II}-Fe^{III} oxides that exist in reduced soil zone. Magnetite and green rust belong to this group. Due to the presence of structural Fe^{II}, mixed Fe^{II}-Fe^{III} oxides are considered more reactive than ferric oxides for remediation purposes. But they are not common in soil system, thus studies to generate them from existing ferric oxides merit to be investigated. Although the Fe^{II}-induced transformation of the least stable ferrihydrite to mixed Fe^{II}-Fe^{III} oxides or other stable Fe^{III} oxides has been reported in literature, the quantification of magnetite or green rust formation versus time is still missing in literature. Moreover the transformation of stable Fe^{III} oxides like goethite and hematite has not been reported till now.

The reactivity of Fe^{II}-bearing minerals was evaluated to catalyze chemical oxidation which has emerged as a viable option for soil remediation. The intense use of fossil organic matter (petroleum and coal) since 18^{th} century for industrial purposes (petroleum extraction, refinery, coking plant, steel industries etc.) has resulted in widespread pollution by polycyclic aromatic hydrocarbons (essentially coal by-products) and aliphatic hydrocarbons (mainly petroleum by-products) that cause environmental and health concerns. As for example, the end of industrial activities based on coal use in France has led to led to thousands of hectares of land especially in Lorraine region (Northeast of France). Different remediation techniques have been explored for such soils including biological, physical and chemical treatments. For the remediation of PAHs contaminated sites, treatments already tested by GISFI group in Lorraine region include phytoremediation, bioremediation, thermal desorption, air oxidation etc. Owing to high persistence in soil, polycyclic aromatic hydrocarbons are pollutants, highly recalcitrant to degradation. On the other hand, bioremediation has proven successful in many

applications to oil contaminated soils. But complete mineralization of oil hydrocarbons cannot be achieved by microorganisms as it leaves complex residues resistant to degradation.

Chemical oxidation has recently been applied for the soil remediation by using various oxidants like Fenton oxidant, persulfate, ozone, permanganate etc. Chemical oxidation treatments have shown promising potential for the degradation of soil hydrocarbons. Some oxidants like H_2O_2 and persulfate require activation for higher oxidation efficiency. This activation can be achieved by Fe^{II} although the chemistry of both oxidants is different. The optimum pH for such reactions is very low (2-4) required to prevent the precipitation of Fe^{II} which results in negative impacts on soil quality. Such a low pH can be avoided by using chelating agents or natural iron minerals for an efficient degradation at circumneutral pH. Ferric minerals like ferrihydrite and goethite were used to catalyze Fenton treatments for PAHs on spiked soil. Recently, magnetite was found as the most reactive iron oxide as compared to other ferric oxides to catalyze Fenton oxidation of various other organic pollutants. But its reactivity has never been evaluated to catalyze chemical oxidation for the degradation of hydrocarbons in soil at circumneutral pH.

Objectives

Our study is composed of two parts: formation of mixed Fe^{II}-Fe^{III} oxides and their reactivity to catalyze chemical oxidation. The first part of study was conducted with the following objectives:

- Synthesis of mixed Fe^{II}-Fe^{III} oxides (magnetite and green rust) by Fe^{II} induced mineralogical transformations of various ferric oxides (ferrihydrite, lepidocrocite, goethite and hematite)
- Determination of formation kinetics by quantifying magnetite or green rust formed by using stoichiometric quantities of soluble Fe^{II} and Fe^{III} oxide.
- Evaluation of key-parameters influencing the formation routes of magnetite or green rust.
- To test the formation of mixed Fe^{II}-Fe^{III} oxides under flow through conditions (column experiments)

The results of first part allow us to design oxidation experiments by using newly generated Fe^{II}-Fe^{III} oxides to catalyze chemical oxidation. The objectives of this part were:

- To test the ability of magnetite to catalyze Fenton-like or persulfate oxidation under batch and flow through conditions.
- To determine the efficiency of magnetite-catalyzed chemical oxidation for the degradation of aliphatic and polycyclic aromatic hydrocarbons.
- To determine the limiting factors for the degradation of pollutants in aged contaminated soils.

Experiments were conducted to achieve these objectives and results would improve understanding of remediation in contaminated soils. This work would allow us to bring new insights for the choice of remediation method. It would also be helpful to the Lorraine region's local community and policy-makers for the rehabilitation of contaminated soils.

Structure of the thesis

The dissertation reports the formation of reactive iron oxides and ultimately their reactivity in chemical oxidation-based remediation of contaminated soils. After a brief review of literature about both aspects separately, the results are presented for ease of understanding and for convenience, under the following two sections in the form of various articles:

***Section 1*:** entitled "Formation of mixed Fe^{II}-Fe^{III} oxides: magnetite and green rust". In this first section, results are presented in three articles describing their formation by Fe^{II} induced transformations of different ferric oxides under static batch and flow through conditions.

***Section 2*:** entitled "Reactivity of magnetite to catalyze chemical oxidation for hydrocarbon remediation in soils". In this section, reactivity of magnetite was evaluated to catalyze Fenton-like and persulfate oxidation. Soil pollution with aliphatic and polycyclic aromatic hydrocarbons was studied. This section comprises four articles, first three describing oxidation in batch slurry system. Oxidation under flow through conditions is reported in last chapter of this section.

Another **two articles** partially related to this dissertation are presented in annexes. Among these two, first reviewed the general properties of iron-based layered double hydroxides (green rust) and second compared magnetite yielded by biotic and abiotic (Fe^{II} induced) ways.

Part I

BACKGROUND

Iron oxides

Iron oxides are group of minerals composed of Fe together with O and/or OH and are abundant in natural environment. They consist of oxides, hydroxides or oxyhydroxides but collectively they are referred to as iron oxides throughout this thesis. Their characteristic features include high stability because of their low solubility, conspicuous colors and high surface area. High specific surface area of iron oxides enables them to act as important sorbents for dissolved species and thereby influence the biogeochemical cycling and availability of elements. They strongly influence the transport and availability of various nutrients (e.g., C, N, and P) (Sulzberger ***et al.***, 1989; Stumm & Sulzberger, 1992; Cornell & Schwertmann, 2003) and the mobility of organic and inorganic contaminants (Elsner ***et al.***, 2004; Hanna ***et al.***, 2010b).

The average iron concentration in the Earth's crust is around 5.6%. There are 17 known iron oxides (Table 1) differing in the composition, Fe valence and in the crystal structure (Cornell & Schwertmann, 2003). Iron oxides are found as minerals containing iron: i) only in the trivalent state (Fe^{III}), ii) exclusively present in the divalent state (Fe^{II}), the only examples are FeO and $Fe(OH)_2$ and iii) mixed Fe^{II}-Fe^{III} compounds like green rusts and magnetite.

Table 1: Overview of iron oxides (Cornell & Schwertmann, 2003)

Oxide-hydroxides and hydroxides		***Oxides***	
Goethite	α-FeOOH	Hematite	α-Fe2O3
Lepodocrocite	γ-FeOOH	Magnetite	Fe_3O_4 ($Fe^{II}Fe^{III}{}_2O_4$)
Akaganéite	β-FeOOH	Maghemite	γ-Fe_2O_3
Schwertmannite	$Fe_{16}O_{16}(OH)_y(SO_4)_z \cdot nH_2O$	-	β-Fe_2O_3
-	δ-FeOOH	-	?-Fe_2O_3
Feroxyhyte	δ'-FeOOH	Wüstite	FeO
High pressure	FeOOH		
Ferrihydrite	$Fe_5HO_8 \cdot 4H_2O$		
Bernalite	$Fe(OH)_3$		
-	$Fe(OH)_2$		
Green rusts	$Fe_x^{III}Fe_y^{II}(OH)_{3x+2y-z}(A^-)_z$; $A^- = Cl^-$; $1/2\ SO_4^{2-}$		

The predominant form of iron in soils is found as solid ferric oxides because of the presence of oxygen and prevailing pH conditions in many natural environments. Common ferric oxides are goethite, ferrihydrite, hematite and lepidocrocite with different characteristics such as crystallinity, stability, specific surface area and reactivity (Stumm & Sulzberger, 1992; Cornell & Schwertmann, 2003). Mixed Fe^{II}–Fe^{III} compounds exist in reduced soil zone as magnetite (Fe_3O_4) or fougerite, the mineral counterpart of the Fe^{II}-Fe^{III} green rust (Trolard ***et al***., 1997; Abdelmoula ***et al***., 1998). Below is the brief description of the applied iron oxides including ferric minerals and mixed Fe^{II}-Fe^{III} minerals (magnetite and green rust).

1. Ferric (Fe^{III}) oxides

This section deals with the different ferric oxides including ferrihydrite, goethite, lepidocrocite and hematite tested in this study.

1.1. Ferrihydrite

Ferrihydrite also termed as “amorphous iron oxide” or “hydrous ferric oxide (HFO)”, is a reddish brown iron oxide and is thought to be most widespread in environment. The composition is variable and an exact formula for ferrihydrite has not established yet because of limitations in precise separation of structural OH and H_2O from adsorbed water, a preliminary formula often used is $Fe_5HO_8{\cdot}4H_2O$. Ferrihydrite, either synthetic or natural, is generally poorly ordered. Two types of ferrihydrite as 2-line and 6-line ferrihydrite are described on the basis of number of reflections in XRD pattern which indicates 2 to 6-8 reflections as structural order increases. The structure of ferrihydrite is still under debate as the low degree of order is the main difficulty to elucidate its structure (Manceau & Gates, 1997; Jambor & Dutrizac, 1998). The morphology of ferrihydrite is spherical and unlike other iron oxides, it exists only as nano crystals resulting in high specific surface areas ranging from 100 - 700 m^2/g (Jambor & Dutrizac, 1998; Cornell & Schwertmann, 2003) depending on the method used to measure the surface area. Ferrihydrite is the least stable iron oxide and is an important precursor for iron oxides of higher crystallinity as it transforms with time into more stable iron oxides.

1.2. Goethite

Goethite (α-FeOOH), a yellow colored iron mineral, is one of the thermodynamically most stable and abundant iron oxides at ambient temperature. Goethite is composed of double chains of edge sharing octahedra which contain Fe ion surrounded by three O_2^- and three OH^- to give $FeO_3(OH)_3$. The double chains are linked by corner sharing and displaced by half a unit cell along the b-axis with respect to its neighbor (Fig. 1). The apparent tunnels in the goethite structure in Figure 1 are not true tunnels but empty octahedral sites. Basic morphology is acicular although goethite exists in range of shapes. The specific surface area of goethite ranges from 8 - 200 m^2/g (Cornell & Schwertmann, 2003).

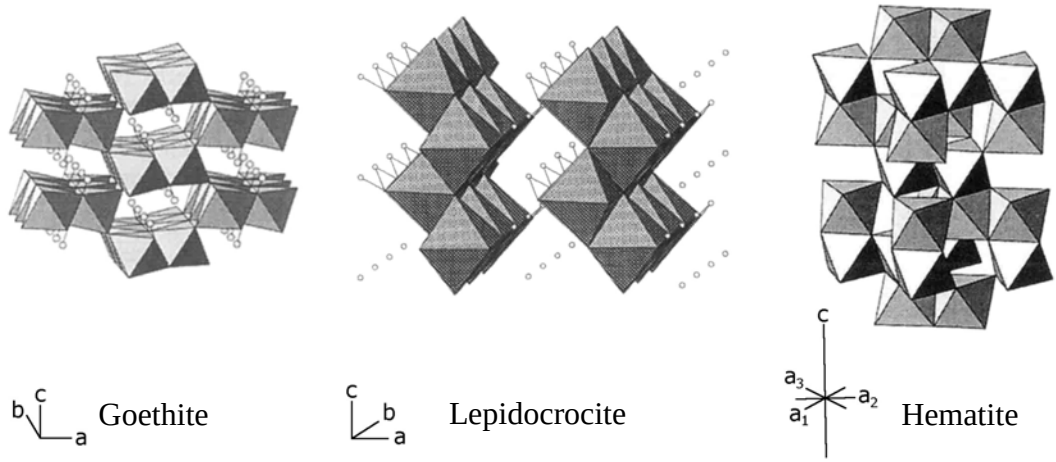

Figure 1: Structure of goethite, lepidocrocite and hematite (Cornell & Schwertmann, 2003). Reproduced with the permission from Wiley VCH.

1.3. Lepidocrocite

Lepidocrocite (γ-FeOOH), an orange colored iron oxide, is much less abundant in soil than goethite. The structure of lepidocrocite consists of double chains of edge sharing octahedra running along the c-axis (Fig. 1). The double chains are linked to adjacent chains by edge sharing, with one chain being displaced by half an octahedral with respect to its neighbor thereby creating corrugated sheets of octahedra. Unlike goethite which has a tunnel structure,

lepidocrocite is a layered compound. The basic morphologies of lepidocrocite are lath-like or tabular and the specific surface area range from 15 - 260 m^2/g (Cornell & Schwertmann, 2003).

1.4. Hematite

Hematite (α-Fe_2O_3) is a blood red iron oxide found widespread in rocks and soils. Like goethite, hematite is very stable. Hematite consists of octahedra sharing edges with three adjacent octahedra in the same plane and one face with an octahedron in a neighboring plane (Fig. 1). The specific surface area ranges from 10 - 90 m^2/g and the most common habits for hematite crystals are rhombohedral, platy and rounded (Cornell & Schwertmann, 2003).

2. Mixed Fe^{II}-Fe^{III} oxides (magnetite and green rust)

The green rust (GR) is a group of mixed Fe^{II}-Fe^{III} hydroxides salts known as GR due to its intense bluish-green colour. Structurally, GR is a member of layered double hydroxides family (LDHs), sometimes also called anionic clays. LDHs are composed of divalent-trivalent ions minerals which are characterized by a crystal structure that consists of the stacking of brucite-like layers carrying a positive charge and layers constituted of anions and water molecules. The positive charge of metal hydroxide sheets is due to the partial replacement of divalent by trivalent metal cations. Our paper with detailed description about iron-based LDH (Ruby *et al.*, 2010) is presented in annex (Annex 1). Their structure and composition depend upon the specific anions they incorporate. The general formula of LDHs is: $[M^{II}_{(1-x)}M^{III}_{x}(OH)_2]^{x+}.[(x/n)\ A^{n-},\ m\ H_2O]^{x-}$ where M^{II} and M^{III} are metallic cations present in brucite-type layers $Mg(OH)_2$, A^{n-} is an intercalated anion or a negatively charged molecule and also the electrostatic charge of both the brucite-type layers and the anionic interlayers and *m* is the number of intercalated water molecules. Most commonly, the values of *x* are found in the range [0.2-0.33] (Khan & O'Hare, 2002).

GR is a particular type of LDHs containing Fe as cation in the brucite type layers i.e. the LDH[Fe^{II}-Fe^{III}] with common intercalated anions are Cl^-, SO_4^{2-}, CO_3^{2-}. On the basis of X-ray diffraction (XRD) main features, GR were initially classified in two types: green rust one, GR1 and green rust two, GR2 (Bernal *et al.*, 1959). GR1 was obtained with the incorporation

of spherical and planar anions (Cl^-, I^-, Br^- and CO_3^{2-}) and it is characterized by a rhombohedral unit cell consisting of 3 repeat units (Fig. 2a) (Refait *et al.*, 1998). The interlayer spaces are composed of a single plane of compensating anions and water. GR2 incorporates three-dimensional tetrahedral anions (SO_4^{2-} and SeO_4^{2-}) and contains a hexagonal unit cell composed of 2 repeat units (Fig.2b) (Simon *et al.*, 2003). In GR2, interlayer spaces are composed of two adjacent planes of anions and water molecules (Simon *et al.*, 2003).

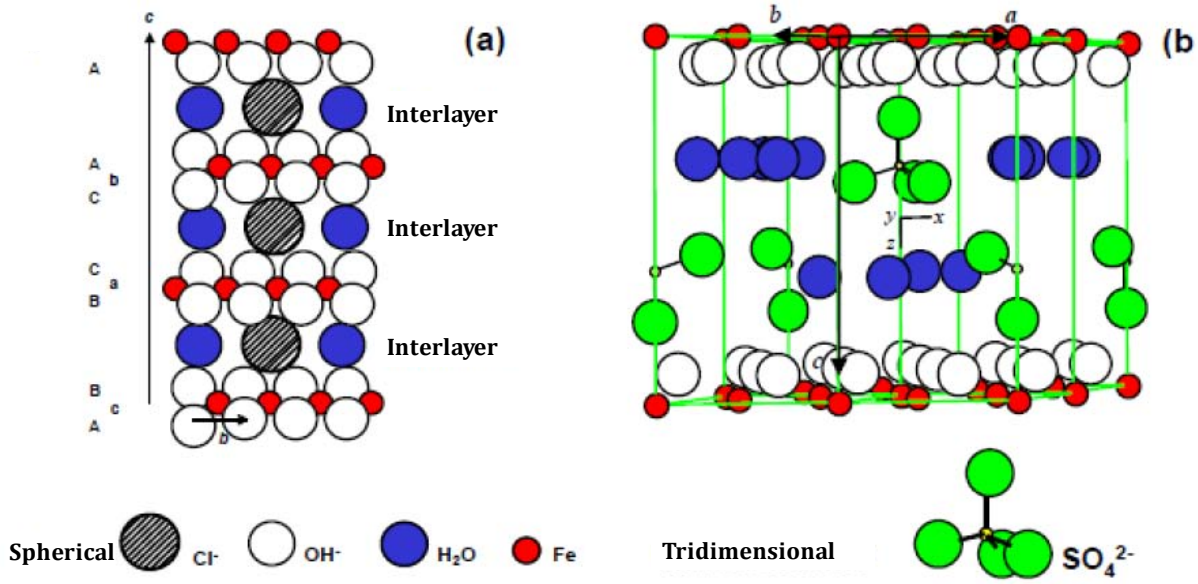

Figure 2: Structure of green rusts: (a) GR1 (Cl^-) (b) GR2 (SO_4) (Refait *et al.*, 1998; Simon *et al.*, 2003). This material was reproduced with the permission of Elsevier.

Magnetite ($Fe^{II}Fe^{III}O_4$) is a black, ferromagnetic mineral and it crystallizes with the spinel structure. The large oxygen ions are close packed in a cubic arrangement and the smaller Fe ions fill in the gaps (Fig.2). Magnetite contains both Fe^{II} and Fe^{III} in its structure with one-third Fe^{II} in octahedral sites and two-third Fe^{III} ions divided between octahedral and tetrahedral sites. Octahedral and tetrahedral layers stacked along [111] in its structure (Fig. 2a). The crystal forms of magnetite include octahedron and rhombodecahedron and the specific surface area ranges from 4-100 m^2/g (Cornell & Schwertmann, 2003).

Magnetite is stable in natural environment with very compact and dense structure. On the other hand, GR is an "opened" and hydrated compound and can be rapidly oxidized upon short exposure to atmospheric oxygen. Stoichiometric GRs ($x \sim 0.33$) contain about two times more structural Fe^{II} than stoichiometric magnetite ($x \sim 0.67$) with the Fe^{II}: Fe^{III} ratio of 1:2.

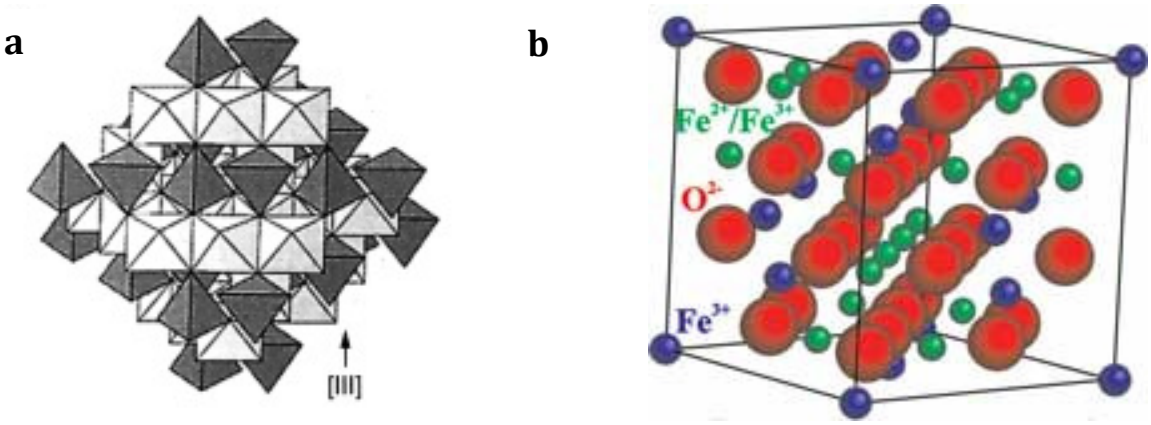

Figure 3: Structure of magnetite (Cornell & Schwertmann, 2003). This material was reproduced with permission of Wiley-VCH.

3. Synthesis of green rust and magnetite

For the first time, the synthesis of GR was reported by Girard & Chaudron (Girard & Chaudron, 1935). Initially GRs had been identified and studied as corrosion products of iron-based materials (Stampfl, 1969). Its first existence as a natural mineral in soil was evidenced by Trolard and coworkers from our lab (Trolard *et al.*, 1997). It was christened fougerite (IMA 2003-057) since the first extracted samples came from the hydromorphic gley soil located in forest of Fougères (Brittany-France). Another occurrence of GR in nature was recently observed in ground water (Christiansen *et al.*, 2009). Various synthetic procedures for GR or magnetite formation have been developed that are believed to mimic those operative in the environment, including biotic and abiotic pathways. Brief discussion of these synthesis routes is provided in following sections.

3.1. Abiotic synthesis

Abiotic synthesis pathways includes co-precipitation of soluble Fe^{II} and Fe^{III} species, oxidation of hydroxylated Fe^{II} species and ferric oxides transformations and are discussed below.

3.1.1. Co-precipitation of soluble Fe^{II} and Fe^{III} species

Co-precipitation of Fe^{II} and Fe^{III} species is a simple method that consists of adding a basic solution to a mixture of both Fe^{II} and Fe^{III} dissolved species. Synthesis of Fe^{II}-Fe^{III} mixed compounds in different kinds of aqueous solutions by this method has been widely reported in literature (Arden, 1950; Hansen, 1989; Jolivet *et al.*, 1992; Géhin *et al.*, 2002; Refait *et al.*, 2003; Ruby *et al.*, 2003; Aissa *et al.*, 2006; Ruby *et al.*, 2006a; Ruby *et al.*, 2006b). An illustration of synthesis routes of magnetite or GR by co-precipitation and oxidation in the mass balance diagram is presented in figure 4.

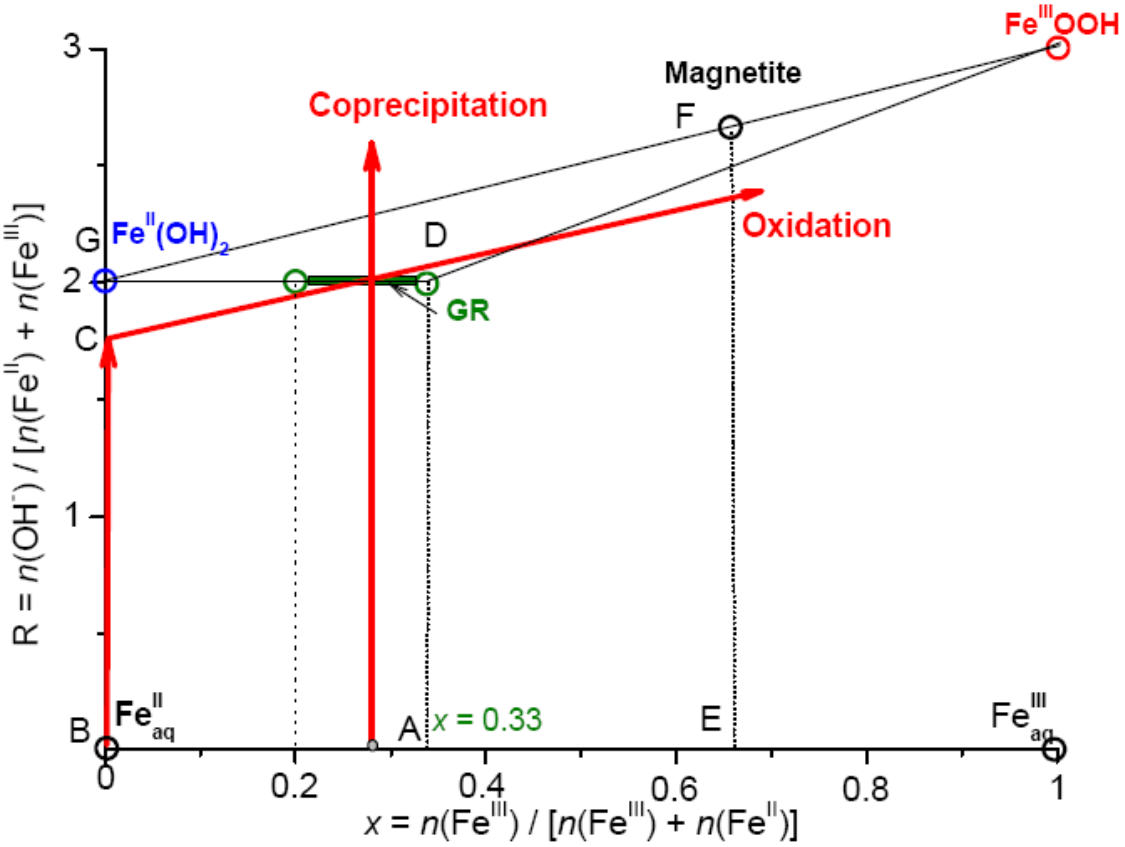

Figure 4: Fe^{II}–Fe^{III} mass-balance diagram showing the co-precipitation and oxidation [Adapted from Fig. 1 of (Ruby *et al.*, 2006a; Ruby *et al.*, 2010)]

The ordinate R= $n(OH^-) / [n(Fe^{II}) + n(Fe^{III})]$ represents the number of hydroxyl species per mole of iron that are consumed during the precipitation of a given compound (Fig. 4). The molar fraction of Fe^{III} is the abscissa $x= n(Fe^{III}) / [n(Fe^{II}) + n(Fe^{III})]$ in figure. Abundance and nature of formed iron compound is governed by these two parameters i.e. R and x. The position of the initial aqueous species Fe^{II}_{aq}, Fe^{III}_{aq} and solid compounds produced like $Fe^{II}(OH)_2$, the GR, the spinel $Fe^{II}Fe^{III}_2O_4$ and the oxyhydroxide $Fe^{III}OOH$ is indicated. The synthesis of GR or magnetite is achieved by the addition of a basic solution to a solution of (Fe^{II}_{aq}, Fe^{III}_{aq}). Vertical paths [AD] and [EF] correspond to the formation of GR and that of magnetite respectively. The formation of magnetite (Eq. 1) and GR (Eq. 2) from the stoichiometric quantities of Fe^{II} and Fe^{III} correspond to the following chemical reactions.

$$Fe^{II} + 2Fe^{III} + 8OH^- \rightarrow Fe^{II}Fe^{III}_2O_4 + 4H_2O \qquad (1)$$

$$4Fe^{II} + 2Fe^{III} + 12OH^- + SO_4^{2-} \rightarrow Fe^{II}_4\, Fe^{III}_2\, (OH)_{12}SO_4 \qquad (2)$$

The possibility to adjust accurately the x value of the initial solution, in order to determine the flexibility of the Fe^{III} molar fraction, is the major advantage of this method. The flexibility of the x values of $GR(SO_4)$ (Ruby *et al.*, 2003) and $GR(CO_3)$ (Ruby *et al.*, 2006a) was determined by using the co-precipitation method. These experiments were conducted in a gas-tight reactor with continuous N_2 bubbling in aqueous solution in order to avoid the oxidation of ferrous ions Fe^{II}. A systematic study of the titration of Fe^{II} and Fe^{III} by NaOH in a sulfate solution showed that $GR(SO_4)$ with a unique composition x=0.33 was formed (Ruby *et al.*, 2003). Co-precipitation at $x > 0.33$ or $x < 0.33$ resulted in the formation of [$GR(SO_4$–x=0.33), Fe_3O_4] and [$GR(SO_4$–x=0.33), $Fe(OH)_2$] mixtures respectively while at x=0.67, magnetite was formed.

The synthesis and mechanism of formation of $GR\text{-}SO_4$ by co-precipitation (Ruby *et al.*, 2003; Ruby *et al.*, 2006a; Ruby *et al.*, 2006b) involves the initial precipitation of ferric oxyhydroxide (Fig. 5). Partial hydroxylation of the Fe^{II} species takes place due to an increase in pH followed by their adsorption along with sulfate anions onto the surface of the precipitated ferric oxyhydroxide. Olation of sorbed Fe^{II} species immediately forms $GR\text{-}SO_4$.

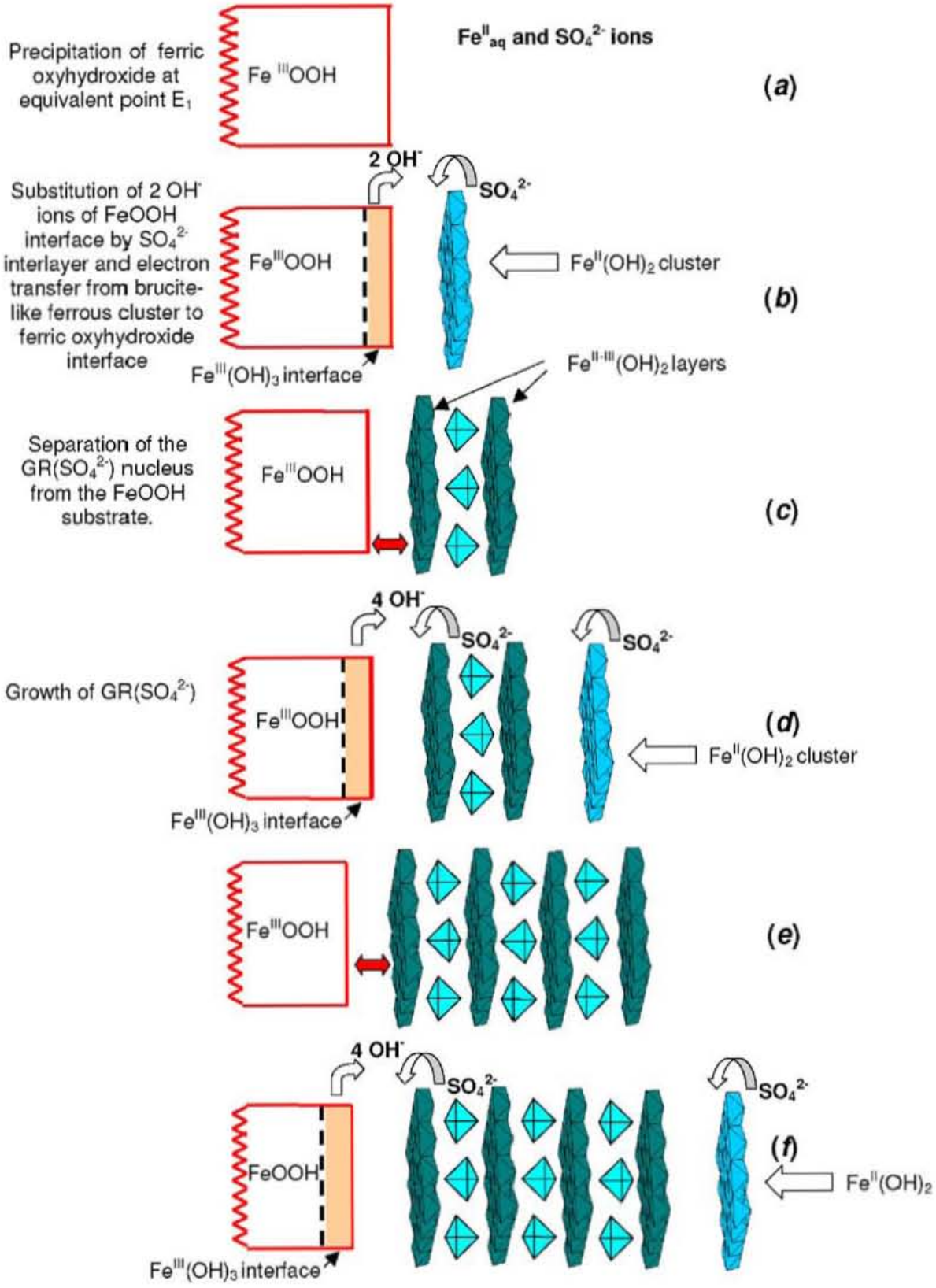

Figure 5. Formation mode of GR-SO_4 by the co-precipitation method. Reproduced with permission from Elsevier.(Ruby *et al.*, 2006a)

3.1.2. Oxidation of hydroxylated Fe^{II} solution

Partial chemical oxidation of soluble Fe^{II} or $Fe(OH)_2$ precipitates is another common method to synthesize the mixed Fe^{II}-Fe^{III} oxides. Oxidation can be carried out by O_2 bubbling in controlled environment, addition of an oxidant or by aerial oxidation. To achieve the desired end product i.e. GR or magnetite, constant monitoring of pH or electrode potential is required during synthesis. Synthesis of magnetite was conducted by aerial oxidation of Fe^{II} solution at basic pH (Ishikawa *et al.*, 2002) and oxidizing an aqueous solution containing Fe^{II} and the anion to intercalate yielded GR (Schwertmann & Fechter, 1994). The mechanism of formation of GR starts with initial oxidation of Fe^{II} into Fe^{III} followed by the precipitation of Fe^{III} as poorly ordered Fe^{III} oxide which ultimately reacts with Fe^{II} and OH^- forming GR (Schwertmann & Fechter, 1994).

Mixed Fe^{II}-Fe^{III} compounds were also synthesized by the partial oxidation of $Fe(OH)_2$ at neutral pH (Kiyama, 1974; Tamaura *et al.*, 1981; Olowe & Génin, 1991; Refait & Génin, 1993; Génin *et al.*, 1996; Génin *et al.*, 2006a). This method involves the precipitation/oxidation route (Fig. 4) with two steps: (i) base addition for initial precipitation of Fe^{II} solution into $Fe^{II}(OH)_2$ or [$Fe^{II}(OH)_2$, Fe^{II}_{aq}) (Fig. 4. Path BC) and (ii) oxidation of divalent species to from GR (Path CD) or magnetite (Path GF). Nature of the oxidant determines the slope of line CD (Fig. 4).

The easiest way of oxidation is agitating the $Fe^{II}(OH)_2$ suspension in contact with air and controlling the redox potential (Eh) of the suspension to follow the oxidation steps. Other oxidants such as hydrogen peroxide H_2O_2, iodine I_2 or persulfate $S_2O_8^{2-}$ can also be used. The advantage is to know the oxidation state of the product by controlling the amount of added oxidant. In sulfate and chloride solutions (Génin *et al.*, 2006a), only suspensions containing a specific amount of soluble Fe^{II} species led to the formation of pure GR. For example in sulfated medium, this excess of Fe^{II}_{aq} is described by the following chemical reaction:

$$5\ Fe^{II}(OH)_2 + Fe^{2+}_{aq} + SO_4^{2-} + 1/2\ O_2 + H_2O \ <=>\ Fe^{II}_4\ Fe^{III}_2\ (OH)_{12}\ SO_4 \qquad (3)$$

Addition of NaOH solution with ratio $r = n(OH^-) / n(Fe^{II})$ of exactly 5/3 resulted in partial precipitation of initial Fe^{II}_{aq} solution and thus yielding GR(SO_4). Precipitation of Fe^{II} species with ratio $r = 2$ resulted in the formation of pure $Fe(OH)_2$ without any excess of Fe^{II}_{aq}. And the oxidation of this formed $Fe(OH)_2$ resulted in pure magnetite. For $5/3 < r < 2$, the formation

of [GR(SO_4) and Fe_3O_4] mixture was observed. Other experiments were carried out by using persulfate ions $S_2O_8^{2-}$ as oxidant (Ruby *et al.*, 2006b). In this case; the oxidation of pure $Fe(OH)_2$ led to the formation of pure GR according to the following reaction :

$$6Fe^{II}(OH)_2 + S_2O_8^{2-} <=> Fe^{II}_4\ Fe^{III}_2\ (OH)_{12}\ SO_4 + SO_4^{2-} \quad (4)$$

Magnetite formation by air oxidation of pure $Fe(OH)_2$ was represented by following chemical reaction (Ruby *et al.*, 2006b).

$$6Fe^{II}(OH)_2 + O_2 <=> 2Fe^{II}Fe^{III}O_4 + 6H_2O \quad (5)$$

3.1.3. Fe^{II} induced mineralogical transformations of Fe^{III} oxides

Possible inter-conversions between the different species are a characteristic of iron oxide system. Fe^{II} induced transformation of iron oxides is still a matter of debate but structurally the transformations may proceed via two principally different mechanisms. (i) solid-state transformation (also called topotactic) and (ii) dissolution/re-precipitation (or reconstructive/re-crystallization). Topotactic transformations involve the transformation of the initial phase within a solid phase without dissolution therefore a correspondence in three dimensions between the initial and final structure is required. While in reconstructive transformations, dissolution of the initial phase is the first step followed by the crystallization of a new secondary phase. And therefore no structural relationship is required between the precursor and the transformation product. In this latter case, the oxide transformation occurs through the interfacial electron transfer reactions between adsorbed Fe^{II} and iron oxides involving reductive dissolution and then re-precipitation of the adsorbed ferrous ions on oxides particle surfaces (Tronc *et al.*, 1992). The penetration of electron into the oxide particle can destabilize the crystal, promoting its disintegration and release of the entered electron as a reduced Fe^{II} species (Williams & Scherer, 2004; Larese-Casanova & Scherer, 2006). On the other hand, direct dissolution of ferric oxide produced ferric ion which will form a redox couple with the added Fe^{II}. This redox couple in solution could potentially cause an electron transfer reaction between the Fe^{II} solution and the solid. The electron transfer reactions may destabilize the ferric oxide structure and promote its dissolution (Yang *et al.*, 2010), which would potentially increase the solution Fe^{III} concentration.

The driving force for the transformations of iron oxides is the thermodynamic instability of the more unstable iron oxides such as ferrihydrite and lepidocrocite. Under oxic conditions, goethite and hematite are thermodynamically the most stable compounds and are therefore the end member of many transformation pathways (Cornell & Schwertmann, 2003). The interactions of iron oxyhydroxides with aqueous Fe^{II} induce their structural modification and bulk phase transformation which depend upon various factors like molar ratio $x(Fe^{II}) = Fe^{II}/[Fe^{II} + Fe^{III}]$ (Tamaura *et al*., 1983; Tronc *et al*., 1992; Hansel *et al*., 2005), pH (Jeon *et al*., 2003), anionic media (Liu *et al*., 2008), OH^-/Fe ratio (Ishikawa *et al*., 1998; Ruby *et al*., 2003) and structure of initial iron oxyhydroxide substrate (Pedersen *et al*., 2005).

The presence of Fe^{II}, either added as Fe^{II}-salts or produced by iron oxide reduction, may lead to iron oxide transformations into ferric and/or mixed Fe^{II}-Fe^{III} phases. In the presence of low concentration of Fe^{II}, ferrihydrite was transformed either into goethite (Tronc *et al*., 1992; Jeon *et al*., 2003; Yee *et al*., 2006; Liu *et al*., 2008), lepidocrocite (Pedersen *et al*., 2005; Liu *et al*., 2008) or hematite (Liu *et al*., 2009). At high Fe^{II} amount, mixed Fe^{II}- Fe^{III} minerals such as magnetite (Tamaura *et al*., 1983; Mann *et al*., 1989; Jolivet *et al*., 1992; Tronc *et al*., 1992; Ishikawa *et al*., 1998; Pedersen *et al*., 2005; Kahani & Jafari, 2009) or green rust (Tamaura, 1985; Ruby *et al*., 2003; Larese-Casanova & Scherer, 2008) were formed from different ferric oxyhydroxides (Hansen, 2001).

To synthesize GR or magnetite, high Fe^{II} to Fe^{III} ratio ($x > 0.2$) and hydroxylation ratio ($R=OH^-/Fe$) of (2 for GR < R< 2.67 for magnetite) are required. The procedure involves the introduction of soluble Fe^{II} species into a suspension that contains the ferric oxyhydroxide at a pH close to 7. This pH allows a sufficient hydroxylation rate of the Fe^{II} species necessary to activate the reaction. The transformation of ferrihydrite at pH 8 and room temperature at varying Fe^{II}/Fe^{III} ratios was examined (Jolivet *et al*., 1992; Tronc *et al*., 1992) and it was found that at a low Fe^{II} concentration, ferrihydrite was transformed into goethite whereas at a higher Fe^{II} concentration magnetite was formed. Same results with varying Fe^{II}/Fe^{III} ratios were obtained with lepidocrocite that was transformed into magnetite at high Fe^{II} concentration while remained unchanged at low Fe^{II} concentration whereas no transformation into other phases was observed for goethite and hematite (Pedersen *et al*., 2005). It was found that α-, β- and γ-FeOOH react with $Fe(OH)_2$ to produce Fe_3O_4 in the order of β-FeOOH > γ-FeOOH > α-FeOOH (Ishikawa *et al*., 1998).

A heterogeneous reaction that would occur during the formation of GR at the surface of the ferric oxyhydroxide was described by our laboratory group (Ruby *et al.*, 2006b). The GR-SO_4 can be prepared by fixing the hydroxylation rate R = n(OH-)/[n(Fe^{II}) + n(Fe^{III})] at a exact value of 7 with a basic solution such as NaOH (Ruby *et al.*, 2003). This ratio corresponds to the formation of a mixture [FeOOH, $2Fe(OH)_2$] that was hypothesized to be the precursor of the formation of the GR-SO_4. Thus the interactions of aqueous Fe^{II} with the host ferric minerals can cause structural changes, potentially resulting in the formation of Fe^{II}-bearing minerals (green rust and magnetite).

3.2. Biotic formation of mixed Fe^{II}-Fe^{III} oxides

Dissimilatory iron-reducing bacteria (DIRB), which are ubiquitous in soils and aquifers, couple the oxidation of organic matter or H_2 with the reduction of various Fe^{III} oxide phases to obtain energy for growth and function. The biotic formation of GR or magnetite has been reported by iron reducing bacteria known to be key players in the biogeochemical cycling of Fe. It would be the most feasible way to explain the existence of Fe^{II}-Fe^{III} oxides (Berthelin *et al.*, 2006) which are produced by co-precipitation reaction between biogenic Fe^{II} and ferric oxides. Various strains of the DIRB *Shewanella putrefaciens* produce green rusts or magnetite as secondary products of microbial reduction of lepidocrocite and ferrihydrite. And this production of secondary minerals (GR *vs.* magnetite) was found dependent on medium composition and properties, bacterial cell density, rate of Fe^{II} supply, solid phase and aggregate pattern consisting of both iron oxide and bacteria etc. (Fredrickson *et al.*, 1998; Ona-Nguema *et al.*, 2002; Zachara *et al.*, 2002; O'Loughlin *et al.*, 2007; Zegeye *et al.*, 2007; Oloughlin *et al.*, 2010; Zegeye *et al.*, 2010).

The kinetics of Fe^{III} bioreduction has also been proposed as the main factor governing the formation of GR versus magnetite (Ona-Nguema *et al.*, 2002), with high rates of bioreduction being essential for magnetite (bio)mineralization. It has also been observed that once the microbial activity was exhausted, GR was no longer stable in the presence of ferrihydrite and was transformed into magnetite (Ona-Nguema *et al.*, 2002). It was suggested that bacterial cell/γ-FeOOH ratio could be the main parameter controlling the formation of GR versus magnetite as high cell numbers lead to the formation of GR while low cell numbers results in magnetite (Zegeye *et al.*, 2007; Oloughlin *et al.*, 2010; Zegeye *et al.*, 2010). Lepidocrocite,

goethite and hematite are formed from ferrihydrite when ferrihydrite is in great excess compared to the electron donor, while a lower electron donor to acceptor ratio leads to small particle-size lepidocrocite and goethite, and finally when the electron donor is in excess, ferrihydrite is transformed into fine-grained magnetite (Zachara *et al.*, 2002). During microbially mediated reduction of the iron oxides at pH 6-8, goethite and hematite remained unchanged at conditions where ferrihydrite transformed into magnetite (Zachara *et al.*, 2002). The synthesis of magnetite or green rust is primarily related with bacterial Fe^{III} reduction in the environment. Moreover, the GR and magnetite formation has also been reported during microbial Fe^{II} oxidation coupled to denitrification (Chaudhuri *et al.*, 2001) offering an alternative environmental source of biogenic Fe^{II}-Fe^{III} oxides.

4. Role of Mixed Fe^{II}-Fe^{III} oxides in environment

Both magnetite and green rust are considered as more reactive compounds than ferric oxides due to the presence of structural Fe^{II}. They play an important role in environmental fate and transport of various organic and inorganic pollutants. The use of GR has been extensively reported for the reductive tranformations of inorganic pollutants like nitrate, U^{VI}, Cr^{VI}, Se^{IV} and TcO_4^- (Erbs *et al.*, 1999; Fredrickson *et al.*, 2004; O'Loughlin & Burris, 2004) as well as organic contaminants (Elsner *et al.*, 2004; Larese-Casanova & Scherer, 2008; Kone *et al.*, 2009). Considerable interest has been given to reduction of NO_3^-, which is widely known as an agricultural pollutant (Hansen *et al.*, 1996; Hansen & Koch, 1998; Hansen *et al.*, 2001). Its reduction helps to protect groundwater from high NO_3^- concentrations. Magnetite was also found involved in contaminant reduction (Gorski *et al.*, 2009; Gorski & Scherer, 2009).

Due to the presence of Fe^{II}, they can serve as an iron source to catalyze Fenton oxidation of various pollutants. The role of magnetite has been widely investigated in oxidation through Fenton reaction for various pollutant like pentachlorphenol (Xue *et al.*, 2009a; Xue *et al.*, 2009c), trinitrotoluene (Matta *et al.*, 2007), rhodmadine B (Xue *et al.*, 2009b), azo dye (Hanna *et al.*, 2008). Only few studies have reported the use of GR in Fenton oxidation like phenol (Matta *et al.*, 2008) and azo dye etc. (Kone *et al.*, 2009). Till date, the reactivity of magnetite or GR has not been tested for the oxidation (Fenton or persulfate) of polycyclic aromatic hydrocarbons or aliphatic hydrocarbons which is briefly explained in next sections.

Fenton and Persulfate based chemical oxidation for hydrocarbon remediation

1. Soil Pollution

Soil pollution comprises the pollution of soils with materials, mostly chemicals that are out of place or are present at concentrations higher than normal threshold level which may have adverse effects on human beings or other organisms. It is a serious worldwide problem and the ever-increasing pollution of the environment has been one of the greatest concerns for science and the general public in the last fifty years. Main causes of pollution in natural ecosystems are the rapid industrialization of agriculture, construction works, military activities, expansion of the chemical industry and the need to generate cheap energy forms. As a consequence, the atmosphere, bodies of water, and many soil environments have become polluted by a large variety of toxic compounds. Many of these compounds at high concentrations or following prolonged exposure have the potential to produce adverse effects in humans and other organisms. In this study, two types of pollutants that are widespread in soil are addressed: Polycyclic aromatic hydrocarbons (PAHs) originated from coking plant sites and aliphatic hydrocarbons (AHs) originated from oil contamination.

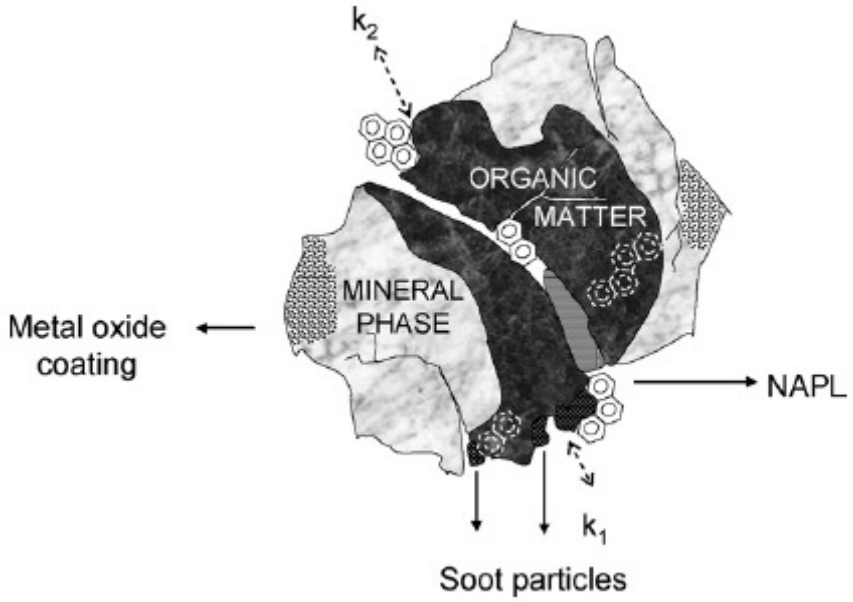

Figure 6: Conceptual model of a soil particle (Jonsson *et al.*, 2007). Reproduced with the permission of Elsevier.

The conceptual soil particle in Fig. 6 illustrates the presence of contaminants (PAHs) in various forms and processes involved when the pollutants are released into soil. PAHs in soil

can be strongly sorbed to soil organic matter (SOM), encapsulated in soil mineral, and can also be present in dense non-aqueous phase liquid (DNAPL) (Fig. 6), which makes the remediation process difficult. When contaminants are released into the ground, they undergo sequestration in the soil matrix. Susceptibility of the contaminants to remediation processes is reduced with sorption strength of contaminants which increases over time. Effective remediation techniques can be developed after understanding of the processes, known to influence the sequestration and degradability of organic pollutants. For example, PAHs are efficiently adsorbed onto the surface of the soil organic matter (SOM) and slowly start to penetrate into cavities and/or diffuse into the organic soil fraction. However, SOM is not homogenous with varying proportions of combustion residues, non-aqueous phase liquids (NAPLs), and natural organic matter (NOM) in its composition. All these components of SOM vary in their affinity for contaminants.

1.1. Polycyclic Aromatic Hydrocarbons

Polycyclic Aromatic Hydrocarbons (PAHs) are hydrophobic organic compounds which contain two or more fused benzene rings in linear, angular or clustered arrangements (Figure 7). They are among the most frequently detected environmental pollutants. PAHs are released during the incomplete combustion of coal, petroleum products and wood. Major route of entry of PAHs into the environment is by anthropogenic sources including combustion, gasification and liquefaction of fossil fuels, coke production, asphalt production, coal tar production, fuel processing, oil and diesel spills, waste incineration and motor vehicle emissions but there are also natural sources, e.g. volcanic eruptions and forest fires (Wild & Jones, 1995; Harvey, 1997; Henner *et al.*, 1997; O'Mahony *et al.*, 2006).

Their occurence in environmental matrices is of great concern due their high toxicity, carcinogenic effects and environmental persistence (Wild & Jones, 1995; Henner *et al.*, 1997). PAHs are highly persistent in the environment in particular, due to their hydrophobic nature and low water solubility (Harvey, 1997; Henner *et al.*, 1997). They have been subject of detailed research for more than 30 years (Wild & Jones, 1995; Henner *et al.*, 1997; Haapea & Tuhkanen, 2006; O'Mahony *et al.*, 2006). Such studies are often limited to 16 PAHs, designated as priority pollutants by the United States Environmental Protection Agency (US-

EPA) and by the European Community (Wild & Jones, 1995; Henner ***et al.***, 1997). Structure of these 16 PAHs is represented below in Fig. 2.

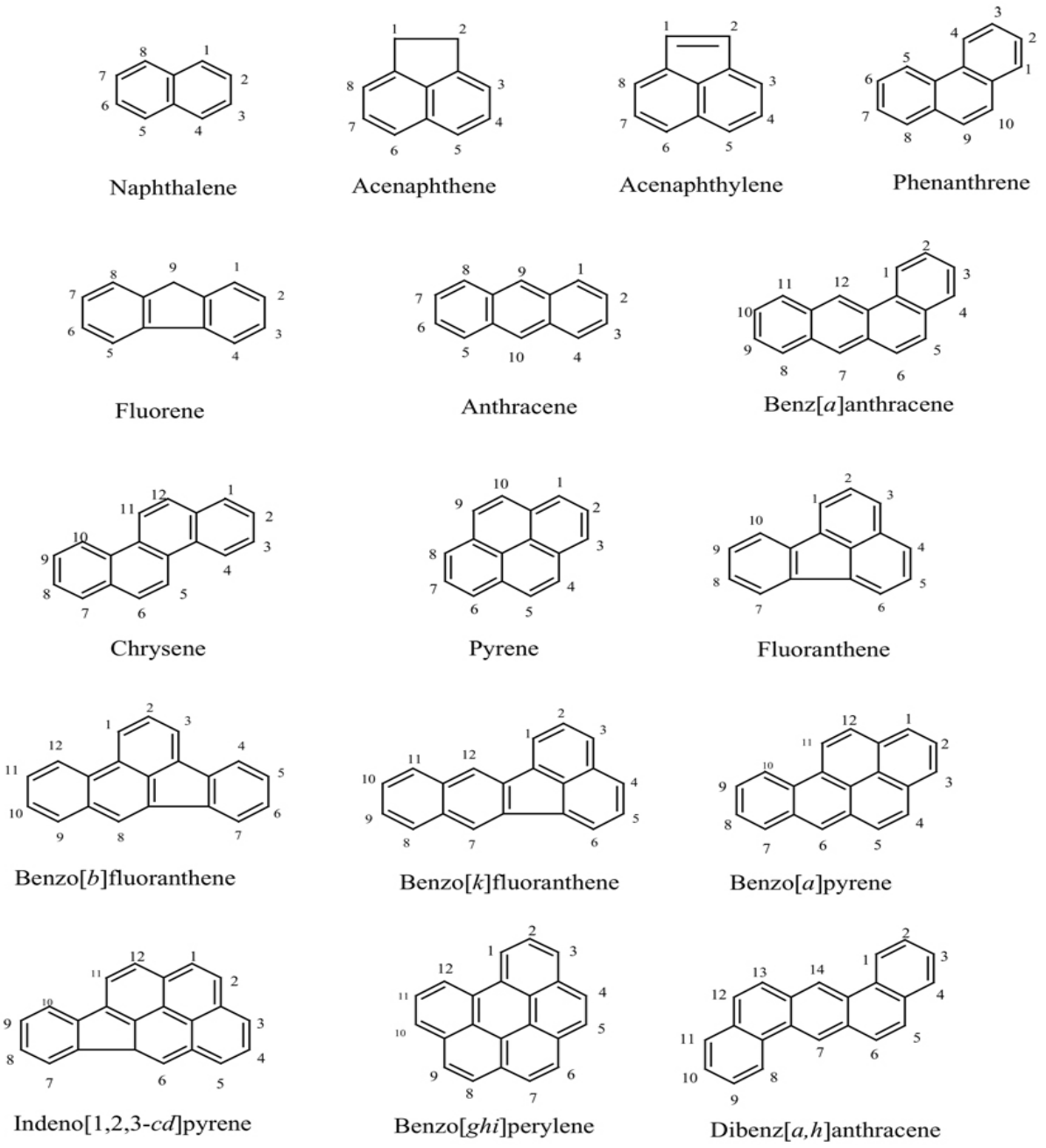

Figure 7: Structures and nomenclatures of the 16 PAHs on the US EPA priority pollutant list (Yan *et al.*, 2004)

Generally, PAHs are lipophilic compounds that show high affinity for organic matter and hydrophobic with low solubility and low volatility (Table 2). However individual PAHs differ substantially in their physical and chemical properties. As shown in Table 1, properties such

as aqueous solubility and vapor pressure range in five and twelve orders of magnitude, respectively, moving from two to six benzene rings in the PAH-molecule. As for PAH species, the lower molecular weight PAHs (LMW PAHs) are more volatile, water soluble and less lipophilic than the high molecular weight PAHs (HMW PAHs) which are highly hydrophobic (Mackay *et al*., 1992; Henner *et al*., 1997). Octanol-water partitioning coefficient (K_{OW}) also reflects this difference in hydrophobicity and lipophilicity as shown in Table 2. Coefficient K_{OW} is the ratio of the concentration of a chemical in octanol and in water at equilibrium and at a specified temperature. It is often used to indicate the fate of pollutants in the environment, as it represents the tendency of a chemical to remain sorbed onto organic matter (high K_{OW} values) or to dissolve in water (low K_{OW} values).

Table 2: Physico-chemical properties of the PAHs listed in US EPA list and considered in this study (Mackay *et al*., 1992).

PAH species	Chemical formula	Number of rings	Molecular weight	Aqueous solubility (mg/l)	Vapor pressure (Pa)	Log(K_{ow})
Naphthalene	$C_{10}H_8$	2	128	31	$1.0x10^{2}$	3.37
Acenaphtylene	$C_{12}H_8$	2	152	16	$9.0x10^{-1}$	4.00
Acenaphtene	$C_{12}H_{10}$	3	154	3.8	$3.0x10^{-1}$	3.92
Fluorene	$C_{10}H_{10}$	3	166	1.9	$9.0x10^{-2}$	4.18
Phenantrene	$C_{14}H_{10}$	3	178	1.1	$2.0x10^{-2}$	4.57
Anthracene	$C_{14}H_{10}$	3	178	0.045	$1.0x10^{-3}$	4. 54
Pyrene	$C_{16}H_{10}$	4	202	0.13	$6.0x10^{-4}$	5.18
Fluoranthene	$C_{16}H_{10}$	4	202	0.26	$1.2x10^{-3}$	5.22
Benzo(a)anthracene	$C_{18}H_{12}$	4	228	0.011	$2.8x10^{-5}$	5.91
Chrysene	$C_{18}H_{12}$	4	228	0.006	$5.7x10^{-7}$	5.91
Benzo(b)fluoranthene	$C_{20}H_{12}$	5	252	0.0015	-	5.80
Benzo(k)fluoranthene	$C_{20}H_{12}$	5	252	0.0008	$5.2x10^{-8}$	6.00
Benzo(a)pyrene	$C_{20}H_{12}$	5	252	0.0038	$7.0x10^{-7}$	5.91
Dibenzo(a,h)antracene	$C_{22}H_{14}$	6	278	0.0006	$3.7x10^{-10}$	6.75
Benzo(g,h,i)perylene	$C_{22}H_{12}$	6	276	0.00019	-	6.50
Indeno(1,2,3-cd)pyrene	$C_{22}H_{12}$	6	276	0.00026	$1.4x10^{-8}$	6.50

These physico-chemical properties also determine the environmental behavior of different PAHs species, as the transfer and turnover of LMW-PAHs will be more rapid than the HMW-PAHs (Wild & Jones, 1995). PAHs are persistent organic pollutants and this persistence increases with number of benzene rings as it was found that the greater the number of benzene

rings in the PAH molecule, the greater the resistance to degradation (Bossert & Bartha, 1986; Henner *et al.*, 1997).

Due to strong sorption of PAHs in soil to soil organic matter (SOM), encapsulated in soil mineral, and can also be present in dense non-aqueous phase liquid (DNAPL) (Fig. 1) makes the remediation process difficult. PAHs are very persistent showing extended natural attenuation times. The half life of PAHs in contaminated soils can be as long as 5.7 years and 9.1 years for low molecular weight and high molecular weight PAHs respectively (Wild *et al.*, 1991). PAHs could stay for longer periods than reported by Wild *et al.* (1991) depending on their sorption, soil type, SOM contents and their availability thus demonstrating the need for remediation processes to accelerate the clean-up of PAH-contaminated soils. For example, the strong adsorption of PAHs to soot carbon (Næs *et al.*, 1998) or its partitioning into humic matter (Sun *et al.*, 2003), will affect the success of any remediation process. However, even in soils with low organic content, the availability of PAHs may be low due to entrapment in pores and voids (Bogan & Trbovic, 2003). Clay minerals were reported to have greater adsorption capacities than SOM, thus influencing the contaminant sequestration (Hwang & Cutright, 2003). Inorganic surfaces, which consist of minerals, oxides, and metals, may also have an impact on PAH availability (Kong *et al.*, 1998b; Watts *et al.*, 1999b; Amellal *et al.*, 2001; Sun *et al.*, 2003; Flotron *et al.*, 2005). Thus all these factors could affect degradability of PAHs in soils.

1.2. Aliphatic Hydrocarbons

Aliphatic hydrocarbons (AHs) are the hydrocarbons which do not contain a benzene ring. The soil and groundwater pollution by oil compounds is a serious environmental and health concern worldwide. Soils contaminated with crude oil fail to support plant growth and are a source of groundwater contamination (Wang & Bartha, 1990). Petrochemical industries and petroleum refineries generate large amounts of priority pollutants. The major pollutants found in these industries are petroleum hydrocarbons, specifically aliphatic hydrocarbons, arising from storage of crude oil, spills, wash downs and vessel clean-outs from processing operation. Aliphatic or saturated compounds are mainly composed of *n*-alkanes, iso-alkanes, isoprenoids and cyclo-alkanes.

The ***n***-alkanes are ubiquitous compounds and can be synthesized ***via*** biotic and abiotic pathways. The origins of biogenic n-alkanes are numerous; they can be directly synthesized by many organisms or be derived from the diagenesis of functionalized linear compounds. Their distribution may nevertheless provide information on their origin. Thus the abundance of n-alkanes, consisting of long chains with a predominance of odd number of carbon atoms, is a characteristic of higher plants contribution because they are derived from cuticle wax while the short-chained ***n***-alkanes are preferentially synthesized by algae and marine organisms. Iso-alkanes have one or more alkyl groups along the hydrocarbon chain. Certain of these molecules are very specific biomarkers others, such as pristane and phytane, are used as indicators of the deposit medium and may provide clues to the degree of biodegradation. Hopanes or pentacyclic triterpenes, belonging also to aliphatic hydrocarbons, are fossil biomarkers mainly inherited from bacteria. They are used as indicators of source and maturity of fossil organic matter in petroleum organic geochemistry (van Duin ***et al.***, 1997).

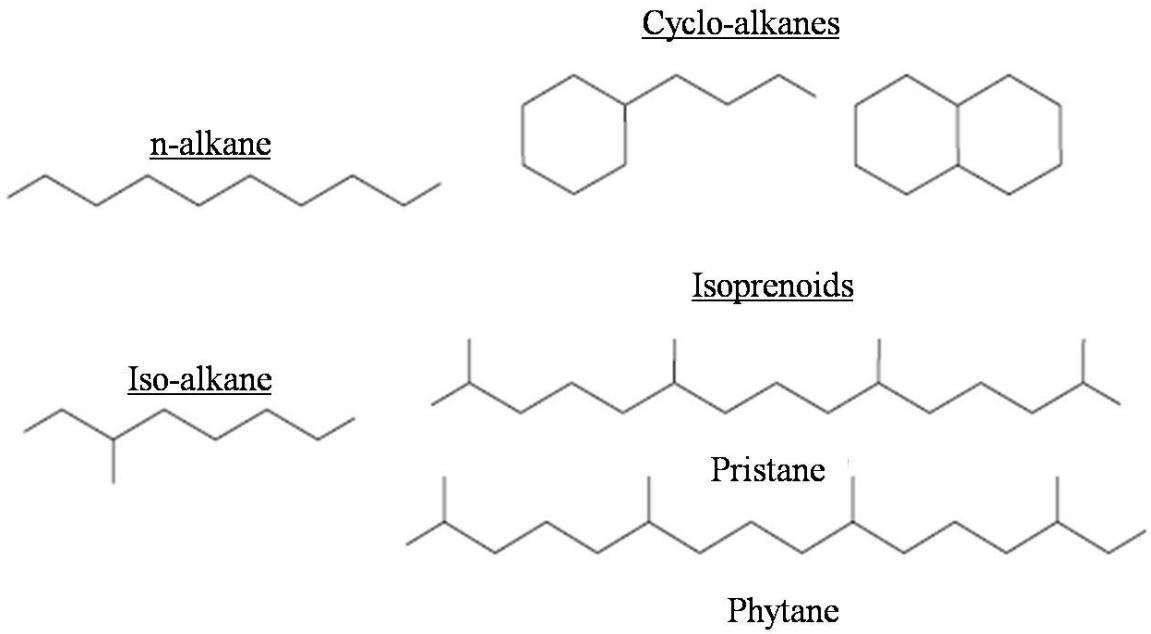

Figure 8: Examples of aliphatic hydrocarbons

2. Soil Remediation by Chemical oxidation

The term 'soil remediation' refers to actions designed to eliminate or minimize the risk associated with contaminated soil. This goal may be achieved in several different ways and the selected method depends on factors such as the contaminants present, the site conditions and the cost. The ultimate goal of any degradation process is complete mineralization of the organic contaminants, resulting in carbon dioxide, water and other inorganic compounds. Many types of remediation technologies have been explored for the removal of PAHs or AHs from soils, using chemical (Ferguson *et al.*, 2004; Ferrarese *et al.*, 2008; Do *et al.*, 2010; Lu *et al.*, 2010a; Yap *et al.*, 2011; Yen *et al.*, 2011), thermal (Haapea & Tuhkanen, 2006; Biache *et al.*, 2008), biological (Taylor & Jones, 2001; Chaîneau *et al.*, 2003; Franco *et al.*, 2004; Cai *et al.*, 2007; Silva *et al.*, 2009) or combined approaches (Allen & Reardon, 2000; Piskonen & Itävaara, 2004; Kulik *et al.*, 2006; Lu *et al.*, 2010b). Although, bioremediation techniques have become popular in recent years for treatment of PAHs contaminated soils (Wilson & Jones, 1993; Boopathy, 2000), these methods have shown limited capacity to degrade recalcitrant high molecular weight PAHs (Wilson & Jones, 1993; Henner *et al.*, 1997; Andersson *et al.*, 2003; Lundstedt *et al.*, 2003). On the other hand, bioremediation has proven successful for AHs in oil contaminated soils as the majority of molecules in crude oil spills and refined products are biodegradable (Prince, 1993). However, also bioremediation is often unable to reduce the level of contamination and long term soil toxicity below the stringent environmental cleanup standards (Płaza *et al.*, 2005). Moreover, a complete mineralization of oil to CO_2 and H_2O cannot be achieved by soil microorganisms and always leaves more or less complex residues (Atlas, 1995) like PAHs. Also bioremediation has limited application to biorefractory materials especially asphaltenes (Gough & Rowland, 1990; Chaîneau *et al.*, 2003; Chaillan *et al.*, 2006).

Faster and more efficient degradation of recalcitrant PAHs, oil hydrocarbons and biorefractory materials can be achieved using advanced oxidation processes (AOPs) (Kawahara *et al.*, 1995; Watts & Dilly, 1996; Kong *et al.*, 1998a; Nam *et al.*, 2001; Watts *et al.*, 2002; Ferrarese *et al.*, 2008; Lu *et al.*, 2010a; Yap *et al.*, 2011; Yen *et al.*, 2011). The AOPs are chemical methods which use various combinations of reactants to enhance the formation of highly reactive radicals, which can mineralize even the most recalcitrant organic compounds. The oxidants that are most commonly used for environmental purposes are

ozone, hydrogen peroxide, permanganate and persulfate (Rivas, 2006; Ferrarese *et al.*, 2008). This study deals with the two most common techniques among AOPs; Fenton based oxidation and activated persulfate which are briefly described in the following sections.

2.1. Fenton based oxidation

Fenton treatment is a widely studied technique classified under AOPs. Fenton reactions encompass H_2O_2 reaction with iron ions to form oxygen species which are able to oxidize organic or inorganic compounds. The Fenton reagent was developed by Henry J. H. Fenton in the 1890s when he reported that H_2O_2 could be activated by Fe^{II} salt to oxidize tartaric acid (Fenton, 1894). It has been applied as an oxidizing agent for organic contaminants in industrial wastewaters since 1960s (Huang *et al.*, 1993). However, its potential application in soil remediation was started in 1990s at lab scale (Tyre *et al.*, 1991; Watts *et al.*, 1993; Watts & Dilly, 1996). And Fenton based treatment was first time applied on PAHs-contaminated soil in 1995 (Martens & Frankenberger, 1995) and for aliphatic hydrocarbons in 1996 (Watts & Dilly, 1996).

In general, Fenton reactions can be homogeneously catalyzed by using soluble Fe^{II} as iron source (conventional Fenton and modified Fenton) or heterogeneously catalyzed by using iron minerals instead of soluble Fe (Fenton-like). Both conventional Fenton and Fenton-like reactions are described below.

2.1.1. Conventional Fenton oxidation

2.1.1.1. Background and reaction chemistry

The conventional Fenton oxidation is based on the reactivity of hydroxyl radical ($OH^{\bullet}$), a very reactive species which is generated in aqueous solution when hydrogen peroxide (H_2O_2) is dosed together with a ferrous ion (Fe^{II}) (Haber & Weiss, 1934). The initiation reaction is shown in Eq. (2.1). This reaction leads to the production of hydroxyl radicals $^{\bullet}OH$, which are very strong non-selective oxidizing agents (standard oxidation potential about 2.8 V), able to react both with alkanes and aromatic compounds (Watts *et al.*, 2002; Rivas, 2006).

$$Fe^{II} + H_2O_2 \quad \rightarrow \quad Fe^{III} + HO^{-} + HO^{\bullet} \qquad (2.1)$$

In Fenton oxidation, besides the initiation reaction (Eq. 2.1) many secondary reactions occur simultaneously that may co-oxidize the contaminants and compete with or scavenge the $OH^{\bullet}$ radicals (Table 2). Various other important radicals are produced in these secondary reactions like perhydroxyl radicals ($HO^{\bullet}_2$), superoxide radicals ($O^{\bullet}_2$) and hydroperoxide anions $(HO_2)^{\bullet}$ which are also involved in the oxidation of contaminants. These radicals are highly reactive and can degrade even most recalcitrant compounds or sorbed contaminants (Watts *et al.*, 2002; Flotron *et al.*, 2005; Ferrarese *et al.*, 2008). However, under acidic condition, $OH^{\bullet}$ radicals remain the principal oxidant species in the process.

Table 3: Principal Fenton reactions and related radical reactions. This table was reproduced from (Yap *et al.*, 2011) with the permission of Elsevier.

Principal initiation	
1. $Fe^{2+} + H_2O_2 \rightarrow Fe^{3+} + {}^{\bullet}OH + OH^-$	(Walling, 1975)
Secondary reactions	
2a. $Fe^{3+} + H_2O_2 \leftrightarrow Fe{-}OOH^{2+} + H^+$	(Walling & Goosen, 1973)
2b. $Fe{-}OOH^{2+} \rightarrow Fe^{2+} + HO^{\bullet}_2$	(Walling & Goosen, 1973)
3. $HO^{\bullet}_2 + Fe^{2+} \rightarrow H_2O_2 + Fe^{3+}$	(Buxton *et al.*, 1988)
4. $HO^{\bullet}_2 + Fe^{3+} \rightarrow Fe^{2+} + O_2 + 2H^+$	Beltran *et al.* (1998)
5. $HO^{\bullet}_2 \leftrightarrow O_2^- + H^+$	(Stumm & Morgan, 1996)
6. $O_2^{\bullet-} + Fe^{2+} \rightarrow H_2O_2 + Fe^{3+}$	(Buxton *et al.*, 1988)
7. $O_2^{\bullet-} + Fe^{3+} \rightarrow Fe^{2+} + O_2$	(Buxton *et al.*, 1988)
8. $HO^{\bullet}_2 + O_2^{\bullet-} \rightarrow HO^-_2 + O_2$	(Buxton *et al.*, 1988)
9. ${}^{\bullet}OH + HO_2^{\bullet} \rightarrow H_2O + O_2$	(Buxton *et al.*, 1988)
10. ${}^{\bullet}OH + O_2^{\bullet-} \rightarrow OH^- + O_2$	(Buxton *et al.*, 1988)
11. $Fe^{2+} + O_2 + OH^- \rightarrow Fe^{3+}$	(Stumm & Morgan, 1996)
Termination	
12. ${}^{\bullet}OH + H_2O_2 \rightarrow O_2^{\bullet-} + H_2O$	(Buxton *et al.*, 1988)
13. ${}^{\bullet}OH + Fe^{2+} \rightarrow Fe^{3+} + OH^-$	(Farhataziz & Ross, 1977)
14. $2{}^{\bullet}OH \rightarrow H_2O_2$	(Buxton *et al.*, 1988)

The optimum pH for conventional Fenton reaction is 2–4 (Di Palma, 2005; Langwaldt, 2005) required to avoid Fe^{III} precipitation as an oxyhydroxide and to keep Fe^{II} in solution which is known for its rapid oxidation at circumneutral pH. Since in environmental conditions iron is mainly found as Fe^{III}, such low pH can also be used to increase the availability of Fe^{II}. As for the regeneration of Fe^{II} from Fe^{III}, acidification of solution to pH < 5 is required (Kwan and Voelker, 2002), as shown in the following equation.

$$Fe^{III} + H_2O_2 \quad \rightarrow \quad Fe^{II} + H + HO^{\bullet}_2 \qquad (2.2)$$

To attain this pH, large amounts of acid (usually sulfuric acid) must be added to the reaction medium. Application of homogeneous Fenton process without pH adjustment can result in the production of large amounts of ferric hydroxide sludge, creating disposal and other environmental problems, thus making is impractical to apply in natural conditions. As in soil systems, such low pH in conventional Fenton reaction results in negative impacts on soil properties and quality and is incompatible with subsequent revegetation or biodegradation (Sahl & Munakata-Marr, 2006; Sirguey *et al.*, 2008). Hence, Fenton reaction has been modified to achieve its application to native circumneutral soil pH conditions. These modifications result from any deviation from the classical Fenton reaction and the reaction is referred to as modified Fenton. Application of biodegradable chelating agents in application to modified Fenton reagents were considered important in this regard. Various chelating agents such as citric acid, cyclodextrins, catechol, nitrilotriacetic acid (NTA), disodium ethanol diglycine (HEIDA), ethylene diamine tetra-acetic acid (EDTA) and gallic acid have been tested on PAH contaminated soils, either as a sole treatment or in combination with secondary biological treatment (Nam *et al.*, 2001; Ferrarese *et al.*, 2008; Gryzenia *et al.*, 2009; Lu *et al.*, 2010a). The chelating agents are able to dissolve Fe^{III} precipitation by forming complexes, thus increasing Fe^{II} availability.

2.1.1.2. Mechanism and reactivity

Once hydroxyl radical ($^{\bullet}OH$) have been created, degradation of organic compounds can be achieved by their reaction with this $^{\bullet}OH$ radical. There are two common ways of degradation reported which are: (i) hydrogen atom abstraction (Eq. 2.2) or (ii) hydrogen or hydroxyl addition (Eq. 2.3 or Eq. 2.4) (Legrini *et al.*, 1993; Flotron *et al.*, 2005). Electron transfer can be a third mechanism but $OH^{\bullet}$ is more likely to participate in hydrogen addition or subtraction reactions.

$$ROH + {}^{\bullet}OH \rightarrow {}^{\bullet}R + H_2O \quad (2.2)$$

$$R + {}^{\bullet}OH \rightarrow {}^{\bullet}ROH \quad (2.3)$$

Or

$$R^{\bullet} + H_2O_2 \rightarrow ROH + {}^{\bullet}OH \quad (2.4)$$

In the former (Eq. 2.2), $OH^{\bullet}$ radicals abstract hydrogen atoms from organic compounds to produce organic radicals. These organic radicals can further react with H_2O_2 to generate more $OH^{\bullet}$ radicals leading to the propagation of chain reactions. The hydrogen abstraction paths on aromatic compounds such as PAHs always form an oxygen- centred phenoxyl type radical and a water molecule (Yeh *et al.*, 2008). In the addition reaction (Eq. 2.3 and 2.4) to an unsaturated C–C bond, $OH^{\bullet}$ radicals attack ring carbons with their unpaired electrons. Upon contact, C–O bonds are formed. Under normal circumstances, if the Fenton oxidation is carried to completion, the complete mineralization of organic molecules into carbon dioxide (CO_2) and water is achieved (Eq. 2.5):

$$\text{Oxidized organics} + {}^{\bullet}OH \rightarrow CO_2 + H_2O \quad (2.5)$$

Fenton oxidation was studied for PAHs by various authors (Kawahara *et al.*, 1995; Watts *et al.*, 2002; Flotron *et al.*, 2005; Jonsson *et al.*, 2007; Ferrarese *et al.*, 2008) etc. and for AHs or oil hydrocarbons (Watts & Dilly, 1996; Ferguson *et al.*, 2004; Mater *et al.*, 2007; Lu *et al.*, 2010a; Yen *et al.*, 2011). The application of Fenton based reactions by various researchers is shown in Table 2.

2.1.2. Fenton-like oxidation

2.1.2.1. Background and reaction chemistry

The optimal pH for conventional Fenton reaction (pH= 2-4) results in negative impact on soil properties and soil quality (Sirguey *et al.*, 2008). Above this pH (>4) in conventional Fenton reaction, the generation of $OH^{\bullet}$ radicals is slower due to the precipitation of Fe^{II} to ferric-hydroxo complexes and the decomposition of H_2O_2 (Di Palma, 2005; Langwaldt, 2005). To avoid the low pH, iron minerals are used instead of soluble Fe^{II} homogeneous catalyst to conduct oxidation at circumneutral pH, and the reaction is defined as a Fenton-like reaction. Iron minerals are able to catalyze Fenton-like reactions over a wide range of pH values. This

is because the Fe species in iron minerals are "immobilized" within the structure and in the pore/ interlayer space of the catalyst. As a result, the ability of iron catalyst to generate hydroxyl radicals from H_2O_2 can be maintained and iron hydroxide precipitation is prevented. Heterogeneous catalysts including native or added iron oxides or certain transition metals can catalyze the Fenton-like oxidation at circumneutral pH. The Fenton-like reaction catalyzed by goethite has been shown to give the highest PAHs degradation efficiency at near neutral pH, i.e. pH of 7.0–8.0 (Watts *et al.*, 2002; Kanel *et al.*, 2003; Kanel *et al.*, 2004).

To date, the study of Fenton-like oxidation on PAH-contaminated soils is limited to the use of native iron as catalyst. The iron oxides present in the soil matrix such as goethite, hematite, magnetite and ferrihydrite are all capable of catalyzing H_2O_2 (Tyre *et al.*, 1991). After the application of H_2O_2, iron on the internal surfaces of the soil structure undergoes a redox cycle to produce the $OH^{\bullet}$ radicals. These non-chain reactions are different from that of homogeneous Fenton reactions as represented below (Eq. 2.6-2.11) (Huling *et al.*, 1998; Lin & Gurol, 1998b; Kanel *et al.*, 2004).

$$\equiv Fe^{3+}\!-\!OH + H_2O_2 \rightarrow \equiv Fe^{2+}\cdot O_2H + H_2O^{\bullet} \quad (2.6)$$

$$\equiv Fe^{2+}\cdot O_2H \rightarrow \equiv Fe^{2+} + HO_2^{\bullet} \quad (2.7)$$

$$2\equiv Fe^{2+} + 3H_2O_2 \rightarrow 2\equiv Fe^{3+}\!-\!OH + OH^{\bullet} + {+}HO_2^{\bullet} + H_2O \quad (2.8)$$

$$\equiv Fe^{2+} + O_2 + H_2O \rightarrow \equiv Fe^{3+}\!-\!OH + HO_2^{\bullet} \quad (2.9)$$

$$HO_2^{\bullet} \rightarrow H^{+} + O_2^{\bullet-} \quad (2.10)$$

$$3\equiv Fe^{2+} + 2H_2O_2 + 4HO_2^{\bullet} + HO_2^{\bullet}/O_2^{\bullet-} \rightarrow 3\equiv Fe^{3+}\!-\!OH + H_2O/OH^{-}; {+}OH_2^{\bullet} + 2O_2 + H_2O \quad (2.11)$$

2.1.2.2. Mechanism and reactivity

Formation of a surface complex between H_2O_2 and iron oxides is the first step in Fenton-like oxidation. This step is followed by an electron transfer inside the complex, leading to Fe^{II} and $HO^{\bullet}_2$ radical. This complex further dissociates and this dissociation is non-reversible due to the high reactivity of the radical. The PAH contaminants in the aqueous phase will then be

oxidized or reduced by reducing species generated in Fenton-like reaction (Lin & Gurol, 1998b; Watts *et al.*, 2002; Kanel *et al.*, 2003). Continuous removal of pollutant from the aqueous phase increases the concentration gradient which ultimately results in mass transfer increase from the sorbed phase to the dissolved phase. The average rate of H_2O_2 reaction was considered to be far lower on the surface of iron oxides, than its diffusion rate through the external films or internal pores (Lin & Gurol, 1998b). Hence, the oxidation process is likely to be limited by the intrinsic reactions of H_2O_2 on the oxide surfaces rather than the mass transfer rate of H_2O_2 to the surfaces (Lin & Gurol, 1998b; Valentine & Ann Wang, 1998).

The degradation of PAHs by Fenton-like reaction catalyzed by various Fe^{III} oxides like ferrihydrite, hematite or goethite were investigated for the degradation of PAHs on spiked soil (Watts *et al.*, 2002; Kanel *et al.*, 2003; Kanel *et al.*, 2004) and AHs (Watts & Dilly, 1996; Kong *et al.*, 1998a). Magnetite was found reactive for oil hydrocarbons to catalyze Fenton oxidation at an acidic pH of 3 (Kong *et al.*, 1998a). While the reactivity of mixed Fe^{II}-Fe^{III} oxides like magnetite have never been evaluated to activate Fenton-like oxidation for PAHs and AHs at circumneutral pH. This magnetite was found effective to catalyze Fenton-like oxidation of other organic pollutants. Up till now, Fenton-like oxidation experiments are reported on spiked soil while real soil oxidation is still missing.

2.2. Persulfate oxidation

2.2.1. Background and reaction chemistry

Persulfate ($S_2O_8^{2-}$) is widely applied in many industrial processes, e.g. polymerization, metal surface oxidation and organic chemical manufacturing (Watts & Teel, 2006). However the use of persulfate for *in situ* chemical oxidation has emerged within the last decade as a more recent addition to the list of possible oxidants (Liang *et al.*, 2003; Liang *et al.*, 2004; Watts & Teel, 2006; Killian *et al.*, 2007; Ferrarese *et al.*, 2008; Liang *et al.*, 2008; Gryzenia *et al.*, 2009; Yen *et al.*, 2011). The most suitable persulfate salt for *in situ* application is sodium persulfate ($Na_2S_2O_8$) due to its highest solubility as compared to other persulfate salts (Huling & Pivetz, 2006). The persulfate anion is a strong oxidizing agent with a redox potential (Eo) of 2.01 V and its reduction results in the production of sulfate anions as shown below (Latimer, 1952):

$$S_2O_8^{2-} + 2e^- \rightarrow 2SO^{2-}_4 \qquad (2.12)$$

Sulfate anion, although a strong oxidant, is kinetically slow in reacting with many organic compounds (Osgerby, 2006). In addition to direct oxidation, sodium persulfate can be induced to form sulfate radicals ($SO4^{\bullet-}$), thereby providing free radical reaction mechanisms similar to the hydroxyl radical pathways generated by Fenton's chemistry. There are different pathways to activate the persulfate anion either chemically or thermally to generate the intermediate sulfate free radical ($SO4^{\bullet-}$) oxidant (House, 1962; Balazs *et al*., 2002). The $SO4^{\bullet-}$ radical (Eo ~ 2.6 V) is a stronger oxidant than the persulfate anion (Latimer, 1952). Pathways of thermal activation or chemical activation via Fe^{II} are presented in the following equations:

Thermal activation by a temperature of (30-100 °C) or by UV:

$$S_2O_8^{2-} \xrightarrow{\Delta \, ou \, h\nu} 2\,SO_4^{\bullet-} \qquad (2.13)$$ (House, 1962)

Chemical activation by metal catalyst includes:

$$S_2O_8^{2-} + M^{n+} \rightarrow SO_4^{\bullet-} + SO_4^{2-} + M^{n+1} \qquad (2.14)$$

The most common metal catalyst is Fe^{II}.

$$S_2O_8^{2-} + Fe^{2+} \xrightarrow{\text{Chemical activation}} SO_4^{-\cdot} + SO_4^{2-} + Fe^{3+} \qquad (2.15)$$ (Travina *et al*. 1999)

However, as soon as $SO4^{\bullet-}$ is generated via Eq. (2.15), $SO4^{\bullet-}$ contacts with excess Fe^{II} in solution and can convert ferrous ion (Fe^{II}) to the ferric form (Fe^{III}) according to the following equation:

$$SO_4^{-\cdot} + Fe^{2+} \rightarrow Fe^{3+} + SO_4^{2-} \qquad (2.16)$$ (Buxton *et al*., 1997)

During metal activation, the metal activator is involved in both radical generation (Eq. 2.14, 2.15) and radical scavenging (Eq. 2.16). Thus an optimum catalyst dose is required to achieve effective activation without excess scavenging. An overall reaction between persulfate and ferrous ion activator can be described as:

$$S_2O_8^{2-} + 2Fe^{2+} \rightarrow 2Fe^{3+} + 2SO_4^{2-} \qquad (2.17)$$ (Buxton *et al*., 1999)

When $SO4^{\bullet -}$ serves as an oxidant, it accepts a single electron, which also results in sulfate anion formation:

$$SO_4^{\cdot -} + e^- \rightarrow SO_4^{2-} \quad E^\circ = 2.6V \qquad (2.18)$$ (Eberson, 1987)

Under acidic conditions the breakdown of persulfate into sulfate free radicals can be further acid catalyzed as follows (House, 1962):

$$S_2O_8^{2-} + H^+ \rightarrow HS_2O_8^- \qquad (2.19)$$

$$HS_2O_8^- \rightarrow SO_4^{\bullet -} + SO_4^{2-} + H^+ \qquad (2.20)$$

Also, the presence of $SO4^{\bullet -}$ in aqueous solution can result in radical inter-conversion reactions to produce the hydroxyl radical ($^{\bullet}OH$) (Eo = 2.7 V) in accordance with the following reactions (Pennington & Haim, 1968; Hayon *et al.*, 1972).

At all pH values: $SO_4^{\cdot -} + H_2O \rightarrow SO_4^{2-} + \cdot OH + H^+$ (2.21)

At alkaline pH values: $SO_4^{\cdot -} + OH^- \rightarrow SO_4^{2-} + \cdot OH$ (2.22)

Sulfate radical initiation can be achieved through the application of heat, transition metal catalysts or UV radiation. For activation by transition metal catalysis, ferrous iron (Fe^{II}) is the most common and readily available activator, with common forms being ferrous sulfate ($FeSO_4$) and ferrous chloride ($FeCl_2$). Unlike the Fenton mechanism, Fe^{II} activation of persulfate does not involve a ferric iron (Fe^{III}) reduction mechanism, and therefore, a continual source of Fe^{II} is required. Fe^{II} requires highly reducing conditions to remain in solution such as an acidic pH, so a low pH is required as with conventional Fenton system. The problem with the use of Fe^{II} as an activator is its instability which is eventually oxidized by the persulfate to Fe^{III} that, at a pH above 4, is insoluble. The net reaction is:

$$2Fe^{II} + S_2O_8^{2-} \rightarrow 2Fe^{III} + 2SO_4^{-2}; \; Fe^{III} + 3H_2O \rightarrow Fe(OH)_3 \downarrow + 3H^+ \qquad (2.23)$$

This low pH can be avoided by using chelated Fe^{II} catalyst, dual oxidant system with H_2O_2 and alkaline persulfate which allow the oxidation experiments at circumneutral pH. Chelating the transition metal catalyst provides protection from hydration and subsequent precipitation under the neutral pH conditions that may be found in the field (see Eq. 2.23) (Liang *et al.*,

2004; Nadim *et al*., 2006; Killian *et al*., 2007; Gryzenia *et al*., 2009). Examples of chelating agents include: ethylene diamine tetra acetic acid (EDTA), citrate, polyphosphate, glycolic acid, catechol, nitrotriacetic acid (NTA), Tetrahydroquinine (THQ) and others in this class of materials.

A dual oxidant system utilizing hydrogen peroxide and sodium persulfate has been suggested by Block *et al*. (Block *et al*., 2004) and tested by several others (Cronk & Cartwright, 2006; Thompson *et al.*, 2006; Crimi & Taylor, 2007). It is hypothesized that hydrogen peroxide and persulfate may have several synergistic attributes. First, hydroxyl radicals can initiate persulfate radical formation. Similarly, sulfate radicals can stimulate formation of hydroxyl radicals. Secondly, hydrogen peroxide may react with a significant portion of the more reactive contaminants, allowing the sulfate radicals to destroy the more recalcitrant compounds of concern. Other possible roles of H_2O_2 include exothermic H_2O_2 reactions followed by an increase in temperature and thermal-activation of persulfate and Fenton-driven reduction of Fe^{III} to Fe^{II}, and subsequent Fe^{II}-activation of persulfate. Finally, a combination of peroxide and sulfate radicals may provide a multi-radical attack mechanism, yielding either a higher efficiency in destroying contaminants, or allowing for recalcitrant compounds to be more readily degraded.

Persulfate is known to be highly reactive at low pH (< 3), but it is also highly reactive at pH's greater than 10. It should thus be possible to "activate" persulfate by increasing the pH to high values. Initial laboratory testing indicated the persulfate oxidation of contaminants was not just a matter of high pH, but of the buffering capacity as well.

2.2.2. Mechanism and reactivity

Sulfate radicals, like the HO• radical are highly reactive to degrade organic compounds and either radical may predominate over the other depending on pH conditions. Sulfate radical is more stable than the hydroxyl radical and thus able to move greater distances in the sub-surface. Sulfate radicals exhibit a higher standard reduction potential than hydroxyl radicals at neutral pH and both radicals exhibit similar reduction potentials under acidic conditions (Anipsitakis & Dionysiou, 2004). Both $SO^{\bullet}_4$ and $^{\bullet}OH$ radicals react with organic compounds but the mechanism of the reaction can be quite different. They react with organic compounds mainly by three mechanisms: hydrogen abstraction, hydrogen addition, and electron transfer.

In general, $SO^{\bullet}_4$ is more likely to participate in electron transfer reactions than is $^{\bullet}OH$ which is more likely to participate in hydrogen abstraction or addition reactions (Norman, 1979; Minisci *et al*., 1983; Peyton, 1993). The reaction of $SO^{\bullet}_4$ radicals with aromatic compounds occuring by an electron-transfer mechanism is representing below:

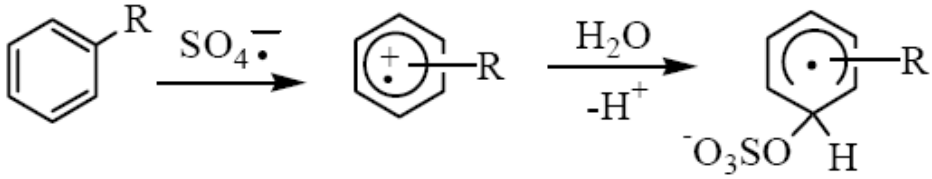

(2.24)

An example is illustrated with carboxylate ions from saturated acids which react with to give carboxy radicals, followed by decarboxylation to generate alkyl radicals (equation 2.25). In contrast, HO• reacts mainly by hydrogen abstraction at the C-H bond (equation 2.26):

$$CH_3CO_2^- + SO^{\bullet}_4 \rightarrow CH_3\,CO_2\bullet + SO_4^{2-} \rightarrow \bullet CH_3 + CO_2 \qquad (2.25)$$

$$CH_3CO_2^- + HO\bullet \rightarrow \bullet CH_2CO_2^- + H_2O \qquad (2.26)$$

The application of persulfate for PAHs and AHs remediation is currently very limited. For these pollutants, persulfate oxidation activated with soluble Fe^{II} (Killian *et al*., 2007; Ferrarese *et al*., 2008; Do *et al*., 2010; Yen *et al*., 2011), chelated Fe^{II} or with heat (Nadim *et al*., 2006) is reported. Reactivity of Fenton's reagent and persulfate oxidation (both catalyzed by soluble Fe^{II}) was compared for the degradation of PAHs (Ferrarese *et al*., 2008) and AHs (Yen *et al*., 2011). Persulfate oxidation can also be used as a mean to predict the PAHs bioavailability in soils (Cuypers *et al*., 2000). Effect of metal oxides on the reactivity of persulfate/Fe^{II} in the remediation of diesel-contaminated soil was investigated at pH=3 (Do *et al*., 2010). The effects of the metal oxides (goethite, hematite, magnetite, and manganese oxide) on the reactivity of persulfate oxidation with and without Fe^{II} indicated that the metal oxides themselves could activate persulfate oxidation, but not as much as metal oxides in combination with Fe^{II} could. Manganese oxide could activate PS as much as Fe^{II} did, and the combination of Fe^{II} and manganese oxide led to the highest degradation of diesel. Iron mineral catalyzed persulfate oxidation of PAHs or AHs at circumneutral pH is still missing in literature.

Part II

RESULTS

Section 1: Formation of mixed Fe^{II}-Fe^{III} oxides: magnetite and green rust

Section 2: Reactivity of magnetite to catalyze chemical oxidation for hydrocarbon remediation in soils

SECTION 1

FORMATION OF MIXED Fe^{II}-Fe^{III} OXIDES: MAGNETITE AND GREEN RUST

Summary

This part of the thesis summarizes the first section of results describing the formation of magnetite or green rust. This section is structured under three articles. The formation of mixed Fe^{II}-Fe^{III} oxides (magnetite or green rust) was investigated by Fe^{II} induced transformation of ferric oxides. Main findings are reported here and readers should refer to the articles for details. Following are the titles of these articles presented in this section:

- Fe^{II} induced mineralogical transformation of ferric oxyhydroxides into magnetite under various experimental conditions
- Formation of green rust *via* mineralogical transformation of ferric oxides (ferrihydrite, goethite and hematite)
- Reactivity of Fe^{III} oxyhydroxides with Fe^{II} in batch and dynamic flow systems

Iron oxides are commonly found in soil environment as ferric (Fe^{III}) oxides like goethite, ferrihydrite, hematite and lepidocrocite with different characteristics such as chemical composition, crystallinity, stability, specific surface area and reactivity. Mixed Fe^{II}-Fe^{III} oxides are more reactive due to the presence of structural Fe^{II} but they are not so common in soil system. Thus studies to generate them from ferric oxides merit investigation.

There are different methods to produce mixed Fe^{II}-Fe^{III} oxides which are detailed in review of literature. But in this study, mixed Fe^{II}-Fe^{III} oxides were synthesized by Fe^{II}-induced mineralogical transformation of ferric oxides. This synthesis method was chosen because there would be a possibility to transform naturally occurring Fe^{III} oxides into Fe^{II} reactive oxides in environmental samples. Moreover, this method would have a possible potential in engineering and environmental application. Indeed, these abiotic transformations could have potential applications in: a) generation of reactive Fe oxides (mixed Fe^{II}-Fe^{III}) from naturally occurring oxides found in contaminated matrices or environmental samples, and b) generation of mixed Fe^{II}-Fe^{III} oxides in column filter systems. Injection of Fe^{II} in column containing Fe^{III} oxide as substrate might be especially advantageous for the waste water treatments or water purification.

In the first step, formation of magnetite or GR was investigated in static batch conditions. Tested ferric oxides include ferrihydrite (F), various kinds of goethite (G1, G2 and G3), lepidocrocite (L) and hematite (H). This is the premier study in which formation of magnetite (Usman ***et al***. 1a, pp: 55-84) or green rust (Usman ***et al***. 1b, pp: 85-100) was quantified versus mineralogy of the ferric oxides and aging time. Also till now, the transformation of thermodynamically stable G and H has not been reported in literature. Stoichiometric quantities of ferric oxides were reacted with hydroxylated Fe^{II} species under static batch conditions to form either GR or magnetite as shown (Fig. 1.1). The initial and final solid products were characterized by X-ray diffraction analysis, transmission electron microscopy and Mössbauer spectroscopy.

Figure 1.1: Transformations of ferrihydrite (F), goethite (G), lepidocrocite (L) and ferrihydrite rich sand (FRS) into magnetite performed in batch slurry systems. Difference in transformation reactivity is prominent for G as shown by its color.

Magnetite formation was quantified from F, G and L at different aging time points (1hour, 1 day, 1 week and 1 month). Ferrihydrite was the most reactive compound to transform into magnetite or green rust. After aging time of one hour, almost 90% of F was transformed into magnetite, as compared to 75% of L and only 4% of G1 (Fig. 1.2). Goethite was the least reactive as 33% was still present after one month. Color of the untransformed G is visible in

Fig. 1.1. The transformation extent into magnetite followed the order: F > L > G1, whereas difference in morphology and particle size of generated magnetite was observed depending on the nature of initial substrates. Smaller magnetite crystals were formed from ferrihydrite while lepidocrocite and goethite yielded magnetite with larger crystals. The green rust formation was quantified from F, G1 and H (Usman ***et al***. 1b, pp: 85-100). Transformation of L into GR was not tested but it is close to ferrihydrite. The formation kinetics of GR was much higher than that observed for magnetite (Fe_3O_4) under similar experimental conditions (Fig. 1.2). This difference of formation kinetics was particularly prominent for G transformations. As after one hour, complete transformation of F into GR was achieved while about half of G or H was transformed although G or H are known for their higher thermodynamic stability. The order of reactivity to transform into GR was found as F > G > H. Higher formation kinetics of GR than magnetite would allow its rapid formation in environment but it is less stable than magnetite.

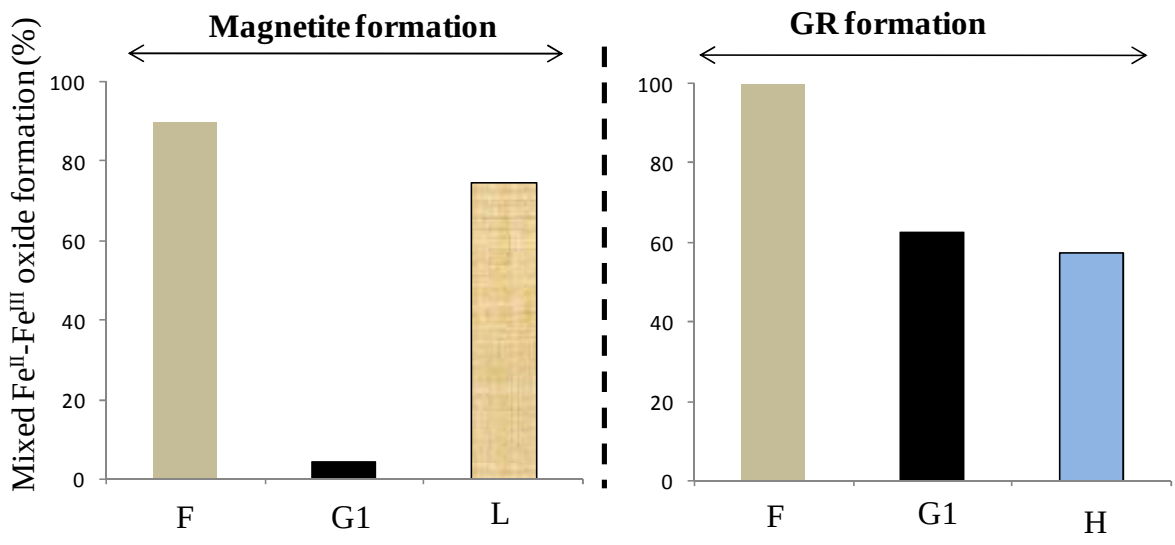

Figure 1.2: Formation extent of magnetite or GR after aging time of one hour from ferrihydrite (■), goethite (■), lepidocrocite (■) and hematite (■). It is represented in % and based on the measurements by Mössbauer spectroscopy. (* Lepidocrocite and hematite are transformed only into magnetite or GR respectively.)

The mineralogical transformations of lepidocrocite into magnetite were also investigated *via* biotic pathway during one month. Stoichiometry of resulting magnetite product was compared with that of the magnetite formed during abiotic Fe^{II}-induced transformations. Our paper

describing these results (Zegeye ***et al.***, 2011) is presented in annexes (Annex 2). After one day of incubation, the departure from stoichiometry, δ, of the bio-generated magnetite was very low (δ ~ 0.025) and rapidly reached values close to zero (Fig. 3 in (Zegeye ***et al.***, 2011)). Such low values of δ were not obtained for magnetite synthesized via abiotic mineralogical transformations. As Fe^{II}/ Fe^{III} ratio is relatively high in this biotic magnetite, its use in reduction of contaminants would be interesting. However, biogenic magnetite contains bacteria and polymers which could influence decontamination reaction. Finally, reactivity of biotic GR and magnetite merit to be explored in future.

Also the transformation extents of three kinds of lab-synthesized goethite (G1, G2 and G3) into magnetite were compared (Usman ***et al***. 1a). These three goethites have different crystal structures, morphologies and surface properties. The reactivity of goethites to transform into magnetite was found as: G1 > G2 > G3 although a reverse order was found for their surface area (G3> G2> G1). Additional experiments showed that the sorption capacity determined at low Fe^{II} concentration and pH 6.6, follows the order G1 > G2 > G3, whereas the first order kinetic rate constant of the reductive dissolution was found: G1 ($1x10^{-3}$ h^{-1}) > G3 ($6x10^{-4}$ h^{-1}) ~ G2 ($5x10^{-4}$ h^{-1}). These experiments helped us to discuss mechanism of transformations. In general, the secondary mineralization pathways can be distinguished through two main mechanisms: (i) solid-state transformation (also called topotactic) and (ii) dissolution/re-precipitation (or reconstructive/re-crystallization). The high Fe^{II}-sorption capacity as well as the highest initial reduction dissolution rate of G1 may explain its higher reactivity, emphasizing the importance of the crystal-faces specific reactivity. The coordination of Fe^{II} at the ferric oxide surface via the formation of bidentate or tridentate complex is a prerequisite to electron transfer, a key step to initiate reductive dissolution reaction or solid-state transformation process. The initiation of transformation reaction by Fe^{II} adsorption to singly coordinated sites through the formation of inner-sphere surface complexes seems to be the most plausible hypothesis. Microscopic level characterizations such as crystal structure and surface site density are therefore needed to describe the transformation extent of iron oxides.

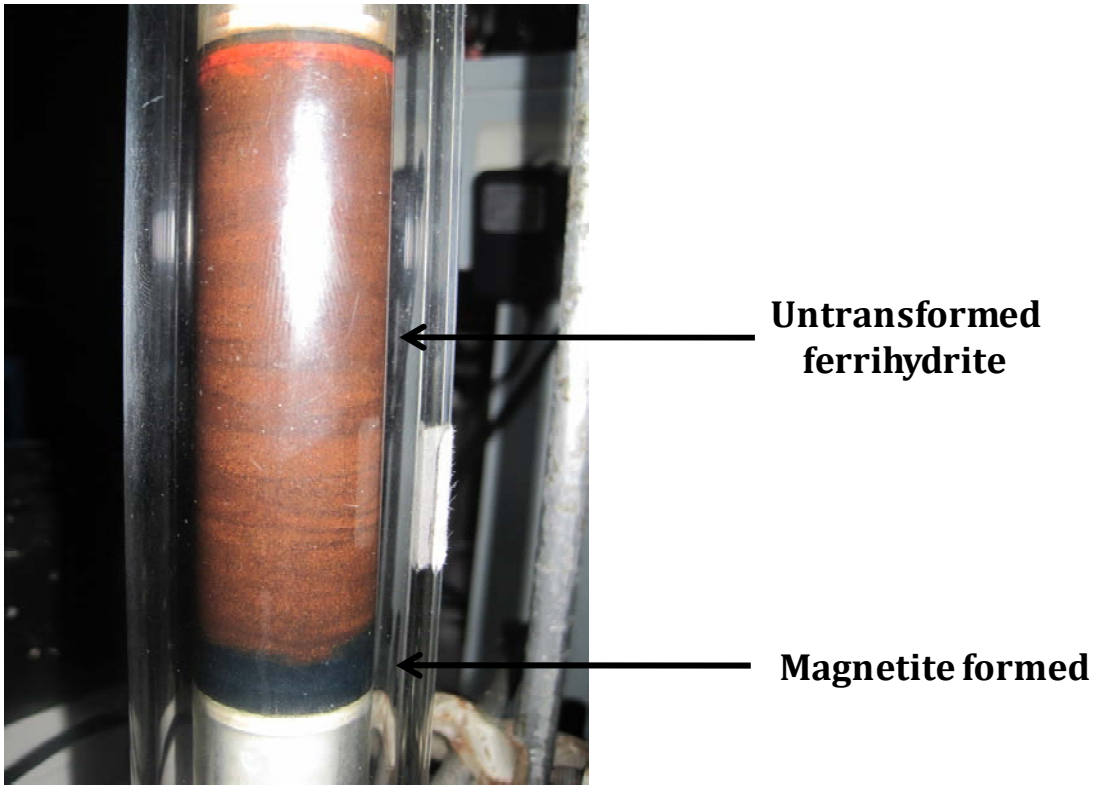

Figure 1.3: Column experiment showing the transformations of ferrihydrite rich sand (FRS) into magnetite

Fe^{II} induced transformations were also investigated in various matrices like ferrihydrite rich sand (FRS) and pristine soil under static batch and flow through conditions (Usman ***et al***. 1c, pp: 101-108). Ferrihydrite in FRS was completely transformed into magnetite or GR under static batch conditions. However, partial transformation of ferrihydrite was achieved in column experiments as represented by color gradient (Fig. 1.3). Only a small amount of mixed Fe^{II}-Fe^{III} oxide was formed while large amount of F was still present untransformed.

The abiotic synthesis of magnetite or GR from ferric oxides seems difficult because injection of $Fe(OH)_2$ (colloidal suspension) in flow solutions affects the hydraulic properties of the column system. However biotic synthesis of GR from bio-reduction of Fe^{III} oxides in column seems more appropriate. It was shown in the preliminary results of PhD thesis of Ms A.S. Sergent of our lab (Co-directed by Pr. K. Hanna and Dr. F. Jorand), where the production of Fe^{II}-Fe^{III} oxides such as GR and magnetite was achieved under flow through conditions.

Fe^{II} induced mineralogical transformation of ferric oxyhydroxides into magnetite under various experimental conditions

M. Usman [a, b], K. Hanna [a], M. Abdelmoula [a], P. Faure [b], C. Ruby [a].

[a] Laboratoire de Chimie Physique et Microbiologie pour l'Environnement, LCPME, UMR 7564, Institut Jean Barriol, CNRS-Nancy Université, 405 rue de Vandoeuvre, 54600, Villers-lès-Nancy, France.

[b] Géologie et Gestion des Ressources minérales et énergétiques, G2R, UMR 7566, 54506, Vandœuvre-lès-Nancy, France.

Abstract

The Fe^{II}-induced mineralogical transformations of Fe^{III} oxides into magnetite were quantified against mineralogy of the ferric oxyhydroxides and aging time. The initial and final solid products were characterized by X-ray diffraction analysis, transmission electron microscopy and Mössbauer spectroscopy. All these results consistently show that the ferrihydrite was the most reactive compound to transform into magnetite. After one hour of reaction, almost 90% of ferrihydrite (F) was transformed into magnetite, as compared to 75% of lepidocrocite (L) and only 4% of goethite (G1). Goethite was the least reactive as 33% was still present after one month. The transformation extent into magnetite followed the order: F > L > G1, whereas difference in morphology and particle size of generated magnetite was observed depending on the nature of initial substrates. Smaller magnetite crystals were formed from ferrihydrite while lepidocrocite and goethite yield magnetite with larger crystals. The transformation extents of three kinds of lab-synthesized goethite (G1, G2 and G3) having different crystal structures, morphologies and surface properties were then compared. The reactivity of three kinds of goethite to transform into magnetite was found as: G1 > G2 > G3. Additional experiments showed that the sorption capacity determined at low Fe^{II} concentration and pH 6.6, follows the order G1 > G2 > G3, whereas the first order kinetic rate constant of the reductive dissolution was found: G1 ($1x10^{-3}$ h^{-1}) > G3 ($6x10^{-4}$ h^{-1}) ~ G2 ($5x10^{-4}$ h^{-1}). The high Fe(II)-sorption capacity as well as the highest initial reduction dissolution rate of G1 may explain its higher reactivity, emphasizing the importance of the crystal-faces specific reactivity. The coordination of Fe(II) at the ferric oxide surface via the formation of bidentate or tridentate complex is a prerequisite to electron transfer, a key step to initiate reductive dissolution reaction or solid-state transformation process. The presence of strong chelating ligand (e.g. phosphate) is expected to hinder the adsorption sites and therefore can affect both topotactic and reconstructive processes. The initiation of transformation reaction by Fe (II) adsorption to singly coordinated sites through the formation of inner-sphere surface complexes seems to be the most plausible hypothesis. Microscopic level characterizations such as crystal structure and surface site density are therefore needed to describe the transformation extent of iron oxides.

1. Introduction

Iron oxyhydroxides are abundant in the environment and influence the biogeochemical cycling and availability of elements. In soils and sediments, iron oxides and oxyhydroxides are commonly found as ferric minerals like goethite, ferrihydrite, hematite and lepidocrocite with different characteristics such as crystallinity, stability, specific surface area and reactivity (Stumm & Sulzberger, 1992; Cornell & Schwertmann, 1996). Due to their high specific surface area, iron oxyhydroxides act as important sorbents for dissolved species. They strongly influence the transport and availability of various nutrients (e.g., C, N, and P) (Sulzberger *et al.*, 1989; Stumm & Sulzberger, 1992; Cornell & Schwertmann, 1996) and the mobility of organic and inorganic contaminants (Elsner *et al.*, 2003; Hanna *et al.*, 2010b). In reduced soil zone, they exist as mixed Fe^{II}-Fe^{III} compounds such as magnetite (Fe_3O_4) or fougerite, the mineral counterpart of the Fe^{II}-Fe^{III} green rust (Trolard *et al.*, 1997; Abdelmoula *et al.*, 1998). Due to the structural Fe^{II}, these mixed valence oxides are very reactive and are involved in the reductive transformations of inorganic contaminants (Fredrickson *et al.*, 1998; Gorski & Scherer, 2010) as well as the organic pollutants (Elsner *et al.*, 2003; Tobler *et al.*, 2007; Gorski & Scherer, 2009; Kone *et al.*, 2009). Fe^{II} species are one of the most abundant reductants typically present in aquatic and terrestrial environments under suboxic and anoxic conditions (Postma, 1993; Rügge *et al.*, 1998). Because of the presence of oxygen and prevailing pH conditions in many natural environments, the predominant form of iron is trapped in solid ferric (Fe^{III}) oxyhydroxides while Fe^{II} species move much more rapidly because they are more easily dissolved. As mixed Fe^{II}-Fe^{III} minerals are more reactive but not so common in soil system, studies to generate them from ferric oxyhydroxides merit investigation.

The interactions of iron oxyhydroxides with aqueous Fe^{II} induce their structural modification and bulk phase transformation which depend upon molar ratio $x(Fe^{II}) = Fe^{II}/[Fe^{II} + Fe^{III}]$ (Tamaura *et al.*, 1983; Tronc *et al.*, 1992; Hansel *et al.*, 2005), pH (Jeon *et al.*, 2003), anionic media (Liu *et al.*, 2008), OH^-/Fe ratio (Ishikawa *et al.*, 1998; Ruby *et al.*, 2003) and structure of initial iron oxyhydroxide substrate (Pedersen *et al.*, 2005). The interaction of iron oxides with aqueous Fe^{II} may lead to their transformations into ferric and/or mixed Fe^{II}-Fe^{III} phases. In the presence of low concentration of Fe^{II}, ferrihydrite was transformed either into goethite

(Tronc *et al.*, 1992; Jeon *et al.*, 2003; Yee *et al.*, 2006; Liu *et al.*, 2008), lepidocrocite (Pedersen *et al.*, 2005; Liu *et al.*, 2008) or hematite (Liu *et al.*, 2009). At high Fe^{II} amount, mixed Fe^{II}- Fe^{III} minerals such as magnetite (Tamaura *et al.*, 1983; Jolivet *et al.*, 1992; Tronc *et al.*, 1992) or green rust (Ruby *et al.*, 2003) were formed from different ferric oxyhydroxides.

Although the transformation of ferric oxides into magnetite has been widely investigated, quantification of magnetite formation *vs.* time has not been performed yet. Also the Fe^{II} induced transformation of goethite into magnetite has seldomly been reported. In this work, experiments were conducted on three different iron oxyhydroxides including ferrihydrite, goethite and lepidocrocite, and the transformation extent into magnetite was quantified against aging time (1 hour, 1 day, 1 week and 1 month). The solid characterization of the initial and final products was done by X-ray diffraction (XRD), Mössbauer spectrometry and transmission electron microscopy (TEM).

On the other hand, little is known about the relationships between crystalline/surface properties of goethite and its ability to be transformed into mixed-valence oxides. In the present study, the transformation extent of three kinds of goethite (G1, G2 and G3) having different crystal structures, morphologies and surface properties was compared. The reductive dissolution and the Fe(II) sorption capacity of the three goethites were also performed. To our best knowledge, there are no previous reports of the sorption of Fe(II) onto different kinds of goethite and the impact of the crystal-faces specific reactivity on interfacial electron transfer process. The transformation dependency of the surface characteristics and the hypothesis of the main mechanism involving in the secondary mineralization process were also discussed.

2. Materials and methods

2.1. Chemicals

Ferric chloride hexahydrate ($FeCl_3.6H_2O$), ferrous sulfate heptahydrate ($FeSO_4.\ 7H_2O$), ferrous chloride tetrahydrate ($FeCl_2.\ 4H_2O$), sodium phosphate ($Na_3PO_4.12H_2O$) and 2-hydroxybenzoic acid (salicylic acid) with a purity greater than 99% were purchased from Sigma Aldrich.

2.2. Sample preparation

2.2.1. Initial ferric oxyhydroxides substrates

Experiments were conducted with three synthetic iron oxyhydroxides: 2-line ferrihydrite (F), lepidocrocite (γ -FeOOH) (L) and goethite (α-FeOOH) (G1). The 2-line ferrihydrite (F) was synthesized according to the method of Schwertmann and Cornell (Schwertmann & Cornell, 2000). It was prepared by neutralizing a 0.2 M ferric chloride solution with 1 M NaOH to a pH of around 7.5. The lepidocrocite sample (γ-FeOOH) was synthesized by vigorous air oxidation of the (0.228 M $FeCl_2.4H_2O$ + 0.4 M NaOH) aqueous mixture at neutral pH. All the Fe^{III} precipitates were washed several times to remove electrolytes, centrifuged and then dried.

Three different types of goethite previously synthesized in the context of earlier studies by our research group (Gaboriaud & Ehrhardt, 2003; Prélot *et al.*, 2003) were used. These goethites are referred as G1, G2 and G3 and their main characteristics are explained in the section 3.1.

2.2.2. Batch experiments

The mineralogical transformations of synthetic ferric oxyhydroxides were examined in batch experiments at room temperature (20 ± 1°C). Firstly, a suspension of Fe^{III} oxyhydroxide was prepared (0.267 M as Fe^{III} molar concentration) and purged for one hour with filter-sterilized N_2 (99.99%) in order to ensure the evacuation of dissolved oxygen which is known to rapidly oxidize Fe^{II} in the presence of oxides at circumneutral pH (Tamura *et al.*, 1980). The reaction was started by adding of $FeSO_4.7H_2O$ with Fe^{II} molar concentration corresponding to 0.133 M. An appropriate amount of NaOH (1M) was then added to the mixture (Fe^{II}/Fe^{III}-oxyhydroxide) to provide the ratio n (OH^-) / n (Fe^{III}) = 1 where n represents the number of moles. The total iron concentration was 0.4 M. Stoichiometric magnetite (Fe^{III} (Fe^{II} Fe^{III}) O_4) contains the Fe^{II}: Fe^{III} ratio of 1:2. The transformation into magnetite was achieved through the following reaction:

$$2Fe^{III}OOH + Fe^{II} + 2OH^- \Rightarrow Fe^{II}Fe^{III}{}_2O_4 + 2H_2O \quad (1)$$

The suspensions are vigorously stirred for 1 hour, and then aged without stirring at room temperature for 1 hour, 1 day and 1 month for F and L, and 1 hour, 1 day, 1 week and 1 month for G1.

All batch series were conducted in glove box, an anoxic (N_2:H_2= 98:2) chamber. At specified aging time, the corresponding batch was withdrawn from the series, centrifuged and the solid was dried in glove box for further analysis. The dissolved and total Fe(II) concentrations were measured at each time point (Table 1) by phenanthroline method and ICP/AES, respectively. The pH of the suspensions was also measured at each time point and reported in the Table 1.

Transformation of goethite (G1) was also studied in the presence of salicylate (SA, 1 mM) or phosphate (P, 1mM), which were chosen as model compounds of naturally occurring organic and inorganic ligands, respectively. The initial pH of these batch reactors was adjusted at 7 ± 0.2. After one hour of stirring, aliquots of solutions of SA and P were withdrawn and analyzed by UV-visible spectroscopy (CARY 5G UV-Vis-NIR Spectrophotometer) and ion chromatography (Metrohm, IC) respectively to determine the sorbed amount. Then the addition of Fe^{II} and NaOH was done following the same procedure previously described. After a specified aging time, the suspensions were filtered and the solid was dried and then analyzed.

The sorption of Fe(II) on three goethites was carried out *vs* Fe(II) concentration (0-5 mM) at pH 6.6 ± 0.1. The residual Fe(II) concentration was measured by 1-phenanthroline method, after 30 min of equilibration time (Liu *et al.*, 2001). Before analysis, the suspensions were filtered through 0.22 µm polyvinylidene fluoride (PVDF) syringe filters (Millipore) that were shown not to sorb or oxidize ferrous ion.

The ascorbic acid promoted reductive dissolution of goethites at pH 3 was also determined according to the method described elsewhere (Larsen & Postma, 2001). The Fe^{II} formation was monitored against time (0-48h), and the generated Fe(II) concentration was measured by 1-phenanthroline method. To compare the intrinsic reactivity for all goethites, 50 m^2/L was used as solid concentration for both sorption and reductive dissolution experiments, representing the amount of exposed surface area per volume unit. All experiments were conducted in triplicates and in glove box (N_2:H_2= 98:2) under O_2 free atmosphere.

2.2.3. Sample characterization

In order to identify the crystal structure of minerals, solid samples were analyzed by X-ray powder diffraction (XRD). The XRD data were collected with a D8 Bruker diffractometer, equipped with a monochromator and a position-sensitive detector. The X-ray source was a Co anode (= 0.179 nm). The diffractograms were recorded in the 3–64° 2θ range, with a 0.0359° step size and a collection of 3 s per point.

Solid samples were also analyzed by Mössbauer spectroscopy. Reflection Mössbauer spectroscopy using the miniaturized Mössbauer spectrometer MIMOS II (Klingelhöfer ***et al.***, 1996) has been employed to determine the oxidation state of iron and the iron mineralogy of the samples. The filtered samples were inserted into a ~ 3 cm^2 holder specially designed to perform Mössbauer reflexion analyses at room temperature. Reemitted backscattered γ-rays (14.4 keV) were selected by four Si-PIN-diodes detectors. Centre shifts *CS* were reported with respect to that of -Fe at room temperature. Mössbauer spectra were computer-fitted with either a sum of Lorentzian shape lines or a Voigt profile analyses (Rancourt & Ping, 1991).

Transmission electron microscopy (TEM) observations were carried out with a Philips CM20 TEM (200 kV) coupled with an EDX energy dispersive X-ray spectrometer. The solid powder was re-suspended in 2 mL ethanol under ultrasonication, and a drop of suspension was evaporated on a carbon-coated copper grid which was placed on filter paper.

The specific surface area of synthesized solids was determined by multipoint N_2-BET analysis using a Coulter (SA 3100) surface area analyzer and was found to be 190, 59 and 38 m^2/g for F, L and G1 respectively.

3. Results

3.1. Characterization of initial ferric oxyhydroxides

XRD diffractogram of the synthesized Fe^{III} minerals confirmed the identity of the expected Fe^{III} oxyhydroxides, i.e. ferrihydrite, goethite and lepidocrocite (Fig. 1a). The main features of the ferrihydrite XRD peaks represented by arrows correspond to 2-line ferrihydrite (Schwertmann & Cornell, 2000). The d-space values of the main peaks correspond to the more intense lines of goethite or lepidocrocite (Fig. 1a), in accordance with literature (Schwertmann & Cornell, 2000). The Mössbauer spectra were also recorded for all ferric substrates and confirm the features typical of ferrihydrite, goethite and lepidocrocite (Fig. 1b).

(Figure 1a)

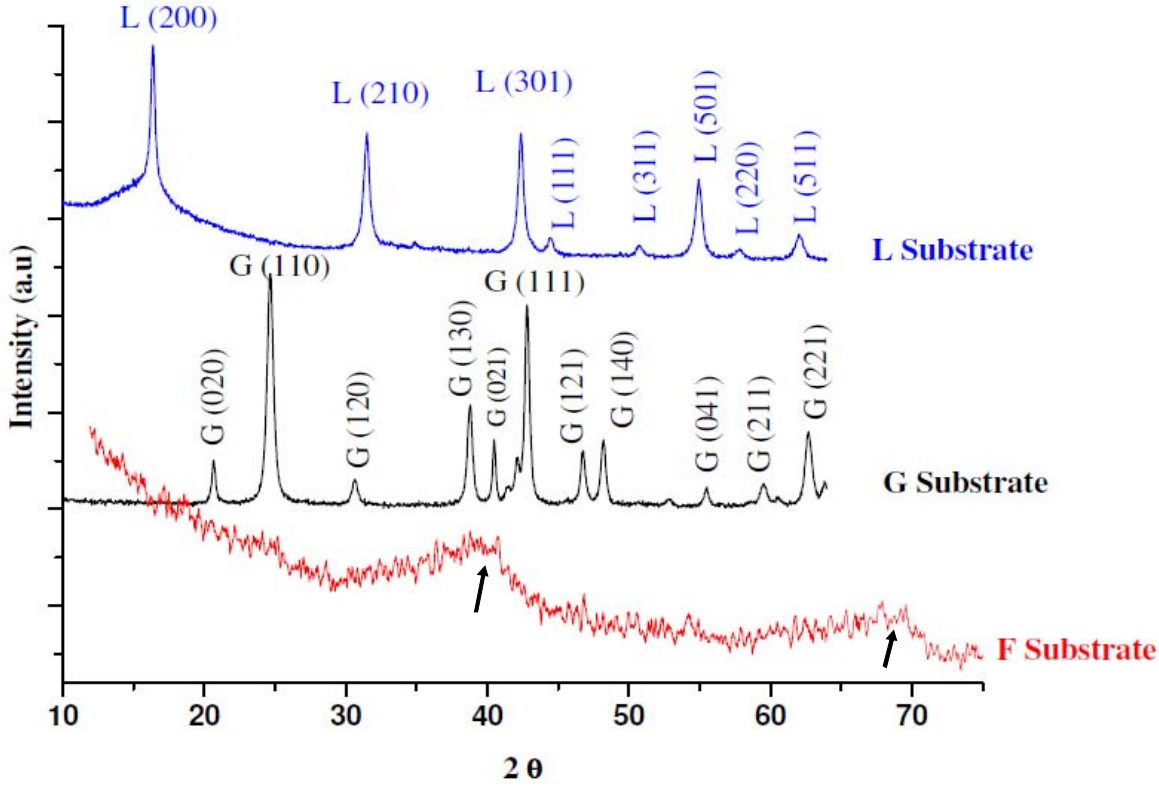

Fig. 1b)

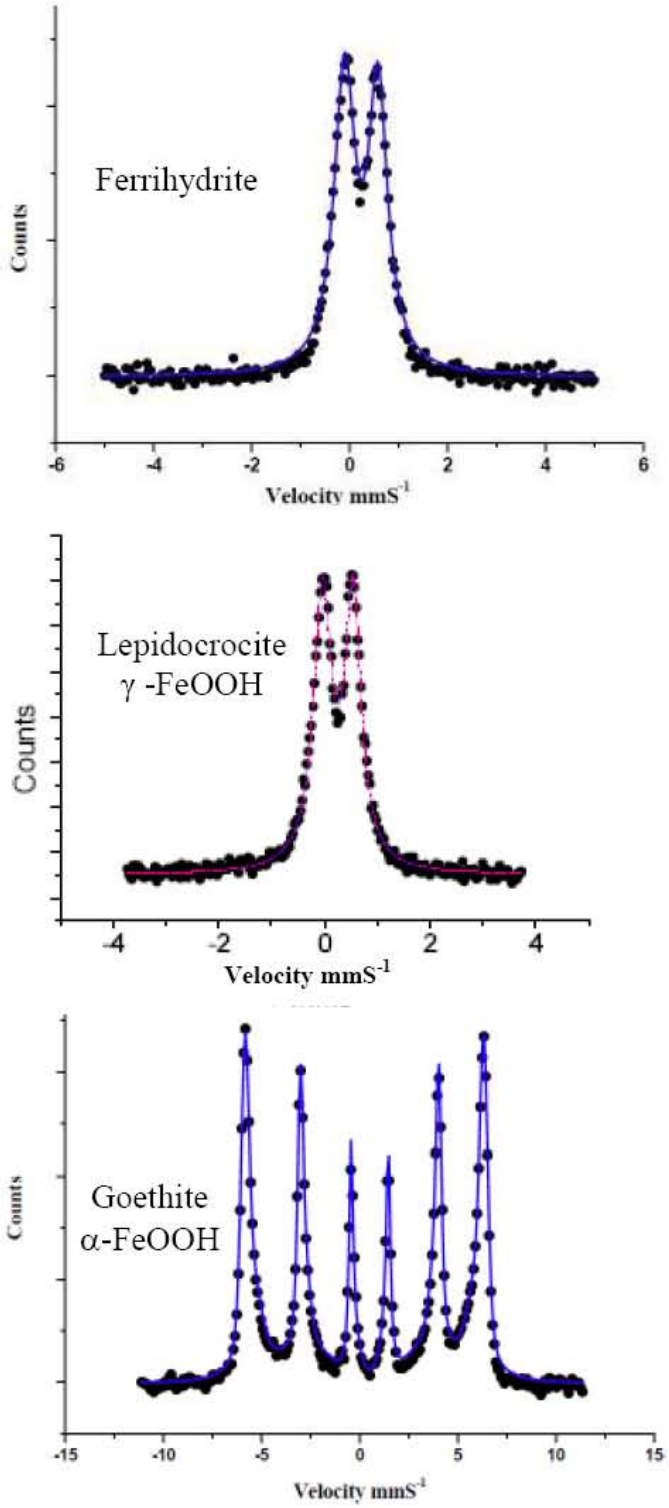

Figure 1: **XRD diffractograms (a) and Mössbauer spectra (b) of original ferric substrates, ferrihydrite (F), goethite (G1) and lepidocrocite (L)**

Table 1: Total and soluble Fe(II) concentration, pH in the oxide suspensions at specified aging times during transformation process.

Solid	Ferrihydrite (F)			Lepidocrocite (L)			Goethite (G1)		
	Total Fe^{II} (± 2mM)	Soluble Fe^{II} (± 0.1 mM)	pH ± 0.1	Total Fe^{II} (± 2mM)	Soluble Fe^{II} (± 0.1 mM)	pH ± 0.1	Total Fe^{II} (± 2mM)	Soluble Fe^{II} (± 0.1 mM)	pH ± 0.1
T_0	50	50	9.7	50	50	9.6	50	50	9.7
1 hour	49	0.5	6.8	47	0.4	7.8	49	0.5	8.4
1 day	48	1.1	6.0	48	1.2	6.5	48	0.4	8.3
1 month	49	7.2	5.5	49	5.7	5.6	47	0.3	7.5

The morphology of the particles produced is available to clarify the transformation mechanism of ferric oxyhydroxides into magnetite. Figure 2 displays the TEM pictures of initial ferric oxyhydroxides, where ferrihydrite particles are very small and heavily aggregated (Fig. 2a). These poorly defined morphologies (or poorly crystallized structures) make difficult identification of the different crystal planes. The lepidocrocite crystals (Fig. 2a) are lath-like and elongated with gradually tapering ends like spindles. The length of the crystals is almost homogeneous and varies between 200-300 nm. Unlike goethite, the different crystal faces of lepidocrocite are not well known.

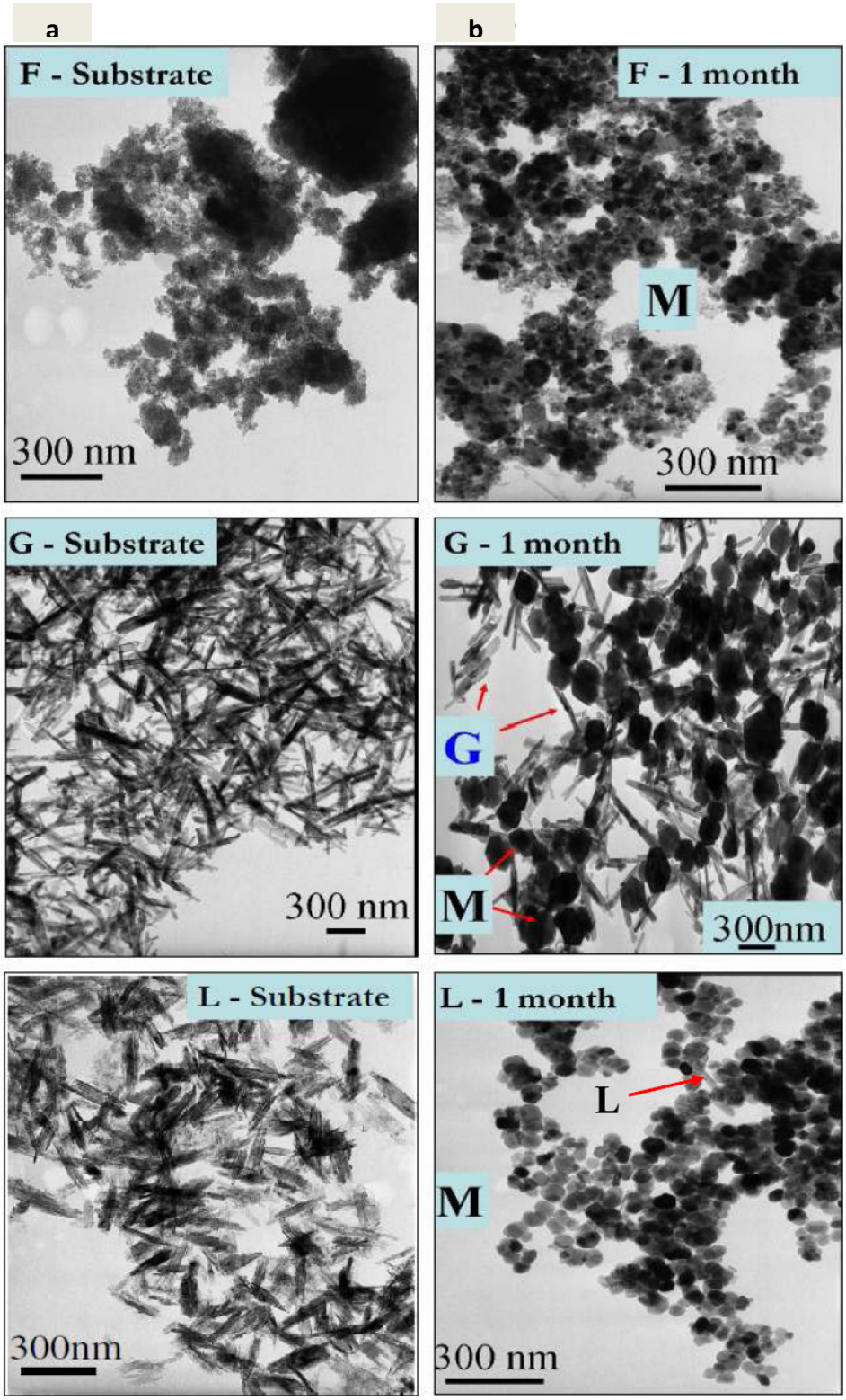

Figure 2: Bright field TEM images showing (a) initial ferric substrates (ferrihydrite (F), goethite (G1) & lepidocrocite (L)) and (b) after their transformations into magnetite (M) at one month of aging time.

Crystal needle shapes were identified for goethite G1 (Fig. 2a). These crystals vary between 300 and 400 nm in length. Two additional goethites are also used in this study. TEM and AFM images showed typical acicular shapes for all goethites samples. As all three goethites were synthesized in the context of the previous studies (Gaboriaud & Ehrhardt, 2003; Prélot *et al.*, 2003), their characterization and modeling parameters will be used to discuss the reactivity of goethites against Fe^{II}. The main characteristics of three types of goethite G1, G2, G3 are reported in Table 2. The AFM images demonstrated that (101) and/or (001) faces are always dominant on crystallized goethites. The crystal faces (101) and the (001) were identified on the single goethite crystals of G2 and G3, while the main crystallographic faces of G1 particles were found as (001), (101) and (121) or (021) (Gaboriaud & Ehrhardt, 2003; Prélot *et al.*, 2003).

Table 2: Some main characteristics of three kinds of goethites (G1, G2 and G3) (Gaboriaud & Ehrhardt, 2003; Prélot *et al.*, 2003).

Solid	BET area (m^2/g)	PZC	Site* 1 density (sites/nm^2)
G1	38	9.0	3.59
G2	49	9.0	3.07
G3	95	9.1	3.03

*: Density of singly coordinated site

The goethite surface displays singly, doubly, and triply coordinated oxygens, denoted as $FeO^{3/2-}$; Fe_2O^{1-} ; $Fe_3O^{1/2-}$, respectively (Hiemstra *et al.*, 1996; Venema *et al.*, 1998). The doubly coordinated sites were not thought to be reactive in our pH range. A simplification was made by adopting the "1pK approximation" approach (Hiemstra & Van Riemsdijk, 1996), whereby the proton affinity constants of $FeOH^{1/2-}$ and $Fe_3O^{1/2-}$ are set to the point of zero charge (pzc) (Table 2).

Furthermore, only singly coordinated sites are considered to participate in surface complexation reactions of iron ion with mineral oxide. Doubly and triply coordinated sites are expected to play a minor role in surface complexation reactions. We attempt to determine the density of the singly coordinated surface groups for the three tested goethites by using the

data of Gaboriaud and Ehrahrdt (Hiemstra & Van Riemsdijk, 1996; Barrón *et al.*, 1997), and Prélot et al. (Hiemstra & Van Riemsdijk, 1996; Barrón *et al.*, 1997). A maximum of 3.0 sites/nm^2 of the $FeOH^{-1/2}$ site on the (110) plane, 3.1 sites/nm^2 on the (001) plane, and 8.2 sites /nm^2 on the 121/021 faces was proposed. The overall site density of the singly coordinated surface groups of goethite can be therefore calculated assuming (3.0 sites/nm^2 x f{110/101} + 3.1 sites/nm^2 x f{001} + 8.2 sites /nm^2 x f{121/021}). According to the spectroscopic investigations, the fraction of each crystal plan can be estimated as f {101} = 20%, f {001} = 70% and f {021} = 10% for G1; f {101} = 30% and f {001} = 70% for G2; f {101} = 70% and f {001} = 30% for G3 (Gaboriaud & Ehrhardt, 2003; Prélot *et al.*, 2003). This leads to an estimation of the maximum density of singly coordinated sites per surface unit (Table 2). On the other hand, Boily et al. (Boily *et al.*, 2000) suggested that surface roughness and edge surface sites could enhance surface site densities.

3.2. Transformation of ferrihydrite, goethite and lepidocrocite into magnetite

In this part, the transformation extent of ferric oxyhydroxides was monitored at three aging times. The XRD diffractograms of ferric substrates after specified aging times of 1 hour, 1 day and 1 month are shown in Figure 3. Figure 3a indicates the F-to-M transformation in which six diffractogram peaks were assigned to magnetite. The d-space values of these peaks were 4.85, 2.96, 2.53, 2.42, 2.09 and 1.71 Å which correspond to the more intense lines 111, 220, 311, 222, 400 and 422, respectively of magnetite (Schwertmann & Cornell, 2000). F peaks were no more visible after one hour of aging. Thus XRD diffractograms show that ferrihydrite was transformed completely into magnetite within the detection limit. In contrast, the peaks corresponding to L and G are clearly identified in the XRD diffractograms together with magnetite peaks (Fig. 3). The intensity of the most intense magnetite peaks increased prominently with an increase in aging time. Presence of untransformed lepidocrocite was evidenced by the three peaks corresponding to lepidocrocite after aging time of one hour (Fig. 3b). These L peaks disappeared after one month of reaction. For G1, the intensity of all peaks especially that of main peaks i.e. 110, 111 and 130 decreased against aging time, while a progressive increase in main magnetite peaks was noted. After one month of reaction, goethite peaks were still present in the diffractogram (Fig. 3c) showing that transformation of goethite into magnetite was not fully accomplished. From XRD analyses, the effect of nature of initial

ferric substrates can be demonstrated by comparing the appearance of peaks corresponding to magnetite which follows the order: F > L > G.

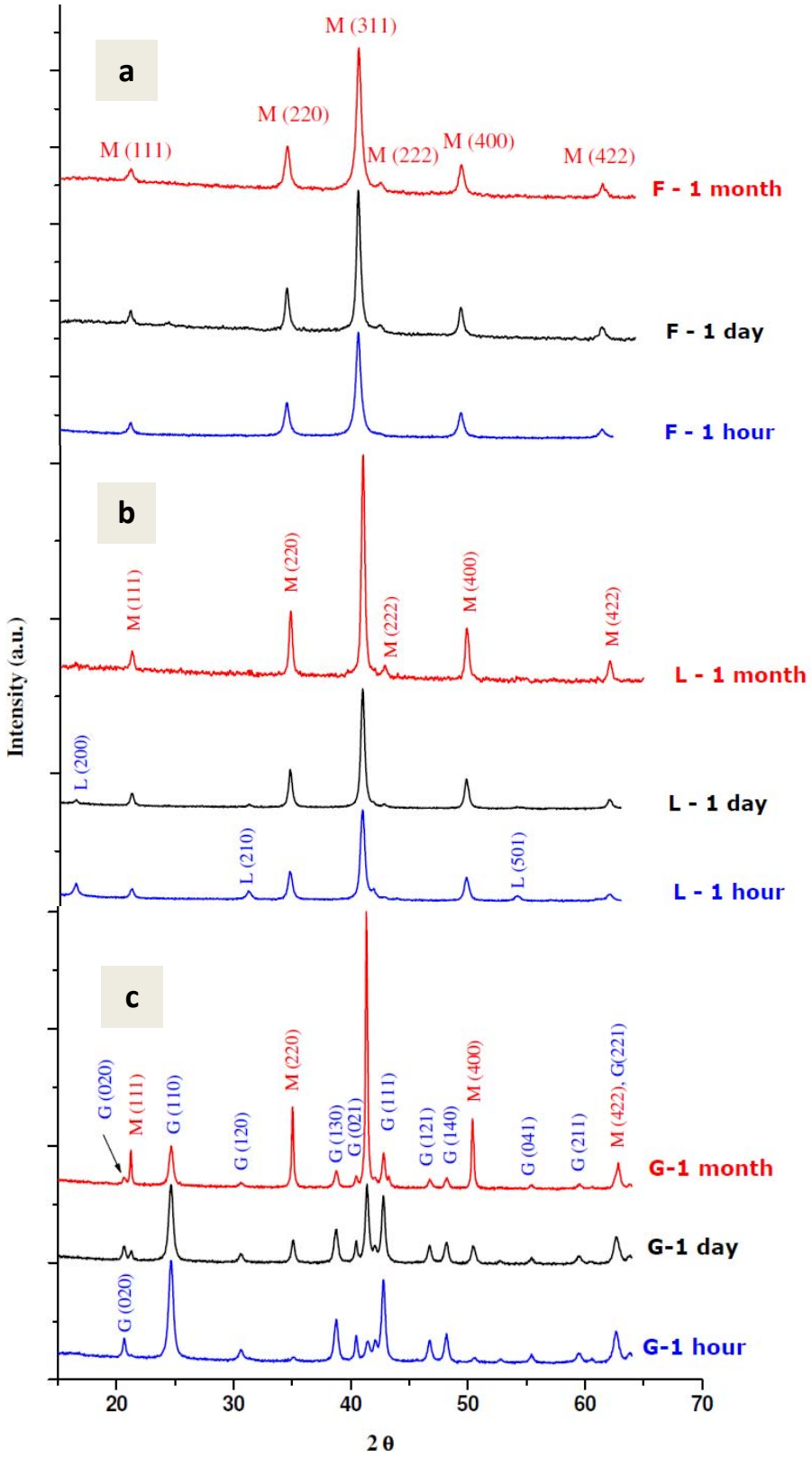

Figure 3: XRD diffractograms of the transformation products of (a) ferrihydrite-F, (b) lepidocrocite-L and (c) goethite- G1, obtained after aging time of 1 hour, 1 day and 1 month.

TEM images for magnetite (Fig. 2b, F-1 month) generated from ferrihydrite indicate that magnetite particles are not uniform in terms of size or shape. On the other hand, the particles of magnetite originating from lepidocrocite and goethite substrates are relatively large particularly when goethite is used as a substrate. The shape of magnetite particles are between hexagonal to octahedral from both goethite and lepidocrocite substrates (Fig. 2b, G-1month, L-1month). TEM images show that there is still large amount of goethite which is not transformed into magnetite, while traces of lepidocrocite are also visible (Fig 2b). Hence difference in morphology and particle size of generated magnetite was observed depending on the nature of initial substrates.

To quantify the transformation extent, Mössbauer analysis of generated magnetite was investigated. Magnetite (Fe_3O_4) at room temperature (RT) has a spinel structure whose Mössbauer spectrum at RT is constituted by a superposition of two subspectra associated with the distribution of the iron in the octahedral (B) and tetrahedral (A) sites represented by S_B and S_A respectively. The two valence states on octahedral sites are not distinguishable due to a fast electron hopping between Fe^{II} and Fe^{III} in octahedral sites. Thus, the ideal magnetite has only two distinct sextets at RT (Murad & Johnston, 1984).

The different Mössbauer spectra (Fig. 4) are presented here along with the corresponding hyperfine parameters (Table 3) to show the transformation of ferric oxyhydroxides into magnetite at each time point. It was easy to distinguish the appearance of magnetite sextets (S) produced from ferrihydrite and lepidocrocite substrates than from goethite as both F and L are characterized by doublets (D) in Mössbauer spectra at RT. In contrast, goethite is characterized by sextets like magnetite. In this case, distinction by fitting the spectrum and calculations are required to determine accurately the proportions of goethite and magnetite.

The F-M transformations are shown in Fig. 4. After one hour of reaction (Fig. 4a), a doublet is present in the centre of spectrum which reveals the presence of untransformed ferrihydrite, along with magnetic sextets corresponding to a spinel (magnetite). The magnetic components were very broad and it was necessary to fit the spectrum with a distribution of sextets. The relative abundance of doublet decreases with the increase in time (Fig. 4a). After one hour, the sextets are broad which probably correspond to the stage of crystal growth of the poorly

crystallized magnetite. These sextets become more resolved and narrow as the time proceeds from one hour to one month, which could be linked to the increase in the crystallinity of magnetite. Therefore, only two sextets S_A and S_B were used to fit the spectrum. Same trend was observed in case of lepidocrocite or goethite (Fig. 4b, 4c), except that the transformation extent was relatively low. The sextets corresponding to magnetite are also more resolved and narrow as compared to magnetite from ferrihydrite.

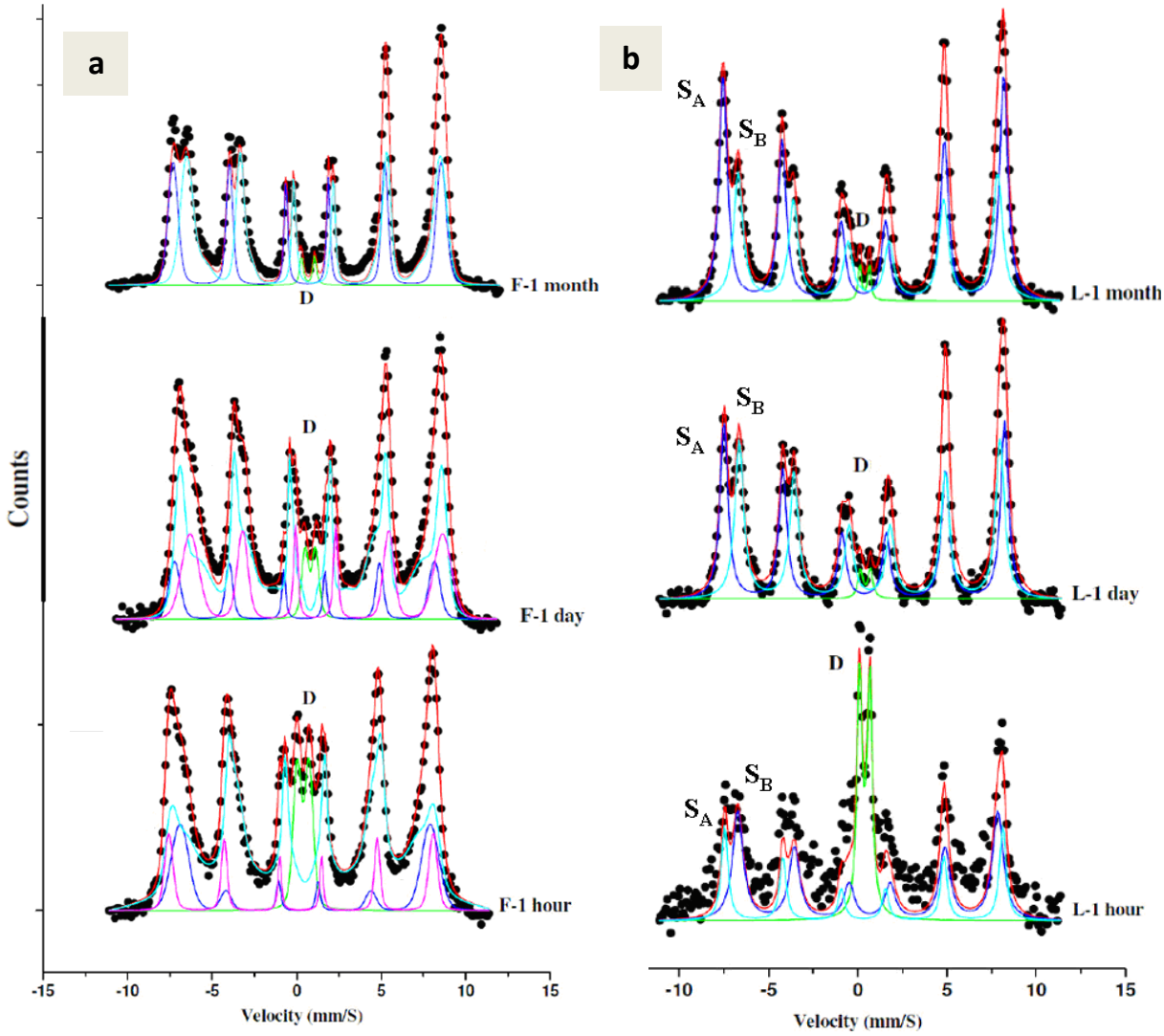

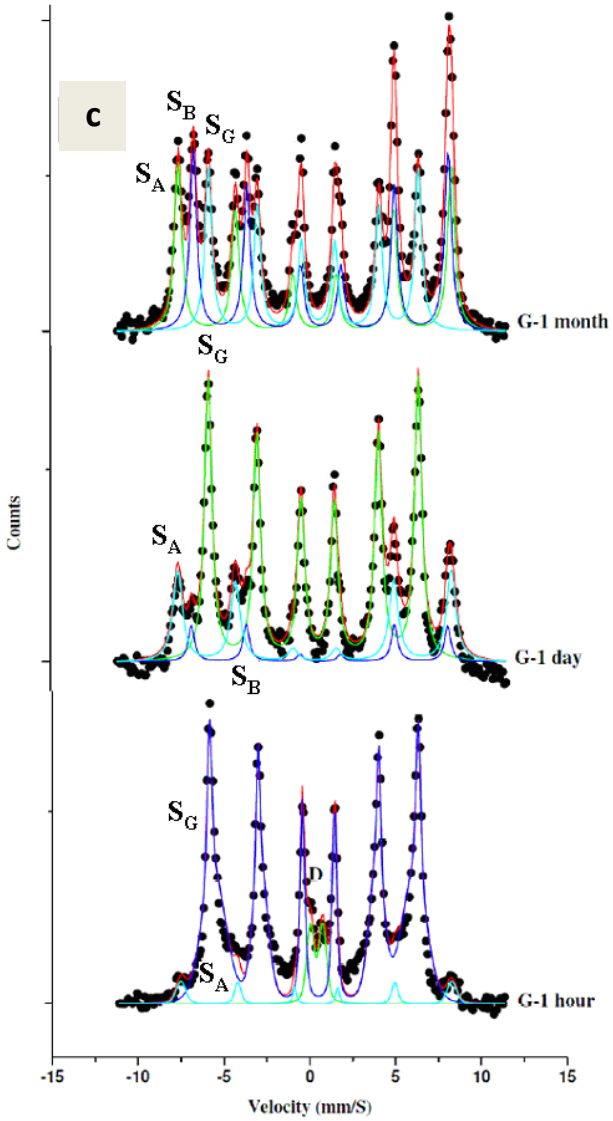

Figure 4: Mössbauer spectra of the transformation products of (a) ferrihydrite-F, (b) lepidocrocite-L and (c) goethite-G1, obtained after aging time of 1 hour, 1 day and 1 month.

Mössbauer spectroscopy can be a useful technique to estimate the magnetite stoichiometry (Voogt *et al.*, 1999; Gorski & Scherer, 2010). The degree of stoichiometry (δ) of magnetite was quantitatively determined by using the relative area of the two sextets S_A and S_B (Table 3). A slight departure from stoichiometry ($0.04 < \delta < 0.08$) was found for final magnetite obtained from all substrates after one month. According to XRD analysis, the ferrihydrite was fully disappeared after one hour and lepidocrocite after one month (Fig. 3) while Mössbauer spectroscopy reveals the presence of untransformed ferrihydrite and lepidocrocite at these time points. This difference between the XRD and Mössbauer results comes from the lower sensitivity of XRD for poorly crystallized compounds.

Table 3: Mössbauer hyperfine parameters of the spectra presented in figure 4. *CS:* centre shift with respect to metallic α-Fe at room temperature; *Δ*: quadrupole splitting in the paramagnetic state or : quadrupole shift; *H:* Hyperfine magnetic field; *RA:* relative area and δ: departure from stoichiometry of non-stoichiometric magnetite ($Fe_{3-\delta}O_4$) determined by classical Mössbauer analysis (δ =0 for stoichiometric magnetite, Fe_3O_4).

Sample	Component	*CS* (mm s^{-1})	*Δ or* (mm s^{-1})	*H* (kOe)	*RA* (%)	Stoichiometry δ
Ferrihydrite	D	0.35	0.68	-	100	
F-1 hour	D	0.38	0.71	-	9	
	S1	0.30	0.20	459	13	
	S2	0.42	-0.07	430	68	
	S3	0.25	0.01	485	10	
F-1 day	D	0.34	0.61	-	4	
	S1	-0.01	0.005	476	12	
	S2	0.346	0.02	407	59	
	S3	0.678	0.02	462	25	
F-1month	D	0.30	0.77	-	2	
	S_A	0.27	0	479	40	**δ = 0.041**
	S_B	0.64	0	444	58	
Goethite	S_G	0.38	-0.13	351	100	
G-1 hour	D	0.39	0.72	-	7	
	S_G	0.37	0.31	364	89	
	S_A	0.37	0	491	4	
G-1 day	S_G	0.38	-0.13	378	68	
	S_B	0.64	-0.02	460	7	
	S_A	0.32	-0.004	491	25	
G-1 week	S_A	0.29	-0.007	489	27	
	S_B	0.24	-0.002	456	14	
	S_G	0.26	-0.13	376	59	
G-1month	S_A	0.31	0.008	491	32	
	S_B	0.66	-0.003	458	35	**δ = 0.079**
	S_G	0.38	-0.14	377	33	
Lepidocrocite	D	0.48	0.54	-	100	
L-1 hour	D	0.39	0.56	-	26	
	S_A	0.32	0.01	484	25	
	S_B	0.61	-0.05	452	49	
L-1 day	D	0.39	0.56	-	2	
	S_A	0.33	0.006	488	47	
	S_B	0.63	0	453	51	
L-1 month	D	0.40	0.53	-	2	
	S_A	0.33	0.01	490	41	**δ = 0.046**
	S_B	0.58	-0.02	456	57	

All these results consistently show that the ferrihydrite was more reactive to transform into magnetite. Almost 90% of ferrihydrite was transformed into magnetite after one hour of reaction, as compared to 75% of lepidocrocite and 4% of goethite. Only traces of lepidocrocite were found after one month, while a large amount of goethite (32%) was still present. The percentage of formed magnetite quantified by Mössbauer analysis was plotted *vs* time in Figure 5.

Although the magnetite quantification was done at only a few reaction times (three points for F and L and four for G1), we have attempted to describe the kinetic mechanism by using the well-known kinetic models. Among them, it appears that the pseudo-second-order rate expression provided the best fitting kinetic model for the experimental data. In our system, the equation of pseudo-second-order can be written as:

$$\frac{dP}{dt} = k_2 (P_{\max} - P_t)^2 \qquad (2)$$

where P_{max} is the maximum amount of magnetite formed (%), P_t is the amount of magnetite formed (%) quantified by Mössbauer analysis at any time t, and k_2 (1/%h) is the pseudo-second-order rate constant. Integrating Eq. (2) gives

$$\frac{1}{P_{\max} - P_t} = \frac{1}{P_{\max}} + k_2 t \qquad (3)$$

Rearranging the Eq. (3) into a linear form we obtained

$$\frac{t}{P_t} = \frac{1}{k_2 P_{\max}^{\ 2}} + \frac{1}{P_{\max}} t \qquad (4)$$

The pseudo-second-order rate constant (k_2) and P_{max} were calculated from the slope and intercept of the plots of t/P_t versus t. The plots show good linearity, with regression coefficients higher than 0.98 (Table 4). Therefore, the order of reactivity as well as the kinetic rate constant can be classified as ferrihydrite > lepidocrocite > goethite, which is consistent with previous findings (Pedersen *et al.*, 2005). They reported that the transformation extent decreases by approximately one order of magnitude going from ferrihydrite to lepidocrocite to goethite and the main control on the transformation yield appears to be affiliated with the properties and crystallinity of the iron oxide mineral.

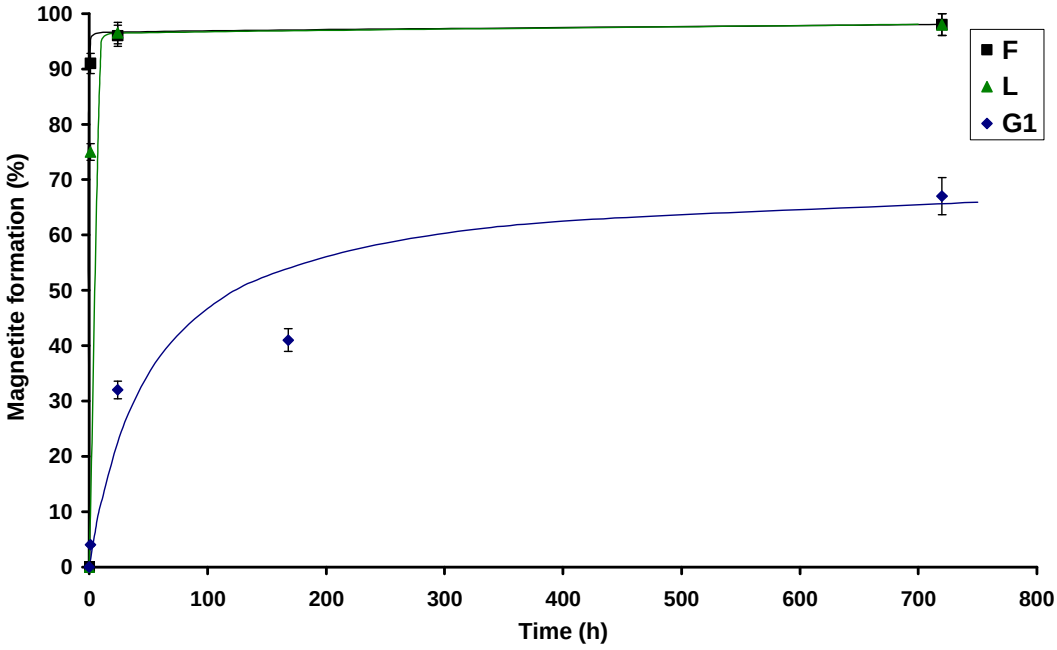

Figure 5: The percentage of the magnetite formed *vs*. time as determined by Mössbauer analysis (F, L and G1).

Table 4. Pseudo-second order kinetic constants of magnetite formation for F, L and G1.

	F (r^2= 0.999)	L (r^2=0.999)	G1 (r^2= 0.981)
P_{max} (%)	98.1	98.1	70.4
k_2 (1/%h)	0.034	0.029	$2.84\ 10^{-4}$

3.3. Transformation of three goethites into magnetite

The transformation of three goethites into magnetite was monitored at three aging times (1 hour, 1 day and 1 week). The XRD diffractograms of three kinds of goethite after aging time of one week are shown in Figure 6a. The intensity of the peaks assigned to magnetite follows the order: G1 > G2 > G3 while reverse is the case for goethite peaks. G1 seems to be more reactive to transform into magnetite.

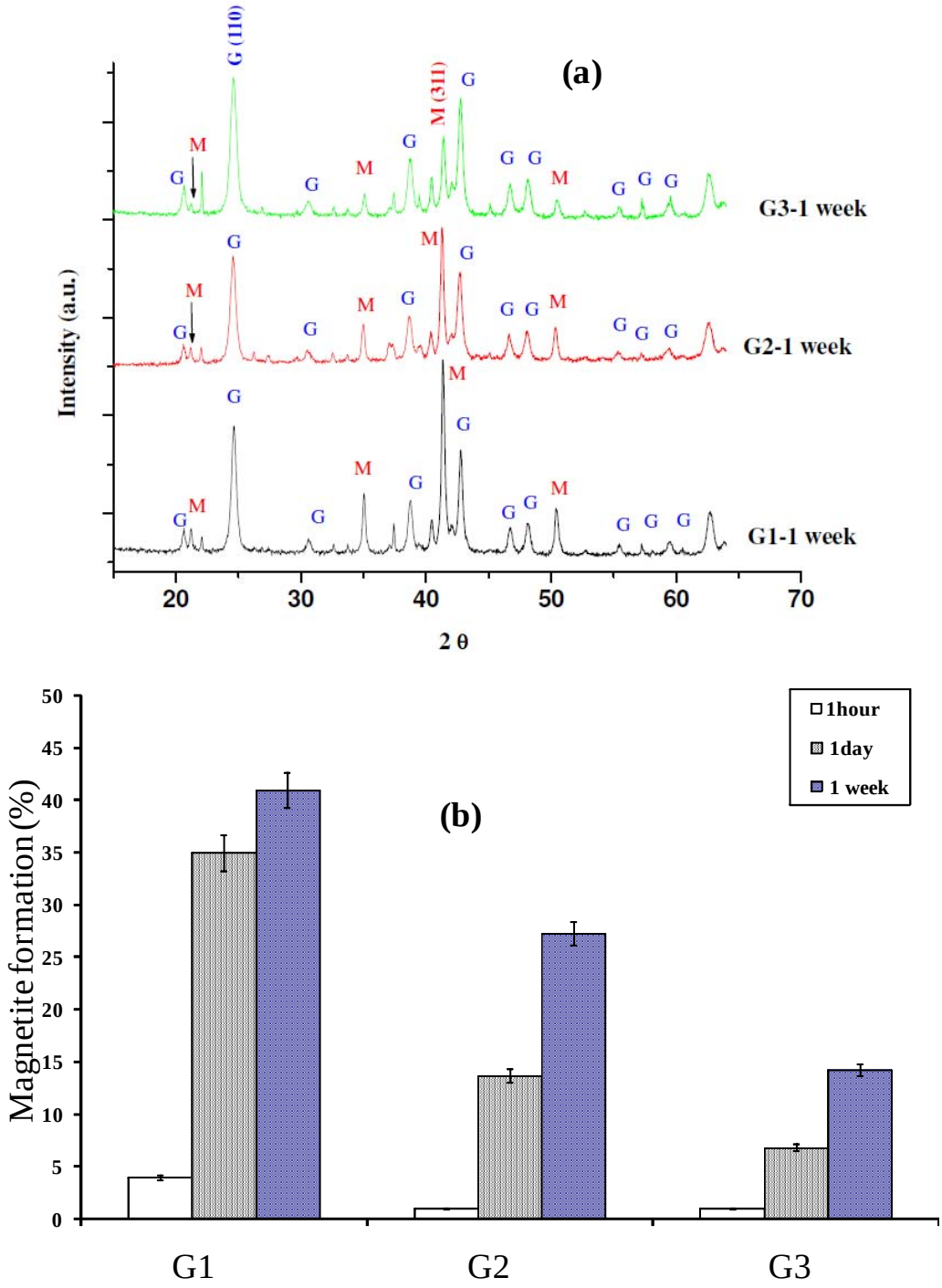

Figure 6: (a) XRD diffractograms of the transformation products of three kinds of goethite (G1, G2 and G3), obtained after aging time of 1 week and (b) the histogram comparing the magnetite formed (%) from three goethites after aging time of 1 hour, 1 day and 1 week.

A correlation between the XRD findings and quantities measured by Mössbauer spectroscopy can be established from the G1 transformations. Firstly, the ratio IM/(IM+IG) was determined from XRD diffractograms, where IM is the intensity of the most intense peak of magnetite

(311) and IG is the intensity of the most intense peak of goethite (110). This ratio was then plotted versus the amount of magnetite measured by Mössbauer spectroscopy at each time point (Table 5). The plot shows very good linearity, with a correlation coefficient of 0.9986. Thus, this regression equation was used to estimate the quantity of formed magnetite for G2 and G3 after 1 hour, 1 day and 1 week (Fig. 6b). Therefore, the reactivity of three kinds of goethite to transform into magnetite was found as: G1 > G2 > G3, implying that more magnetite was generated when G1 was reacted with Fe^{II} under our experimental conditions. This reactivity sequence follows the inverse order of the specific surface area determined by BET method (Table 2).

Table 5: IM/(IM+IG) against percentage of magnetite amount formed (%) after various aging times. Where IM is the intensity of most intense magnetite peak (311) and IG is that of goethite (110) determined from XRD diffractograms.

Solid	IM /(IM+IG) from XRD	Magnetite formed (± 2%) from Mössbauer spectroscopy
G1-1hour	0.29	4
G1-1day	0.50	35
G1-1 week	0.57	41
G1-1month	0.80	67

The impact of organic (salicylate SA) and inorganic (phosphate P) ligands on the transformation of G1 was also tested after aging time of one week. The total ligand loading per surface unit is relatively high and lies at 26 µmol/m^2. The sorbed amount of SA and P on the goethite surface (G1) was determined by depletion method and was found to be respectively 0.05 and 0.30 µmol/m^2. The magnetite appeared when SA was present in reaction medium while no magnetite peaks can be identified in the presence of P alone or a mixture of P + SA (data not shown). According to the correlation IM/(IM+IG) *vs.* magnetite amount explained above, a slight reduction (from 41 % to 37 %) in the amount of formed magnetite was noted for salicylate while the presence of phosphate completely hindered the generation of magnetite (from 41 % to less than 1 %).

4. Discussion

The transformations of iron oxides and hydroxides and the Fe(II) induced mineralization pathways are complex and the exact mechanism of the Fe(II)-catalyzed transformation of iron oxides is still a matter of debate. In general, the secondary mineralization pathways can be distinguished through two main mechanisms: (i) solid-state transformation (also called topotactic) and (ii) dissolution/re-precipitation (or reconstructive/re-crystallization). The first involves the transformation of the initial phase within a solid phase without dissolution, while in the second the initial phase is dissolved following by the crystallization of a new secondary phase. In this latter case, the oxide transformation occurs through the interfacial electron transfer reactions between adsorbed Fe(II) and iron oxides involving reductive dissolution and then reprecipitation of the adsorbed ferrous ions on oxides particle surfaces (Tronc ***et al.***, 1992). The penetration of electron into the oxide particle can destabilize the crystal, promoting its disintegration and release of the entered electron as a reduced Fe(II) species (Williams & Scherer, 2004; Larese-Casanova & Scherer, 2006). On the other hand, direct dissolution of ferric oxide produced ferric ion which will form a redox couple with the added Fe(II). This redox couple in solution could potentially cause an electron transfer reaction between the Fe(II) solution and the solid. The electron transfer reactions may destabilize the ferric oxide structure and promote its dissolution(Yang ***et al.***, 2010), which would potentially increase the solution Fe(III) concentration.

Therefore, the dissolution reaction may act as the main mechanism in the secondary mineralization processes. However, the aqueous Fe measurements did not permit a direct evidence of Fe^{2+}-promoted reductive dissolution or Fe^{3+} release in our experimental system. Indeed, the total Fe concentration remained very low along the course of experiment (Fig. 7a; Table 1).

Nevertheless, the order of reactivity found in the present work (ferrihydrite > lepidocrocite > goethite) is comparable with the dissolution data previously reported in literature. Firstly, the direct dissolution rate of iron oxyhydroxides is often found as: ferrihydrite > lepidocrocite > goethite which is the inverse order of the degree of crystallinity determined by XRD analysis (Schwertmann, 1991; Cornell & Schwertmann, 1996). Crystal size and crystal order are important determinative factors, affecting dissolution rate of iron oxides. For example,

ferrihydrite, an unstable Fe oxide with a large specific surface is highly soluble, whereas crystallized iron oxides such as goethite are thermodynamically stable with a relatively low dissolution rate (Schwertmann, 1991; Pedersen *et al.*, 2005; Yee *et al.*, 2006).

The reductive dissolution of iron oxyhydroxides was compared elsewhere and dissolution rate was found strongly dependent of the mineralogy for the initial phase (Larsen & Postma, 2001; Pedersen *et al.*, 2005). Indeed, among different iron oxides, the crystallinity and morphological properties were the control factor of the reductive dissolution rate, which follows the order ferrihydrite > lepidocrocite > goethite.

On the other hand, the reductive dissolution of goethites was determined in this work according to the method described in (Larsen & Postma, 2001). The Fe^{II} formation was monitored against time at pH 3 and the experimental data was then fitted to the first order kinetic model (Fig.7b). The initial rate constant was found: $1x10^{-3}$ h^{-1} (G1), $5x10^{-4}$ h^{-1} (G2), $6x10^{-4}$ h^{-1} (G3), following this order: G1 > G3 ~ G2. The initial rate is therefore independent of the specific surface area among three tested goethites, emphasizing the importance of crystal structure. This is in agreement with the transformation data where the G1 was found to be the most reactive goethite to transform into magnetite.

Based on the observation that magnetite, formed by the action of Fe(II), has morphology and particle size similar to those of the initial oxyhydroxides, a topotactic conversion of initial compounds to magnetite can also be proposed (Ardizzone & Formaro, 1983; Tronc *et al.*, 1992; Fredrickson *et al.*, 1998). Indeed, the transformation of small particles of ferrihydrite produced small magnetite particles while those formed by the Fe(II)-catalysed transformation of lepidocrocite or goethite have larger crystal size (Fig. 2). In addition, the Mössbauer spectra of magnetite formed from ferrihydrite displays broad lines, often caused by a structural disorder. This observation is also in favor of a topotactic formation of magnetite onto poorly crystallized ferrihydrite. In contrast, well ordered magnetite with sharp Mössbauer lines was obtained from crystallized iron oxides (i.e. L and G) (Fig. 4).

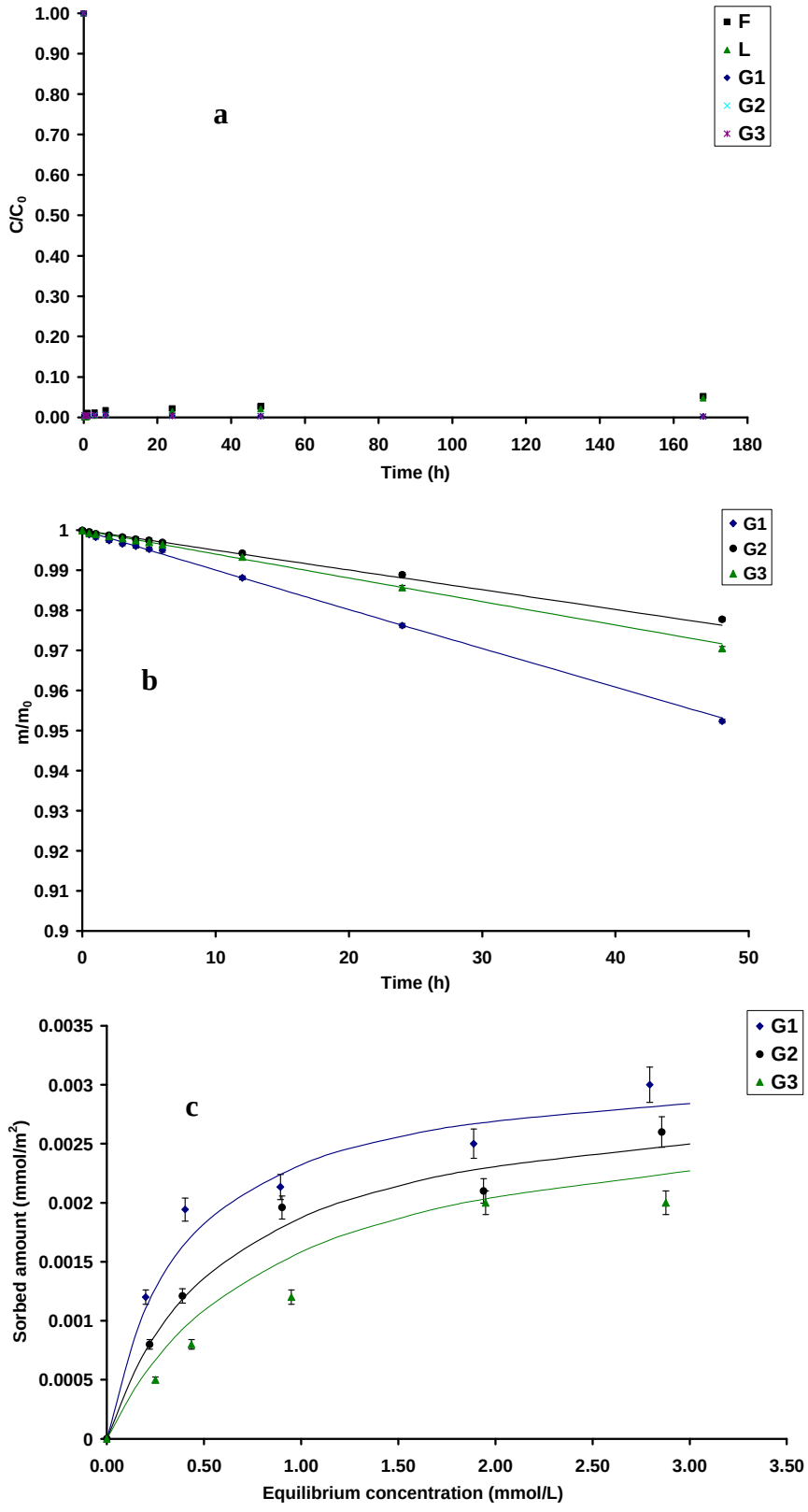

Figure 7: (a) Relative concentration (C/C_0) of aqueous Fe(II) during the transformation reaction. Input concentration C_0=50 mM, the pH values are reported in Table 1. (b) Reductive dissolution rate of three goethites at pH3. m/m_0 is the fraction of undissolved iron oxide. [ascorbic acid] =10 mM, [solid] = 50 m^2/L;

T = 20±1 °C; the lines represent a fit of the data to the first-order kinetic model. (c) Fe(II) sorption data on three goethites at pH 6.6±0.1, [solid]= 50 m^2/L; T = 20±1°C; the lines represent the Langmuir isotherm model. The Langmuir constants are reported in table 6.

This topotactic transformation process is initiated by the Fe(II) surface adsorption and interfacial electron transfer (Belleville *et al.*, 1992; Jolivet *et al.*, 1992; Tronc *et al.*, 1992). Crystallization of magnetite occurred only if high Fe(II) amount is fixed on the oxide surface and then excess electrons can diffuse within the particle. In this work, the adsorption of ferrous ion was strong under our experimental conditions (high Fe (II) concentration and alkaline pH). Indeed, almost 98% of the input Fe(II) amount was rapidly removed from the aqueous solution (Fig. 7a). In this case, Fe(II)-to-Fe(III) electron transfer and precipitation processes are contributing to the observed sorption phenomena. A decrease in pH was observed against aging time, which can be positively correlated with the transformation extent (Table 1). Therefore, the addition of HO^- together with Fe^{2+} would have the effect of accelerating and strengthening the sorption and then surface electron transfer reactions. The total number of electrons that can be transferred per surface unit of oxide is important and therefore the magnetite conversion can be faster. Due to its electrical conducting properties, the magnetite nuclei formed would further enhance electron injection into oxide particles, as it is the case for electron transfer in mixed-valent Fe^{II}-Fe^{III} minerals (Williams & Scherer, 2004).

The inhibition of magnetite formation caused by the adsorption of phosphate provides also a data that is in favor of such a mechanism. Indeed, the strong phosphate bonding minimizes site accessibility for Fe^{2+}, thereby preventing the electron delocalization at the interfacial sites and the solid-state reaction. Phosphate forming strong inner sphere complexes with the iron oxide surface are generally believed to inhibit magnetite nucleation and precipitation regardless of Fe(II) concentration (Biber *et al.*, 1994; Benali *et al.*, 2001). However, loosely bonded ligand such as salicylate anion did not significantly affect the magnetite formation. These results are consistent with the findings of previous works where phosphate was found to interfere with the transformation of ferrihydrite to crystalline oxyhydroxides (Barrón *et al.*, 1997; Borch *et al.*, 2006). Therefore, this lack of transformation into magnetite in the presence of strongly bonded ligand point out the key role of Fe(II) surface sorbed and electron injection within the oxide particle.

According to the aqueous Fe(II) measurements, the residual aqueous Fe(II) concentration was very low along the course of experiment and did not significantly differ between the tested oxides (Fig. 7a). These observations are consistent with literature (Liger *et al.*, 1999) who found that the Fe^{II} adsorption edge was the same for the three oxyhydroxide phases: goethite, hematite, and ferrihydrite. At pH > 7.5, the adsorption of Fe^{II} onto iron oxyhydroxide phases reach 100 % regardless of the tested oxide. Calculations using PHREEQC2 (Parkhurst & Appelo, 1999) of the pH dependence of adsorption of Fe^{II} on F, L or G confirms that all Fe^{II} is adsorbed at a pH higher than 7. However that adsorption, oxidation and electron transfer processes were reported to differ significantly depending on Fe-phase(Hiemstra & van Riemsdijk, 2007). The Fe^{II} adsorption of goethite and ferrihydrite can be explained by Fe^{II} binding with and without electron transfer, while interactions of Fe^{II} with lepidocrocite can be explained as due to a complete surface oxidation of adsorbed ferrous iron via electron transfer to the solid (Hiemstra & van Riemsdijk, 2007).

Table 6. Langmuir isotherm constants (r^2 = 0.97-0.98) of Fe^{2+} sorption onto goethites.
[solid] = 50 m^2/L ; [Fe^{2+}]= 0-0.5 mM; pH= 6.6±0.1; T = 20±1 °C.

	G1	G2	G3
b (L/mmol)	2.64	1.66	1.20
q_m (µmol/m^2)	3.25	3.0	2.9

In fact, the determination of Fe^{II} adsorption extent is difficult because sorbent solid (ferric oxyhydroxide) rapidly transforms into other compounds, via Fe(II)-to-Fe(III) electron transfer processes. In order to overcome this limitation, the adsorption was evaluated using the least reactive compound (i.e. goethite) at a low range of Fe(II) concentration and at pH 6.6 ± 0.1. This adsorption experiment was done with G1, G2 and G3 and the residual Fe(II) concentration was measured after 30 min of equilibration time as described elsewhere (Liu *et al.*, 2001). The sorbed amount was then estimated by depletion method and the sorption isotherms were best fitted to the Langmuir equation (Table 6, Fig.7c). The sorption capacity follows the order G1 > G2 > G3, which is in agreement with the amount of site density of the singly coordinated surface groups (Table 2) and also their reactivity to transform into magnetite. These results are also consistent with those of Torrent *et al.* (Torrent *et al.*, 1990) who tested the phosphate sorption onto several goethites and reported that multidomainic

crystals of goethite (like G1 in our study) have a higher retention capacity than monodomainic crystals.

In addition, the difference in reactivity of ferric oxides against Fe^{II} may result from the molecular interaction characteristics of ferrous ion with oxide surface. Some authors showed that the microscopic sorption mechanism (i.e. inner or outer sphere complexation) could affect the sharing of electrons between ferric crystal and Fe^{II} and so the transformation rate (Williams & Scherer, 2004; Larese-Casanova & Scherer, 2006). An inner sphere complex may be required to achieve Fe^{II}-Fe^{III} interfacial electron transfer and ultimately their transformations into magnetite (Tronc *et al.*, 1992; Jeon *et al.*, 2003). As the inner-sphere complexation is most likely to take place at sites with singly coordinated surface groups, Fe^{II} adsorption on the singly coordinated surface should be the controlling step for the mineralogical transformation of Fe^{III} oxides (Hiemstra & Van Riemsdijk, 1996; Liger *et al.*, 1999; Larese-Casanova & Scherer, 2006). Consistently, the difference in the transformation extent (G1 > G2 > G3) can be positively correlated with the amount of site density of the singly coordinated surface groups calculated above.

In some cases, the surface complexes of adsorbed Fe^{II} have an edge sharing coordination environment similar to that found in mixed-valent Fe minerals. In the case where the environment of an Fe^{II} ion adsorbed on an Fe^{III} oxide is similar to that of adjacent Fe^{II}-Fe^{III} octahedra in mixed-valent Fe minerals, the interfacial electron transfer would be favorable (Williams & Scherer, 2004; Larese-Casanova & Scherer, 2006). For instance, formation of bidentate or tridentate complex between divalent ion and oxide surface may favor the electron transfer.

So, one can imagine that the difference in reactivity between G1, G2 and G3 may come also from the difference in type of surface complexes formed between ferrous ion and the different crystal faces of goethite. It is known that divalent ion can form either double corner bidentate surface complexes or tridentate complex (Hiemstra & Van Riemsdijk, 1996). It was suggested (Manceau *et al.*, 2000; Spadini *et al.*, 2003) that the adsorption behavior of divalent cation may probably be dominated by the crystal faces that terminate the chains (021/001 like faces) and the presence of the face 021 or 121 favored the formation of bidentate or tridentate complex. In addition to the 021 face, the 110 face was likely implied in the adsorption of the ferrous ions especially at a high Fe^{II} loading (Dixit & Hering, 2006).

Finally, the high reactivity of G1 observed here could be the result of the presence of the faces (021) or (121) and also (001) that favor the formation of bidentate or tridentate complex and therefore the electron transfer. For G3, the low reactivity may come from the lack in the crystal faces (001) (30% only of the total surface area) and (021), being responsible of the formation of inner sphere complexes.

5. Conclusion

Transformation of ferric oxyhydroxides in the presence of Fe^{II} can be affected by many factors including mineralogy of starting compound, aging time and solution chemistry.

The transformation of iron oxides by the catalytic action of Fe(II) involves the adsorption of Fe(II) on the oxide surface and then electron exchange. These interfacial electron transfer reactions between adsorbed Fe(II) and iron oxides enable both (i) rapid formation of mixed-valence state upon surface adsorption of high Fe(II) amount, and/or (ii) reductive dissolution and then reprecipitation of the adsorbed ferrous ions on ferric oxide surface. Under our experimental conditions, both topotactic and reconstructive transformations may occur simultaneously.

Both transformation reactions are initiated by Fe (II) adsorption to singly coordinated sites via the formation of inner-sphere surface complexes. The coordination of Fe(II) at the ferric oxide surface via the formation of bidentate or tridentate complex is a prerequisite to electron transfer, a key step to initiate both the mentioned processes. The presence of strong chelating ligand like phosphate is expected to hinder the adsorption sites and therefore affect reductive dissolution reaction or solid-state transformation. The high intrinsic reactivity of G1 as shown by its higher Fe^{II}-adsorption capacity and initial reduction dissolution rate emphasizes the importance of crystal faces reactivity for the transformation process. Microscopic level characterizations such as crystal structure and surface site density are therefore needed to describe the transformation extent of iron oxides.

Acknowledgements

The authors would like to thank the Higher Education Commission of Pakistan (HEC) and "Agence Nationale de la Recherche (ANR) and Agence de la Maitrise de l'énergie (ADEME)

for financial support (Programme ECOTECH 2009 (“Production durable de Technologies de l’environnement, CERVEAU NP, décision attributive d’aide n° 0994C0103). We gratefully acknowledge Dr F. Gaboriaud for providing the three goethites samples (G1, G2 and G3). The authors thank J. Ghanbaja and G. Ollivier for TEM and XRD analyses, respectively.

Formation of green rust *via* mineralogical transformation of ferric oxides (ferrihydrite, goethite and hematite)

M. Usman[a, b], K. Hanna[a,§], M. Abdelmoula[a], A. Zegeye[a], P. Faure[b] and C. Ruby [a]

[a] *Laboratoire de Chimie Physique et Microbiologie pour l'Environnement, LCPME, UMR 7564, Institut Jean Barriol, CNRS-Nancy Université, 405 rue de Vandoeuvre, 54600, Villers-lès-Nancy, France.*

[b] *Géologie et Gestion des Ressources minérales et énergétiques, UMR 7566, CNRS-Nancy Université-CREGU, 54506, Vandœuvre-lès-Nancy, France.*

[§] *Present address :*

Ecole Nationale Supérieure de Chimie de Rennes

UMR CNRS 6226 "Sciences Chimiques de Rennes"

Chimie et Ingénierie des Procédés

Avenue du Général Leclerc, 35708 Rennes Cedex 7

Abstract

This laboratory study describes the abiotic mineralogical transformation of ferrihydrite (F), goethite (G) and hematite (H) into mixed Fe^{II}-Fe^{III} green rust (GR). Stoichiometric quantities of ferric oxides were reacted with hydroxylated Fe^{II} species under static batch conditions at a final pH of ~ 6.3 for 2 hours. Mössbauer spectroscopy and transmission electron microscopy (TEM) was used to characterize initial and resulting transformation products. Results indicate that the order of reactivity to transform into GR is F > G > H. Complete transformation of F into GR was achieved while about half of G or H was transformed although G or H are known for their higher thermodynamic stability. As expected, the concentration of soluble iron at the end of the experiment followed the order H > G > F which is in agreement with the predictions of Fe^{II}-Fe^{III} mass balance diagram. The formation kinetics of GR is much higher than that observed for magnetite (Fe_3O_4) under similar experimental conditions. Therefore in the environment, when hydroxylated Fe^{II} species interact with ferric oxides, fougerite, the mineral counter part of GR, could be preferentially formed.

Key Words: Iron; Green rust; Mössbauer; Fougerite; Layered double hydroxides.

1. Introduction

Iron oxides are abundant in the environment and play a key role in the fate of Fe via the redox couple connecting solid ferric oxides and soluble Fe^{II} species. This Fe^{II}-Fe^{III} redox couple is closely linked to various important elemental cycles, (e.g. C, N, and P) and to the mobility of soil and groundwater contaminants (organic and inorganic) due to adsorption, redox and surface precipitation processes (Stumm & Sulzberger, 1992; Cornell & Schwertmann, 1996). In soils and sediments, iron minerals are commonly found as ferric oxides like goethite, ferrihydrite, hematite and lepidocrocite with different surface and crystal characteristics (Cornell & Schwertmann, 1996; Larsen & Postma, 2001). Ferrihydrite is a poorly crystallised ferric oxyhydroxide, while goethite and hematite are generally well crystallised and thermodynamically more stable (Cornell & Schwertmann, 1996; Majzlan *et al.*, 2003). Another type of iron mineral includes the mixed Fe^{II}-Fe^{III} compounds such as magnetite (Fe_3O_4) or fougerite, the mineral counterpart of Fe^{II}-Fe^{III} green rust GR (Trolard *et al.*, 1997). Fougerite was found in a hydromorphic gley soil of the forest of Fougères (Britanny, France).

The synthetic homologue GR is an Fe^{II}-Fe^{III} hydroxide salts belonging to the general class of layered double hydroxide family or LDHs, sometimes also called anionic clays. GR is characterized by the general formula $[Fe^{II}_{(1-x)}Fe^{III}_{x}(OH)_2]^{x+}[\frac{x}{n}A^{n-}, mH_2O]^{x-}$ where A^{n-} is the intercalated anions (A^{n-} = Cl^-, SO_4^{2-}, CO_3^{2-}...) and *x* is the Fe^{III} molar fraction (Génin *et al.*, 1998; Hansen *et al.*, 2001). Due to the presence of structural Fe^{II}, GR is very reactive and thus plays a central role in the redox cycling of iron in many aquatic and terrestrial environments (Génin *et al.*, 1998; Hansen *et al.*, 2001; Génin *et al.*, 2006b). Stoichiometric GRs ($x \sim 0.33$) contain about two times more structural Fe^{II} than magnetite $Fe^{II}Fe^{III}{}_2O_4$ and are therefore considered as powerful reductants (Myneni *et al.*, 1997; Hansen *et al.*, 2001; Elsner *et al.*, 2004; Kone *et al.*, 2009; Ona-Nguema *et al.*, 2009).

Various synthetic procedures have been developed for GR formation that are believed to mimic those operative in the environment, including biotic and abiotic pathways. Indeed, GR was shown to be the secondary product of microbial reduction of lepidocrocite and ferrihydrite (Ona-Nguema *et al.*, 2002; Zachara *et al.*, 2002; Zegeye *et al.*, 2007). Abiotic methods include chemical or electrochemical oxidation (Abdelmoula *et al.*, 1996; Peulon *et al.*, 2004) of zero-valent iron, partial oxidation of hydroxylated Fe^{II} solution (Génin *et al.*, 2006b) or co-precipitation of Fe^{II} and Fe^{III} salts in aqueous solutions (Ruby *et al.*, 2006a). The interactions of aqueous Fe^{II} with the host ferric minerals can cause structural changes, potentially resulting in the formation of Fe^{II}-bearing minerals (green rust and magnetite). These solid state transformation are governed by various factors, including the structural relationship between precursor and final product as well as experimental conditions, e.g. pH, values of the ferric molar fraction *x* and the hydroxylation rate (Tamaura *et al.*, 1983; Jolivet *et al.*, 1992; Tronc *et al.*, 1992; Ruby *et al.*, 2003; Pedersen *et al.*, 2005). Due to its low degree of order, the solid state transformation of ferrihydrite has been the subject of several studies (Tamaura *et al.*, 1983; Tamaura *et al.*, 1984; Jolivet *et al.*, 1992; Hansel *et al.*, 2005; Pedersen *et al.*, 2005). Up to now, generation of GR by abiotic transformation of goethite and hematite has not been explored, probably because they exhibit a higher thermodynamic stability. However the E_h-pH Pourbaix Diagram describes a relatively large stability domain of GR at higher Fe^{II} concentrations (Génin *et al.*, 1996; Ruby *et al.*, 2010). Thus, the main focus of this study was the transformation of the three most abundant iron oxides, i.e. ferrihydrite, goethite and hematite into GR. Therefore, the reactivity of these minerals against

aqueous Fe^{II} species and the extent of their mineralogical transformations into green rust under static batch conditions were investigated. The initial and final solid compounds were characterized by Mössbauer spectroscopy and transmission electron microscopy (TEM).

2. Experimental section

2.1. Sample preparation

2.1.1. Initial ferric oxides/hydroxides substrates

Experiments were conducted with three synthetic ferric substrates: 2-line ferrihydrite (F), goethite (-FeOOH) (G) and hematite (α-Fe_2O_3) (H). The 2-line ferrihydrite (F) was synthesized according to the method of Schwertmann and Cornell (Schwertmann & Cornell, 2000). It was prepared by neutralizing a 0.2 M ferric chloride solution with 1 M NaOH to a pH of around 7.5. The goethite (G) sample was prepared by air oxidation of a hydrolyzed $FeSO_4$ solution following a procedure described by Olowe ***et al***. (1990). The hematite (H) sample (α-Fe_2O_3) was synthesized as proposed by Schwertmann and Cornell (2000). Ferric chloride was placed in 0.002 mol/ L HCl and incubated at 98 °C in a closed vessel for 7 days. After centrifugation, the solids were washed and then dried. The specific surface area of synthesized solids was determined by multipoint N_2-BET analysis using a Coulter (SA 3100) surface area analyzer. It was found to be 190, 38 and 11 m^2/g for F, G and H, respectively.

2.1.2. Transformations of ferric oxyhydroxides in batch experiments

The mineralogical transformations of synthetic ferric oxyhydroxides were examined in batch experiments at ambient temperature (22 ± 2°C). The experiments were designed to investigate the effect of the initial ferric oxyhydroxides (F, G or H) on these transformations, and were conducted by their reaction in parallel against Fe^{II} to synthesize sulphate containing green rust $GR(SO_4)$ of formula $Fe^{II}_4\,Fe^{III}_2\,(OH)_{12}\,SO_4$. Stoichiometric GR has an Fe^{II}: Fe^{III} ratio of 2:1 so their quantities were taken accordingly. To make a specific Fe^{III} concentration in suspensions, the Fe^{III} oxides were dissolved in concentrated HCl and analyzed through Inductively Coupled Plasma Atomic Emission Spectroscopy (ICP-AES) to determine the resulting Fe^{III} concentration. A suspension of Fe^{III} oxide was prepared and purged for one

hour with filter-sterilized N_2 (99.99%) in order to ensure the evacuation of dissolved oxygen which is known to rapidly oxidize Fe^{II} in the presence of oxides at circumneutral pH (Tamura *et al*. 1980). The reaction was started by adding $FeSO_4.7H_2O$ at an Fe^{II} molar concentration corresponding to 47.6 mM. An appropriate amount of NaOH (1 M) was then added to the mixture (Fe^{II}/Fe^{III}-oxyhydroxide) to provide the ratio $[OH^-]$ / $[Fe^{III}]$ = 3. This ratio ($[OH^-]$ / $[Fe^{III}]$ = 3) is required to synthesize stoichiometric GR as shown in reactions (1) and (2) below. The concentration of total iron in the final solution was 71.4 mM ($[Fe^{III}]$ = 23.8 mM and $[Fe^{II}]$ = 47.6 mM). As an example, the expected reaction of transformation for G and H can be written as following:

$$2\ FeOOH + 4Fe^{II} + 6\ OH^- + 2\ H_2O + SO_4^{2-} = Fe^{II}_4Fe^{III}_2(OH)_{12}SO_4 \quad (1)$$

$$Fe_2O_3 + 4Fe^{II} + 6\ OH^- + 3\ H_2O + SO_4^{2-} = Fe^{II}_4Fe^{III}_2(OH)_{12}SO_4 \quad (2)$$

The characteristic bluish green color of GR was observed immediately after the addition of NaOH. The suspensions were vigorously stirred for 1 hour and then aged without stirring at room temperature for 1 hour. All experiments were conducted in a glove box, an anoxic chamber (N_2:H_2= 98:2). After one hour of aging, a portion of the suspension was centrifuged and the solid was dried in a glove box for Mössbauer analysis. Another portion of the suspension was analyzed by TEM.

2.2. Sample characterization

2.2.1. Mössbauer Spectroscopy

In order to identify the nature and the relative quantity of the various Fe-bearing minerals, the initial substrates and their products were analyzed by Mössbauer spectroscopy. The filtered samples were inserted into a ~7 cm^2 holder and were set into a gas tight cell specially designed to perform Mössbauer reflexion analyses at room temperature under a continuous inert N_2 gas flow as explained by Naille and co-workers (Naille *et al.*, 2010). Reemitted backscattered γ-rays (14.4 keV) were selected by four Si-PIN-diodes detectors. Centre shifts *CS* were reported with respect to that of α-Fe at room temperature. Mössbauer spectra were computer-fitted with either a sum of Lorentzian shape lines or a Voigt profile analyses.

2.2.2. Transmission electron microscopy

TEM observations were carried out with a Philips CM20 TEM (200 kV) coupled with an EDX energy dispersive X-ray spectrometer. For initial ferric substrates, the solid powder was re-suspended in 2 mL ethanol under ultrasonication to prepare their suspensions while for final products; they were kept as suspensions in air tight flasks to avoid their oxidation. One drop of the suspension was laid on a carbon-coated copper grid, which was introduced in the microscope under a 10^{-8} Torr vacuum.

2.2.3. Analyses of soluble iron species by UV-Visible spectroscopy

To measure the aqueous concentration of Fe^{II} at the end of the experiment, aliquots were sampled from the batches, filtered through 0.22 µm filters and added to a tube that contained 2N HCl. The total Fe^{II} in a given solution was determined colorimetrically by the ferrozine assay as previously reported elsewhere (Viollier *et al.*, 2000).

3. Results

3.1. Initial ferric oxyhydroxides

Initial ferric oxyhydroxides (F, G and H) were characterized by Mössbauer spectroscopy at room temperature (Fig. 1). Their hyperfine parameters are presented in Table 1. The first spectrum (Fig. 1a) shows broadened quadrupole Fe^{III} doublet attributed to poorly crystallized F. The spectrum of the second sample (Fig. 1b) consists of a sextet with lines that are asymmetrically broadened corresponding to a magnetically ordered goethite. The spectrum in Fig. 1c is characterized by sextet attributed to H and a small doublet. This doublet is attributed to the presence of ferric impurities (< ~ 5%), probably ferrihydrite.

The morphology of the initial iron oxides particles is displayed to illustrate their evolution into GR (Fig. 2). The TEM picture of F displays very small sized and heavily aggregated particles (Fig. 2a). While for G, typical acicular needle shapes were identified (Fig. 2b) with crystals varying between 300 and 400 nm in length. As shown in Fig. 2c, the TEM image indicates that the H particles were more or less rhombohedral in shape.

Table 1: Mössbauer hyperfine parameters of the spectra presented in Fig. 1. *CS:* centre shift with respect to metallic -Fe at room temperature; *Δ*: quadrupole splitting in the paramagnetic state or : quadrupole shift; *H:* Hyperfine magnetic field; *RA:* relative area.

Fig.	Component	*CS* (mm s^{-1})	*Δ or* (mm s^{-1})	*H* (kOe)	*RA* (%)
Ferrihydrite	D_1 (Fe^{III}) F	0.35	0.68	-	100
F- Product	D_1 (Fe^{II}) GR	1.13	2.52	-	66.8
	D_2 (Fe^{III}) GR	0.36	0.55	-	33.2
Goethite	S_1 (Fe^{III}) G	0.38	-0.13	351	100
G- Product	D_1 (Fe^{II}) GR	1.13	2.29	-	41.0
	D_2 (Fe^{III}) GR	0.30	0.46	-	21.5
	D_3 (Fe^{III}) G	0.50	0.85	-	11.9
	S_1 (Fe^{III}) G	0.35	-0.13	364	25.6
Hematite	D_1 (Fe^{III}) F	0.32	0.64	-	4.8
	S_1 (Fe^{III}) H	0.37	-0.10	507	95.2
H- Product	D_1 (Fe^{II}) GR	1.24	2.30	-	34.7
	D_2 (Fe^{III}) GR+ impurities	0.14	0.58	-	22.8
	S_1 (Fe^{III}) H	0.37	-0.11	511	42.5

3.2. Transformation products

3.2.1. Mössbauer spectroscopy

The Mössbauer spectra of the resulting products obtained by abiotic Fe^{II} induced transformation of initial ferric oxide/hydroxides are presented in Fig. 1 (d, e and f). Mössbauer spectroscopy is a useful tool for an accurate quantitative determination of the relative proportions of Fe^{II} and Fe^{III} species. The Mössbauer spectrum of the F transformation product (Fig. 1-d) displays only two doublets D_1 and D_2 typical of GR (SO_4) (Génin *et al*, 1998b): D_1 with a large quadrupole splitting Δ = 2.52 mms^{-1} corresponds to high spin Fe^{II} ions in octahedral sites, and D_2 with a small quadrupole splitting Δ = 0.55 mms^{-1} corresponds to high spin Fe^{III} ions in octahedral sites. The expected ferric molar fraction x_{GR} = 33 % of GR(SO_4) was found (Table 2) . The GR(SO_4) was the only product formed during the F transformation process, suggesting that almost all F was transformed into GR. The transformation into GR was also significant in the case of G as doublets D_1 and D_2 are the most intense components of the spectrum at the end of the experiment (Fig. 1e). Nevertheless, G is not fully transformed as identified by the sextet and a new doublet D_3 (Fig. 1e and Table 1). This Fe^{III} doublet suggests a superparamagnetic G (Olowe *et al*., 1990), which is in agreement with the TEM results (section 3.2.2). Almost 63 % of initial G was transformed into GR. This GR contained a ferric molar fraction x_{GR} of 34 % (Table 2), which is very close to the expected value (x_{GR} = 33 %). Concerning the H, the transformation was slower to some extent because 42 % was still untransformed at the end of reaction (2 hours) as shown by the H sextet in the spectrum (Fig. 1-f). Nevertheless, the rest of the H was transformed into GR with a ferric molar fraction $RA(D_2)/ [RA(D_1)+ RA(D_2)]$ = 39.5 %. By taking into account the relative quantity of ferric impurities present in the initial H, i.e. 4.8 %, the ferric molar fraction obtained for GR was again 34 % (Table 2).

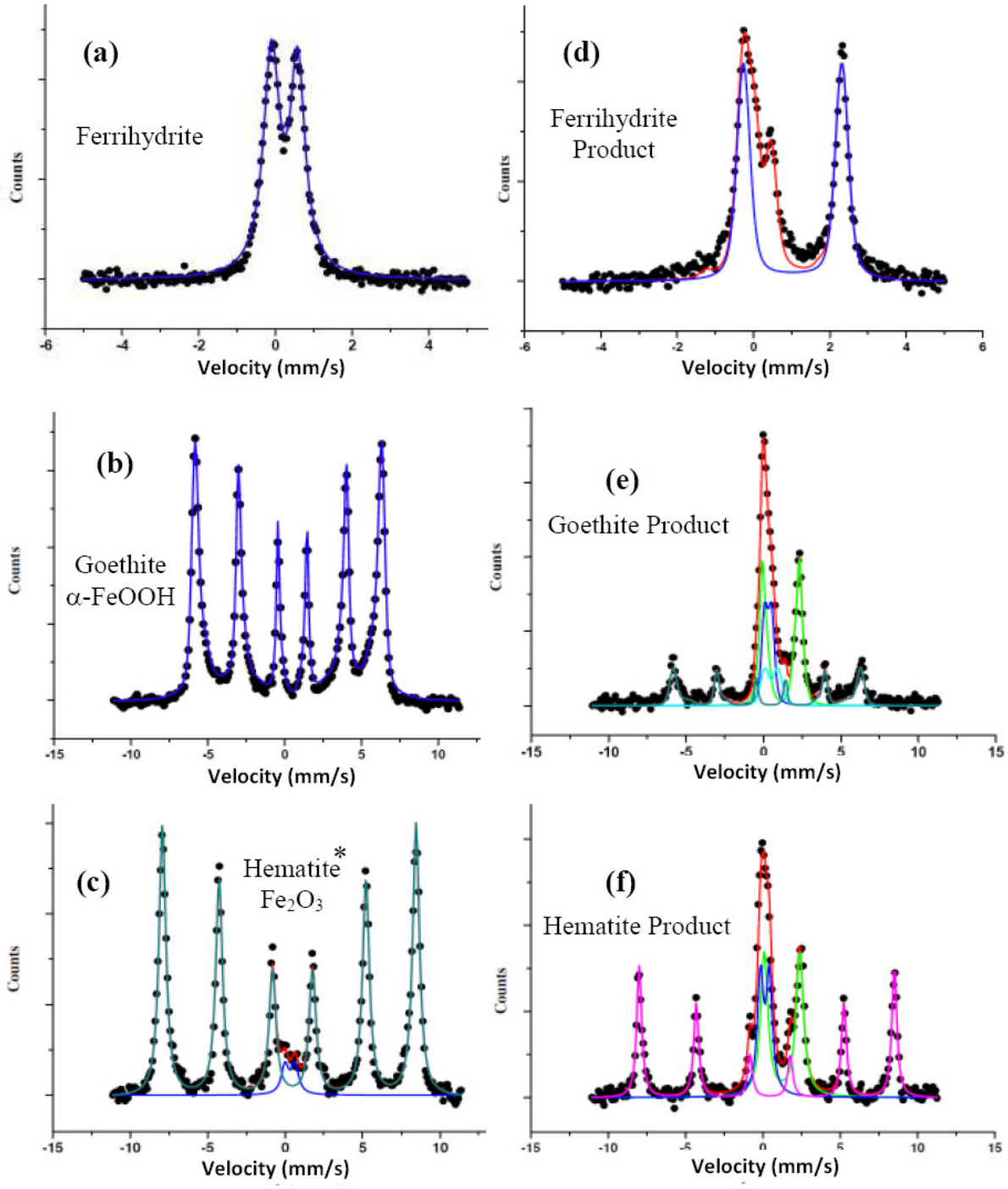

* The initial sample of hematite contains ferrihydrite impurities (< 5%).

Figure 1: Mössbauer spectra of initial ferric substrates (a: ferrihydrite, b: goethite and c: hematite) and their transformation products (d: ferrihydrite product, e: goethite product and f: hematite product).

3.2.2. Transmission electron microscopy (TEM)

To illustrate the morphology evolution of the initial iron oxides particles after transformation, the products were analyzed by TEM (Fig. 2- d, e and f). These TEM images were consistent with the Mössbauer results.

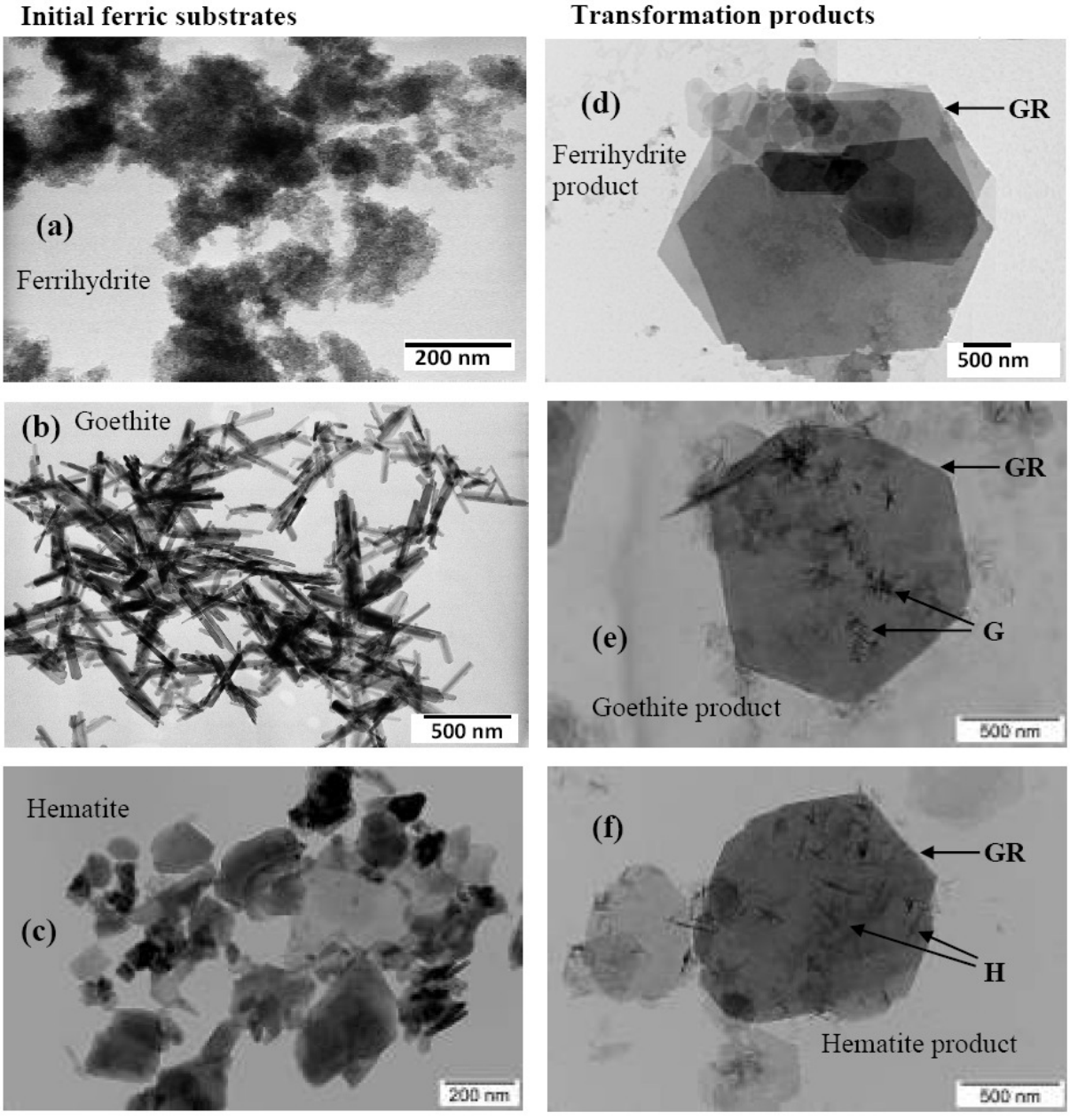

Figure 2: TEM images of initial ferric substrates (a: ferrihydrite, b: goethite and c: hematite) and their transformation products (d: ferrihydrite product, e: goethite product and f: hematite product).

Well-defined hexagonal crystals of GR were identified as secondary mineral when the initial iron oxide is F or G while GR crystals resulting from H transformation are less defined (Fig. 2 d-f). Almost no traces of F were found in the case of F product (Fig. 2d) while along with GR, the remaining G acicular needle shaped crystals (Fig. 2-e) and H crystals (Fig. 2-f) were still present (untransformed) in the final products as also shown by the Mössbauer results. Note that the size of the remaining G crystals is decreased (~ 4 times) as compared to the initial G substrate. This might be related to a progressive dissolution of the G crystals during the transformation. This smaller crystal size is a possible explanation of the appearance of superparamagnetic doublet in G product as observed by Mössbauer spectroscopy (Fig. 1e). The F yields GR with large crystals (~ 1 m) while the size of GR particles from G and H is less uniform and ranges between ~ 100 and ~ 500 nm.

Table 2: Ferric molar fraction of the products and transformation rate of ferrihydrite (F), goethite (G) and hematite (H) measured by Mössbauer Spectroscopy. The extent of transformation corresponds to the relative proportion of iron atoms present in the desired final product, i.e. GR or Fe_3O_4. The values of pH and concentration of soluble iron species are also given.

Samples :	Ferrihydrite product	Goethite product	Hematite Product
$x = n(Fe^{III})/n(Fe)$ (%)	33	59	65
$x_{GR} = \{n(Fe^{III})/n(Fe)\}_{GR}$ (%)	33	34	34
Extent of transformation into GR (%)	100	62.5	57.5
Extent of transformation into Fe_3O_4 (%)	91	4	-
$[Fe^{II}]$ expected (mM)	0 mM	31[(a)]	33[(a)]
$[Fe^{II}]$ measured[(b)] (mM)	0.3 mM	9.9	11.2
pH of the final suspension	6.2	6.3	6.3

[(a)] Values calculated by doing the mass-balance of reactions (1) and (2) and assuming that all unreacted Fe^{II} species remain in the solution.

[(b)] Fe^{II} soluble species measured by the ferrozin assay.

3.2.3. Concentration of soluble iron and mass balance diagram

According to Mössbauer spectroscopy and TEM, the extent of reactions (1) and (2) were not complete since untransformed G and H were observed. The ferric molar fraction *x* of the final solid products measured by Mössbauer spectroscopy, i.e. *x* = 59 % and 65 % for the G and H products respectively (Table 2), was almost 2 times higher than the *x* value (*x* =33.3 %) of the initial suspension that contains a mixture of soluble aqueous Fe^{II} species and the Fe^{III} mineral. Therefore, a significant concentration of unreacted soluble Fe^{II} species were present in the aqueous suspension, in particular because the final pH of ~ 6.3 (Table 2) is situated below the saturation pH for precipitation of $Fe(OH)_2$ (> ~ 7 for $[Fe^{II}]$ = 71mM). The total Fe^{II} concentration of the final suspension (transformation product and solution) was measured at the end of experiment and it was almost the same as the initial concentration (47.6 mM) suggesting the absence of Fe^{II} oxidation. The relative proportion of soluble Fe^{II} species may be quantified by using the Fe^{II}-Fe^{III} mass balance diagram as previous described in Ruby ***et al.*** (2006). The segment [OB] illustrates the full transformation of G into GR, i.e. reaction (1) (Fig. 3). The solid mixture {62.6 % GR, 37.4 % G} measured by Mössbauer spectroscopy is represented by point M. The experimental point N is the intersection between the segment [AM] and the reaction path [OB]. It is included inside the triangle ABC corresponding to the ternary system {Fe^{2+}_{aq}, GR, G}. The relative proportion of iron present as soluble Fe^{II} species is given by the lever rule NM/AM = 43.4 %. Then, the expected concentration of soluble Fe^{II} species is computed (Table 2). A similar diagram (not shown) and calculation can be constructed for the transformation of H into GR and leads to slightly higher expected values (Table 2). The concentration of Fe^{II} in the final solution measured by UV-Visible spectroscopy followed quite well the trends of the expected values (Table 2). The maximal concentration of soluble iron (11.2 mM) was measured for H which represents the lowest extent of transformation. F was fully transformed into GR and the concentration of remaining soluble iron was very low (0.3 mM). However, lower experimental values were found for the H and G products, which are probably due to the sorption and/or partial oxidation of the Fe^{II} species on iron oxide surface as reported elsewhere (Jolivet ***et al.***, 1992; Williams & Scherer, 2004).

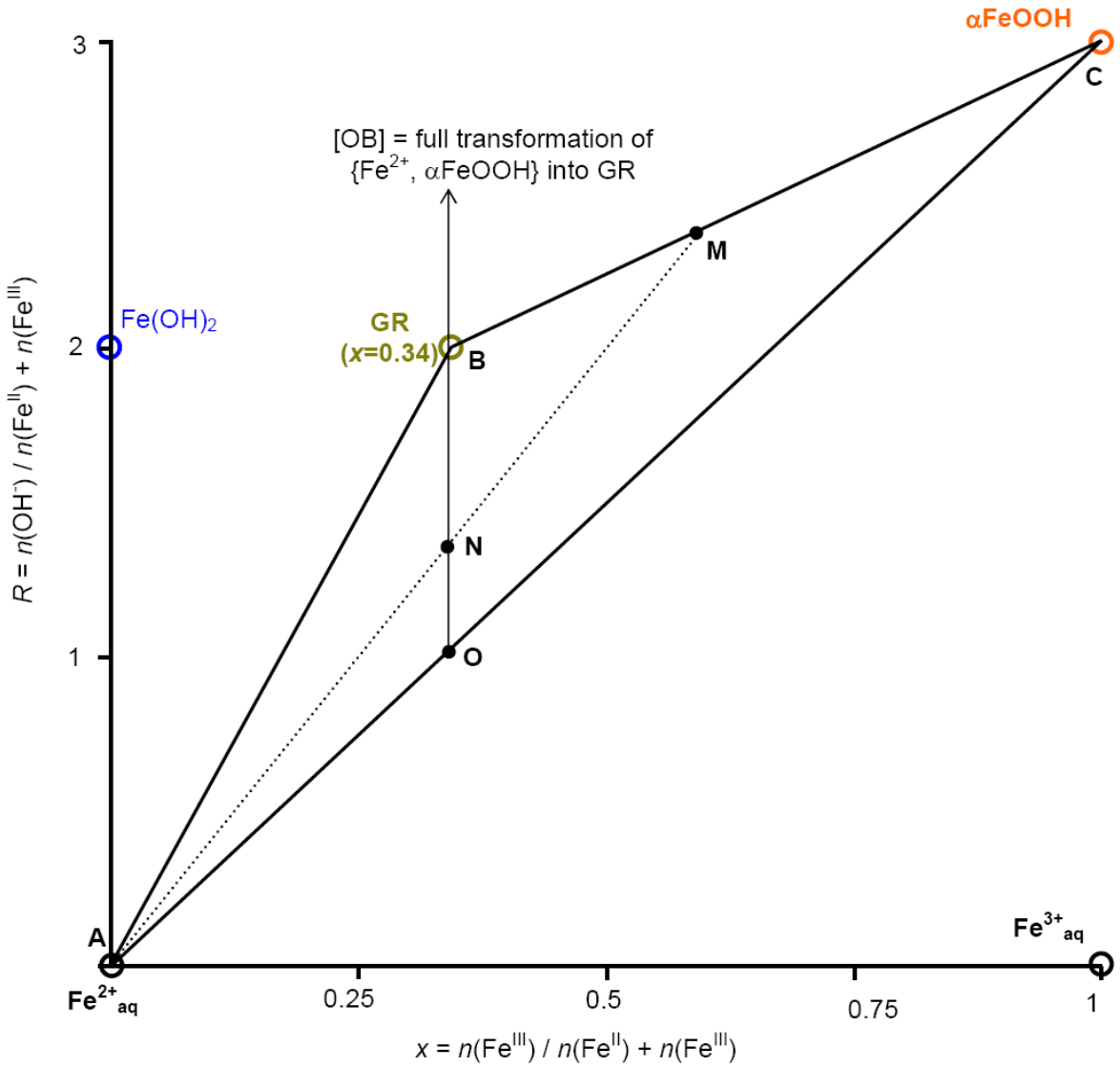

Figure 3: Fe^{II}-Fe^{III} Mass balance diagram showing the reaction path [OB] corresponding to reaction (1) (see experimental section). Point M corresponds to the mixture {62.6 % GR, 37.4 % FeOOH} measured by Mössbauer spectroscopy where MC/BC = 62.6% and MB/BC = 37.4 %. Point N corresponds to the ternary system {Fe^{II}, GR, FeOOH} where the ratio MN/AM ~ 43.4 % is the expected relative proportion of iron present as soluble Fe^{II} species.

4. Discussion

4.1. Order of reactivity of the various ferric oxides

The order of reactivity to transform into GR was found to be F > G > H. This difference in reactivity can be explained by the differences in the properties and surface characteristics of the investigated ferric oxides including structure, particle size, thermodynamic stability and specific surface area. F consists of small units of double chains of edge sharing octahedra cross-linked together in a disordered way by double corners to form chains (Jambor & Dutrizac, 1998). Due to smaller Fe–Fe distances (Waychunas ***et al.***, 1993), the length of these chains is extremely short, thereby resulting in a tremendous increase in chain terminations and ultimately an increase in unshared sites available for adsorption. On the other hand, the length of the octahedral chains is long for G (Manceau, 1995). The G consists of double bands of edge-sharing octahedra. The double bands are linked by corner sharing in a fashion that forms extremely small 2 × 1 octahedra "tunnels" that are crossed by hydrogen bridges (Schwertmann & Cornell, 2000). The H consists of octahedra sharing edges with three adjacent octahedra in the same plane and one face with an octahedron in a neighbouring plane. Thus, due to their mineralogical structure, both H and G have fewer reactive sites than ferrihydrite. The specific surface area as well as the thermodynamic stability of these minerals is also in the same order as their reactivity to transform into GR.

It is very well known that at ambient temperature, G and H are thermodynamically the most stable phases in the iron oxide system while F is the least stable (Cornell & Schwertmann, 1996). It was observed that while F transformed into magnetite during microbially mediated reduction of iron oxides at pH between 6 and 8, G and H remained unchanged (Zachara ***et al.***, 2002). Lack of reactivity was also observed for G and H during Fe^{II}-catalysed transformation (Pedersen ***et al.***, 2005), while F transformed into more stable compounds such as goethite in the presence of ferrous species (Yang ***et al.***, 2010). The unexpected transformation of H and G into GR observed in this study is most probably due to the careful control of the initial suspension. In particular, both parameters of the Fe^{II}-Fe^{III} mass balance diagram were controlled, i.e. the ferric molar fraction $x = n(Fe^{III}) / n(Fe)$ and the extent of hydroxylation $R = n(OH^-)/ n(Fe)$. The relative proportions of the reactants present in reaction (1) and (2) were fixed at the stoichiometric values for a favourable reaction. Kinetic effects limited the extent

of mineral transformation reactions which were not fully accomplished after 2 hours of reaction. Nevertheless, the concomitant appearance of doublets $D_1(Fe^{II})$ and $D_2(Fe^{III})$ observed by Mössbauer spectroscopy is a direct proof that the Fe^{II} and the Fe^{III} species present at the surface of the initial ferric oxides interact to form the GR.

4.2. Formation of green rust versus magnetite

The results of this study show that GR can be formed by reacting Fe^{II} with any of the three most common ferric compounds, i.e. F, G or H. For comparison purpose, the extent of transformation of F and G into mixed Fe^{II}-Fe^{III} magnetite (Fe_3O_4) was also quantified under the following experimental conditions: (i) equivalent iron concentration and reaction time of 2 hours, (ii) ferric molar fraction ***x*** fixed at 0.67 and a ratio OH^-/Fe^{III} of 1 required to form stoichiometric magnetite. These conditions are required to synthesize a stoichiometric magnetite according to the reaction:

$$2\ FeOOH + Fe^{II} + 2\ OH^- = Fe^{II}Fe^{III}{}_2O_4 + 2\ H_2O \qquad (3)$$

The results (Table 2) show the absence of G transformation into magnetite and an incomplete transformation of F. In contrast to GR, magnetite is a compact and very dense ferric oxide and a full deprotonation of the initial ferric and ferrous hydroxylated species is needed during its formation. GR is an “opened” and hydrated compound that may form much more quickly in aqueous solution. Our results reveal that the transformation of ferric oxides to GR was much rapid than to magnetite suggesting that fougerite, the mineral counterpart of GR, could be quickly formed when hydroxylated Fe^{II} interact with ferric oxyhydroxides. Despite the fact that magnetite was thermodynamically more stable than GR (Refait ***et al.***, 2003), the kinetics of formation of Fe_3O_4 was slower.

5. Conclusion

The order of the reactivity of ferric oxides to transform into green rust (GR) was ferrihydrite (F) > goethite (G) > hematite (H). For the first time, a significant transformation into GR of the thermodynamically most stable iron oxides, G and H, was observed. These findings have implications for natural environments where these oxides are abundant. The kinetics of formation of other mixed Fe^{II}-Fe^{III} compound such as magnetite is much slower. So we can

suggest that in anoxic environments, when soluble Fe^{II} species interact with ferric minerals, the generation of GR will be favoured. The formation of fougerite in hydromophic gleysoil could be due to a fast reaction between biogenerated Fe^{II} species and poorly ordered ferric oxyhydroxides, such as ferrihydrite. However, its instability and its fast air-oxidation make the monitoring of GR in environmental settings more difficult and sensitive than that of other stable minerals such as magnetite or goethite.

Acknowledgments

The authors would like to thank the Agence Nationale de la Recherche (ANR) and Agence de la Maitrise de l'Energie (ADEME) for financial support (Programme ECOTECH 2009, CERVEAU NP, décision attributive d'aide n° 0994C0103). The authors thank also Dr. J. Ghanbaja (Université Henri Poincaré -Nancy University) for TEM analyses. We are grateful to Pr Dean Hesterberg and the reviewers for suggestions that helped us to improve this manuscript.

Reactivity of Fe^{III} oxyhydroxides with Fe^{II} in batch and dynamic flow systems

M. Usman[a,b], K. Hanna[a], M. Abdelmoula C. Ruby [a] and P. Faure[b]

[a] Laboratoire de Chimie Physique et Microbiologie pour l'Environnement, LCPME, UMR 7564 CNRS, 405 rue de Vandoeuvre, 54600, Villers Les Nancy, France.

[b] Géologie et Gestion des Ressources minérales et énergétiques, G2R, UMR 7566, 54506, Vandoeuvre Les Nancy, France.

Abstract:

Ferrihydrite is a poorly crystallized mineral and one of the most abundant iron minerals found in soils and sediments. The mineralogical transformation of ferrihydrite into Fe^{II} bearing minerals represents a potential way to improve the soil self-remediation capacity. Indeed, reduction by Fe^{II} may be a significant abiotic pathway in the natural attenuation of environmental contaminants including organic and inorganic pollutants. The aim of this laboratory study was to investigate the Fe^{II} induced mineralogical transformations of three matrices: ferrihydrite, ferrihydrite-rich sand and a pristine soil under static batch and flow through conditions. Since sorbed or structural Fe^{II} is more reactive than minerals bearing only Fe^{III} to promote the remediation of various soil pollutants, generation of Fe^{II} bearing minerals in soil-packed columns was optimized. The starting and resulting solids were characterized by X-ray diffraction (XRD), Mössbauer spectrometry, transmission electron microscopy (TEM) and scanning electron microscopy (SEM).

1. Introduction

Iron oxyhydroxides are abundant in the environment and influence the biogeochemical cycling and availability of Fe via the redox couple connecting solid phase ferric oxides and soluble Fe^{II} species. Iron oxides and oxyhydroxides are present in the soils as a wide range of minerals most commonly goethite, ferrihydrite, hematite and lepidocrocite with different characteristics such as stability, specific surface area and reactivity (Cornell & Schwertmann, 1996). In the reduced soil zone, they exist as mixed Fe^{II} and Fe^{III} compounds such as magnetite (Fe_3O_4) or fougerite, the mineral counterpart of the Fe^{II} Fe^{III} green rust (Trolard ***et al.***, 1997). Ferrihydrite is a poorly crystallized mineral, one of the most abundant iron minerals found in soils and sediments. It plays a substantial role in soil due to its high surface area and intrinsic reactivity.

The chemistry of Fe in aquatic and soil/sediment systems also strongly influences the transport and availability of various nutrients (e.g., C, N, and P) and contaminants (organic and inorganic) due to adsorption and surface precipitation processes (Elsner ***et al.***, 2004). The ubiquitous presence of iron suggests that reduction by iron may be a significant abiotic pathway in the natural attenuation of environmental contaminants. Fe^{II} is one of the most

abundant reductants typically present in aquatic and terrestrial environments under suboxic and anoxic conditions (Rügge *et al*., 1998) but sorbed Fe^{II} and structural Fe^{II} are often more powerful reductants than dissolved Fe^{II}. Indeed, contaminants such as carbon tetrachloride, nitro benzenes, and U(VI) are readily reduced by sorbed or structural Fe^{II} but not by aqueous Fe^{II} complexes (Amonette *et al*., 2000). This Fe^{III}-Fe^{II} redox couple is implicated in the fate and mobility of various soil contaminants including organic and inorganic pollutants (Elsner *et al*., 2004). The stability and reactivity of iron oxyhydroxides are strongly affected by their interactions with aqueous Fe^{II} inducing their structural modification and bulk phase transformation which depend upon Fe^{II}/Fe^{III} molar ratio, pH, anionic media and structure of initial iron oxyhydroxide substrate (Pedersen *et al*., 2005). Therefore, *in situ* generation of Fe^{II} bearing minerals in soil could modify the soil capacity for natural remediation of environmental contaminants. The objective of this study is to monitor the mineralogical transformations in three matrices: ferrihydrite, ferrihydrite-rich sand and a pristine soil under static batch and flow through conditions. The reactivity of Fe^{II} with the endogenous iron mineral fraction in a pristine soil with low organic carbon was investigated.

2. Methods

Experiments were conducted with synthetic ferrihydrite (F) and ferrihydrite rich sand (FRS). The 2-line ferrihydrite (F) was synthesized according to the method of Schwertmann and Cornell (Schwertmann & Cornell, 2000).The quartz sand (Fontainebleau, France) 150-300 µm was cleaned with 1 M HCl for 48 hours, and then rinsed with pure water. The FRS was synthesized by a heterogeneous suspension method. The final FRS was stored at ambient temperature for further use. The soil sample was collected from a pristine site. Particle size, carbon, nitrogen and soil moisture content analyses were performed. The soil is mainly composed of sand and clay with a very low organic carbon content. The clay size fraction of soil (< 2µm) was composed of 35 % smectite, 30 % illite/muscovite, 30 % kaolinite and 5 % chlorite. The main physicochemical properties are reported in table 1.

The Fe^{II} induced reaction test was conducted with the the 2 mm size soil fraction. The mineralogical transformation of substrates was conducted by reacting them against Fe^{II} and NaOH in to synthesize either magnetite or green rust (GR). To prepare magnetite, firstly a suspension of Fe^{III} oxyhydroxide was prepared in water by taking their amounts equivalent to

a Fe^{III} concentration of 2.67 $\times 10^{-1}$ M followed by the addition of $FeSO_4.7H_2O$ in quantity corresponding to the Fe^{II} concentration of 1.33 $\times 10^{-1}$ M. While for green rust, Fe^{III} concentration of 1.33 $\times 10^{-1}$ M and Fe^{II} concentration of 2.67 $\times 10^{-1}$ M was used. Both conditions lead to the final iron concentration of 0.4 M. This mixture was blended with appropriate amount of NaOH (1M). All samples were stirred for one hour in a gas tight reactor with continuous N_2 bubbling in aqueous solution in order to ensure the evacuation of dissolved oxygen and to avoid the oxidation of Fe^{II}. Final pH was 5.6 for magnetite batch and 6.25 for GR.

Table 1. Characteristics of the soil used.

Natural pH_{H2O}	8.0
CEC (meq/100 g)	15.1
Soil particle density (g/cm^3)	2.69
Clay content < 2µm (%)	29.4
Carbonates (%)	1.30
Organic carbon (%)	0.22
Ignition loss (%)	3.33
	(%)
SiO_2	76.2
Al_2O_3	9.90
Fe_2O_3	4.10
MgO	0.75
CaO	0.71
Na_2O	0.81
K_2O	1.86
TiO_2	0.86
P_2O_5	0.12

Column studies were conducted to evaluate the Fe^{II} induced transformations of FRS under flow through conditions. In a glass chromatographic column of 40 cm length and 2.6 cm internal diameter (XK 26/20, GE Healthcare), the FRS particles were packed to a height of 9.5 cm, corresponding to a dry mass of 76 g. The dry porous bed had a uniform bulk density ( ) of 1.23 ±0.01g/cm^3. After packing, the column was cautiously wetted upward with the background electrolyte solution (NaCl, 10^{-2} mol/L). Throughout the experiments, the flow rate was held constant at 0.5 ml/min, corresponding to a pore water velocity of 0.09 cm/min, the flow direction was from bottom to top of the column. Dissolved iron and aqueous silica concentrations in the outflow were measured by ICP-AES. The starting and resulting solids

from both batch and column tests (0.5ml/ minute) were characterized through X-ray diffraction (XRD), Mössbauer spectrometry and Transmission electron microscopy (TEM).

3. Results

3.1. Static batch conditions

In the presence of Fe^{II}, the poorly crystallized iron oxide, ferrihydrite, can be transformed either into green rust (Fe^{II}:Fe^{III}=2:1) or magnetite (Fe^{II}:Fe^{III}=1:2). The Mössbauer spectra of end-products of these transformations are shown in Figure 1. Mössbauer spectroscopy is a powerful technique for determining accurately the relative proportion of Fe^{II} and Fe^{III} species.

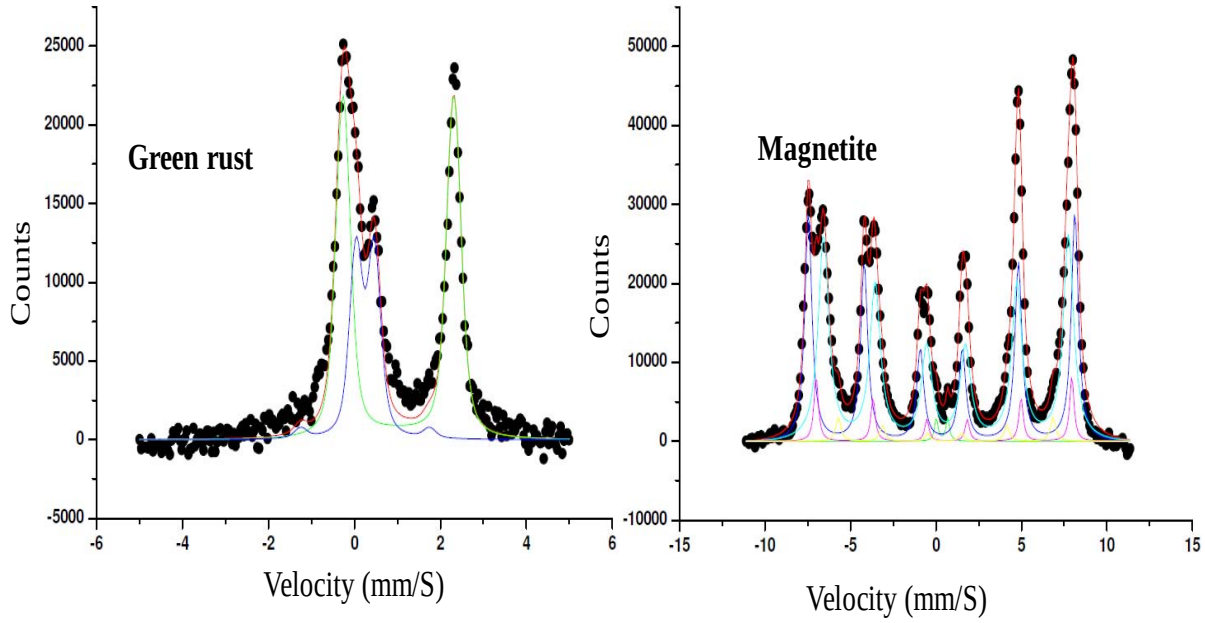

Figure 1. Mössbauer spectra of GR (A) and magnetite (B) generated through Fe^{II} reaction with Ferrihydrite.

The Mössbauer spectrum of figure 1a is essentially composed of two doublets with a ratio Fe^{II}: Fe^{III}=66:33, which could be attributed to green rust. The spectrum in figure 1b was fitted with two sextets assigned to magnetite, it is constituted by a superposition of two subspectra associated to the distribution of the iron in the octahedral and tetrahedral sites. The two valence states on octahedral sites are not distinguishable (valence $Fe^{2.5+}$) due to a fast electron hopping between Fe^{2+} and Fe^{3+} in octahedral sites. This magnetite is non-stoichiometric and

poorly crystallized. The same spectrum was obtained when ferrihydrite was initially mixed with sand quartz (i.e. FRS) & transformed to magnetite and GR.

Five diffraction peaks at 2θ = 21.2°, 35°, 41.2°, 50.4° and 62.8° are shown in the XRD diffractograms, which could be assigned to Fe_3O_4, magnetite (Fig. 2). The d-space values of theses main peaks were 2.53, 2.96, 2.09, 4.85 and 1.71 Å which may correspond to the more intense lines 311, 220, 400, 111 and 422, respectively of magnetite (Schwertmann & Cornell 2000). In addition to the diffraction peaks of magnetite, the transformation product of FRS showed the peaks of quartz represented by Q.

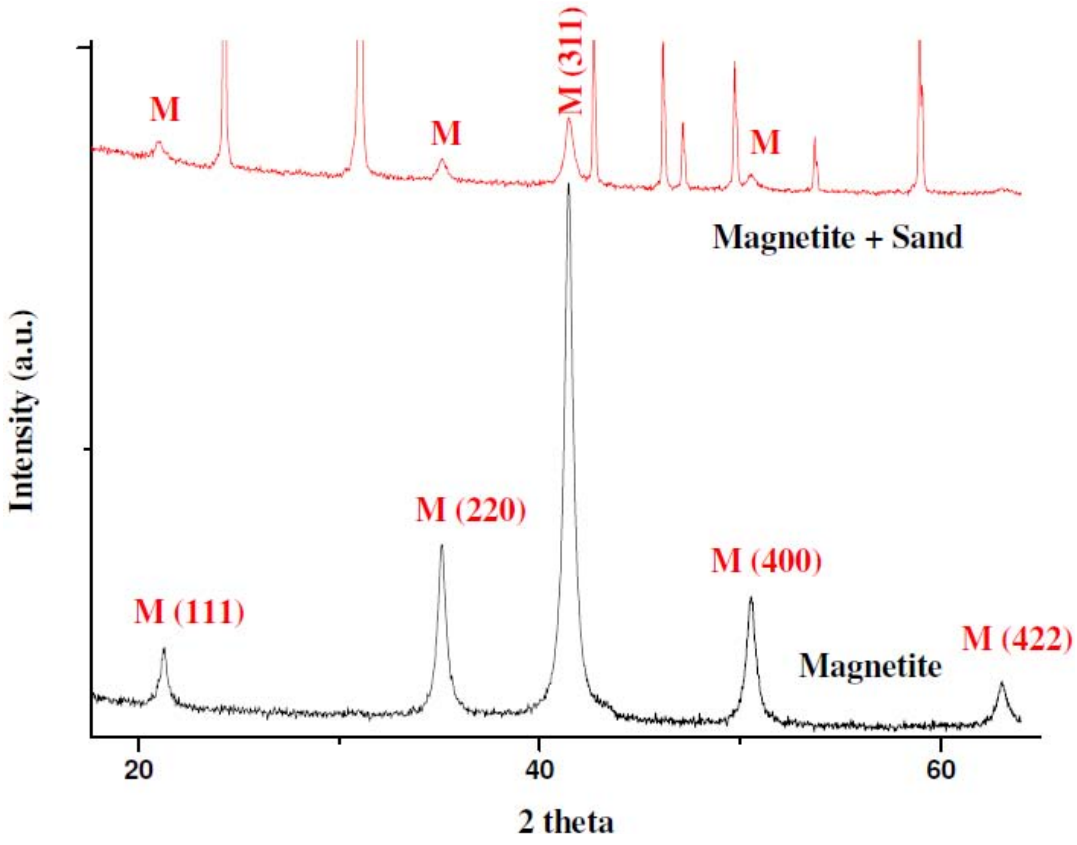

Figure 2. XRD for magnetite (from ferrihydrite) and magnetite with sand (from FRS).

Figure 3 shows the morphological features of the initial F substrate and final magnetite. It shows that particles of F are very small and strongly aggregated, which makes it almost impossible to identify single crystals in TEM. The TEM image for magnetite indicates that its particles are poorly crystallized and their size is not uniform. The shape of crystals varied from round to octahedral.

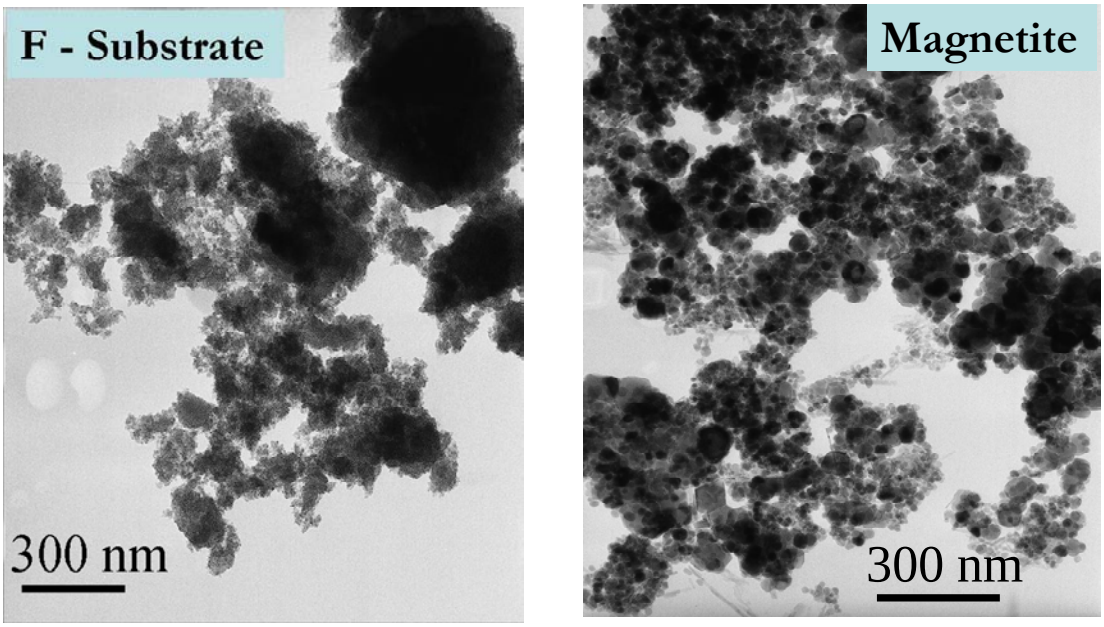

Figure 3. TEM of ferrihydrite and generated magnetite.

3.2. Saturated column test

In the column where Fe^{II} solution was injected in an open system, the FRS color was darkened at the bottom of the column, while it remained unchanged in the rest of column (i.e. red-brown; see Fig. 4 top). This color modification was noted after 2h corresponding to the injection of 4 porous volume of Fe^{II} (0.4mM) solution (pH~6.5) at flow rate of 0.5mL/min. Mössbauer and XRD analyses showed this black color was likely due to the formation of mixture of magnetite (Fe_3O_4) and goethite (α-FeOOH) (Fig. 4). A darkening was however observed in the whole column when Fe^{II} solution was injected in a closed loop system (see Fig. 4). No color stratification was noted. Mineralogical characterization of the latter showed that there are at least three mineral phases: untransformed ferrihydrite (proposed formula, $Fe_5HO_8{\cdot}4H_2O$), small quantities of magnetite (Fe_3O_4) and hematite (α-Fe_2O_3). Increasing crystallinity of Fe-oxide together with formation of Fe^{II} -mineral species were observed.

For soil column experiment, poor crystallinity and low concentrations of Fe oxides explain the difficulty in their identification and quantification by spectroscopic techniques. In addition, the reaction of Fe^{II} with soil iron oxides would be affected due to the high clay content of the soil used, which may uptake a significant amount of added iron. However chemical analyses showed an increase in the degree of crystallinity of Fe oxides. This

parameter was evaluated from the ratio of amounts of Fe extracted with oxalate-oxalic acid and with bicarbonate-citrate-dithionite mixtures. This step is crucial for the application of the above mentioned transformation processes in soil remediation by using the reactivity of Fe^{II}. Further study is still needed in order to optimize the reaction of Fe^{II} with soil iron minerals under flow through conditions.

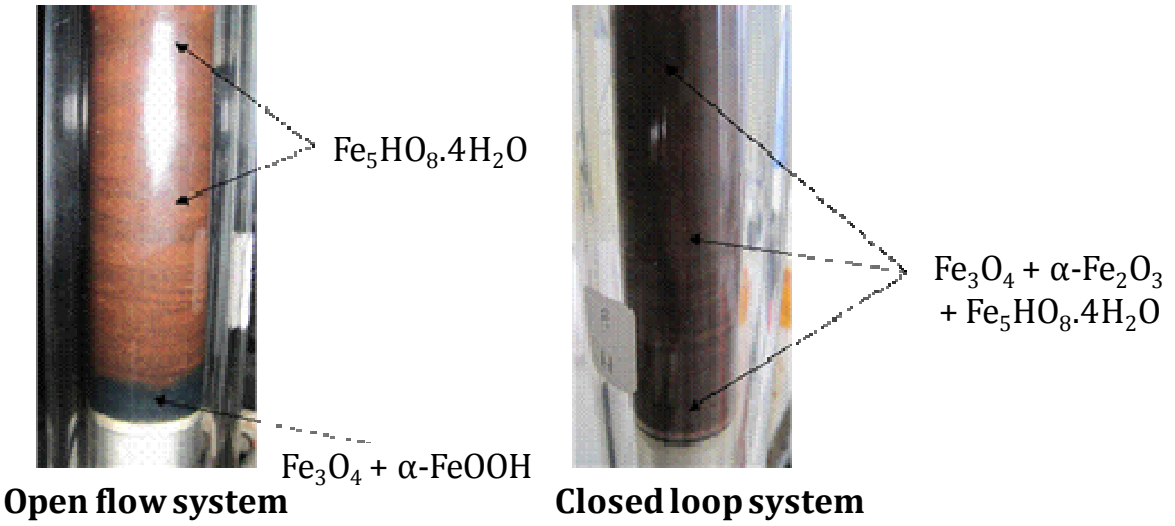

Figure 4. Pictures of FRS bed in columns.

4. Conclusions

Fe^{II}-induced mineralogical transformation of ferrihydrite involved the generation of more reactive iron (II) bearing minerals for remediation under batch test. Formation of Fe^{II} -mineral species as well as increasing crystallinity of Fe-oxides were however observed under flow through conditions. Fe^{II}-induced mineralogical transformation test in a pristine soil did not provide desired results, probably due to the low Fe soil content and air oxidation of the newly iron (II) formed. A current study is under progress to monitor ***in situ*** the mineral transformation using miniaturized Mössbauer spectroscopy implanted in the front of the column. These results have important implications in the understanding of biogeochemical processes of iron in environment and prediction of natural attenuation of environmental contaminants.

SECTION 2

REACTIVITY OF MAGNETITE TO CATALYZE CHEMICAL OXIDATION FOR HYDROCARBON REMEDIATION IN SOILS

Summary

Magnetite was used to catalyze chemical oxidation in this section. This section is composed of four articles. A brief summary of main results describing the reactivity of magnetite to catalyze chemical oxidation is presented below. For details, readers should refer to the articles presented in this section. Below are the titles of these articles:

- Application of magnetite catalyzed chemical oxidation (Fenton-like and persulfate) for the remediation of oil hydrocarbon contamination
- Remediation of PAH-contaminated soils by magnetite catalyzed Fenton-like oxidation
- Application of magnetite-activated persulfate oxidation for the degradation of PAHs in contaminated soils
- Magnetite as a catalyst for chemical oxidation of hydrocarbons spiked on sand under flow through conditions

A widespread pollution by polycyclic aromatic hydrocarbons (PAHs) and oil (aliphatic) hydrocarbons was caused by the intense use of fossil organic matter (petroleum and coal) since 18^{th} century for industrial purposes (petroleum extraction, refinery, coking plant, steel industries etc.) that cause environmental and health concerns. This problem is a serious hazard in Lorraine region of France. Different remediation techniques have been explored for their removal from complex matrices like soils or sediments. Among them, chemical oxidation treatments are showing great potential as viable remediation technology for rapidly treating contaminated soils.

The two oxidants tested in this study are H_2O_2 and persulfate, both of which require activation to produce stronger radicals. Fe^{II} can be used to activate both oxidants. But the optimum pH required for soluble Fe^{II} to act effectively as catalyst is very low (~3) which is its main limitation. Such a low pH is results in negative impact on soil quality and microbial community. Also it is impractical in soils because of their buffering capacity. But this low pH can be avoided by using iron minerals instead of soluble Fe^{II} to produce stronger radicals at circumneutral pH. Magnetite was found as the most reactive iron mineral to catalyze Fenton-like oxidation of other organic pollutants. Till now, the reactivity of magnetite has never been

tested to activate chemical oxidation for the remediation of PAHs and aliphatic hydrocarbons at circumneutral pH in contaminated soils.

This section reports the premier application of the magnetite to catalyze chemical oxidation (Fenton-like and persulfate) at circumneutral pH for the remediation of hydrocarbon contaminated soils. It could be an economically and environmentally feasible way for ***in-situ*** chemical oxidation (ISCO*)*. Hydrocarbon pollution of two types (PAHs and aliphatic hydrocarbons) was treated. Catalytic reactivity of magnetite was compared with that of soluble Fe^{II} under the same experimental conditions. Magnetite is considered as reactive due to the presence of structural Fe^{II}. But green rust (Fe^{II}: Fe^{III}= 2:1) contains two times more structural Fe^{II} than magnetite (Fe^{II}: Fe^{III}= 1:2). Thus green rust could be more reactive to catalyze chemical oxidation but magnetite was used as catalyst because of its excellent structural and catalytic stabilities and possibility to re-use for several oxidation cycles. Use of green rust exhibits however some constraints such as high solubility and instability in O_2 rich water and against air. Despite these constraints, the reactivity of GR to promote adsorption, reduction and Fenton-like oxidation have been studied in our lab at bench scale (Matta ***et al.***, 2008; Kone ***et al.***, 2009; Hanna ***et al.***, 2010a; Kone ***et al.***, 2011). One of these studies was co-authored by me (Kone ***et al.***, 2011). In addition, comparison of reactivity between magnetite and GR showed that GR is the most reactive compound of mixed valence Fe^{II}-Fe^{III} oxides (Hanna ***et al.***, 2010a). However, its fast oxidation and transformation into un-reactive compounds (ferrihydrite or goethite) when mixed with soil samples would have made its handling difficult for experiments. This ease of handling was provided by the highly stable magnetite.

In first part of this section (Usman ***et al.*** 2a, pp: 115-132) the degradation of oil hydrocarbons was investigated by magnetite catalyzed Fenton-like (FL) and activated persulfate (AP) oxidation. A magnetite rich sandy soil was spiked with (i) an organic extract from a soil contaminated by weathered oil (WO) and (ii) a fresh crude oil (CO) and was subjected to oxidation in batch slurry system at circumneutral pH. Contaminated soil was sampled from oil fields of Pechelbronne located in Alsace area of France. The WO abatement achieved after one week was 85% and 73% by FL and AP respectively. Higher oxidation efficiency was also observed for CO abatement (92% and 84% by FL and AP). Experiments conducted with or without soluble Fe^{II} as catalyst instead of magnetite caused only 10-15% of degradation.

Magnetite-catalyzed chemical oxidation was effective for the remediation of both weathered and crude oil.

In second part of this section (Usman ***et al***. 2b, pp: 133-156), oxidation experiments using H_2O_2 were conducted at circumneutral pH for the degradation of PAHs in two soils from ancient coking plant sites. These two soils (Homécourt (H) and Neuves Maisons (NM)) are located in Northeast of France (Lorraine region). Coking activities and steel industry had started on this site at the beginning of the 20th century and had ended in 1983.This site had also been used as a dump from 1953 to 1990. In the past 15 years, the slag resulting from previous industrial activities has been exploited. Various remediation treatments were tested on these soils by GISFI group including phytoremediation, bioremediation, air oxidation, thermal desorption, etc. Our contribution in these treatments is the magnetite-catalyzed chemical oxidation to treat PAHs contaminated soils. Oxidative degradation of PAHs was investigated at circumneutral pH. In first step, complete oxidation of a model PAH compound (Fluorenone) was achieved in the FL system, while it did not exceed 20% with or without Fe^{II} as catalyst. Negligible oxidation of PAHs was, however, observed in two PAHs polluted soils regardless of the catalyst used: ferrous salt or magnetite. When the soil organic extracts previously isolated from the soil were subjected to oxidation, more than 90% of PAHs degradation was obtained in FL treatment. If the organic extracts were oxidized in the presence of original soil matrix, almost 50% of PAHs removal efficiency was observed. When soils were treated with PAHs availability-enhancement agents such as ethanol or cyclodextrin prior to oxidation, about 15-20% of PAHs degradation was obtained. Almost the same results were obtained with AP in all treatments (Usman ***et al***. 2c, pp: 157-180). In all cases, application of soluble Fe^{II} as catalyst did not enhance the degradation as compared to treatment without Fe^{II}. Thus Fe^{II} was unable to act as catalyst at circumneutral pH. All these results point out the importance of catalyst type for oxidation, PAHs availability in soils and the soil matrix effect.

Then chemical oxidation of both hydrocarbon types (PAHs and aliphatic hydrocarbons) was investigated by FL and AP oxidation under flow through conditions (Usman ***et al***. 2d, pp: 181-190). Column experiments were designed to conduct oxidation of organic extracts from oil contaminated soil (WO soil) and two other PAHs contaminated soils (H and NM) that were spiked on magnetite rich sand. Significant abatement of both types of hydrocarbons (60-

70%) was observed by both FL and AP under flow through conditions. FL showed better degradation efficiency than AP in all experiments. No by-products were observed by FL oxidation but AP resulted in some oxygenated by-products.

Whatever the treatment (FL or AP), no by-products were observed by GC-MS and μFTIR in all batch slurry oxidation experiments which suggests the complete degradation of all hydrocarbons. Some by-products were exhibited by AP oxidation in column experiments while FL did not yield such by-products. Non-selective degradation was observed for FL which degraded all PAHs without preference. While AP showed a selective degradation with less efficiency towards high molecular weight n-alkanes in crude oil as well as high molecular weight PAHs in contaminated soils.

Results of this study suggest that magnetite can be used as iron source to activate both Fenton and persulfate oxidation at circumneutral pH. This study has important implications in the remediation of hydrocarbon polluted soils by ***in-situ*** chemical oxidation. But there are still questions about the ***in situ*** application of magnetite-catalyzed chemical oxidation.

Application of magnetite catalyzed chemical oxidation (Fenton-like and persulfate) for the remediation of oil hydrocarbon contamination

M. Usman[a,b], P. Faure[b], K. Hanna[c], M. Abdelmoula[a], and C. Ruby [a]

[a] LCPME UMR 7564, Nancy Université, CNRS, 405 rue de Vandoeuvre, 54600, Villers-lès-Nancy, France.

[b] G2R UMR 7566, Nancy Université, CNRS, BP 239, 54506, Vandoeuvre-lès Nancy, France.

[c] Ecole Nationale Supérieure de Chimie de Rennes, UMR CNRS 6226 "Sciences Chimiques de Rennes", Avenue du Général Leclerc, 35708 Rennes Cedex 7, France.

Abstract

The chemical oxidative degradation of oil hydrocarbons was investigated by magnetite catalyzed Fenton-like (FL) and activated persulfate (AP) oxidation. An artificial soil composed of silica sand and magnetite was synthesized and characterized by XRD and Mössbauer spectroscopy. This magnetite rich sandy soil (MRS) was then spiked with (i) an organic extract from a soil contaminated by weathered oil (WO) and (ii) a fresh crude oil (CO) and was subjected to oxidation in batch slurry system at circumneutral pH. Experimental results indicate that approximately 70-80% of WO removal was achieved by both FL and AP treatments after one week. Moreover significant CO abatement was also observed by both oxidants (80-90%). Non-selective degradation was evaluated for FL while AP showed less reactivity towards higher molecular weight n-alkanes. Experiments were also conducted with soluble Fe^{II} as catalyst instead of magnetite and only 10-15% of degradation was achieved for oxidation experiments with or without soluble Fe^{II} addition. Whatever the treatment (FL and AP), no by-products were observed after oxidation experiments which indicate the complete degradation of oil hydrocarbons. Results of this study suggest that magnetite can be used as iron source to activate both Fenton and persulfate oxidation at circumneutral pH. This study has important implications in the remediation of oil polluted soils by FL or AP oxidation.

Keywords: Soil; oil; magnetite; oxidation; Fenton; persulfate.

1. Introduction

The soil and groundwater pollution by oil compounds is a serious environmental and health concern worldwide. Soils contaminated with crude oil fail to support plant growth and are a source of groundwater contamination (Wang & Bartha, 1990). Due to the discovery of thousands of oil-contaminated sites, various remediation technologies have been developed using chemical (Ferguson *et al.*, 2004; Do *et al.*, 2010; Lu *et al.*, 2010a; Yen *et al.*, 2011), biological (Prince, 1993; Atlas, 1995; Chaîneau *et al.*, 2003; Franco *et al.*, 2004) and

combined approaches (Mater *et al.*, 2007; Lu *et al.*, 2010b). Bioremediation has proven to be successful in many applications to oil contaminated soils. It may remove the contaminants to a large extent as the majority of molecules in crude oil spills and refined products are biodegradable (Prince, 1993). However, bioremediation is often inefficient in lowering contamination level and long term soil toxicity below the stringent environmental cleanup standards reported by environmental regulations (Płaza *et al.*, 2005). Moreover, a complete mineralization of oil to CO_2 and H_2O cannot be achieved by soil microorganisms and always leaves more or less complex residues (Atlas, 1995). Also bioremediation has limited application to biorefractory materials especially asphaltenes (Gough & Rowland, 1990; Chaîneau *et al.*, 2003; Chaillan *et al.*, 2006). Chemical oxidation methods especially Fenton treatments are showing great potential as viable remediation technology for rapidly treating oil contaminated soils (Ferguson *et al.*, 2004; Lu *et al.*, 2010a; Lu *et al.*, 2010b; Yen *et al.*, 2011). Fenton treatments utilize the high reactivity of hydroxyl radical ($^{\bullet}OH$), a very reactive chemical species, which is generated through Fenton's reaction (Fenton, 1894):

$$Fe^{II} + H_2O_2 \rightarrow Fe^{III} + HO^- + HO^{\bullet} \quad (1)$$

This conventional Fenton's process is limited by the optimum pH (~3) and such low pH results in negative impacts on soil properties and quality and is incompatible with subsequent revegetation or biodegradation (Sahl & Munakata-Marr, 2006; Sirguey *et al.*, 2008). Iron minerals or organic chelating agents can be applied to extend its range of applicability at soil neutral pH (Watts & Dilly, 1996; Kong *et al.*, 1998a; Lu *et al.*, 2010a; Yen *et al.*, 2011). Iron minerals are used instead of soluble iron to produce hydroxyl radical for an efficient degradation of the organic molecules at circumneutral pH and the process is known as Fenton-like oxidation. This process may be especially advantageous for *in situ* remediation of contaminated matrices where pH cannot be adjusted. A more recent alternative oxidant used for oxidation is persulfate ($S_2O_8^{2-}$) (Do *et al.*, 2010; Yen *et al.*, 2011). Persulfate anion ($S_2O_8^{2-}$) is a strong oxidant (E^0 = 2.01 V), but kinetically slow in destroying most of organic contaminants (Osgerby, 2006). The persulfate anion can be chemically or thermally activated to generate the intermediate sulfate free radical ($SO_4^{\bullet-}$) oxidant which is stronger oxidant (E^0 = 2.6 V) than the persulfate anion. In addition to its oxidizing strength, persulfate oxidation has several advantages over other oxidant systems. The $SO_4^{\bullet-}$ radical is more stable than the hydroxyl radical and thus able to transport greater distances in the sub-surface where it can persist for weeks (Huang *et al.*, 2002). Moreover, persulfate show less affinity for natural soil

organics than does the permanganate ion (Brown & Robinson, 2004) and is thus more efficient in high organic soils. Generation of sulfate free radical by Fe^{II} activation is achieved through the following reaction.

$$S_2O_8^{2-} + Fe^{II} \rightarrow SO_4^{\bullet -} + SO_4^{2-} + Fe^{III} \quad (2)$$

In case of heterogeneous catalysis, iron minerals can be used to activate both oxidants to produce stronger radicals in order to degrade pollutants at circumneutral pH. Magnetite, mixed Fe^{II}-Fe^{III} oxide was found to be the most effective catalyst as compared to only Fe^{III} oxides for the chemical oxidation of petrol hydrocarbons (pH=3) (Kong *et al.*, 1998a) and other organic pollutants (Matta *et al.*, 2007; Hanna *et al.*, 2008; Yan *et al.*, 2010) because of the presence of Fe^{II} in its structure. In soils and sediments, iron is mainly found as Fe^{III} and ferrihydrite is the most abundant Fe^{III} oxyhydroxide. Therefore its transformation into magnetite constitutes the first part of this study and its characterization was done through XRD, Mössbauer spectroscopy and scanning electron microscopy. To date, the reactivity of magnetite has not been explored in heterogeneous catalysis of chemical oxidation for oil degradation at circumneutral pH. The main objectives of this study were to: 1) evaluate the feasibility of magnetite to activate hydrogen peroxide and persulfate for oil removal, 2) determine the efficiency of oxidation to degrade both weathered and fresh crude oil. For this purpose, batch experiments were conducted to evaluate the reactivity of this newly-generated magnetite to catalyze Fenton-like and persulfate oxidation. Both oxidants were tested for the degradation of weathered oil (WO) present in organic extract from an oil contaminated soil under natural attenuation and a fresh crude oil (CO). The oxidation was studied versus time and organic analyses were performed by GC-MS, GC-FID and µFTIR.

2. Experimental Section

2.1. Chemicals

Fresh crude oil (CO) was provided by "Le Musée du Pétrole" (Pechelbronn, France), Survey 2962. Ferric chloride hexahydrate ($FeCl_3.6H_2O$), ferrous sulfate heptahydrate ($FeSO_4.\ 7H_2O$) and sodium persulfate ($Na_2S_2O_8$) were purchased from Sigma-Aldrich Co. Hydrogen peroxide 35% (H_2O_2) was obtained from Acros Organics. Dichloromethane (DCM) and chloroform were purchased from VWR and used as received. Fontainebleau sand, with a grain size range

of 150–300 μm (mean diameter 257 μm) obtained from VWR (Van Waters and Rogers) was used. The mineralogy of the sand was characterized by X-ray diffraction and was found to be exclusively quartz. Deionized water was produced with a Milli-Q system from Millipore.

2.2. Synthesis and characterization of magnetite rich sandy soil (MRS)

The 2-line ferrihydrite (F) was synthesized according to the method of Schwertmann and Cornell (Schwertmann & Cornell, 2000). It was prepared by neutralizing a 0.2 M ferric chloride solution with 1 M NaOH to a pH of 7–8. Synthesis of ferrihydrite rich sandy soil (FRS) was done as explained earlier (Hanna, 2007) by using 10g of ferrihydrite and 90g of sand (10% w/w). Then FRS was transformed into magnetite rich sandy soil (MRS) by taking its amount equivalent to a Fe^{III} concentration of 0.267 M followed by the addition of $FeSO_4.7H_2O$ in quantity corresponding to the Fe^{II} concentration of 0.133 M leading to the final iron concentration of 0.4 M. An appropriate amount of NaOH (1M) was then added to the mixture to provide the ratio n (OH^-) / n (Fe^{III}) = 1 where n represents the number of moles. These conditions are required to form stoichiometric magnetite ($Fe^{II}\,Fe^{III}_2\,O_4$) with a Fe^{II}: Fe^{III} ratio of 1:2. The suspension was stirred for two days, centrifuged and solid was dried. All experiments to synthesize MRS (10% w/w) were conducted in glove box, an anoxic chamber (N_2:H_2= 98:2).

2.3. Iron mineral characterization

In order to identify the crystal structure of minerals, solid samples were analyzed by X-ray powder diffraction (XRD). The XRD data were collected with a D8 Bruker diffractometer, equipped with a monochromator and a position-sensitive detector. The X-ray source was a Co anode (= 0.179 nm). The diffractograms were recorded in the 3‑64° 2θ range, with a 0.0359° step size and a collection of 3 s per point.

Solid samples were also analyzed by Mössbauer spectroscopy. Reflection Mössbauer spectroscopy using the miniaturized Mössbauer spectrometer MIMOS II (Klingelhöfer *et al.*, 1996) has been employed to determine the oxidation state of iron and the iron mineralogy of the samples. The filtered samples were inserted into a ~ 3 cm^2 holder specially designed to perform Mössbauer reflexion analyses at room temperature. Reemitted backscattered γ-rays

(14.4 keV) were selected by four Si-PIN-diodes detectors. Centre shifts *CS* were reported with respect to that of α-Fe at room temperature. Mössbauer spectra were computer-fitted with either a sum of Lorentzian shape lines or a Voigt profile analyses.

The surface morphological characterization of solid samples was done by Scanning Electron Microscopy (SEM) using a HITACHI FEG 54800 apparatus. The solid powder was glued on an adhesive surface and metalized with a thin layer of gold. SEM studies were performed in backscattered mode to identify the elemental differences on the surfaces and thus estimate the location of coated and non-coated surfaces.

2.4. Sample preparation

This focuses on: 1) weathered oil (WO) isolated from an oil contaminated forest soil under natural attenuation from Pechelbronn oil field (Alsace, France) and 2) Pechelbronn crude oil (CO) corresponding to type III oil (reference). For WO organic extract, oil-contaminated soil samples were freeze-dried, sieved at 2 mm and extracted using an automatic extractor Dionex® ASE 200 (Accelerated Solvent Extractor) at 100° C and 130 bars with dichloromethane (DCM). CO was previously "dried" under N_2 flow in order to remove volatile compounds and dissolved in DCM. To avoid cross contamination, before use, all vessels were rinsed with DCM.

The MRS was spiked by adding WO and CO to obtain a final concentration of 4000 mg/Kg of MRS. The DCM was allowed to evaporate with a continuous mixing to ensure homogeneous contaminant distribution. This spiked sand was considered as reference (T_0).

2.5. Oxidation experiments

The oxidative degradation of oil hydrocarbons was conducted by using two oxidants: H_2O_2 and persulfate with two catalysts (magnetite and soluble Fe^{II}). Here is the detailed description of treatments including: *i)* Fenton-like (FL = H_2O_2 + magnetite), *ii)* Fenton (F = H_2O_2 + soluble Fe^{II}), *iii)* H_2O_2 without iron activation (HP), *iv*) activated persulfate (AP- sodium persulfate + magnetite) v) sodium persulfate + soluble Fe^{II} (P) and vi) sodium persulfate without iron activation (SP). Oxidation was performed with oxidant:Fe molar ratio equal to 10:1 (H_2O_2) and 1:1 (persulfate) in soil slurry. Batch series were prepared by assigning one batch for each time point (1 hour, 6 hours, 24 hours, 48 hours and 1 week) to study the kinetic

degradation. In the standard procedure, slurries were prepared by adding water to solid matrix (2 g for sand); the amount of water to be added was determined in order to have a final solution volume (including the oxidant volume to be added) of 20 mL. After stirring the suspension for 15 minutes, the H_2O_2 oxidant or sodium persulfate was slowly added. The slurries were treated for specified reaction times under vigorous magnetic-stirring. After specified reaction time, corresponding batch was withdrawn from the series and was frozen to stop reaction. After two days, the samples were freeze dried to remove water. All experimental runs were performed within a temperature range of 20–25 °C without light obtained by aluminum foil coverings to avoid any photolytic degradation. The pH was adjusted at 6.7 ± 0.3 during the whole course of oxidation for all experiments. Blank experiments were carried out on spiked MRS under the same conditions except no oxidant was added, to study possible desorption or degradation of the pollutants.

2.6. Instrumental analysis

The freeze dried samples were extracted in chloroform during 45 min at 60°C. The organic extract volume was reduced to 20 mL under nitrogen flow and 5mL of the solution was dried and weighed to determine the amount of extractable organic matter (EOM).

The hydrocarbon oil index (IH) was measured according to ISO 16703:2004 procedure using a GC-FID 7890 Agilent technologies

GC-MS quantification of reactant and products were performed by adding internal standards to the samples. An internal n-alkanes standard mix ($C_{16}D_{34}$, $C_{20}D_{42}$, $C_{24}D_{50}$, and $C_{30}D_{62}$) as well as an internal deuterated PAHs standard mix (naphthalene-d_8, acenaphthene-d_{10}, phenanthrene-d_{10}, chrysene- d_{12}, and perylene-d_{12}, supplied by Cluzeau) were added. A 2 μL amount of solution was then injected into an Agilent 5890 gas chromatograph equipped with a DB 5-MS (length: 60 m; diameter: 250 µm) capillary column coupled to an Agilent 5973 Inert mass spectrometer operating in full scan mode. The temperature program was the following: 60 to 250 °C at 15 °C min^{-1}, then 250 to 315 °C at 3 °C min^{-1}, and 60 min holds at 315 °C. The carrier gas was helium at 1.5 mL min^{-1} constant flow.

The micro Fourier Transform Infrared (µFTIR) spectroscopic analysis were performed on an infrared spectrometer Bruker IFS55 coupled with a Multipurpose Bruker IR microscope

equipped with a MCT detector cooled with liquid N_2. EOM were analyzed as described by (Faure *et al.*, 1999) using a diamond window. The spectra were recorded with the following conditions: size of the analyzed area 60 μm^2, 64 accumulations (32 s), spectral resolution 4 cm^{-1}, gain 4.

3. Results and Discussion

3.1. Characterization of magnetite rich sand (MRS)

The iron oxide rich sand was characterized by XRD (Fig. 1a) and Mössbauer spectroscopy (Figure 1b). The XRD diffractograms of the initial ferrihydrite rich sand (Fig. 1a, FRS) show only the peaks corresponding to quartz. As ferrihydrite is very poorly crystallized Fe oxide, no corresponding peaks can be identified in the presence of quartz. After transformation reaction with Fe^{II} (Fig. 1a, MRS), the occurrence of magnetite was evidenced by the main peaks corresponding to magnetite (Schwertmann & Cornell, 2000). The results were confirmed by Mössbauer spectroscopy that reveals the doublets of ferrihydrite in the FRS and sextets corresponding to magnetite in MRS (Fig. 1b). Almost all the ferrihydrite was transformed into magnetite as only the sextets corresponding to magnetite were observed in MRS.

Investigations through SEM were carried out in backscattered mode on the FRS before (Fig. 1c-FRS) and after its transformation into MRS (Fig.1c-MRS). The grains of silica sand which exhibit elements with low atomic number such as Si are grey as observed in Fig. 1c. However, the white patches on these grains are indicative of the coating which contains elements of high atomic number i.e. Fe. Free white particles of iron were also observed as the FRS contains high contents of ferrihydrite (10% w/w), since the maximum of ferrihydrite sorbed on the surface of Fontainebleau sand lies at ~ 6 mg/ g of sand (Hanna, 2007).

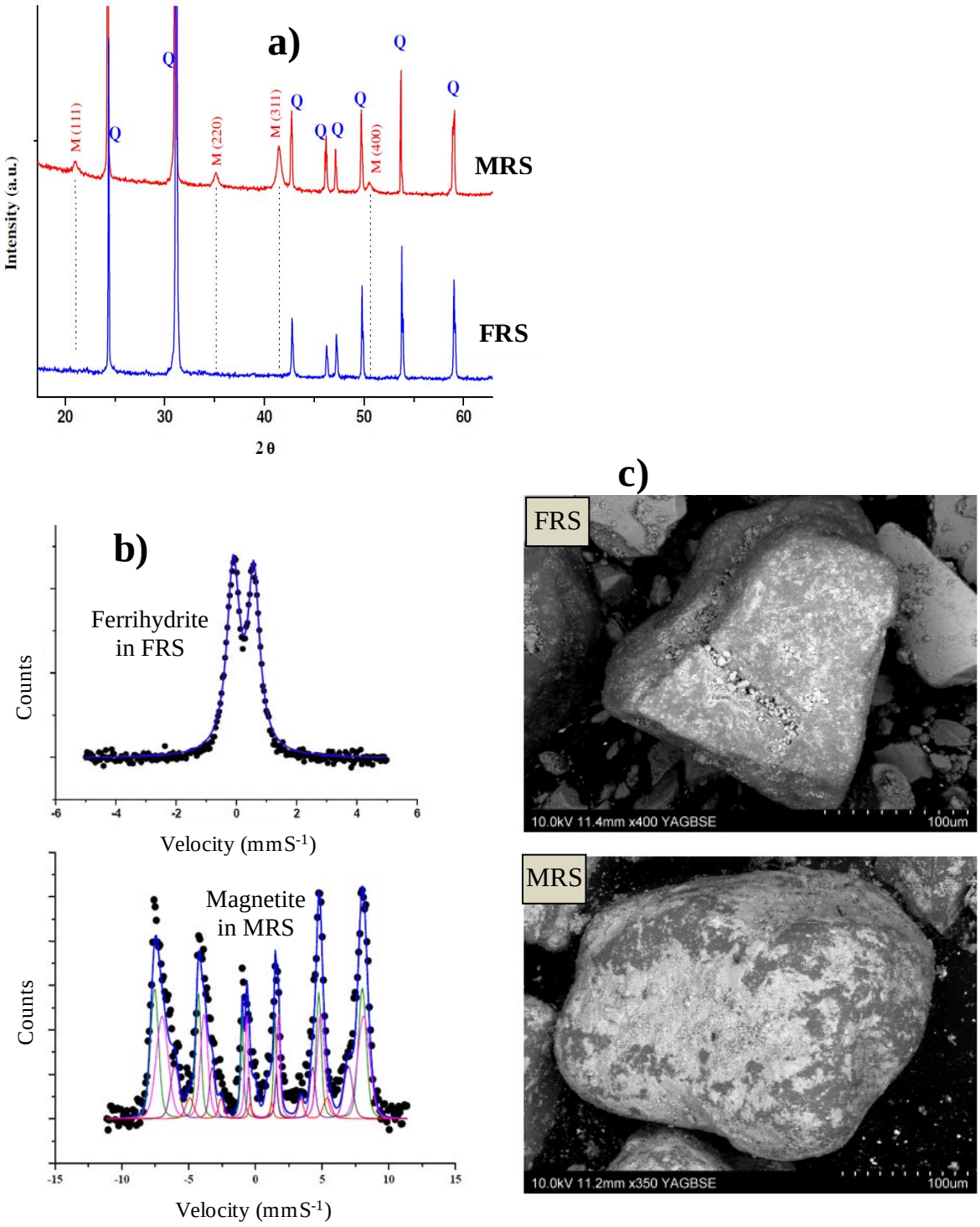

Figure 1: XRD diffractograms (a), Mössbauer spectra (b) and SEM characterization (c) of initial ferrihydrite rich sandy soil (FRS) and its transformation product magnetite rich sandy soil (MRS). Almost all ferrihydrite was transformed into magnetite.

3.2. Kinetic degradation of oil hydrocarbons

3.2.1. Extractable organic matter (EOM) and hydrocarbon index (HI)

In order to determine the effectiveness of oxidation for oil-hydrocarbons degradation, experiments were performed by using H_2O_2 or persulfate catalyzed by magnetite or soluble Fe^{II}. The EOM evolution was obtained by the weight of extract before and after oxidation. m/m_0 was plotted against time where m is the mass at specific time point while m_0 is the mass at T_0 (figure 2). The EOM recovered at T_0 was ~4mg/g (initially added amount) representing the complete recovery of EOM from MRS. Due to very low organic carbon contents of MRS after extraction, total organic carbon (TOC) analyses cannot be performed. Complete recovery of organic matter from the sand indicates that no carbon was trapped in sand and ultimately there is no effect of matrix (quartz sand) as observed elsewhere (Ghislain ***et al.***, 2010). Analyses of extracted organic solutions by Gel Permeation Chromatography (data not shown) did not show any change in molecular weight underscoring the absence of carbon condensation in matrix. Blank experiments (conducted in the absence of any oxidant) revealed almost negligible degradation (<3%). Significant reduction (80-90%) in EOM was obtained for WO (Fig. 2a) and CO (Fig. 2b) by FL and AP when magnetite was used as catalyst. Both oxidants did not show the same trend of EOM evolution. Indeed, the reaction of FL seems to be faster than AP. The experimental data did not fit with any kinetic model. Hydrocarbon index (HI) determined by GC-FID (Fig. 3) was in accordance with EOM calculations. It was observed that approximately 84% of WO removal was achieved by FL in the course of one week of oxidation as compared to 73% by AP. Significant degradation was also observed for CO oxidation by both FL (92%) and AP (83%). For both pollution types, magnetite was highly reactive to catalyze chemical oxidation of oil contaminants. Although H_2O_2 and persulfate oxidants can be activated by Fe^{II} as widely reported in literature (Lu ***et al.***, 2010a; Yen ***et al.***, 2011), low degradation (10-15%) was achieved in these experiments (F and P). This is probably due to the precipitation of added Fe^{II} at circumneutral pH (6.7) which prevents the soluble Fe^{II} to act as catalyst. It should be noted that approximately the same degradation (10-15%) was achieved for oxidation without iron addition (HP and SP). This similar degradation extent with and without soluble Fe^{II} activation reveals the unavailability of soluble Fe^{II} to act as catalyst under tested experimental conditions.

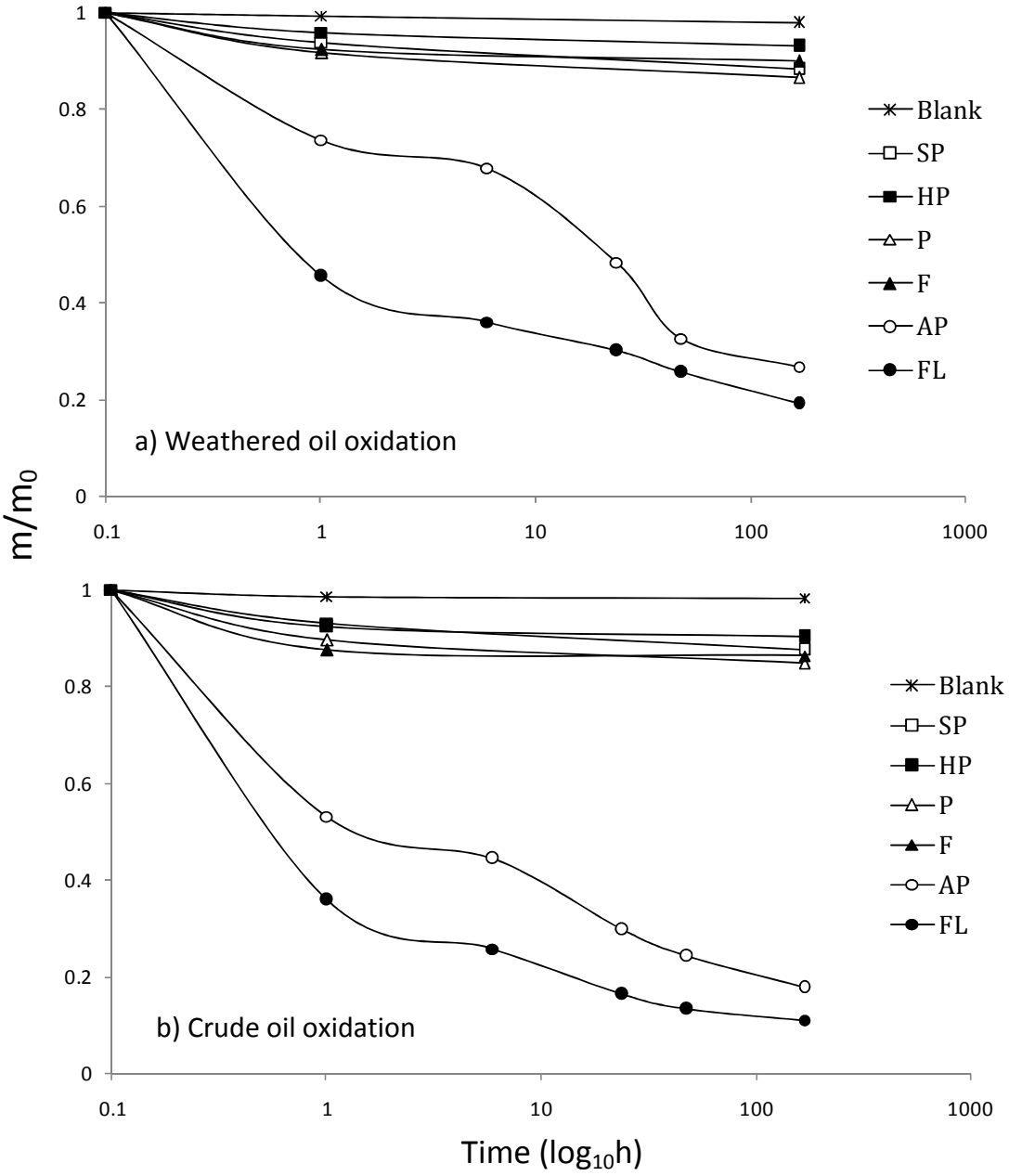

Figure 2: Extractable organic matter (EOM) evolution during oxidation experiments for (a) organic extract containing weathered oil (WO) and (b) crude oil (CO) by: H_2O_2 with magnetite activation (FL-●), sodium persulfate with magnetite activation (AP-○), H_2O_2 with soluble Fe^{II} activation (F-▲), sodium persulfate with soluble Fe^{II} activation (P-Δ), hydrogen peroxide without iron activation (HP-■), sodium persulfate without iron activation (SP-□) and blank (⁎). This evolution is represented in terms of m/m_0 where m is the amount of EOM at specified time and m_0 is EOM at T_0.

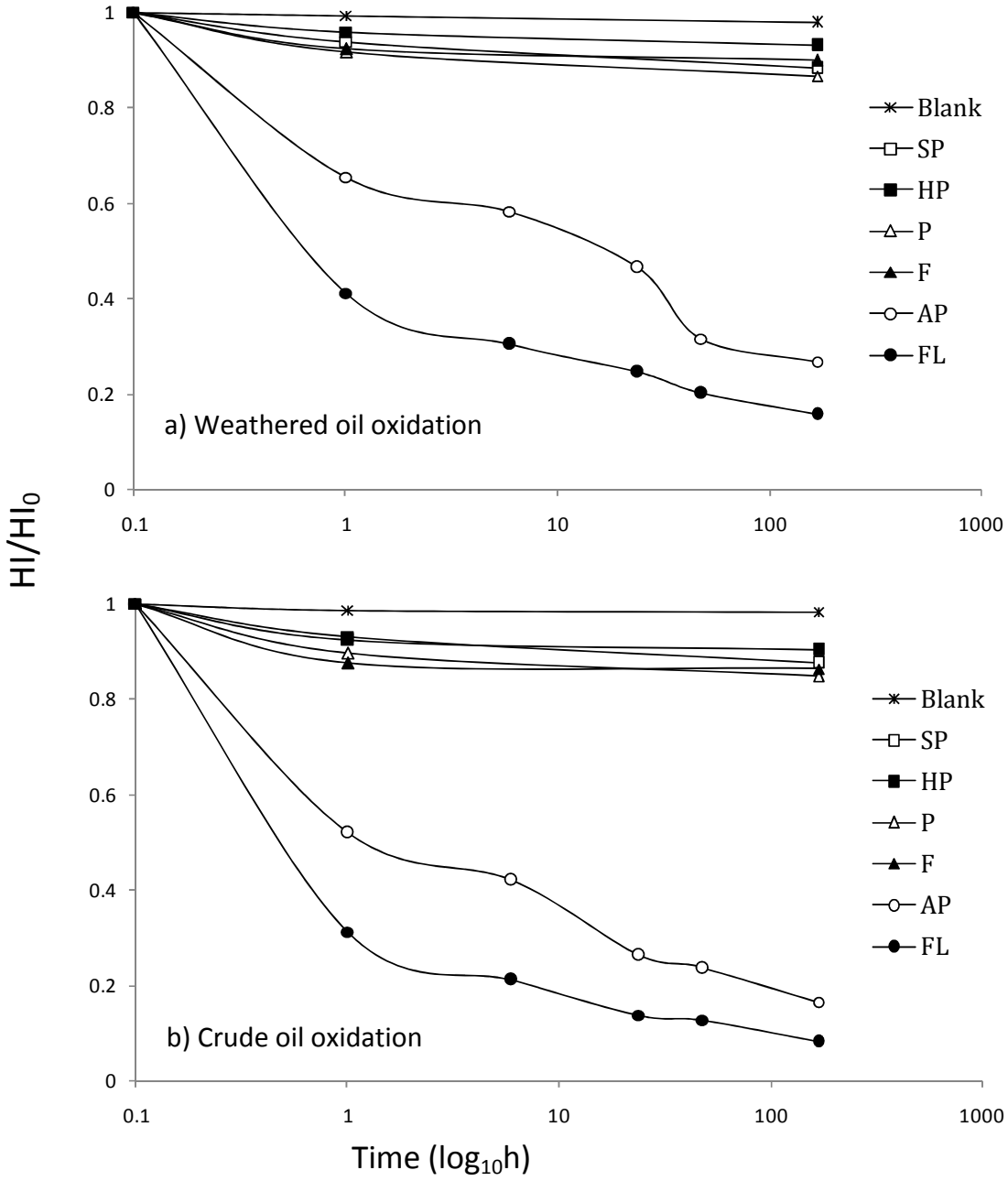

Figure 3: GC-FID measured Hydrocarbon index (HI) evolution during oxidation experiments for (a) organic extract containing weathered oil (WO) and (b) crude oil (CO) by: H_2O_2 with magnetite activation (FL-●), sodium persulfate with magnetite activation (AP-○), H_2O_2 with soluble Fe^{II} activation (F-▲), sodium persulfate with soluble Fe^{II} activation (P-Δ), hydrogen peroxide without iron activation (HP-■), sodium persulfate without iron activation (SP-□) and blank (⁎). This evolution is represented in terms of HI/HI_0 where HI is the HI value at specified time and HI_0 is the value at T_0.

The GC-FID chromatograms for WO (Fig. 4a) represents the existence of a large area of the raised baseline hump describing an intense unresolved complex mixture (UCM) for T_0 generally considered as an iso- and cyclo-alkanes mixture (Gough & Rowland, 1990). The sampled soil area was under natural attenuation for years which cause the degradation of n-alkanes that are easily biodegradable (Chaillan ***et al.***, 2006). As UCM is totally refractory to microbial attack (Gough & Rowland, 1990; Chaillan ***et al.***, 2006) so it existed as the sole reactant in T_0. In this study, a significant UCM degradation was found by both oxidants FL and AP (Fig. 4a). GC-FID chromatograms representing the CO oxidation are presented in Fig. 4b. CO was rich in n-alkanes along with pristane and phytane (Fig. 4b, T_0). The n-alkanes distribution was decreased prominently for both oxidants with time. Thus, the oxidation was found effective for the hydrocarbons resistant to biodegradation (UCM) as well as main constituents of the crude oil (n-alkanes).

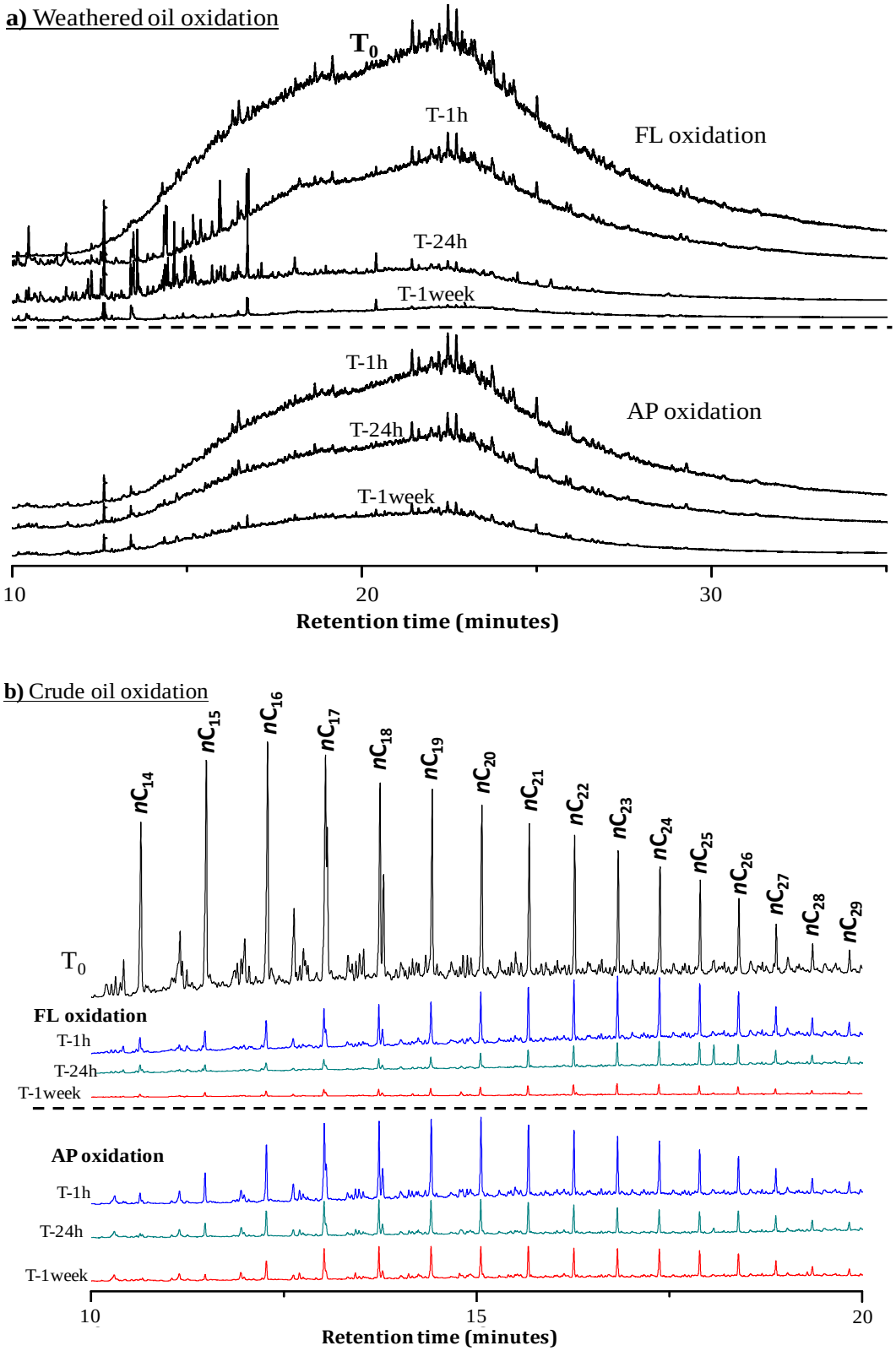

Figure 4: GC-FID chromatograms of (a) weathered oil-WO and (b) crude oil-CO before (T_0) and after oxidation (1hour, 24hours and 1week) by Fenton-like (FL- H_2O_2 with magnetite activation) and activated persulfate (AP- sodium persulfate with magnetite activation). Intensities of chromatograms are proportional to the oil concentration.

3.2.2. GC-MS characterization

The oxidation experiments on CO (rich in n-alkanes) allow us to observe the degradation of individual n-alkanes by both oxidants. This is not possible in WO due to the intense abundance of UCM that is difficult to characterize by GC-MS. Thus only the molecular characterization of CO was performed by GC-MS in the course of oxidation (Fig. 5). For T_0, the sum of n-alkanes was 3200 µg/g with a ratio of low molecular weight n-alkanes (LMW: sum of C_{13}-C_{20} concentrations) to higher molecular weight n-alkanes (HMW: sum of C_{21}-C_{30} concentrations) LMW/HMW of 2.63 suggests the predominance of LMW-n-alkanes. The FL reduced the n-alkanes sum to 200 µg/g (LMW/HMW= 0.69) as compared to 542 µg/g (LMW/HMW= 0.80) by AP after one week of oxidation. AP exhibited a selective behavior as the HMW-n-alkanes (C_{31}-C_{36}) showed almost negligible degradation. On the contrary, these molecules were fully disappeared at the end of experiment by FL. The degradation extent obtained by GC-MS (>80%) confirmed the EOM results (Fig. 2b) and GC-FID data (Fig. 3b). GC-MS molecular analysis of the n-alkanes distribution in crude oil does not represent any difference in the chromatograms from the two oxidation systems of existing molecules (chromatograms not shown). No new reaction products were detected after oxidation indicating the removal of oil hydrocarbons principally by mineralization processes and probably by volatilization for low molecular mass compounds due to the experimental device (open batch system). Moreover, the parallel evolution of the HI and the EOM suggests that no condensation processes and stabilization in mineral matrix occur. Indeed, such condensation leads to an increase in the molecular mass of organic compounds (Ghislain ***et al.***, 2010) not observed at molecular level (Fig. 4) in our experiments whatever the oxidant used.

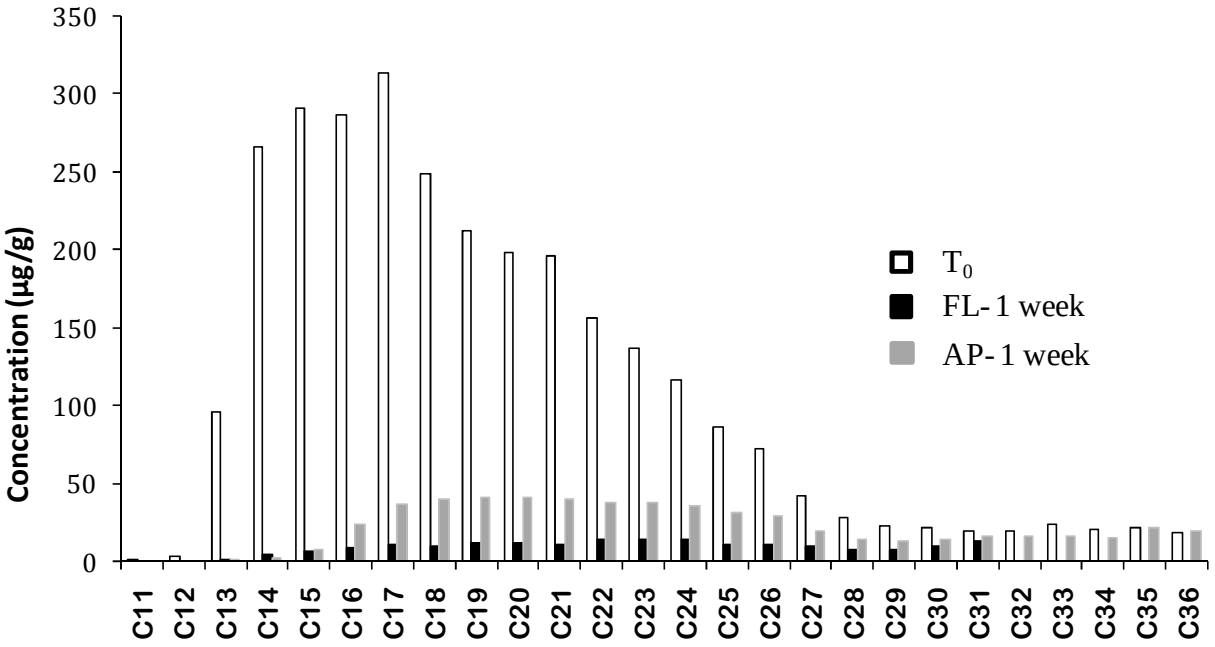

Figure 5: Molecular distribution obtained by GC-MS for crude oil (CO) before (T_0) and after 1 week of oxidation by Fenton-like (FL- H_2O_2 with magnetite activation) and activated persulfate (AP- sodium persulfate with magnetite activation)

3.2.3. µFTIR characterization

Investigations by µFTIR revealed that WO and CO organic extracts are dominated by aliphatic bands (CH_{ali} : 3000 – 2800 cm^{-1} and ΔCH_{ali} : 1470 – 1360 cm^{-1}) with a CH_3/CH_2 ratio values weaker for WO compatible with the predominance of iso and cyclo-alcanes (UCM). The occurrence of the $r(CH_2)_n$ band (720 cm^{-1}) only in CO confirms the presence of long aliphatic chains in the fresh oil. After, oxidation, spectra remain almost unchanged except the appearance of one weak oxygenated band (C=O: 1745 – 1705 cm^{-1}) in all samples whatever the oxidant (Fig. 6). This oxygenated band represents a limited intensity compared to other bands (especially aliphatic bands) and suggests minor chemical changes in the remaining organic fractions as significant degradation (>80%) has occurred. Both oxidants $^{\bullet}OH$ and $SO_4^{\bullet-}$ attack organic compounds in a different way: •OH is more likely to do it through hydrogen abstraction or addition while $SO_4^{\bullet-}$ participates in electron transfer reactions (Minisci ***et al.***, 1983). Thus different intermediates may be obtained when they react with oil hydrocarbons but in this study, minor structural modification revealed by FTIR spectra suggests that no significant intermediate products were formed. It suggests the complete degradation of oil hydrocarbons.

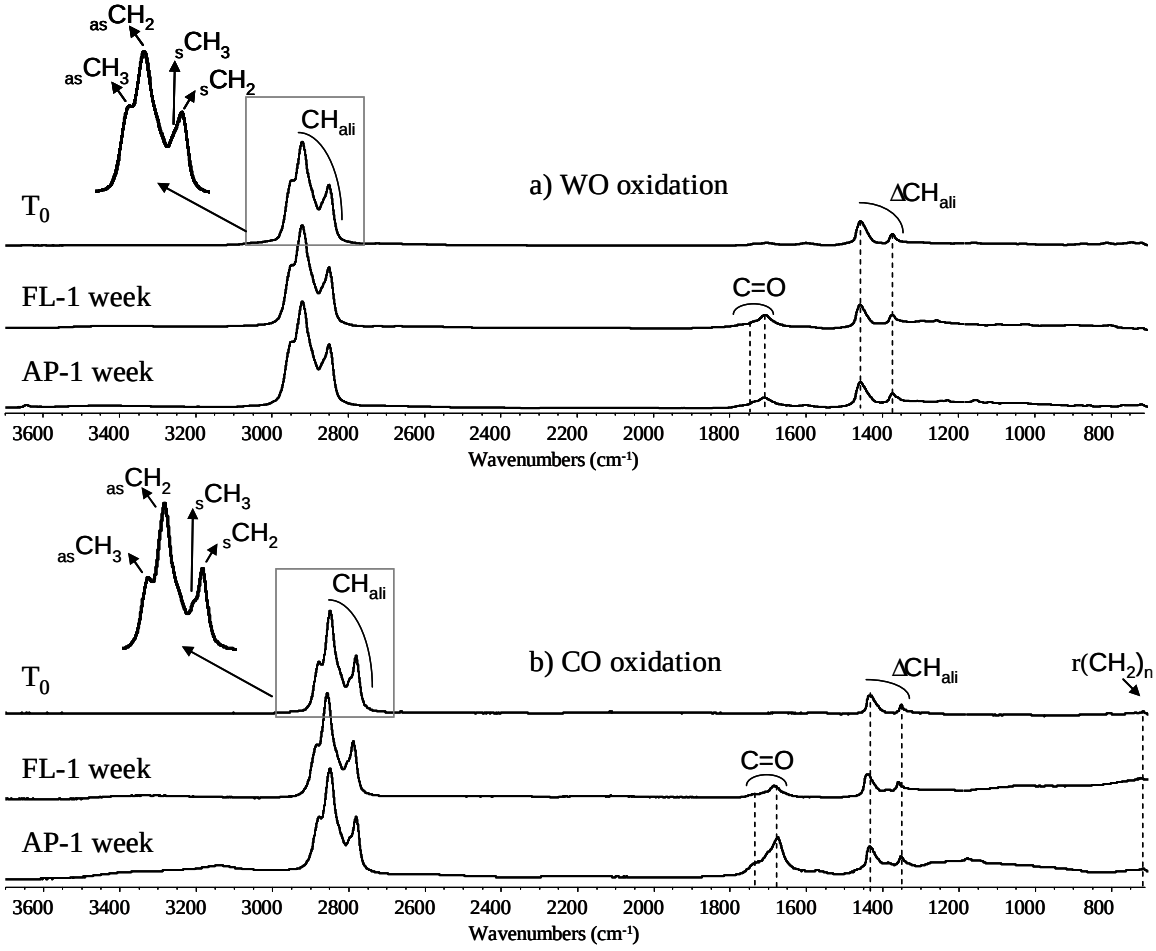

Figure 6: FTIR spectra of (a) WO- weathered oil and (b) CO- crude oil before (T_0) and after oxidation (1week) by Fenton-like (FL- H_2O_2 with magnetite activation) and activated persulfate (AP- sodium persulfate with magnetite activation).

Conclusion

This study reported the ability of magnetite to catalyze Fenton and persulfate oxidation in order to destroy refractory oil residues (UCM, etc.) as well as normal n-alkanes in a highly contaminated soil. All results (GC-FID, GC-MS and EOM mass balance) indicated the high degradation (>80%) by both oxidants when magnetite was used as catalyst (FL and AP) at circumneutral pH. Soluble Fe^{II} was found unable to activate H_2O_2 (F) and persulfate (P) under our experimental conditions as the presence or absence of soluble Fe^{II} caused the same low

degradation (10-15%). Non-selective degradation was achieved by FL while AP showed less reactivity towards high molecular weight n-alkanes. Both oxidants greatly reduced the contamination level without significant by-products. This highlights the role of magnetite to promote chemical oxidation of oil contamination, which should be addressed in real systems. This study has important implications in the remediation of polluted soils by using the reactivity of synthetic or endogenous iron as a feasible source of iron catalyst to promote chemical oxidation.

Acknowledgements

The authors gratefully acknowledge the financial support of the GISFI (French Scientific Interest Group - Industrial Wasteland, www.gisfi.prd.fr) project.

Remediation of PAH-contaminated soils by magnetite catalyzed Fenton-like oxidation

M. Usman[a,b], P. Faure[b], C. Ruby [a] and K. Hanna[c]

[a] Laboratoire de Chimie Physique et Microbiologie pour l'Environnement, LCPME, UMR 7564 CNRS-Université de Lorraine, 405 rue de Vandoeuvre, 54600, Villers Les Nancy, France.

[b] Géologie Géologie et Gestion des Ressources minérales et énergétiques, G2R, UMR 7566, CNRS-Université de Lorraine, 54506, Vandoeuvre Les Nancy, France.

[c] Ecole Nationale Supérieure de Chimie de Rennes, UMR CNRS 6226 "Sciences Chimiques de Rennes", Avenue du Général Leclerc, 35708 Rennes Cedex 7, France.

Abstract

This is the premier study reporting the degradation of polycyclic aromatic hydrocarbons (PAHs) through Fenton-like oxidation catalyzed by magnetite. Kinetic degradation of PAHs was studied at circumneutral pH by treatments: (i) H_2O_2 + soluble Fe^{II} (F), (ii) H_2O_2 + magnetite as iron source (FL) and (iii) H_2O_2 alone without catalyst (HP). Results show that oxidation of a model PAH compound (Fluorenone) spiked on sand resulted in its complete removal by FL treatment but degradation did not exceed 20% in HP or F systems. However, in two PAHs polluted soils (sampled from coking plant sites), negligible oxidation of 16 PAHs was observed regardless of the catalyst used: soluble Fe^{II} or magnetite. Then organic extract separated from these soils was added to sand and after evaporation of the solvent, oxidation was performed which resulted in more than 90% of PAHs removal by FL as compared to 15% by F or HP systems. These removal extents decreased by a factor of two when the organic extracts were oxidized in the presence of original soil. PAHs degradation extent was improved in soils pre-treated with availability-enhancement agents such as ethanol or cyclodextrin. Degradation was non-selective and no by-products were observed by GC-MS and µFTIR. Treatment efficiency was highly limited by PAHs availability in soils and the soil matrix effect. This study points out the promising efficiency of magnetite for PAHs oxidation at circumneutral pH over soluble Fe^{II} in contaminated soils, and has important implications in the remediation of contaminated soils.

Keywords: soil; polycyclic aromatic hydrocarbons; Fenton; magnetite; oxidation.

1. Introduction

Polycyclic aromatic hydrocarbons (PAHs) are toxic organic contaminants of great environmental and health concern, which consist of two or more fused aromatic rings. The 16 PAHs in the US EPA list are considered as priority pollutants by US EPA and European community. Soil matrices contaminated with PAHs abound at the sites of coke-oven gas plants, refineries, and many other major chemical industries. Owing to the persistence of PAHs in soil and sediments and their toxic, mutagenic, and carcinogenic effects, the remediation of PAH-contaminated sites is an important environmental issue. Different remediation techniques have been explored for the removal of persistent PAHs from complex matrices like soils or sediments. ***In situ*** chemical oxidation (ISCO) has emerged as a cost-effective and viable remediation technology for the treatment of several pollutants in ground waters, soils and sediments. The most common oxidants used in ISCO techniques are permanganate, persulfate and H_2O_2 combining with iron (Fenton's reagent) (ITRC, 2005). Fenton treatments are showing great potential to oxidize PAHs in contaminated soils (Watts ***et al.***, 2002; Kanel ***et al.***, 2003; Flotron ***et al.***, 2005; Ferrarese ***et al.***, 2008). Fenton treatments utilize the high reactivity of hydroxyl radical ($^{\bullet}OH$), a powerful oxidant that attacks organic pollutants generating smaller molecules (Fenton, 1894).

The Fenton's process is limited by the optimum pH (~3) required to inhibit the Fe^{II} precipitation and by the production of large amounts of ferric hydroxide sludge. In soil systems, such low pH in conventional Fenton reaction results in negative impacts on soil properties and quality and is incompatible with subsequent re-vegetation or biodegradation (Sahl & Munakata-Marr, 2006; Sirguey ***et al.***, 2008). This low pH can be avoided by using iron minerals or chelating agents (Kanel ***et al.***, 2003; Ferrarese ***et al.***, 2008). But chelating agents can act as hydroxyl radical scavenger (Xue ***et al.***, 2009c), thereby reducing the oxidation efficiency. Hence, Fenton-like oxidation is developed to extend its range of applicability to native soil circumneutral pH. In Fenton-like oxidation, iron minerals are used instead of soluble iron to produce hydroxyl radical for an efficient degradation of organic contaminants at circumneutral pH (Kong ***et al.***, 1998b; Lin & Gurol, 1998a; Kanel ***et al.***, 2003; Kanel ***et al.***, 2004).

The degradation of PAHs has been reported by Fenton-like reaction catalyzed by various Fe^{III} oxides like ferrihydrite, hematite or goethite (Watts *et al.*, 2002; Kanel *et al.*, 2003; Kanel *et al.*, 2004) but all these investigations were based on spiked or artificially contaminated soils. Recently, Fe^{II}-bearing minerals like magnetite (Fe_3O_4) were found to be the most effective catalyst as compared to the only Fe^{III} oxides for heterogeneous catalytic oxidation of organic pollutants (Kong *et al.*, 1998b; Matta *et al.*, 2007; Hanna *et al.*, 2008; Xue *et al.*, 2009a). To date, the reactivity of magnetite has not been explored in heterogeneous catalysis of PAHs chemical oxidation. This is the first study investigating the removal of PAHs from two different contaminated soils through Fenton-like oxidation catalyzed by magnetite. To attain this goal, batch experiments were conducted to evaluate the ability of magnetite to catalyze Fenton-like oxidation at circumneutral pH. For comparison purpose, PAHs degradation was also investigated by using H_2O_2 catalyzed by soluble Fe^{II} and H_2O_2 alone without iron activation at circumneutral pH. Kinetic degradation of PAHs was studied over a period of one week. In first part of the study, oxidation of fluorenone (used as model compound) was investigated. Then the ability of magnetite or soluble Fe^{II} was tested to catalyze H_2O_2 decomposition for the degradation of PAHs found in two former coking plant soils. These soils are located in the Northeast of France. The limiting factors such as soil matrix effect or PAHs availability were addressed by conducting oxidation experiments on: i) soil organic extracts spiked on sand and ii) soils pretreated using extracting agents (chloroform, ethanol or cyclodextrin). The oxidation was studied versus time and organic analyses were performed by GC-MS and μFTIR.

2. Experimental section

2.1. Chemicals

Pure fluorenone 98%, ferric chloride hexahydrate ($FeCl_3.6H_2O$) and ferrous sulfate heptahydrate ($FeSO_4.\ 7H_2O$) were purchased from Sigma-Aldrich Co. Hydroxypropyl-β-cyclodextrin (HPCD) was supplied by Sigma-Aldrich and used without further purification. Hydrogen peroxide 35% (H_2O_2) was obtained from Acros Organics. Ethanol was used as provided by Carlo Erba. Dichloromethane and chloroform were purchased from VWR and used as received. Deionized water was produced with a Milli-Q system from Millipore.

Magnetite used in this study was synthesized and characterized by X-ray powder diffraction and Mössbauer spectroscopy. Synthesis procedure and characterization of the magnetite ($Fe^{II}Fe^{III}_2O_4$) are summarized in the supporting information (Fig. S1). Fontainebleau sand, with a grain size range of 150–300 μm (mean diameter 257 μm) obtained from Prolabo was used as a support for the oxidation experiments. The sand was cleaned with 1 M HCl to remove metal impurities. Rinsing with oxygenated water was done to remove organic matter. The mineralogy of the sand was characterized by X-ray diffraction and was found to be exclusively quartz.

2.2. Soil samples

The study concerns the contaminated soils of two former coking plant sites (Homécourt (H) and Neuves-Maisons (NM)) that were located in the Northeast of France. The properties of both soils are summarized in Table 1 and were previously detailed (Biache ***et al.***, 2008). Both soils are dominated by sand mineral fractions (more than 60%), and are almost similar in the initial PAH contamination and mineral size fraction distributions. As shown in table 1, the total Fe content was also similar in both soils. However, the pH differs from neutral (NM) to basic (H) that could be related to 10 times higher carbonate contents in H than NM soil. Extractable organic matter (EOM) contents were also higher in H than NM. The major element concentrations were approximately the same in both soils. NM soil sample contained significant contents of Zn (~ 2500 mg kg^{-1}) and Pb (~580 mg kg^{-1}) that were, respectively, 10 and 4 times higher than in the H soil sample (Biache ***et al.***, 2008).

Soil samples were crushed to 500 μm. Oxidation was performed on the dried soil samples. Organic extracts of both soils were isolated through automatic extractor Dionex® ASE 200 (Accelerated Solvent Extractor) at 100° C and 130 bar with dichloromethane (DCM). Soil organic extract is composed of EOM which is isolated by organic solvent extraction from soil (mineral fractions and insoluble organic matter (IOM)). IOM is not soluble in organic solvent and thus, could not be extracted by solvent.

2.3. Oxidation procedures

The oxidation experiments with H_2O_2 were investigated in the following different systems: 1) model pollutant, fluorenone spiked on sand, 2) H and NM soil samples, 3) organic extracts of

H and NM soils that were spiked on sand, 4) H and NM organic extracts with soil and 5) H and NM soil pretreated with addition of availability-enhancement agents.

For the first and third systems, quartz sand was served as a support matrix for the oxidation experiments. A solution of fluorenone was added into sand to have 4mg of fluorenone per g of sand. In third system, organic extracts isolated from soils were mixed with sand. The DCM was removed by evaporation under continuous mixing to ensure homogeneous contaminant distribution.

In contrast to the second system where the soil was subjected to oxidation without any preliminary treatment, the soil has undergone different chemical pretreatment before oxidation in the latter two systems. For the forth system, soil samples were agitated in chloroform during 45 minutes at 60°C. Normally, this method is used for organic extraction of soils. But here, organic extract was not withdrawn from the system; instead it was evaporated to dryness. Our purpose here was to increase PAHs availability as it can be achieved by soil extraction. In last system, ethanol and cyclodextrin were used as solubility enhancement agents of PAHs in soils. Pure ethanol (99%) was added (5 mL/g) and next day, it was removed by evaporation. Cyclodextrin solution (10 mM) was mixed with soil overnight prior to oxidation.

All the oxidation experiments were conducted at circumneutral pH with (i) H_2O_2 alone without catalyst (HP), (ii) H_2O_2 + soluble Fe^{II} (F) and H_2O_2 + magnetite (10% w/w) (FL). In order to compare activation ability of both catalysts, an equivalent molar amount of Fe was used. Oxidant dose was used according to H_2O_2:Fe molar ratio of 10:1 and 20:1 for fluorenone and PAHs degradation, respectively (Table 2). A molar ratio of 10:1 for H_2O_2/Fe was employed for fluorenone oxidation according to our previous findings (Xue ***et al.***, 2009a; Xue ***et al.***, 2009c). Higher amount of oxidant (20:1 for H_2O_2/Fe) was used for the oxidation of PAHs because of natural oxidant demand induced by the presence of organic and mineral constituents along with PAHs in soils (Table 1). Blank experiments were carried out with magnetite alone under the same conditions except no oxidant was added, to study possible desorption or degradation of the pollutants (Table 2).

Batch series were prepared by assigning one batch for each time point (1 hour, 6 hours, 24 hours, 48 hours and 1 week) to study the kinetic degradation of PAHs. All batch experiments

were performed in triplicates. All results were expressed as a mean value of the 3 experiments and standard deviation of the three replicates was less than 5%. All experimental runs were performed at room temperature and in the absence of light obtained by aluminum foil coverings to avoid any photolytic degradation. In the standard procedure, soil slurries were prepared by adding water and catalysts (magnetite or soluble Fe^{II}) to solid matrix (2g). The amount of water to be added was determined in order to have a final solution volume (including the oxidant volume to be added) of 20mL. The pH was initially adjusted at 6.8 ± 0.2 for fluorenone and organic extract isolated form soil and then checked during the whole course of oxidation. In the presence of soil, oxidation experiments were performed without pH adjustment. After stirring the suspension for 15 minutes, the H_2O_2 oxidant was slowly added. At a specified reaction time, the corresponding batch was withdrawn from the series and was frozen to stop reaction. The samples were then freeze dried to remove water.

2.4. Instrumental analysis

The freeze dried samples were extracted in chloroform during 45 min at 60°C. The volume was reduced to 20 mL under nitrogen flow and 5mL of the solution was dried and weighed to determine the residual amount of EOM.

GC-MS quantification of reactant and products were performed by adding internal standards to the samples. An internal deuterated PAHs standard mix (naphthalene-d_8, acenaphthene-d_{10}, phenanthrene-d_{10}, chrysene- d_{12}, and perylene-d_{12}, supplied by Cluzeau) was added. A 2 μL amount of solution was then injected into an Agilent Technologies 6890 gas chromatograph equipped with a DB 5-MS (length: 60 m; diameter: 0.125 mm) capillary column coupled to an Agilent Technologies 5973 mass spectrometer operating in full scan mode. The temperature program was the following: 60 to 250 °C at 15 °C min^{-1}, then 250 to 315 °C at 3 °C min^{-1}, and 60 min holds at 315 °C. The carrier gas was helium at 1.5 mL min^{-1} constant flow.

The micro Fourier Transform Infrared (µFTIR) spectroscopic analysis were performed on an infrared spectrometer Bruker IFS55 coupled with a Multipurpose Bruker IR microscope equipped with a MCT detector cooled with liquid N_2. EOM were analyzed as described by (Faure ***et al.***, 1999) using a diamond window in order to avoid drawbacks usually encountered when using bulk infrared on KBr pellets, such as contamination by water adsorbed on the highly hygroscopic KBr (Ruau ***et al.***, 1997). The spectra were recorded with the following

conditions: size of the analyzed area 60 μm^2, 64 accumulations (32 s), spectral resolution 4 cm^{-1}, gain 4.

Table 1: Physico-chemical parameters and total elemental analyses of soil samples

	H soil	NM soil
Clay (<2µm) ($g.kg^{-1}$)	99	126
Fine silt (2-20µm) ($g.kg^{-1}$)	151	164
Coarse silt (20-50µm) ($g.kg^{-1}$)	91	97
Fine sand (50-200µm) ($g.kg^{-1}$)	184	120
Coarse sand (200-2000µm) ($g.kg^{-1}$)	475	493
Agronomic parameters		
pH (water)	8.35	7.20
Total $CaCO_3$ ($g.kg^{-1}$)	369	38
Phosphorus P_2O_5 ($g.kg^{-1}$)	0.090	0.287
Total organic carbon ($g.kg^{-1}$)	102.0	70.6
Total nitrogen ($g.kg^{-1}$)	2.25	2.70
C/N	45.4	25.8
Solvent extractable organic matter ($g.kg^{-1}$)	36.81	13.37
16 PAHs ($mg.kg^{-1}$)	1369	1279
Total elemental analysis (%)		
Al_2O_3	6,78 ± 0,03	7,58 ± 0,40
CaO	13,92 ± 0,49	12,58 ± 0,68
Fe_2O_3	24,34 ± 0,76	24,44 ± 0,38
MgO	1,76 ± 0,06	1,71 ± 0,13
MnO	0,34 ± 0,00	0,93 ± 0,15
P_2O_5	0,65 ± 0,03	0,77 ± 0,03
SiO_2	17,76 ± 0,84	25,66 ± 0,78
K_2O	0,53 ± 0,07	1,37 ± 0,16
Na_2O	0,14 ± 0,08	0,50 ± 0,10
Loss by combustion	29,23 ± 0,68	24,04 ± 1,70
Total	95,46	99,58

Table 2: Batch slurry oxidation tests where FL: H_2O_2 + magnetite F: H_2O_2 + soluble Fe^{II} and HP: H_2O_2 alone without iron activation. Blank experiments were performed in the presence of magnetite but without any oxidant.

Samples *	Test	Catalyst type**	Oxidant dose (H_2O_2/Fe)
1) Fluorenone spiked on quartz sand	FL	Magnetite	10
	F	Soluble Fe^{II}	10
	HP	No iron catalyst	Same oxidant dose as for F and FL***
	Blank	Magnetite	No oxidant
2) H and NM soils	FL	Magnetite	20
	F	Soluble Fe^{II}	20
	HP	No iron catalyst	Same oxidant dose as for F and FL***
	Blank	Magnetite	No oxidant
3) H and NM soil organic extracts spiked on quartz sand	FL	Magnetite	20
	F	Soluble Fe^{II}	20
	HP	No iron catalyst	Same oxidant dose as for F and FL***
	Blank	Magnetite	No oxidant
4) H and NM soils in pretreated soils	FL	Magnetite	20
	F	Soluble Fe^{II}	20
	HP	No iron catalyst	Same oxidant dose as for F and FL***
	Blank	Magnetite	No oxidant

* Detailed description of initial samples is given in experimental section.

** Magnetite was mixed with solid matrix in a ratio of 10% w/w. An equivalent molar amount of Fe was used to compare the catalytic activity of soluble Fe^{II} and magnetite.

*** As no iron was used here so the same oxidant dose was applied as for F and FL treatments.

3. Results and Discussion

3.1. Degradation of fluorenone

Firstly the degradation of fluorenone was studied by applying H_2O_2 alone without a catalyst (HP) or H_2O_2 catalyzed by soluble Fe^{II} (F) or magnetite (FL). The pH was checked along the experiment and stayed almost constant (6.8 ± 0.2). The fluorenone was chosen as model pollutant due to its higher solubility, mobility and abundance in PAHs-contaminated soils (Benhabib *et al.*, 2010). Abatement of fluorenone was monitored by EOM evolution and GC-MS quantification, both of which are in agreement. The recovered EOM from t=0 was ~4mg/g corresponding to the initially added amount of fluorenone. It means that no carbon was condensed in sand and ultimately no effect of matrix (quartz sand) was observed.

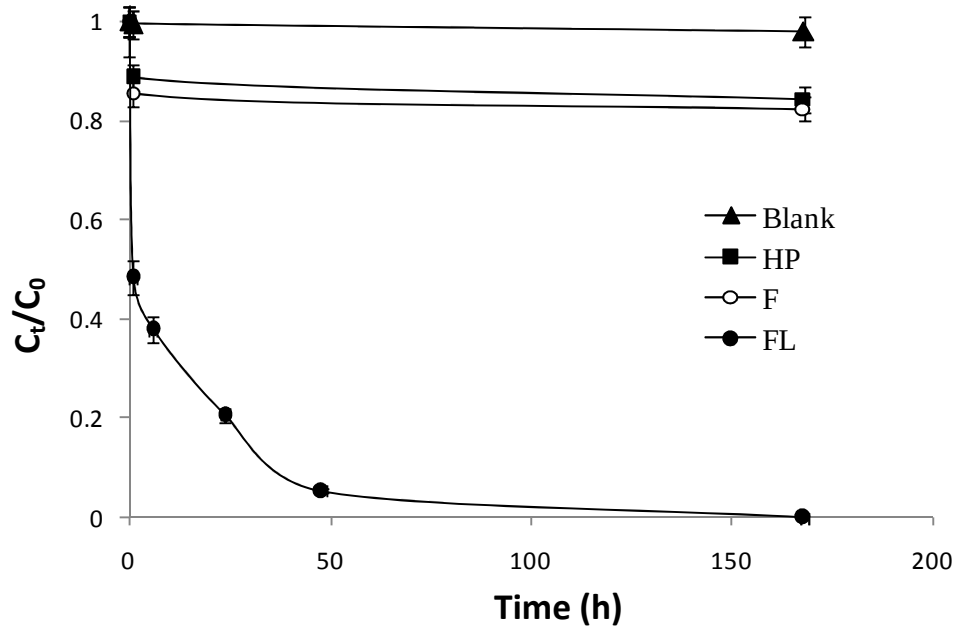

Figure 1: Degradation of fluorenone (spiked on sand) during oxidation experiments by: H_2O_2 alone without iron activation (■-HP), H_2O_2 + soluble Fe^{II} (○-F) and H_2O_2 + magnetite (●-FL). Blank (▲) experiment was performed in the presence of magnetite but without any oxidant. This degradation is represented in terms of C_t/C_0 where C_t is the fluorenone concentration at specified oxidation time and C_0 is the concentration at t=0 (before oxidation) measured by GC-MS. Lines are only visual guide. Experimental conditions were: solid matrix=2g, Volume of solution= 20mL. Oxidant dose was used according to H_2O_2:Fe molar ratio of 10:1.

Fluorenone degradation is represented by C_t/C_0 versus oxidation time (Fig. 1) where C_t is the concentration at specific time point and C_0 is the concentration at t=0 (~3975 µg/g) determined by GC-MS. Blank experiments (conducted with magnetite alone, without oxidant) revealed negligible degradation (< 3%) of fluorenone. When magnetite was the catalyst, almost 90% of fluorenone abatement was achieved within 48h, and after one week of oxidation fluorenone was completely removed. On the contrary, slight decrease (15-20%) was obtained when H_2O_2 was catalyzed by soluble Fe^{II}. The same degradation yield was observed for H_2O_2 without iron activation, thereby underscoring the inability of soluble Fe^{II} to act as catalyst at circumneutral pH.

3.2. Oxidation of two PAHs contaminated soils

Oxidative degradation of PAHs from H and NM soils was investigated by the same treatments including HP, F and FL. A very slight decrease in pH was observed (from 8.35 to 8.10 in H and from 7.20 to 7.10 in NM) after the introduction of reactants and then stayed almost constant throughout experiment. The soil samples of concern showed slightly higher concentration of total PAHs in H soil (~1369 µg/g) than in NM soil (~1279 µg/g). The ratio of low molecular weight PAH (LMW: sum of naphthalene to pyrene concentrations) over high molecular weight PAH (HMW: sum of benzo[a]anthracene to benzo[g,h,i]perylene concentrations) was calculated for each experimental time. LMW/HMW for t=0 suggests the predominance of LMW-PAHs in H soil with a value of 5.36 whereas NM soils is characterized by a higher proportion of HMW-PAHs (0.96). The achieved results exhibit negligible PAHs removal at circumneutral pH whatever the used catalyst (magnetite or soluble Fe^{II}). Increasing of oxidant dose did not improve the PAHs degradation (Fig. S2). This absence of degradation can be caused by several factors related to soil nature and pollution type. These factors may include unavailability of PAHs to oxidation, soil matrix effect or high reactivity of H_2O_2 and $^{\bullet}OH$ radical with soil constituents. To understand this lack of degradation, we firstly isolated organic extract from soil matrix to improve the PAH availability before starting oxidation reaction.

3.3. PAHs degradation in organic extracts spiked on sand

Both H and NM soils were extracted via the procedures given in the section 2.2. The corresponding organic extracts isolated from soil were homogeneously spread on sand and dried followed by their oxidation through HP, F and FL treatments. The oxidant dose was used according to H_2O_2:Fe molar ratio of 20:1 and the pH was 6.8 ± 0.2. The PAHs quantified by GC-MS represented in terms of C_t/C_0 against time are shown in Fig. 2. Negligible degradation was observed for blank experiments. After one week of oxidation in the FL system, almost 90% and 95% of 16 PAHs degradation was achieved in H (i.e. remaining concentration of 16 PAHs: ~125 µg/g) and NM extract (i.e. remaining concentration of 16 PAHs: ~76 µg/g), respectively. A colorimetric test showed that H_2O_2 was still present in the first four points (from 1h to 48h) and disappeared after one week in the FL system. Only 10-15% of degradation was achieved when soluble Fe^{II} was used as catalyst. The same degradation efficiency was found for H_2O_2 alone without iron activation.

To observe the degradation selectivity, the behavior of individual 16 PAHs was studied (Figure 3). Before oxidation (t=0), the total PAHs contents in both H and NM extract–sand mixture were almost the same as in real soil. FL oxidation did not show any preferential degradation for LMW or HMW PAHs (Figure 3). No selective degradation was observed for both soils although the PAHs composition was different in both soils with varying proportions of LMW and HMW-PAHs. These results are in agreement with those obtained with abiotic air oxidation process at 100 °C during 180 days which showed a non-selective PAHs degradation (Biache *et al.*, 2011). However, thermal desorption treatments that consists of exposing the soil to high temperature (650 °C) operated in both H and NM soil samples showed selective PAHs degradation with less efficiency towards HMW-PAHs (Biache *et al.*, 2008). The non-selective degradation way observed here could be explained by the probable production of surfactants which would render HMW-PAHs available in the aqueous phase and ultimately degradable by radical hydroxyl (Ndjou'ou & Cassidy, 2006; Gryzenia *et al.*, 2009). The surfactants can be produced as a result of partial oxidation of hydrocarbons and/or native organics having surfactant-like properties. These surfactants accompanying the Fenton oxidation of hydrocarbons in soil are eventually removed by further chemical oxidation and/or biodegradation (Ndjou'ou & Cassidy, 2006; Gryzenia *et al.*, 2009). In addition

formation of reductants (e.g. superoxide) could act as surfactant and contribute in enhanced desorption of PAHs (Watts ***et al.***, 1999a).

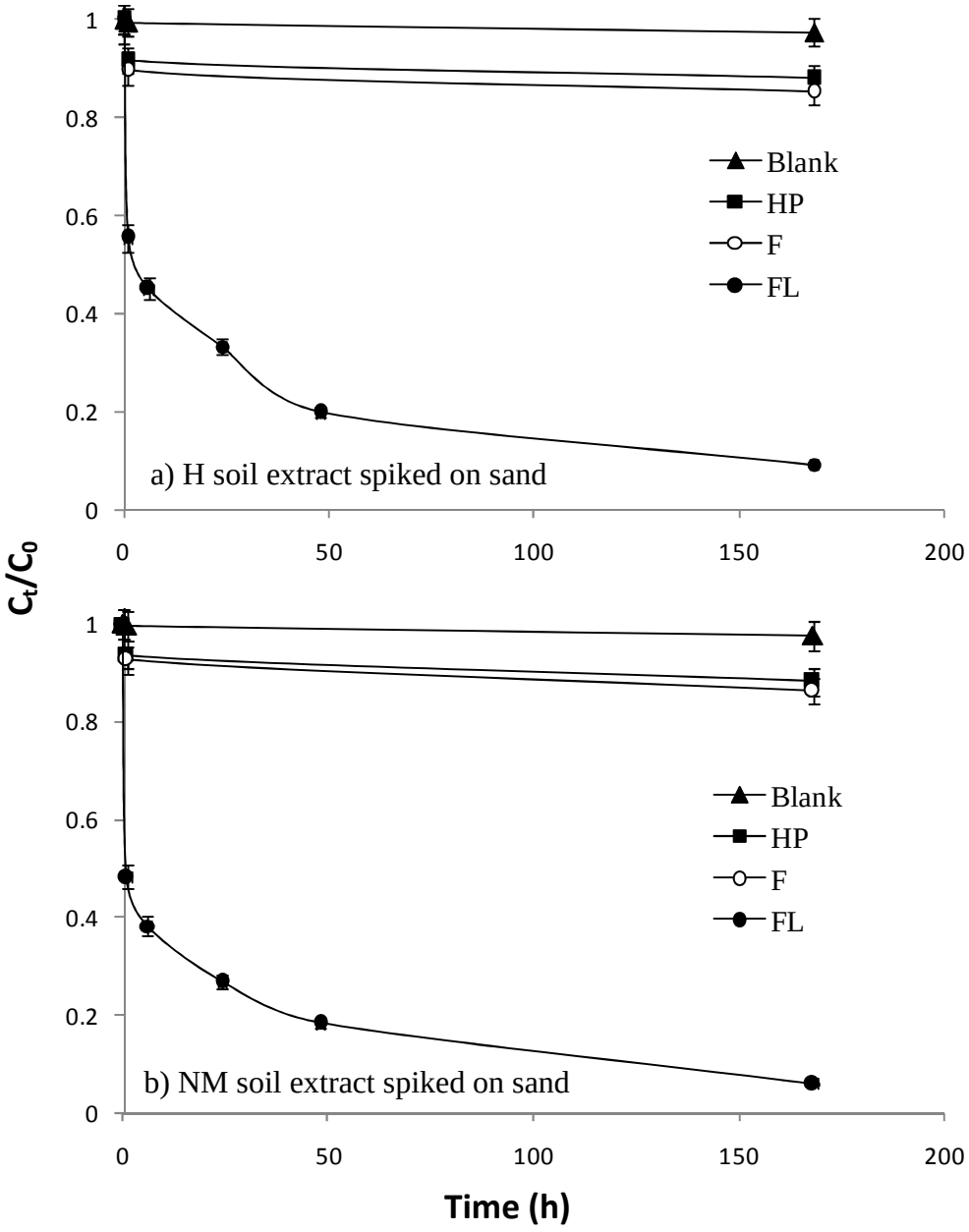

Figure 2: PAHs degradation in H and NM organic extracts (spiked on sand) during oxidation experiments by: H_2O_2 alone without iron activation (■-HP), H_2O_2 + soluble Fe^{II} (○-F) and H_2O_2 + magnetite (●-FL). Blank (▲) experiment was performed in the presence of magnetite but without any oxidant. This degradation is represented in terms of C_t/C_0 where C_t is the sum of 16 PAHs concentration at specified oxidation time and C_0 is their concentration at t=0 (before oxidation) measured by GC-MS. Lines are only visual guide. Experimental conditions were: solid matrix=2g, Volume of solution= 20mL. Oxidant dose was used according to H_2O_2:Fe molar ratio of 20:1.

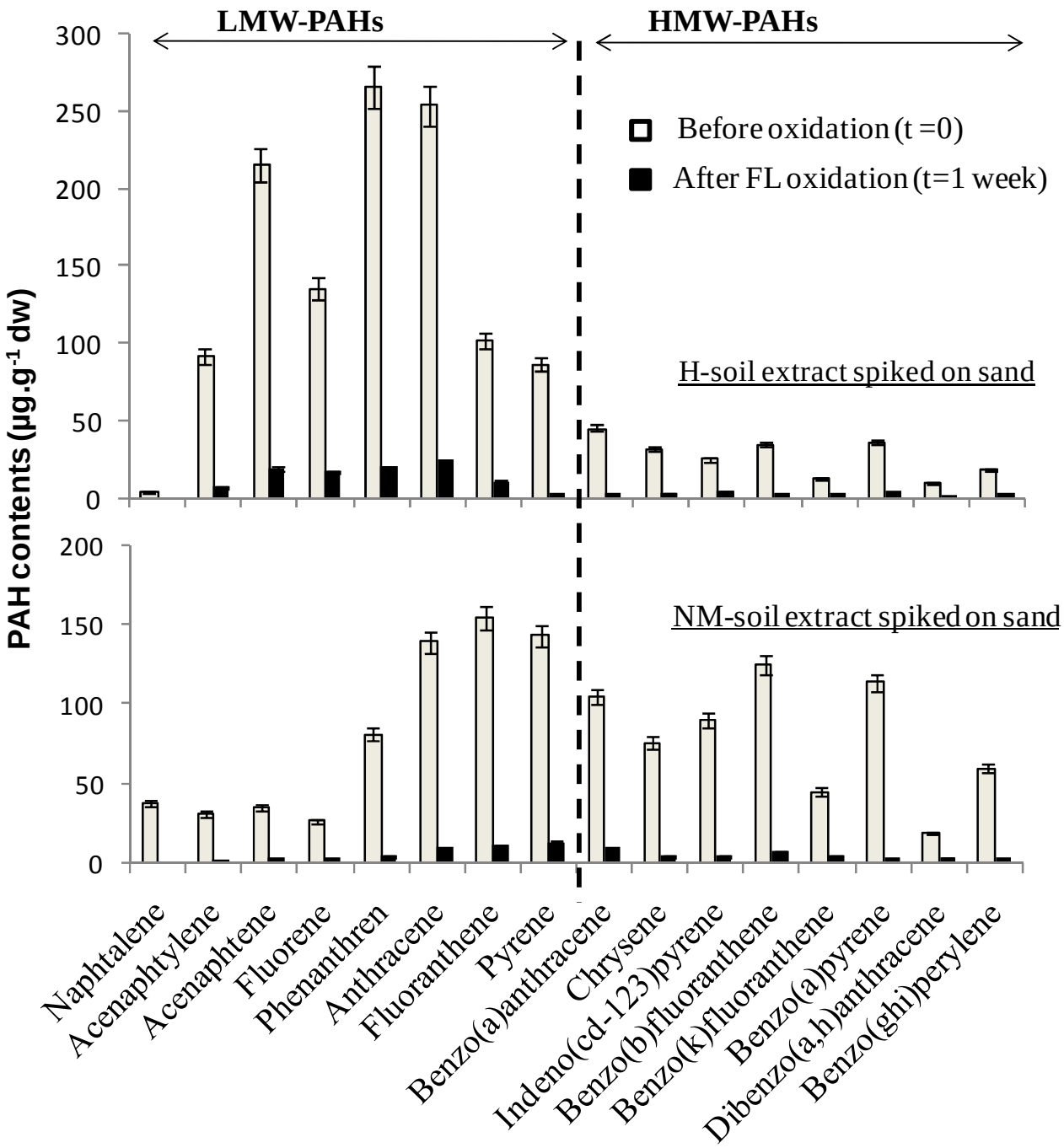

Figure 3: Contents of individual PAHs in H and NM organic extracts (spiked on sand) at t=0 before oxidation (■) and after one week FL oxidation (H_2O_2 + magnetite = □). PAHs contents are based on the measurements by GC-MS. Experimental conditions were: solid matrix=2g, Volume of solution= 20mL. Oxidant dose was used according to H_2O_2:Fe molar ratio of 20:1.

A problem that may arise during PAHs oxidation is the risk of incomplete degradation (mineralization) and the consequent production of degradation by-products. In this study, the identity of the oxidation by-products was determined by GC-MS (Fig. 4) and µFTIR (Fig. 5). The GC-MS molecular analysis of the PAHs distribution in organic extracts of H and NM showed clearly the absence of new reaction products (Fig.4). Molecular distributions are almost the same at different oxidation time points as compared to t=0 for both H and NM extracts suggesting a non-selective degradation.

The findings by µFTIR revealed that the initial EOM characteristics remained unchanged after FL oxidation for both H and NM organic extract (Fig. 5). The stability of the relative intensity of oxygenated bands (especially OH : 3700 – 3100 cm^{-1} and C=O : 1745 – 1705 cm^{-1}) suggests the absence of oxygenated by-products formation. Moreover, the similarity of aliphatic profiles (CH_{ali}: 3000 – 2800 cm^{-1} and ΔCH_{ali}: 1470 – 1360 cm^{-1}) and aromatic profiles (CH_{aro}: 3100 – 3000 cm^{-1}, C=C: 1620 – 1590 cm^{-1} and CH_{aro}: 900 – 700 cm^{-1}) reveals that no major molecular reorganization occured (Fig. 5). These findings are in agreement with µFTIR and suggest the absence of degradation products by FL oxidation in EOM-sand system and a non-selective degradation.

All these results reveal that PAH removal can be achieved when the organic extracts were subjected to oxidation away from the soil matrix. Another interesting point of these results is the strong reactivity of magnetite to catalyze oxidation for PAHs degradation compared to ferrous salt. But its reactivity was observed only when oxidation was operated for PAHs in EOM spiked on sand after its separation from the soil matrix. Once PAH availability was increased by their extraction from soil, oxidation lead to their degradation. This highlights the important role of the PAHs availability in the determination of treatment efficiency in a contaminated soil whatever the catalyst used.

Various soil factors like soil organic matter (SOM) and mineral composition could contribute to hinder PAHs degradation (Bogan & Trbovic, 2003; Goi & Trapido, 2004; Flotron *et al.*, 2005; Jonsson *et al.*, 2007). In general, an increase in SOM will reduce the Fenton oxidation efficiency through scavenging of $^{\bullet}OH$ radicals and increasing of PAHs retention (Flotron *et al.*, 2005; Jonsson *et al.*, 2007). It was stated that the PAH degradation extent was inversely proportional to the total organic carbon (TOC) for the soil with TOC above 5% (Bogan & Trbovic, 2003). In our soil samples, TOC in both soils is close to 10% and 7% for H and NM

respectively (Table 1). Contents of 16-PAHs (1369 and 1279 µg.g^{-1} for H and NM respectively) represent less than 2% of soil TOC and EOM (36 and 13 mg.g^{-1} for H and NM respectively) corresponds to almost 36% and 17% of H and N soil respectively of the TOC of tested soils. Rest of the organic matter was trapped in soil as IOM. This suggests that SOM competition and retention capacity can largely affect oxidation efficiency. In addition to SOM, clay particles contribute to the strong sorption of PAHs in soils (Kawahara ***et al.***, 1995). As a matter of fact, PAHs on sandy soil are degraded easier than PAHs adsorbed on organic rich soils or clay rich soils (Goi & Trapido, 2004). Even if, in our case, H and NM soils are dominated by sand mineral fractions (more than 60%), clay and fine silt (~25%) can induce an efficiency limitation.

Therefore, in addition to the PAH availability, radical scavenging particles such as SOM, fine soil fractions and carbonates could inhibit or limit the degradation extent. This was examined in the following section by increasing the PAHs availability and then oxidizing the organic extract in the presence of soil.

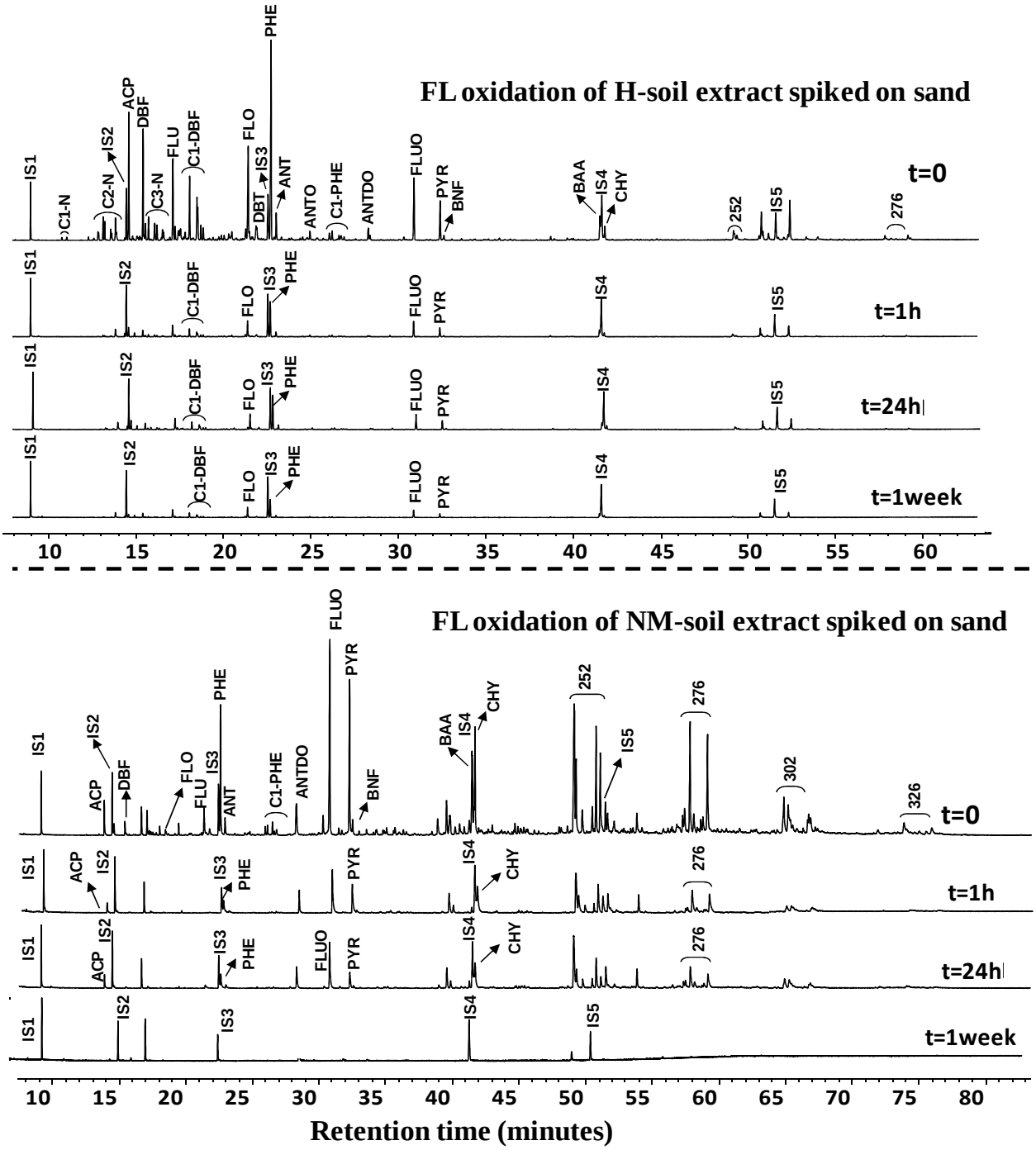

Figure 4: Molecular distribution obtained by GC-MS of H and NM organic extract (spiked on sand) before oxidation (t=0) and after different oxidation times by FL oxidation (H_2O_2 + magnetite). The compounds are detailed in Table S1. Experimental conditions were: solid matrix=2g, Volume of solution= 20mL. Oxidant dose was used according to H_2O_2:Fe molar ratio of 20:1.

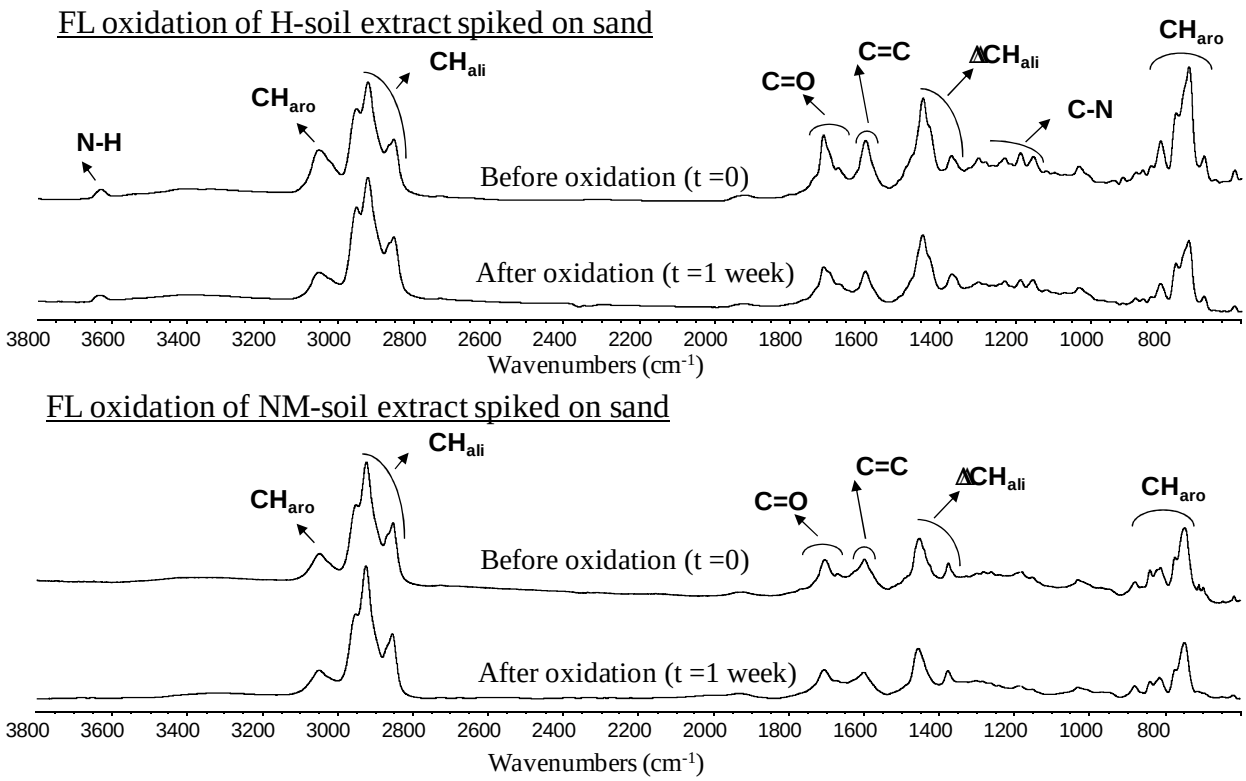

Figure 5: FTIR spectra of (a) organic extract from H soil and (b) organic extract from NM soil before (t=0) and after oxidation (1week) by FL oxidation (H_2O_2 + magnetite). Organic extracts from H and NM soil were added to sand and after evaporation of the solvent, oxidation was performed. Experimental conditions were: solid matrix=2g, Volume of solution= 20mL. Oxidant dose was used according to H_2O_2:Fe molar ratio of 20:1.

3.4. PAHs degradation in pretreated soils

In this section, the same extraction procedures as in the section 3.3 were used but without separation of EOM from solid (mineral + IOM). In other words, soil was agitated in chloroform for 45 minutes at 60°C that was allowed to evaporate before oxidation. The purpose was to increase the PAHs availability, but by keeping the soil matrix. Then, as in previous sections, H_2O_2 oxidation with or without iron catalyst was performed with H_2O_2:Fe molar ratio of 20:1. The observed pH values were 8 ± 0.2 in H and 7 ± 0.2 in NM and stayed almost constant throughout experiment. The concentration of 16-PAH is represented in terms of C_t/C_0 versus time in Figure 6. No oxidation was observed in blank experiments. Very small degradation (<5%) was obtained without or with soluble Fe^{II} activation in HP and F treatments. However, a degradation extent of 50-60% was achieved after one week of oxidation for both soils when magnetite was used as catalyst. After one week, remaining

concentration of 16 PAHs by FL treatment was ~ 678 µg/g and ~594 µg/g in H and NM soils respectively. Here PAHs degradation was significantly improved as compared to soil oxidation without any pretreatment (section 3.2), but reduced as compared to oxidation of organic extract spiked on sand (section 3.3). Therefore, soil matrix effectively contributes to the decrease in the degradation extent (from 90% to 55%). This reduction in degradation extent in soil could be exerted by a natural oxidant demand (NOD) resulting in additional nonproductive oxidant depletion (Haselow ***et al.***, 2003). Such natural materials can include IOM inherited probably from coal, coke, as well as reactive mineral materials including metal-based oxides and carbonates. Higher IOM was observed in both soils from almost 60% and 80% of TOC respectively for H and NM soils which could cause this lower degradation extent. These scavenging soil constituents compete for oxidant radicals with organic contaminants and thus lowering their degradation in soil as compared to organic extracts spiked on sand. Carbonate contents in H soil were 10 times higher than NM soil, but a slight difference in term of degradation efficiency between soils was observed. Thus the impact of carbonate content on PAH removal is not significant in our systems. In conclusion, both soil matrix (IOM and mineral fractions) and PAHs availability were responsible of the lack of PAHs degradation in soils.

Similar to the oxidation of organic extract in sand, GC-MS and µFTIR analyses revealed the absence of by-products in soils (data not shown). Also the PAHs degradation was non-selective in both soils. Results also highlight the importance of catalyst used as magnetite was able to catalyze Fenton oxidation at circumneutral pH. Interestingly, degradation efficiency was almost the same in both cases either with or without soluble Fe^{II}. The rapid oxidation of Fe^{II} and/or the complexation of ferrous ion with soil constituents at circumneutral pH could explain this inability of Fe^{II} to catalyze the H_2O_2 decomposition.

Pretreatments using ethanol or cyclodextrin (CD) as solubility-enhancement agents (or availability-enhancement agents) were also used to increase ***in situ*** the PAHs availability in both soils, and to evaluate the impact of enhancing PAHs availability on oxidation yield. In the magnetite catalyzed Fenton-like oxidation system, ethanol has slightly higher degradation efficiency (20%) than that of cyclodextrin (15%) after one week of reaction time. No significant degradation was, however, noted in the absence of catalyst or in the presence of soluble Fe^{II}. A similar low degradation efficiency (~20%) was previously obtained for

ethanol-Fenton treatment of PAHs contaminated soil compared to Fenton alone (Lundstedt ***et al.***, 2006). This limited-degradation extent may be due to (i) the low capacity of ethanol or CD to enhance the PAH availability, and/or (ii) the scavenging effect. In fact, CD can consume a significant amount of oxidant species that would otherwise be available to degrade contaminants, as previously reported in aqueous solution (Hanna ***et al.***, 2005). So, injection of enhancement solubility agents may increase the oxidant demand of the system. However, the scavenging effect concerns only CD, as ethanol was evaporated from reactor before oxidation.

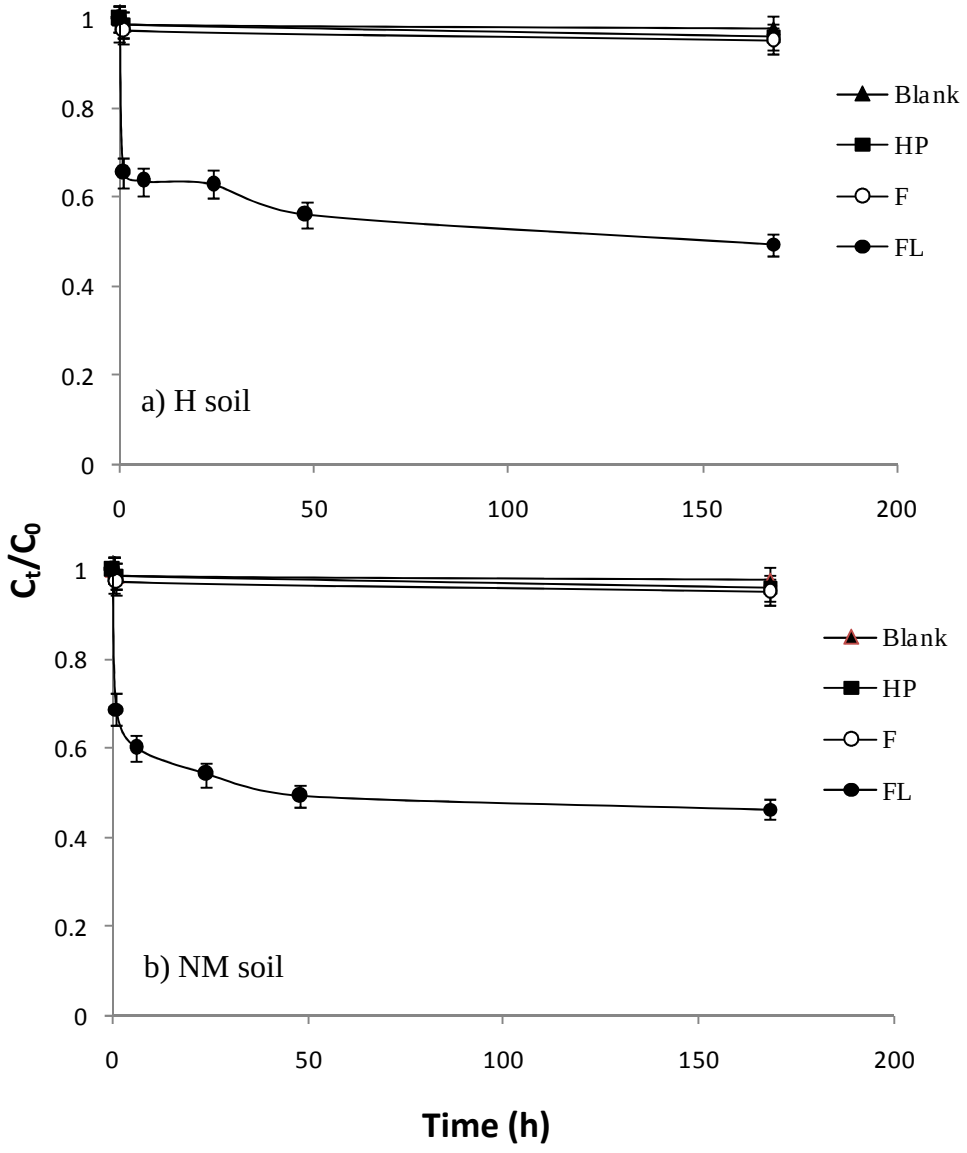

Figure 6: PAHs degradation in organic extracts in the presence of soils (H and NM) during oxidation experiments by: H_2O_2 alone without iron activation (■-HP), H_2O_2 + soluble Fe^{II} (○-F) and H_2O_2 + magnetite (●-FL). Blank (▲) experiment was performed in the presence of magnetite but without any oxidant. Soils were subjected to an extraction pretreatment but without isolation of organic extract and

after evaporation of solvent, oxidation was performed. This degradation is represented in terms of C_t/C_0 where C_t is the sum concentration of 16 PAHs at specified oxidation time and C_0 is the sum concentration at t=0 (before oxidation) measured by GC-MS. Lines are only visual guide. Experimental conditions were: solid matrix=2g, Volume of solution= 20mL. Oxidant dose was used according to H_2O_2:Fe molar ratio of 20:1.

4. Conclusions

This study represents the following important points for ex-situ and *in-situ* chemical oxidation of contaminated soils:

1). Higher efficiency of magnetite to catalyze chemical oxidation at circumneutral pH was the main finding of this study. The use of magnetite as iron source for Fenton oxidation was appeared as a promising and innovative way for chemical oxidation of PAHs. As Fe^{II} was found unable to catalyze the H_2O_2 decomposition at circumneutral pH, injection of magnetite particles in contaminated soils could be especially advantageous for *in-sit*u remediation of contaminated matrices where pH cannot be adjusted. This approach provides a cost effective solution for soil remediation without pH adjustment contrary to other known methods where more than one reagent is used (e.g. iron + chelating agents). In addition, magnetite, non-toxic mineral, is structurally and catalytically stable and can be used for further oxidation cycles.

2). Both PAHs availability and soil matrix seem to be the most influencing parameters in ISCO technologies. Improvement of PAHs availability can be correlated with the enhancement of PAHs oxidation in soil samples. Contents of mineral and organic constituents in soil can affect the oxidation mechanism and degradation efficiency. Before designing an oxidation experiment, evaluation of PAH availability as well as characterization of soil constituents should be carefully carried out. Finally, reactivity of magnetite for application would be more prominent in contaminated soil without such limitations of PAHs availability or significant matrix effect.

These findings regarding the ability of magnetite, the most stable mixed-valence oxide, to promote oxidation in soils have important practical implications for chemical oxidation technologies.

Acknowledgements: The authors gratefully acknowledge the financial support of this work by Higher Education Commission of Pakistan (HEC) and ADEME "Agence de l'Environnement et de la Maîtrise de l'Energie" (Grant N° 0972C0016). We are also thankful to the Région Lorraine and GISFI **(**Groupement d'Intérêt Scientifique sur les Friches Industrielles) for support. Finally, we would like to thank the reviewers who helped to improve the quality of the manuscript.

Supplementary material Available: I. Synthesis and characterization of magnetite. Table S1: Details of the abbreviated compounds enlisted in the GC-MS chromatograms. Figure S1: XRD diffractogram (a) and Mössbauer spectrum (b) of the used magnetite. Figure S2: PAHs degradation in soils (H and NM) during oxidation experiments.

Number of Tables: 1
Number of Figures: 2

I. Synthesis and characterization of magnetite

The magnetite used in this study was synthesized from ferrihydrite by taking its amount equivalent to a Fe^{III} concentration of 0.267 M followed by the addition of $FeSO_4.7H_2O$ in quantity corresponding to the Fe^{II} concentration of 0.133 M leading to the final iron concentration of 0.4 M. An appropriate amount of NaOH (1M) was then added to the mixture to provide the ratio n (OH^-) / n (Fe^{III}) = 1 where n represents the number of moles. These conditions are required to form stoichiometric magnetite ($Fe^{II}\,Fe^{III}_2\,O_4$) with a Fe^{II}: Fe^{III} ratio of 1:2. The suspension was stirred for two days, centrifuged and solid was dried. All synthesis experiments were conducted in glove box, an anoxic chamber (N_2:H_2= 98:2).
At the end of reaction, XRD data (Fig. S1a) and Mössbauer spectroscopy (Fig. S1b) confirmed the magnetite as the only product.

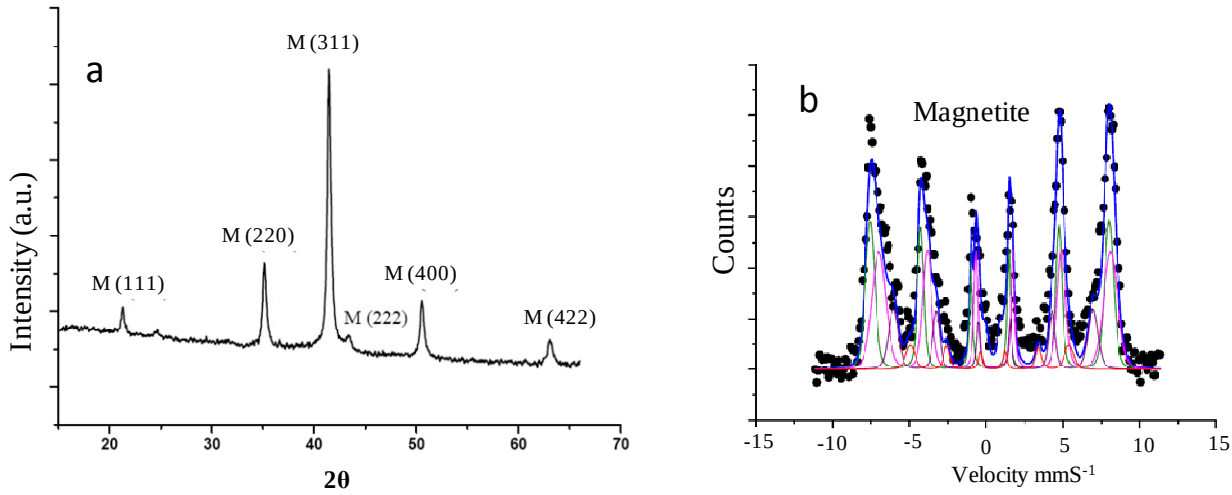

Figure S1: XRD diffractogram (a) and Mössbauer spectrum (b) representing the magnetite formed from ferrihydrite. Whole ferrihydrite was transformed into magnetite.

Table S1. Details of the abbreviated compounds enlisted in the chromatograms of Figure 4.

Code	***Name***
IS-1	*Naphthalene-D8*
C1-N	*methyl-naphthalene*
C2-N	*ethyl & dimethyl-naphthalene*
IS2	*Acenaphtene-D10*
ACP	*Acenaphtene*
DBF	*Dibenzofuran*
C1-DBF	*Methyl-Dibenzofuran*
FLO	*Fluorenone*
DBT	*Dibenzothiopene*
IS3	*Phenanthrene-D10*
PHE	*Phenanthrene*
ANT	*Anthracene*
ANTO	*Anthracenone*
C1-PHE	*Methyl-phenanthren*
ANTDO	*Anthracendione*
FLUO	*Fluoranthene*
PYR	*Pyrene*
BNF	*Benzonaphtofuran*
BAA	*Benzo[a]anthracene*
IS4	*Chrysene-D12*
CHY	*Chrysene*
252	*PAH 252 g/mol*
IS5	*Perylene-D12*
276	*PAH 276 g/mol*

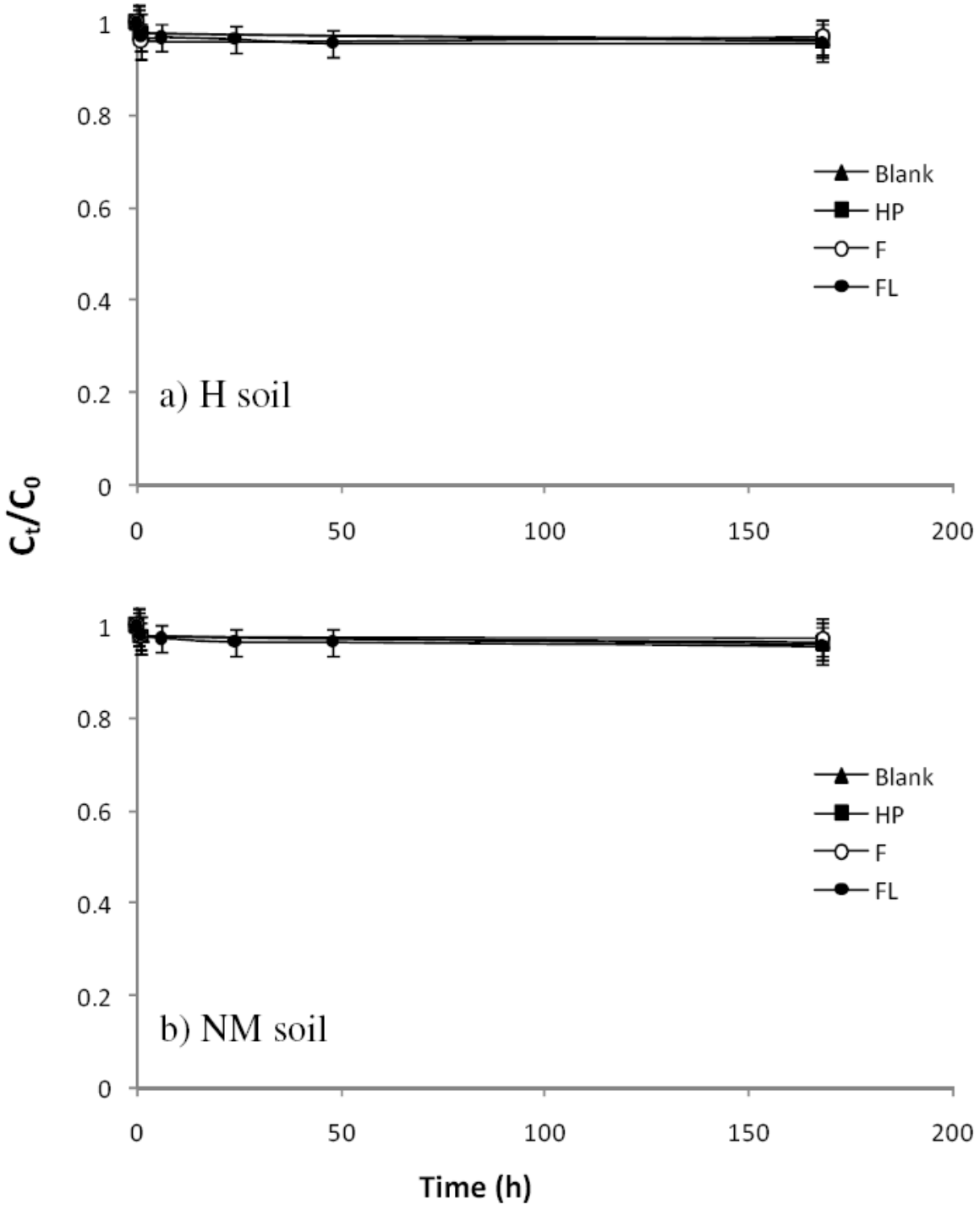

Figure S2: PAHs degradation in soils (H and NM) during oxidation experiments by: H_2O_2 alone without iron activation (■-HP), H_2O_2 + soluble Fe^{II} (○-F) and H_2O_2 + magnetite (●-FL). Blank (▲) experiment was performed in the presence of magnetite but without any oxidant. This degradation is represented in terms of C_t/C_0 where C_t is the sum concentration of 16 PAHs at specified oxidation time and C_0 is the sum concentration at t=0 (before oxidation) measured by GC-MS. Lines are only visual guide. Experimental conditions were: solid matrix=2g, Volume of solution= 20mL. Oxidant dose was used according to oxidant: Fe molar ratio of 20:1. Same were the results with oxidant: Fe molar ratio of 10:1.

Application of magnetite-activated persulfate oxidation for the degradation of PAHs in contaminated soils

M. Usman[a,b], P. Faure[b], C. Ruby [a] and K. Hanna[c, d]

[a] Laboratoire de Chimie Physique et Microbiologie pour l'Environnement, LCPME, UMR 7564 CNRS-Université de Lorraine, 405 rue de Vandoeuvre, 54600, Villers Les Nancy, France.

[b] Géologie et Gestion des Ressources minérales et énergétiques, G2R, UMR 7566, CNRS-Université de Lorraine, 54506, Vandoeuvre Les Nancy, France.

[c] Ecole Nationale Supérieure de Chimie de Rennes, UMR CNRS 6226 "Sciences Chimiques de Rennes", Avenue du Général Leclerc, 35708 Rennes Cedex 7, France.

[d] Université Européenne de Bretagne, France.

Abstract

In this study, feasibility of magnetite-activated persulfate oxidation (AP) was evaluated for the degradation of polycyclic aromatic hydrocarbons (PAHs) in batch slurry system. Persulfate oxidation activated with soluble Fe^{II} (FP) or without activation (SP) was also tested. Kinetic oxidation of PAHs was tracked in spiked sand and in aged PAH contaminated soils at circumneutral pH. Quartz sand was spiked with: i) single model pollutant (fluorenone) and ii) organic extract isolated from two PAH contaminated soils (H and NM sampled from ancient coking plants) and was subjected to oxidation. Oxidation was also performed on real H and NM soils with and without an extraction pretreatment. Results indicate that oxidation of fluorenone resulted in its complete degradation by AP while abatement was very low (< 20%) by SP or FP. In soil extracts spiked on sand, significant degradation of 16 PAHs was observed by AP (70-80%) in one week as compared to only 15% by SP or FP systems. But no PAH abatement was observed in real soils whatever the treatment used (AP, FP or SP). Then soils were subjected to an extraction pretreatment but without isolation of organic extract from soil. Oxidation of this pretreated soil showed significant abatement of PAHs by AP. On the other hand, very low degradation was achieved by FP or SP. Selective degradation of PAHs was observed by AP with lower degradation efficiency towards high molecular weight PAHs. Analyses revealed that no by-products were formed during oxidation. The results of this study demonstrate that magnetite can activate persulfate at circumneutral pH for an effective degradation of PAHs in soils. However, availability of PAHs and soil matrix were found to be the most critical factors for degradation efficiency.

Keywords

Soil; oxidation; polycyclic aromatic hydrocarbons; persulfate; magnetite.

1. Introduction

Chemical oxidation treatments are showing great potential for the remediation of contaminated soils in which strong oxidants are injected into the subsurface. Recently, persulfate oxidation has emerged as an option for chemical oxidation of organic contaminants in soils and sediments (Liang et al., 2004; Liang et al., 2007; Ferrarese et al., 2008; Yen et al.,

2011). Persulfate salts dissociate in aqueous solution to the persulfate anion $S_2O_8^{2-}$ which is a strong oxidant (E^o = 2.01 V). But its reaction kinetics is slow in destroying most of the recalcitrant organic contaminants (Osgerby, 2006). However, persulfate activation can be initiated by thermal or chemical means to form sulfate radical ($SO_4^{\bullet-}$) (House, 1962). The sulfate radical is a stronger oxidant (E^o = 2.6 V) than persulfate anion (Latimer, 1952). Iron is a commonly used transition metal for chemical activation of persulfate anion (Liang et al., 2004).

Due to their high toxicity, environmental persistence and carcinogenic effects, polycyclic aromatic hydrocarbons (PAHs) are of great environmental and health concern and thus are considered as priority pollutants by US EPA and European community (Wild & Jones, 1995). *In situ* chemical oxidation (ISCO) is an increasingly popular method for the remediation of contaminated soils and groundwater in which various oxidants are injected to degrade contaminants (ITRC, 2005). There are few studies on the treatment of PAHs using persulfate oxidation activated by soluble Fe^{II} (Nadim et al., 2006; Ferrarese et al., 2008; Gryzenia et al., 2009). As rapid oxidation and precipitation of ferrous ion could make Fe^{II} inactive, chelating agents were previously used to overcome this limitation and to maintain Fe^{II} in solution (Liang et al., 2004). Another possibility is the use of minerals like ferrihydrite, goethite, manganese oxide and clay that could activate persulfate oxidation for the degradation of trichloroethylene or diesel compounds in recent studies (Ahmad et al., 2010; Do et al., 2010). Recently, Fe^{II}-bearing minerals like magnetite (Fe_3O_4) were found to be the most effective catalyst as compared to the only Fe^{III} oxides for heterogeneous catalytic oxidation of organic pollutants (Kong ***et al.***, 1998b; Matta ***et al.***, 2007; Hanna ***et al.***, 2008; Xue ***et al.***, 2009a). In addition, magnetite exhibited excellent structural and catalytic stabilities and can be used for several oxidation cycles (Xue ***et al.***, 2009a; Xue ***et al.***, 2009c). The objective of this study was to evaluate the ability of magnetite to activate persulfate at circumneutral pH for the oxidation of PAH-contaminated soils. To date, the use of magnetite, the most stable mixed valence oxide instead of soluble Fe^{II} to activate persulfate oxidation has not been tested for PAH degradation in aged contaminated soils.

To achieve this goal, magnetite-activated persulfate oxidation was studied in spiked sand and two PAH contaminated soils in batch slurry system. These soils were sampled from two former coking plants situated in the Northeast of France. Single model pollutant (fluorenone) and organic extract of two soils was spiked on sand followed by oxidation. Kinetic

degradation of 16 PAHs was also tracked in both real contaminated soils with or without an extraction pretreatment. To compare with magnetite, oxidation treatments were also evaluated under the same conditions with persulfate activated by soluble Fe^{II} or without iron activation. The oxidation was studied versus time and organic analyses were performed by GC-MS and µFTIR.

2. Experimental section

2.1. Chemical reactants

Pure fluorenone 98%, ferrous sulfate heptahydrate ($FeSO_4$. $7H_2O$) and sodium persulfate ($Na_2S_2O_8$) were purchased from Sigma-Aldrich Co. Dichloromethane (DCM) and chloroform were purchased from VWR and used as received.

Magnetite ($Fe^{II}Fe^{III}{}_2O_4$) used in this study was synthesized and characterized by X-ray powder diffraction and Mössbauer spectroscopy in the context of our previous work (Usman ***et al.***, 2011a). Fontainebleau sand, with a grain size range of 150–300 µm (mean diameter 257 µm) obtained from Prolabo was used as support for oxidation experiments. The sand was cleaned with 1 M HCl to remove metal impurities. Rinsing with oxygenated water was done to remove organic matter. The mineralogy of the sand was characterized by X-ray diffraction and was found to be exclusively quartz. Deionized water was produced with a Milli-Q system from Millipore.

2.2. Soil samples

In this study, 16 PAHs in two different soils, Homécourt (H) and Neuves-Maisons (NM) were selected as target compounds. These soils were sampled from two former coking plant sites that are located in the Northeast of France. The properties of both soils are presented in the supplementary materials (Table S1). Mineral size fraction distributions were similar for both soils that are dominated by sand mineral fractions (more than 60%) with pH from neutral (7.20 in NM) to basic (8.35 in H). This pH could be related to 10 times higher carbonate contents in H than NM soil. Extractable organic matter (EOM) contents were also higher in H than NM. The major element concentrations were approximately the same in both untreated soils. Samples were crushed to 500 µm and freeze-dried. Oxidation was performed on these

two soil samples. Isolation of organic extracts of both soils was done through automatic extractor Dionex® ASE 200 (Accelerated Solvent Extractor) at 100 °C and 130 bar with DCM (Biache et al., 2008). Soil organic extract is composed of EOM which was separated by solvent extraction from rest of soil (mineral fractions and insoluble organic matter (IOM)). Soil organic matter (SOM) is composed of EOM and IOM. Solvent was unable to extract IOM from soil.

2.3. Oxidation experiments

Before oxidation, all vessels were rinsed with DCM and then several times with deionized milli-Q water. The persulfate mediated degradation of PAHs was evaluated in the following different systems: 1) model pollutant, fluorenone spiked in sand, 2) H and NM organic extracts spiked in sand, 3) H and NM soil samples and 4) H and NM organic extracts in soil.

In first two systems, fluorenone and organic extracts dissolved in DCM was added in sand (4 mg g^{-1} w/w). The DCM was allowed to evaporate to dryness followed by oxidation. In the third system, both soils H and NM were subjected to oxidation. In the last system, soil samples were subjected to an extraction pretreatment by agitating in chloroform during 45 min at 60 °C. Normally, this method is used for organic extraction of soils. But here, chloroform was not withdrawn from the system; instead it was evaporated to dryness. Our purpose here was to increase PAH availability.

Oxidation treatments at circumneutral pH were performed as following: (i) sodium persulfate alone without iron activation (SP), or (ii) sodium persulfate activated with soluble Fe^{II} (FP) or sodium persulfate activated with magnetite (10% w/w) (AP). Equivalent molar amount of Fe was used to compare the efficiency of both catalysts to activate persulfate. Blank experiments were performed by using magnetite alone without oxidant to study possible desorption or degradation of the PAHs. Kinetic degradation of PAHs was studied for one week in batch series by assigning one batch for each time point (1 h, 6 h, 24 h, 48 h and 1 week). All batch experiments were performed in triplicates. All results were expressed as a mean value of the 3 experiments and relative standard deviation (RSD) of the three replicates was less than 5%. The RSD was calculated as described in supplementary material. The kinetic oxidation procedure is also detailed in supplementary materials (SM).

2.4. Extraction and analysis

The freeze dried samples were extracted in chloroform during 45 min at 60 °C. The volume was reduced to 20 mL under nitrogen flow and 5 mL of the solution was dried and weighed to determine the amount of EOM. The organic analyses were performed by GC-MS and µFTIR. All details of analysis procedures are presented in supplementary materials (SM).

3. Results and Discussion

3.1. Oxidation of fluorenone

Magnetite and soluble Fe^{II} were investigated for their potential to activate persulfate oxidation for a single PAH pollutant, fluorenone. It was chosen as a model pollutant due to its higher solubility, mobility and abundance in PAH-contaminated soils (Benhabib et al., 2010). GC-MS quantification and EOM evolution were used to monitor its abatement, both of which are in agreement. The EOM recovered from sand at t = 0 was almost similar to the initially added amount of fluorenone (i.e. ~ 4 mg g^{-1}) which states that no fluorenone was retained in sand. The degradation of fluorenone is represented by plotting C_t/C_0 *vs.* time (Fig. 1). Its concentration was determined by GC-MS where C_t is concentration at specific time point and C_0 is the concentration at t = 0 before oxidation. Blank experiments did not cause any degradation (< 3%) of fluorenone. AP treatment showed rapid degradation of fluorenone resulting in almost 90% of fluorenone abatement within 48 h and complete removal after one week of oxidation. Slight abatement (20-25%) was, however, obtained by FP or SP treatments. This similar degradation yield with or without soluble Fe^{II} activation suggests that the soluble Fe^{II} was unable to activate persulfate oxidation at circumneutral pH. Oxidation and precipitation of Fe^{II} may occur at neutral pH conditions and thus making it unavailable for activation. These results suggest that magnetite was effective to activate persulfate oxidation for fluorenone degradation.

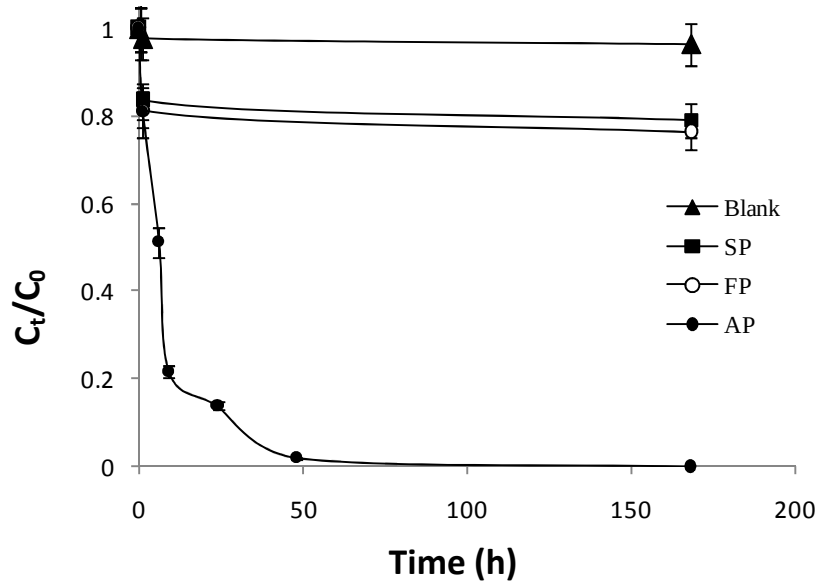

Figure 1: Degradation of fluorenone (spiked on sand) during persulfate oxidation experiments by: sodium persulfate alone without iron activation (■-SP), or (ii) sodium persulfate activated with soluble Fe^{II} (○-FP) or sodium persulfate activated with magnetite (●-AP). Blank (▲) experiments were conducted by using only magnetite without any oxidant. This degradation is represented in terms of C_t/C_0 where C_t is the fluorenone concentration at specified oxidation time and C_0 is the concentration at t = 0 (before oxidation) measured by GC-MS. Lines are only visual guide. Experimental conditions were: solid matrix = 2 g, Volume of solution = 20 mL. Oxidant dose was used according to oxidant: Fe molar ratio of 1:1.

3.2. PAHs degradation in organic extracts spiked on sand

In this section, organic extracts previously isolated from both soils (H or NM) were spiked on sand. After evaporation of solvent, oxidation treatments AP, FP and SP were applied. Degradation of 16 PAHs by persulfate oxidation is represented in terms of C_t/C_0 versus time (Fig. 2). Negligible degradation was observed for blank experiments. After one week of oxidation in the AP system, 16 PAHs were removed by approximately 83% and 72% in H and NM extract respectively. Only 15-20% of degradation was achieved by FP or SP treatments. An iodometric test (Kolthoff & Stenger, 1947) showed that persulfate was still present in the first four points (from 1h to 48h) and disappeared after one week in the AP system. Thus, as observed for fluorenone, magnetite was found as a potential activator for persulfate oxidation of PAHs.

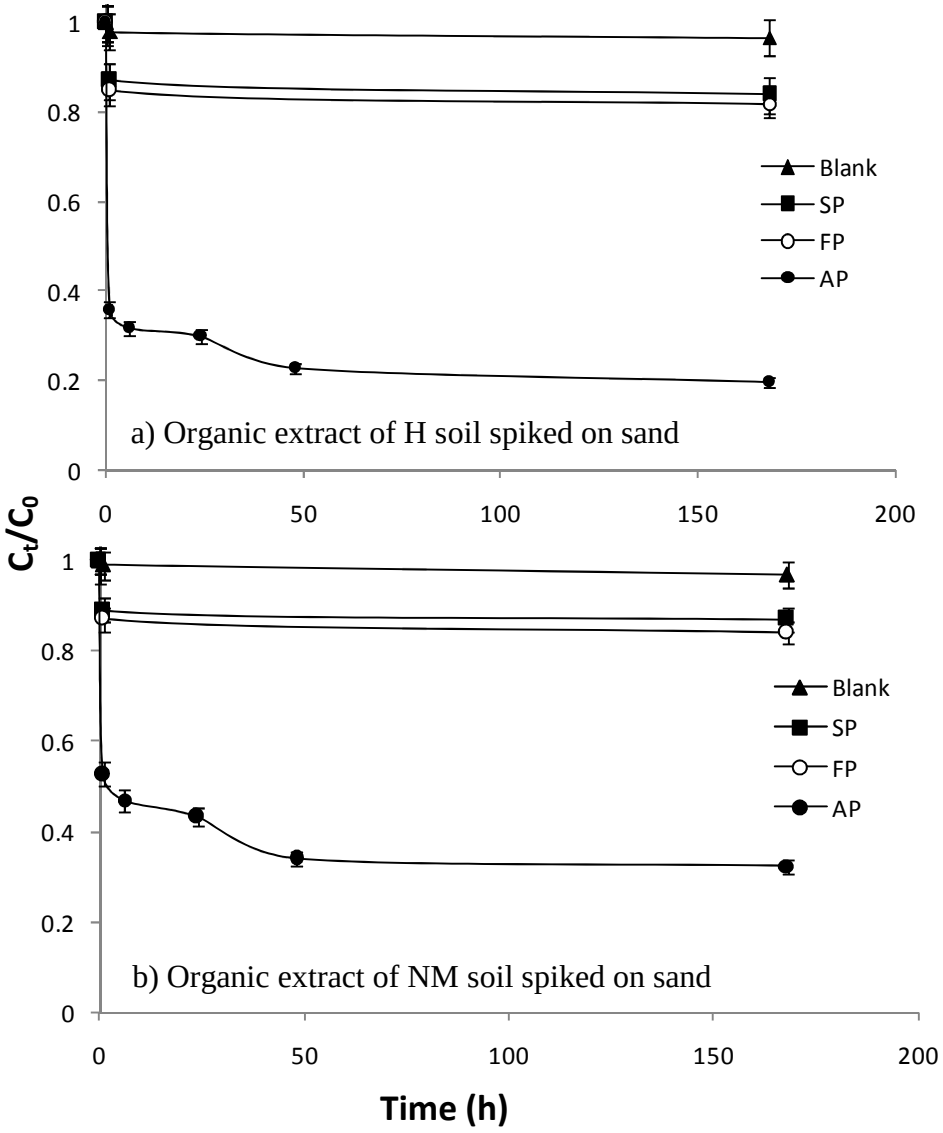

Figure 2: PAH degradation in organic extracts extracted from soils (H and NM) during persulfate oxidation experiments by: sodium persulfate alone without iron activation (■-SP), or (ii) sodium persulfate activated with soluble Fe^{II} (○-FP) or sodium persulfate activated with magnetite (●-AP). Blank (▲) experiments were conducted by using only magnetite without any oxidant. This degradation is represented in terms of C_t/C_0 where C_t is the sum of 16 PAH concentration at specified oxidation time and C_0 is their concentration at t = 0 measured by GC-MS. Lines are only visual guide. Experimental conditions were: solid matrix = 2 g, Volume of solution = 20 mL. Oxidant dose was used according to oxidant: Fe molar ratio of 1:1.

To observe the behavior of individual PAHs during oxidation, the remaining PAHs were quantified for each experiment using GC-MS at each time point. And 16 PAHs present in H and NM before (t = 0) and after one week of oxidation, are shown in Figure 3. For t = 0, the total content of PAHs in H extract was lower (~ 204 µg g^{-1}) than NM extract with almost 348 µg g^{-1} of sand.

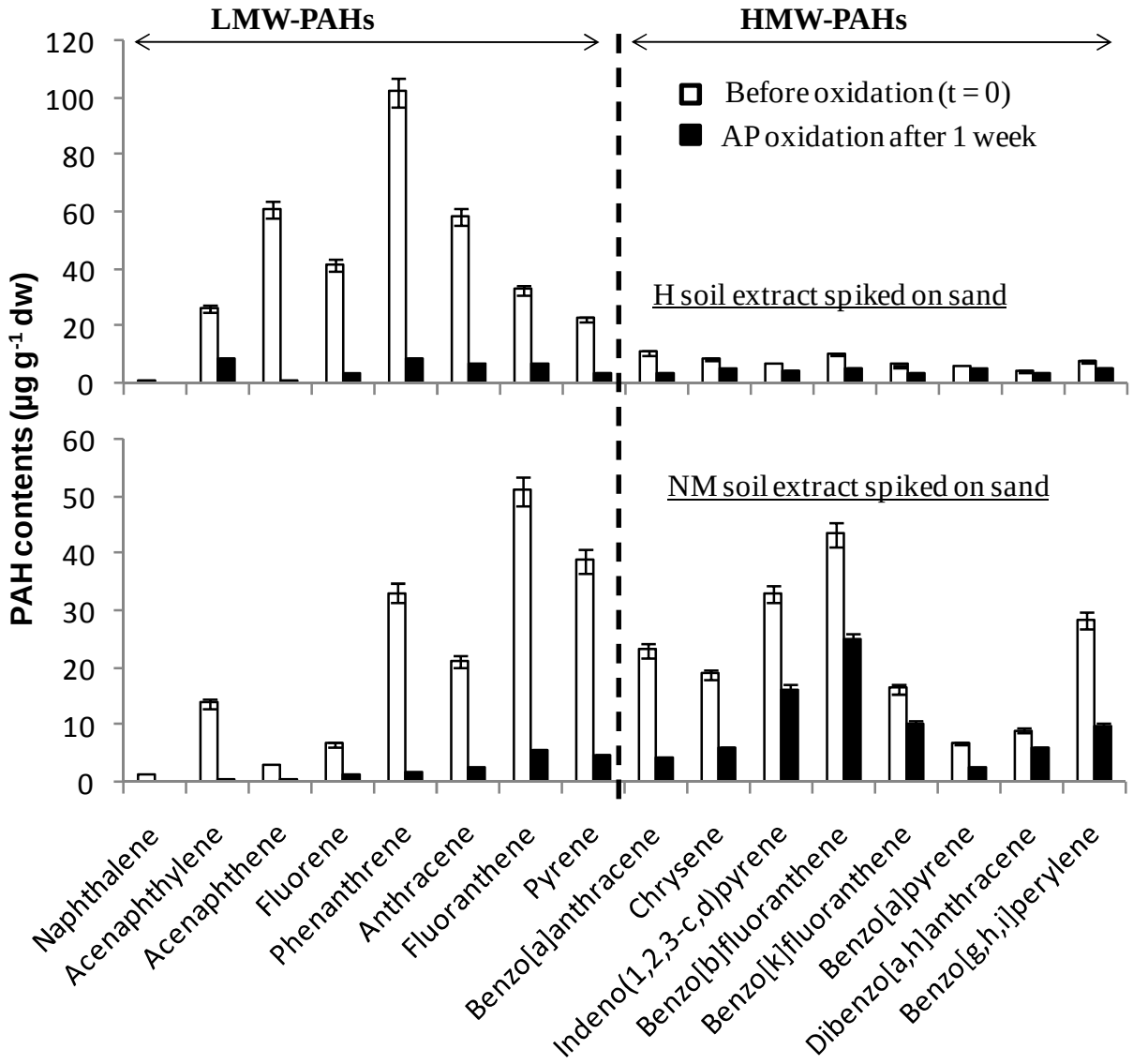

Figure 3: Contents of individual PAHs in organic extracts of both soils (H and NM) at t = 0 before oxidation (□) and after one week of oxidation by magnetite-activated persulfate (■-AP) PAH contents are based on the measurements by GC-MS.

The ratio of low molecular weight PAH (LMW: sum of naphthalene to pyrene concentrations) over high molecular weight PAH (HMW: sum of benzo[a]anthracene to benzo[g,h,i]perylene concentrations) LMW/HMW was different for both soils. The ratio of LMW/HMW suggests the predominance of LMW-PAHs with a value of almost 3.8 in H extract as compared to 0.9 in NM extract with higher proportion of HMW-PAHs. After one week of oxidation, ~ 83% of degradation for 16 PAHs in H extract was achieved by AP (Fig. 2). AP showed better PAH removal efficiency for LMW-PAHs and lower reactivity towards HMW-PAHs. As HMW-PAHs are abundant in NM extract, therefore lower degradation yield (~ 72%) was achieved as compared to H extract (~ 83%). Over time, the PAH composition was displaced towards HMW PAHs as a result of more extensive degradation of the smaller PAHs in NM extract. This might be because the LMW-PAHs are more degradable than HMW-PAHs and were removed by persulfate oxidation during the early stage. It was reported that a selective degradation of PAH can be attributed to the weak oxidation conditions, while vigorous oxidation conditions allowed the equal removal of PAHs (Ferrarese et al., 2008). They stated that limited PAH removal was achieved by activated persulfate, but the combined use of activated persulfate and hydrogen peroxide led to a better removal of both LMW and HMW PAHs. Persulfate oxidation also exhibited slower degradation rate of fuel oil than diesel which was likely to result from more complex components in fuel oil (Yen et al., 2011).

During PAH oxidation, degradation by-products can be produced as a result of incomplete mineralization of PAHs. In this study, the research of the eventual oxidation by-products was carried out by µFTIR (Fig. 4) and GC-MS (Fig. S1) at different oxidation times. The findings by µFTIR revealed that the initial EOM characteristics remain unchanged after AP oxidation for both H and NM organic extract (Fig. 4). The stability of the relative intensity of oxygenated bands (especially OH: 3700–3100 cm^{-1} and C=O: 1745–1705 cm^{-1}) suggests the absence of oxygenated by-products formation. Moreover, the similarity of aliphatic profiles (CH_{ali}: 3000–2800 cm^{-1} and ΔCH_{ali}: 1470–1360 cm^{-1}) and aromatic profiles (CH_{aro}: 3100–3000 cm^{-1}, C = C: 1620–1590 cm^{-1} and CH_{aro}: 900–700 cm^{-1}) reveals that no major molecular reorganization occurs (Fig. 4). Molecular analysis of the PAH distribution by GC-MS in organic extracts of H and NM was in agreement with µFTIR findings (Fig. S1). At different oxidation times, almost the same chromatograms were found with respect to retention time of existing molecules. No reaction intermediates or by-products were detected after oxidation suggesting the complete oxidative degradation of PAHs.

These results reveal that magnetite was effective to activate persulfate oxidation of PAHs in spiked sand, while soluble Fe^{II} seems to be unable to activate persulfate. To test if the magnetite was effective in the presence of soil matrix, oxidation was performed in real soils.

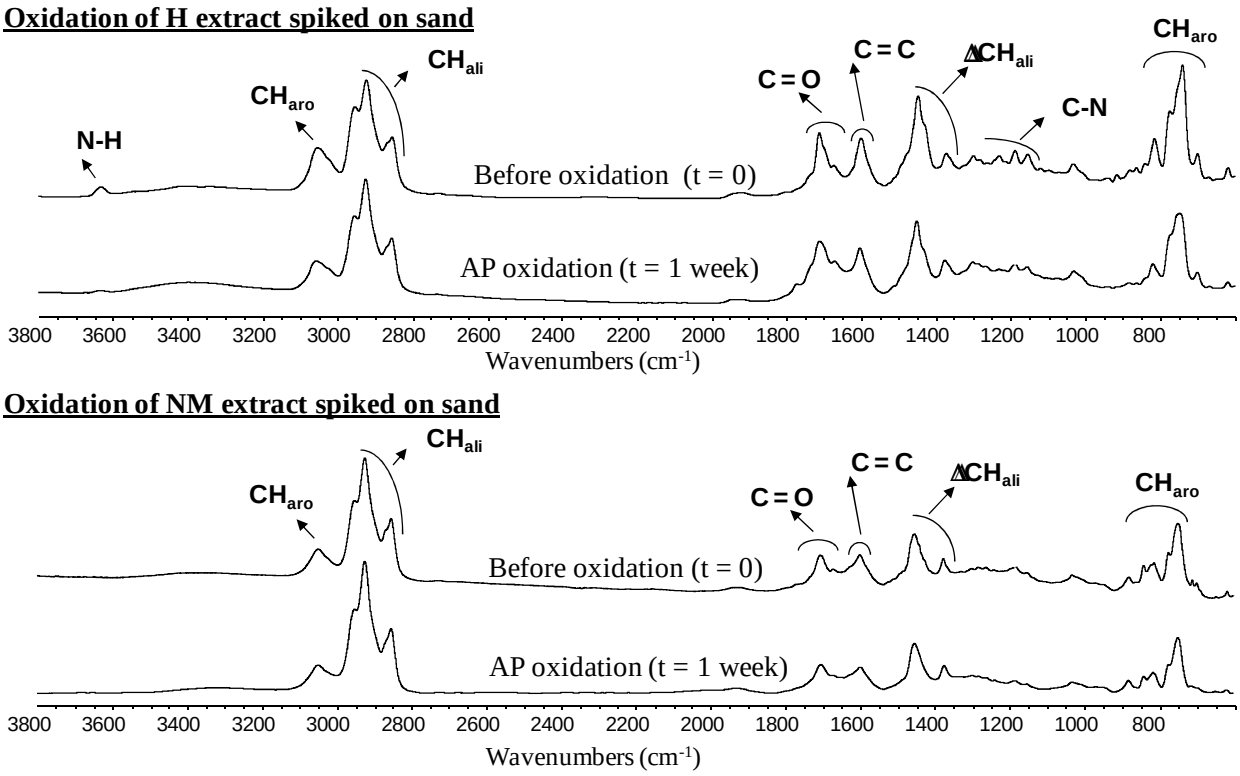

Figure 4: FTIR spectra of (a) organic extract from H soil and (b) organic extract from NM soil before (t = 0) and after oxidation (1 week) by AP oxidation (sodium persulfate + magnetite). Organic extracts from H and NM soil were added to sand and after evaporation of the solvent, oxidation was performed. Experimental conditions were: solid matrix = 2 g, Volume of solution = 20 mL. Oxidant dose was used according to oxidant: Fe molar ratio of 1:1.

.

3.3. PAHs degradation in soils

Before oxidation (t = 0), target soil samples showed higher concentration of 16 PAHs in H soil (~ 1369 µg g^{-1}) than that in NM soil (~ 1279 µg g^{-1}). The value of LMW/HMW PAHs was almost 5.4 and 1.0 in H and NM soil, respectively. The ratio in H soil is higher than observed for its organic extract (Fig. 3) that could be caused by a small loss of LMW compounds during the evaporation of organic extract in spiked sand.

Oxidation treatments applied were AP, FP or SP for the degradation of the 16 PAHs in both soils (H and NM). No PAH removal was observed at pH 8.2 in H and 7.2 in NM, whatever the treatment was used. Same results were obtained even with higher oxidant doses (oxidant:Fe molar ratio of 2:1) (Fig. S2). Thus magnetite-activated persulfate oxidation was effective to degrade PAHs in spiked sand (section 3.2) but not in real soil. The possible explanations for this lack of oxidation in real soil could be PAH unavailability or the soil matrix effect. To determine the possible reason, oxidation was performed in soil after increasing PAH availability by an extraction pretreatment but without isolating the organic extract from soil. In other words, soil extraction was performed as explained in section 2.3 but organic extract was not separated from the rest of soil (mineral + IOM). The chloroform was evaporated from the system and then persulfate oxidation was performed by using oxidant dose according to oxidant:Fe molar ratio of 2:1. The 16 PAHs quantified by GC-MS are represented in terms of C_t/C_0 versus time in Fig. 5. No PAH degradation was observed in blank experiments. Almost 5-10% of degradation was observed with FP or SP. Magnetite activation resulted in degradation extent of PAHs of almost 60% and 50% in H and NM soils, respectively. Thus PAH availability was the crucial factor responsible for the absence of degradation in real soil observed before.

Selective degradation (as observed for organic extracts in section 3.2) resulted in slightly lower PAH degradation in NM soil than H soil. In NM soil, HMW-PAHs are abundant which are difficult to degrade by AP, thus less PAH degradation was observed. Similar to the oxidation of organic extract, GC-MS and µFTIR analyses revealed the absence of by-products (data not shown).

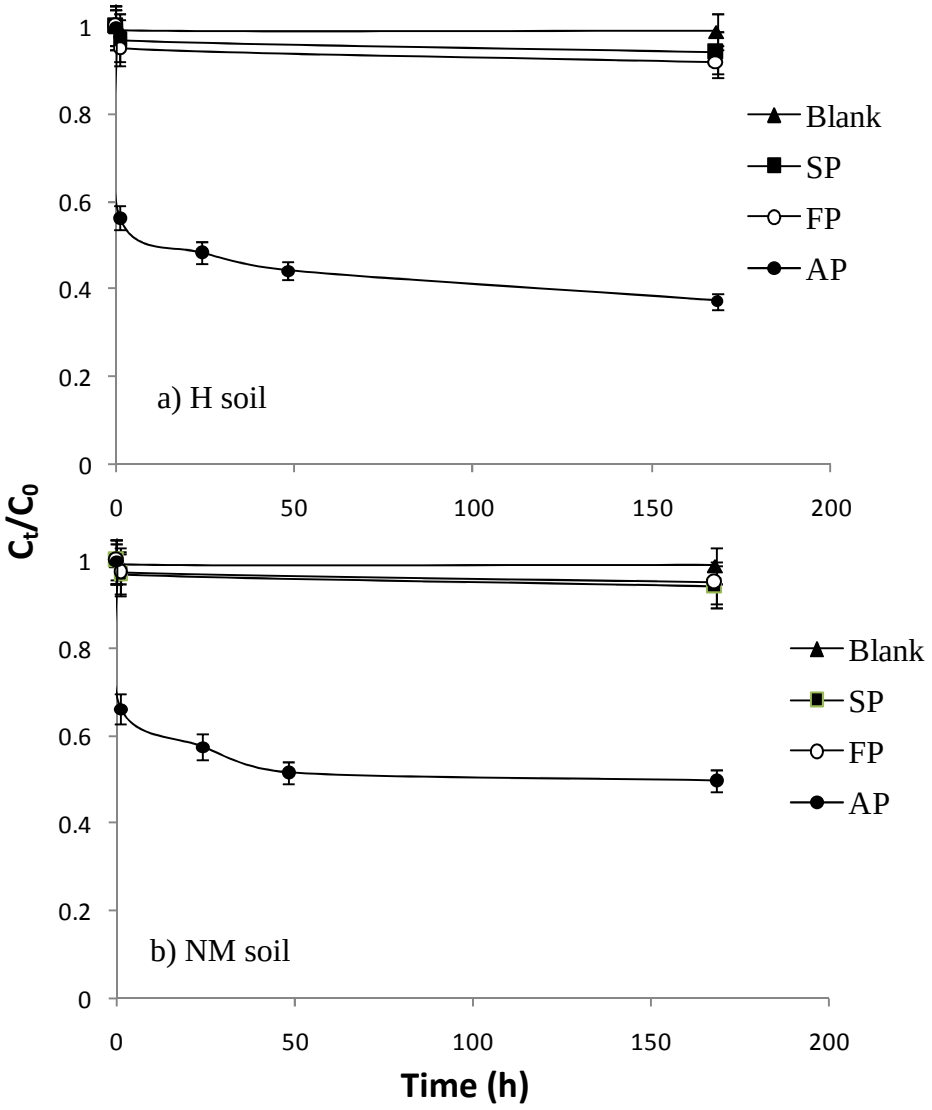

Figure 5: PAH degradation in soils after an extraction treatment (H and NM) during persulfate oxidation experiments by: sodium persulfate alone without iron activation (■-SP), or (ii) sodium persulfate activated with soluble Fe^{II} (○-FP) or sodium persulfate activated with magnetite (●-AP). Blank (▲) experiments were conducted by using only magnetite without any oxidant. This degradation is represented in terms of C_t/C_0 where C_t is the sum of 16 PAH concentration at specified oxidation time and C_0 is their concentration at t = 0 measured by GC-MS. Lines are only visual guide. Experimental conditions were: solid matrix = 2 g, Volume of solution = 20 mL. Oxidant dose was used according to oxidant: Fe molar ratio of 2:1.

These results indicate that once availability of PAHs was increased in tested soils, effective PAH degradation was observed. This highlights the important role of the PAHs availability in the determination of treatment efficiency in a contaminated soil whatever the catalyst used. Degradation extent was, however, decreased in the presence of soil, that can be attributed to the soil matrix effect (mineral and IOM). During persulfate oxidation of trichloroethylene in soil (Liang et al., 2003; Liang et al., 2008) soil constituents exhibited a considerable influence and appeared to scavenge sulfate free radicals. It was stated that the PAH degradation extent by Fenton oxidation was inversely proportional to the total organic carbon (TOC) for the soil with TOC above 5% (Bogan & Trbovic, 2003). TOC in both tested soil samples is close to 10% and 7% for H and NM respectively (Table S.I.1). As the contents of 16-PAHs (~ 1369 and ~ 1279 µg g^{-1} for H and NM respectively) represent less than 2% of soil TOC and EOM (36 and 13 mg g^{-1} for H and NM respectively) corresponds to almost 36% and 17% of H and N soil respectively of the TOC of tested soils. This data represents that most of the SOM is trapped as IOM which would affect oxidation efficiency by oxidant depletion and PAH retention capacity by SOM. The effect of soil matrix is in accordance with previous studies where different soil factors like SOM or the inorganic mineral fractions were found to hinder PAH degradation (Bogan & Trbovic, 2003; Goi & Trapido, 2004; Flotron *et al.*, 2005; Jonsson *et al.*, 2007). In addition to SOM, clay particles contribute to the strong sorption of PAHs in soils (Kawahara et al., 1995), thus making it less available for degradation. However, the impact of soil matrix is less pronounced for persulfate oxidation than Fenton oxidation system. It was previously reported that persulfate can be activated at basic pH by organic compounds similar to those present in soil organic matter (Ahmad et al., 2010). In the same time, some soil mineral components were unable to activate persulfate oxidation, rather they could act as scavenging agents (Ahmad et al., 2010).

The interactions between persulfate and Fe^{II}-Fe^{III} oxide surface (e.g. magnetite) can be explained by heterogeneous reactions analogous to the solution phase reactions and those proposed for heterogeneous Fenton-like oxidation:

$$\equiv Fe^{II} + S_2O_8^{2-} \rightarrow \equiv Fe^{III} + SO_4^{\bullet -} + SO_4^{2-} \quad (1)$$

Since ferric oxides like ferrihydrite and goethite were shown to activate persulfate (Ahmad et al., 2010), Fe^{III}-oxide surface could react with $S_2O_8^{2-}$ to generate sulfate radical but the interactions of persulfate anion with the iron mineral surface are not yet well argued. It was,

however, reported that Fe-surface can act as radical sulfate scavenger as it is known for hydroxyl radical:

$$\equiv Fe^{II} + SO_4^{\bullet -} \rightarrow \equiv Fe^{III} + SO_4^{2-} \quad (2)$$

Other competitive or scavenging reactions may be occurred such as the recombination of sulfate radicals to generate sulfate anion (Mora et al., 2009)

$$2SO_4^{\bullet -} \rightarrow S_2O_8^{2-} \qquad k = 5 \times 10^8 \ M \ s^{-1} \quad (3)$$

On the other hand, hydroxyl radical can be produced at alkaline pH conditions (Mora et al., 2009) *via*: $SO_4^{\bullet -} + HO^- \rightarrow SO_4^{2-} + {}^{\cdot}OH$ (4)

and at all pH values *via:* $SO_4^{\bullet -} + H_2O \rightarrow HO^{\bullet} + HSO_4^-$ (5)

Liang et al. (2007) suggested that the sulfate radical predominates under acidic conditions and the hydroxyl radical under alkaline conditions. Both hydroxyl and sulfate radicals could attack the target contaminants, but they also react with persulfate anion as:

$$HO^{\bullet} + S_2O_8^{2-} \rightarrow HSO_4^- + SO_4^{\bullet -} + \tfrac{1}{2}O_2 \quad \text{or} \quad HO^{\bullet} + S_2O_8^{2-} \rightarrow S_2O_8^{\bullet -} + HO^- \quad (6)$$

$$SO_4^{\bullet -} + S_2O_8^{2-} \rightarrow S_2O_8^{\bullet -} + SO_4^{2-} \quad (7)$$

Finally, radical sulfate may react with organic matter to give organic radical, as for instance:

$$SO_4^{\bullet -} + ROH \rightarrow HSO_4^- + R^{\cdot}OH \quad (8)$$

In the soil slurry system, there should be many reactions with synergic and/or antagonistic effect on the persulfate activation and persulfate oxidation reaction. All the soil matrix factors could contribute in influencing the persulfate oxidation efficiency.

4. Conclusion

This study reported the use of magnetite to activate persulfate oxidation for the degradation of PAHs in spiked sand and in aged contaminated soils at circumneutral pH. All experimental results indicated the higher efficiency of magnetite-activated persulfate oxidation (AP) for PAH removal. Experiments performed with soluble Fe^{II} (FP) or without iron activation (SP) resulted in only 15-20% of PAH removal in spiked sand while 5-10% in real soil. Such similar degradation with or without soluble Fe^{II} exhibits the inability of soluble Fe^{II} to activate persulfate oxidation. However, magnetite was highly reactive to activate persulfate oxidation as almost 5 times higher PAH removal efficiency was observed in the AP oxidation system. This big discrepancy points out the importance of catalyst type sued to activate persulfate decomposition.

On the other hand, the PAH unavailability as well as soil matrix effect seems to be the most important factors for persulfate oxidation process. Selective degradation behaviour was shown by persulfate oxidation with less efficiency towards HMW-PAHs. No by-products were observed in both treated soils. Application of magnetite is therefore effective for significant activation of persulfate at circumneutral pH and could be a promising way for improving chemical oxidation of aged contaminated soils. For ***in situ*** applications, further investigations should be done for the transport study of magnetite and oxidant in soil columns.

Acknowledgements: The authors gratefully acknowledge the financial support of this work by HEC (Higher Education Commission of Pakistan) and ADEME “Agence de l'Environnement et de la Maîtrise de l'Energie” (Grant N° 0972C0016). We are also thankful to the Région Lorraine and GISFI **(**Groupement d'Intérêt Scientifique sur les Friches Industrielles) for support. The authors would like to thank the anonymous reviewers for their valuable comments and suggestions that have improved the manuscript.

Supplementary contents available

Supplementary contents

I. Kinetic oxidation experiments

Oxidation treatments at circumneutral pH were performed as following: (i) sodium persulfate alone without iron activation (SP), or (ii) sodium persulfate activated with soluble Fe^{II} (FP) or sodium persulfate activated with magnetite (10% w/w) (AP). Equivalent molar amount of Fe was used to compare the efficiency of both catalysts to activate persulfate.

Kinetic degradation of PAHs was studied for one week in batch series by assigning one batch for each time point (1 h, 6 h, 24 h, 48 h and 1 week). Oxidation experiments were performed at room temperature and in the absence of light achieved by aluminum foil coverings to avoid any photolytic degradation. Blank experiments were performed by using magnetite alone without oxidant, otherwise rest of the conditions were same, to study possible desorption or degradation of the PAHs. In the standard procedure, water and catalysts (magnetite or soluble Fe^{II}) was added to solid matrix (2 g) to made soil slurries to have a final solution volume of 20 mL. The pH was initially adjusted at 6.8 ± 0.2 for fluorenone and organic extract isolated form soil and then checked during the whole course of oxidation. The oxidant was applied in soil without pH adjustment that remained almost stable throughout the experiment. The suspensions were stirred for 15 minutes followed by the oxidant addition. At a specified reaction time, the corresponding batch was withdrawn from the series and was frozen to stop reaction. The samples were then freeze dried to remove water.

II. Extraction and analysis

The freeze dried samples were extracted in chloroform during 45 min at 60°C. The volume was reduced to 20 mL under nitrogen flow and 5mL of the solution was dried and weighed to determine the amount of EOM.

PAHs were quantified by GC-MS analyses that were performed by adding internal standards to the samples. An internal deuterated PAHs standard mix (naphthalene-d_8, acenaphthene-d_{10}, phenanthrene-d_{10}, chrysene- d_{12}, and perylene-d_{12}, supplied by Cluzeau) was added. A 1 μL amount of solution was then injected into an Agilent Technologies 6890 gas chromatograph equipped with a DB 5-MS (length: 60 m; diameter: 0.125 mm) capillary column coupled to an Agilent Technologies 5973 mass spectrometer operating in full scan mode. The temperature

program was the following: 60 to 250 °C at 15 °C min^{-1}, then 250 to 315 °C at 3 °C min^{-1}, and 60 min holds at 315 °C. The carrier gas was helium at 1.5 mL min^{-1} constant flow.

The micro Fourier Transform Infrared (µFTIR) spectroscopic analysis were performed on an infrared spectrometer Bruker IFS55 coupled with a Multipurpose Bruker IR microscope equipped with a MCT detector cooled with liquid N_2. EOM were analyzed as described by (Faure ***et al.***, 1999) using a diamond window in order to avoid drawbacks usually encountered when using bulk infrared on KBr pellets, such as contamination by water adsorbed on the highly hygroscopic KBr (Ruau ***et al.***, 1997). The spectra were recorded with the following conditions: size of the analyzed area 60 μm^2, 64 accumulations (32 s), spectral resolution 4 cm^{-1}, gain 4.

III. Calculation of relative standard deviation:

The average "mean" of a set of n data x_i:

$$\bar{x} = \frac{\sum x_i}{n}$$

Standard deviation is the most commonly used measure of the spread or dispersion of data around the mean. The standard deviation is defined as the square root of the variance (V). The variance is defined as the sum of the squared deviations from the mean, divided by n-1.

$$s = \sqrt{\frac{\sum (x_i - \bar{x})^2}{n-1}}$$

The relative standard deviation (RSD) is expressed as a fraction, but more usually as a percentage and is then called coefficient of variation (CV):

$$RSD = \frac{s}{\bar{x}} \qquad CV = \frac{s}{\bar{x}} \times 100\%$$

Example: three sets of degradation data of fluorenone during persulfate oxidation experiments by sodium persulfate activated with magnetite (AP). C_t is the fluorenone concentration (mg/g of sand) at specified oxidation time (h).

	1st	2nd	3rd	Average	
Time (h)	C_t	C_t	C_t	C_t	RSD (%)
0	4.33	4.44	4.17	4.31	3.14
1	3.51	3.69	3.47	3.55	3.29
6	2.22	2.31	2.16	2.23	3.38
24	0.61	0.58	0.64	0.61	4.91
48	0.08	0.09	0.08	0.08	5.12
168	0	0	0	0	

The relative standard deviation of the three replicates is then considered around 5% for all data points. This is represented by an error bars in Figure 1.

Table S1. Physico-chemical parameters and total elemental analyses of soil samples

	H soil	NM soil
Clay (<2µm) ($g.kg^{-1}$)	99	126
Fine silt (2-20µm) ($g.kg^{-1}$)	151	164
Coarse silt (20-50µm) ($g.kg^{-1}$)	91	97
Fine sand (50-200µm) ($g.kg^{-1}$)	184	120
Coarse sand (200-2000µm) ($g.kg^{-1}$)	475	493
Agronomic parameters		
pH (water)	8.35	7.20
Total $CaCO_3$ ($g.kg^{-1}$)	369	38
Phosphorus P_2O_5 ($g.kg^{-1}$)	0.090	0.287
Total organic carbon ($g.kg^{-1}$)	102.0	70.6
Total nitrogen ($g.kg^{-1}$)	2.25	2.70
C/N	45.4	25.8
Solvent extractable organic matter ($g.kg^{-1}$)	36.81	13.37
16 PAHs ($mg.kg^{-1}$)	1369	1279
Total elemental analysis (%)		
Al_2O_3	6.78 ± 0.03	7.58 ± 0.40
CaO	13.92 ± 0.49	12.58 ± 0.68
Fe_2O_3	24.34 ± 0.76	24.44 ± 0.38
MgO	1.76 ± 0.06	1.71 ± 0.13
MnO	0.34 ± 0.00	0.93 ± 0.15
P_2O_5	0.65 ± 0.03	0.77 ± 0.03
SiO_2	17.76 ± 0.84	25.66 ± 0.78
K_2O	0.53 ± 0.07	1.37 ± 0.16
Na_2O	0.14 ± 0.08	0.50 ± 0.10
Loss by combustion	29.23 ± 0.68	24.04 ± 1.70
Total	95.46	99.58

I- Characterization by GC-MS

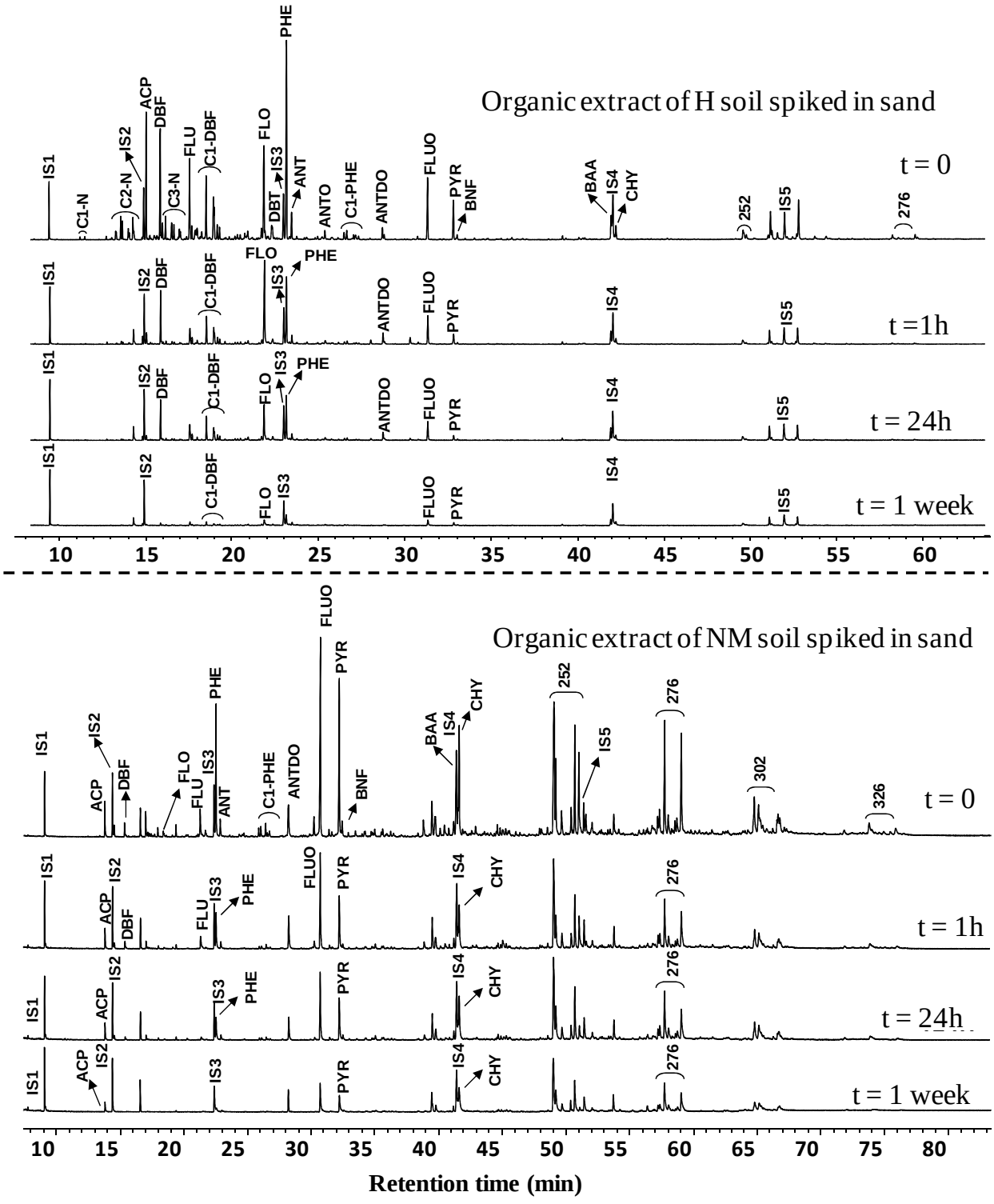

Figure S1: Molecular distribution from GCMS analyses of H and NM organic extract before (t=0) and at different oxidation times by magnetite activate persulfate (AP) oxidation. The compounds are detailed in table S2

Table S2. Details of the abbreviated compounds enlisted in the chromatograms of Figure S1.

Code	*Name*
IS-1	*Naphthalene-D8*
C1-N	*methyl-naphthalene*
C2-N	*ethyl & dimethyl-naphthalene*
IS2	*Acenaphtene-D10*
ACP	*Acenaphtene*
DBF	*Dibenzofuran*
C1-DBF	*Methyl-Dibenzofuran*
FLO	*Fluorenone*
DBT	*Dibenzothiopene*
IS3	*Phenanthrene-D10*
PHE	*Phenanthrene*
ANT	*Anthracene*
ANTO	*Anthracenone*
C1-PHE	*Methyl-phenanthren*
ANTDO	*Anthracendione*
FLUO	*Fluoranthene*
PYR	*Pyrene*
BNF	*Benzonaphtofuran*
BAA	*Benzo[a]anthracene*
IS4	*Chrysene-D12*
CHY	*Chrysene*
252	*PAH 252 g/mol*
IS5	*Perylene-D12*
276	*PAH 276 g/mol*

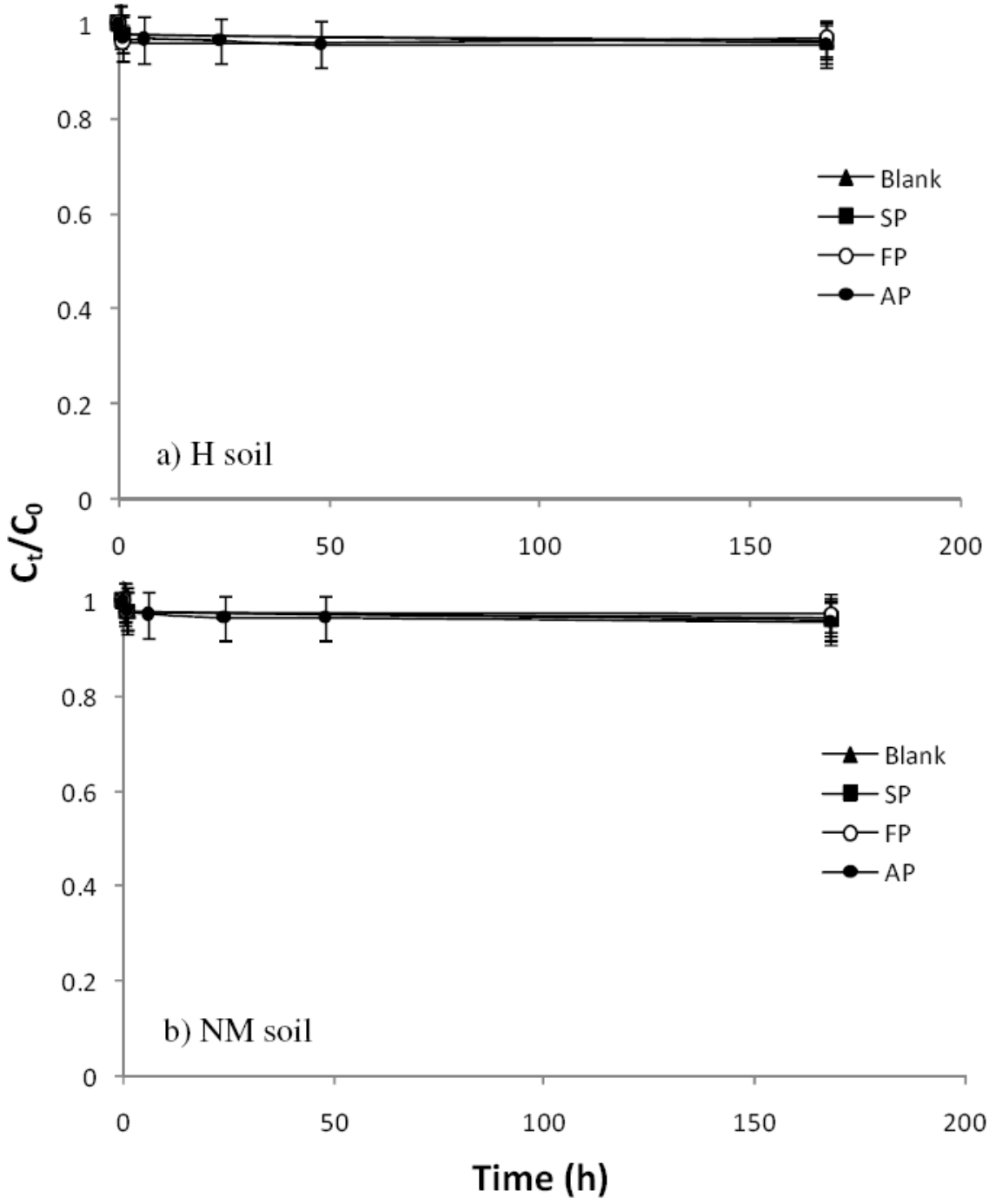

Figure S2: PAH degradation in soils (H and NM) during persulfate oxidation experiments by: sodium persulfate alone without iron activation (■-SP), or (ii) sodium persulfate activated with soluble Fe^{II} (○-FP) or sodium persulfate activated with magnetite (●-AP). Blank (▲) experiments were conducted by using only magnetite without any oxidant. This degradation is represented in terms of C_t/C_0 where C_t is the sum of 16 PAH concentration at specified oxidation time and C_0 is their concentration at t = 0 measured by GC-MS. Lines are only visual guide. Experimental conditions were: solid matrix = 2 g, Volume of

solution= 20 mL. Oxidant dose was used according to oxidant: Fe molar ratio of 2:1. Same were the results with oxidant: Fe molar ratio of 1:1.

Magnetite as a catalyst for chemical oxidation of hydrocarbons spiked on sand under flow through conditions

M. Usman[a,b], P. Faure[b], C. Ruby [a] and K. Hanna[c]

[a] Laboratoire de Chimie Physique et Microbiologie pour l'Environnement, LCPME, UMR 7564 CNRS, 405 rue de Vandoeuvre, 54600, Villers Les Nancy, France.

[b] Géologie et Gestion des Ressources minérales et énergétiques, G2R, UMR 7566, 54506, Vandoeuvre Les Nancy, France.

[c] Ecole Nationale Supérieure de Chimie de Rennes, UMR CNRS 6226 "Sciences Chimiques de Rennes", Avenue du Général Leclerc, 35708 Rennes Cedex 7, France.

Abstract

Soil pollution by hydrocarbons (aromatic and aliphatic hydrocarbons) is a serious environmental issue. The chemical oxidation has been successfully applied for the remediation of hydrocarbon contamination in batch slurry system. In present laboratory study, column experiments were performed to evaluate the efficiency of magnetite catalyzed Fenton-like (FL) and activated persulfate (AP) oxidation for hydrocarbon degradation.

Organic extracts isolated from three different soils (two polycyclic aromatic hydrocarbon polluted soils and one oil-contaminated soil) were spiked on magnetite rich sand. After evaporation of solvent, spiked sand was packed in column and was subjected to oxidation. Oxidant was injected at a flow rate of 0.1 ml/min under water saturated conditions. Organic analyses were performed by GC-MS, GC-FID and µ-FTIR.

Significant abatement of both types of hydrocarbons (60-70%) was observed. No by-products were found after FL oxidation but some oxygenated by-products were detected after AP. Non-selective degradation was evaluated for FL while AP showed less reactivity towards higher molecular weight PAHs. Results of this study confirmed that magnetite-catalyzed chemical oxidation can degrade both kinds of hydrocarbons in column experiments.

.

Keywords: Soil; oil; aromatic hydrocarbons, magnetite; oxidation; Fenton; persulfate.

1. Introduction

The intense use of fossil organic matter (petroleum and coal) since 18th century for industrial purposes (petroleum extraction, refinery, coking plant, steel industries etc.) has resulted in widespread pollution by polycyclic aromatic hydrocarbons (PAHs) and petroleum by-products (aliphatic) hydrocarbons that cause environmental and health concerns. Especially, 16 PAHs in the US EPA list are considered as priority pollutants by US EPA and European community, are well known carcinogenic pollutants. Different remediation techniques have been tested for their removal from contaminated matrixes. Owing to their high persistence in

soil, they are resistant to environmental degradation and imply huge industrial treatments. On the contrary, oil hydrocarbons are easily degradable by bioremediation (Prince, 1993). However, bioremediation showed limited application to biorefractory materials especially asphaltenes (Gough & Rowland, 1990; Chaillan *et al.*, 2006). Application of chemical oxidants has been quite successful in remediating hydrocarbon contamination (Watts & Dilly, 1996; Kong *et al.*, 1998a; Kanel *et al.*, 2004; Ferrarese *et al.*, 2008; Do *et al.*, 2010; Yen *et al.*, 2011).

In our recent studies (Usman *et al.*, 2011a; Usman *et al.*, 2011b; Usman *et al.*, 2011c), magnetite, (Fe^{II}-$Fe^{III}_2O_4$) was found effective to catalyze Fenton-like and persulfate oxidation of PAHs and aliphatic hydrocarbons in batch slurry system at circumneutral pH. The objective of this study is to test the ability of magnetite to catalyze H_2O_2 and persulfate in a column system under flow through conditions. Previous studies stated that the limiting factors influencing the oxidative degradation include iron catalyst type, PAHs availability and soil matrix effect (Usman *et al.*, 2011a; Usman *et al.*, 2011b; Usman *et al.*, 2011c). Oxidation of PAHs was observed only after a PAHs availability enhancement agent in natural soil in batch slurry system. For that reason, the oxidation reaction was conducted on organic extracts in the column system. Organic extracts isolated from three soils (one oil contaminated soil and two different PAH contaminated soils) were spiked on sand and oxidant solution (H_2O_2 or persulfate) were injected into the sand packed column. The hydrodynamic parameters flow rate, velocity and bed height (column length) were chosen to ensure a convective regime. After oxidation, organic analyses were performed by GC-MS, GC-FID and µFTIR.

2. Experimental Section

2.1. Sample preparation

Magnetite rich sand (MRS) (10% of magnetite w/w) was prepared and characterized in context of a previous study and same MRS was used here (Usman *et al.*, 2011a). Oxidative degradation of aliphatic hydrocarbons and PAHs was studied. Aliphatic hydrocarbons present in weathered oil (WO) were extracted from an oil contaminated forest soil that was under natural attenuation from Pechelbronn oil field (located in Alsace, France). Organic extract containing PAHs were isolated from two polluted soils of former coking plant sites

(Homécourt (H) and Neuves-Maisons (NM) located in the Northeast of France)). Properties of both soils were already detailed (Usman ***et al.***, 2011b). For organic extraction, contaminated soil samples were sieved at 2 mm, freeze-dried and extracted using an automatic extractor Dionex® ASE 200 (Accelerated Solvent Extractor) at 100° C and 130 bars with DCM.

These organic extracts from WO, H and NM samples were spiked on MRS to obtain a final concentration of 4g/Kg of MRS. The DCM was evaporated with a continuous mixing to ensure homogeneous contaminant distribution. This spiked sand was considered as reference (t= 0).

2.2. Oxidation under flow through conditions

Three treatments were included to study oxidative degradation of hydrocarbons which were: *i)* Fenton-like (FL = H_2O_2 + magnetite), *ii)* activated persulfate (AP- sodium persulfate + magnetite) and *iii)* blank without any oxidant. Oxidation was performed with oxidant:Fe molar ratio equal to 10:1 and 1:1 for FL and AP respectively under flow through conditions. The schematic diagram of column used in this study is given in Fig. 1. In a glass chromatographic column of 40 cm length and 2.6 cm internal diameter (XK 26/20, GE Healthcare), the spiked MRS particles were packed to a height of 6.5 cm, corresponding to a dry mass of 50 g. The dry porous bed had a uniform bulk density (ρ) of 1.23 ± 0.01 g/cm^3. After packing, the column was cautiously wetted upward with the Milli-Q water (Millipore). Throughout the experiments, the flow rate was held constant at 0.1 mL/min, corresponding to a pore water velocity of 0.019 cm/min, the flow direction was from bottom to top of the column. Flow rate was checked several times by comparing inflow and outflow and was found constant. Porous volume of the MRS column measured by weighing before and after water saturation, was almost 10.5 ± 0.02 mL. Blank experiments were conducted by injecting water only. Dissolved organic carbon (DOC) was almost zero in outflow stating the absence of hydrocarbons degradation or desorption. After blank experiments, oxidant solution (oxidant + water= 500 mL) was injected with same flow rate (0.1 mL/ min) under water saturated conditions. In all experiments, dissolved iron concentrations in the outflow were measured by Inductively Coupled Plasma-Atomic Emission Spectroscopy (ICP-AES). Iron detected in solution was negligible indicating that no magnetite had passed the filter membrane. Effluents from each column after oxidation were collected and analyzed for DOC

but its value was very low (10-15mg/L) with almost negligible difference between the different fractions of effluent and the different treatments (FL or AP). This contaminant loss is ignored in description of results presented in the following sections.

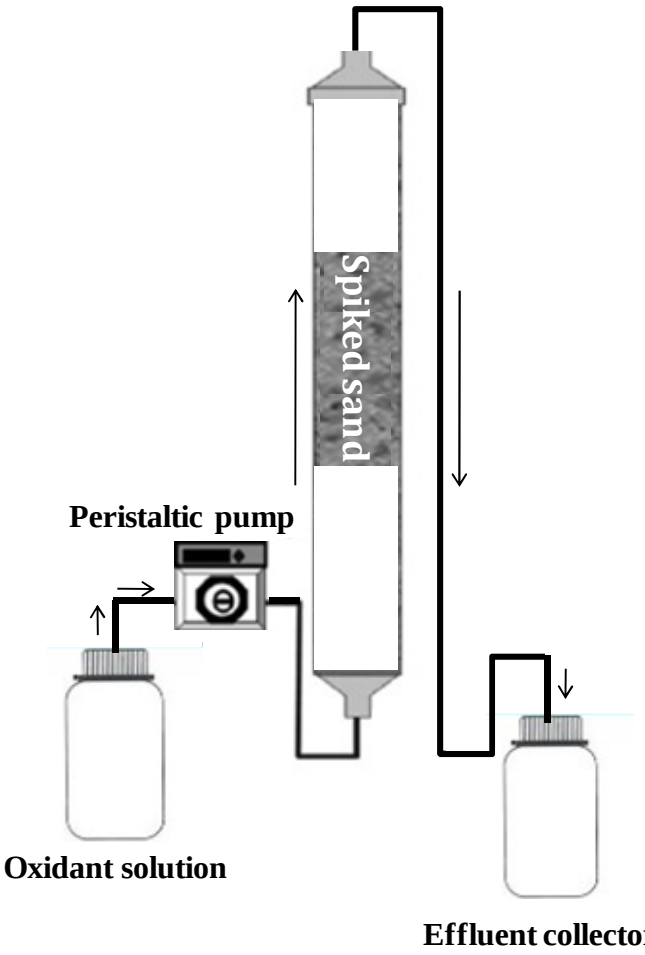

Figure 1: Diagram showing the layout of column used for oxidation experiments

Once whole solution was injected, the treated MRS column was frozen to stop reaction. The samples were then freeze dried to remove water. All experiments were performed without pH adjustment and at room temperature. Blank experiments were carried out on spiked MRS under the same conditions except no oxidant was added, to study possible desorption or degradation of the pollutants.

2.3. Extraction and analysis

After freeze drying, the samples were submitted to five cycles of $CHCl_3$ Soxhlet extractions for 24 h each. The solvent volume was then reduced to 50 mL under a nitrogen flow, and then

5 mL of the solution was dried and weighed in order to determine the amount of extractable organic matter (EOM).

The hydrocarbon oil index (HI) was measured for oil hydrocarbons according to ISO 16703:2004 procedure using a GC-FID 7890 Agilent technologies.

GC-MS quantification of PAHs organic extracts was performed by adding internal standards to the samples. An internal deuterated PAHs standard mix (naphthalene-d_8, acenaphthene-d_{10}, phenanthrene-d_{10}, chrysene- d_{12}, and perylene-d_{12}, supplied by Cluzeau) was added. A 2 μL amount of solution was then injected into an Agilent Technologies 6890 gas chromatograph equipped with a DB 5-MS (length: 60 m; diameter: 0.125 mm) capillary column coupled to an Agilent Technologies 5973 mass spectrometer operating in full scan mode. The temperature program was the following: 60 to 250 °C at 15 °C min^{-1}, then 250 to 315 °C at 3 °C min^{-1}, and 60 min holds at 315 °C. The carrier gas was helium at 1.5 mL min^{-1} constant flow.

The micro Fourier Transform Infrared (µFTIR) spectroscopic analysis were performed on an infrared spectrometer Bruker IFS55 coupled with a Multipurpose Bruker IR microscope equipped with a MCT detector cooled with liquid N_2. EOM were analyzed as described by (Faure *et al.*, 1999) using a diamond window. The spectra were recorded with the following conditions: size of the analyzed area 60 μm^2, 64 accumulations (32 s), spectral resolution 4 cm^{-1}, gain 4.

3. Results and Discussion

3.1. Degradation of oil hydrocarbons

The presence of intense unresolved complex mixture (UCM) before oxidation was observed as demonstrated in previous study (Usman *et al.*, 2011a). It is generally considered as an iso- and cyclo-alkanes mixture (Gough & Rowland, 1990). UCM was the sole reactant in reference sample due to its totally refractory nature to microbial attack (Gough & Rowland, 1990; Chaillan *et al.*, 2006). Initial samples (before oxidation) did not contain n-alkanes because they are biodegradable (Chaillan *et al.*, 2006) and sampled soil area was under natural attenuation for years that caused their degradation. The degradation of oil hydrocarbons was monitored by EOM evolution and hydrocarbon index (HI), both of which

were in agreement. The EOM recovered from MRS before oxidation was ~4mg/g (initially added amount) representing that no EOM was trapped in sand. The GC-FID measured HI is presented before and after oxidation (Fig. 2). Negligible degradation was observed in blank experiments (conducted in the absence of any oxidant) (<3%). Significant reduction in HI was obtained by FL (70%) and AP (62%). Compared to previous batch findings (Usman *et al.*, 2011a), slight reduction in degradation was observed. Results obtained in column experiments confirm previous batch findings (Usman *et al.*, 2011a) and treatment was also effective for the degradation of oil hydrocarbons refractory to biodegradation (like UCM).

3.2. Degradation of PAHs

Before oxidation, the total content of PAHs in H extract was lower (204 µg/g) than NM extract with 348 µg g^{-1} of sand. The ratio of low molecular weight PAH (LMW: sum of naphthalene to pyrene concentrations) over high molecular weight PAH (HMW: sum of benzo[a]anthracene to benzo[g,h,i]perylene concentrations), LMW/HMW was calculated. This ratio suggested the predominance of LMW-PAHs with a value of 3.81 in H extract as compared to 0.94 in NM extract with higher proportion of HMW-PAHs. Organic extracts of both soils (H and NM) were oxidized in the presence of MRS. Blank experiments did not show any degradation. Figure 2 shows the residual concentrations of 16 PAHs achieved after chemical oxidation treatments. Significant PAHs abatement was observed for both H and NM organic extracts (Fig. 2). As can be seen from data shown, both FL and AP were equally efficient for PAHs degradation in H extract (70%). But in NM extract, FL showed higher degradation (78%) than AP (63%). This difference of degradation was due to the selective degradation of PAHs by AP with less efficiency towards HMW-PAHs that are abundant in NM organic extract (data not shown). On the other hand, FL showed non-selective degradation as observed previously (Usman *et al.*, 2011b; Usman *et al.*, 2011c). This difference in reactivity of both oxidants could be attributed to the production of surfactants during oxidation of PAHs in soils as a result of partial oxidation of hydrocarbons and/or native organics having surfactant-like properties (Ndjou'ou & Cassidy, 2006; Gryzenia *et al.*, 2009). Surfactants could solubilize HMW-PAHs and render them chemically more available. A higher production of surfactant was reported with Fenton oxidation compared to persulfate oxidation, which allows a better removal of HMW-PAHs, and consequently a non-selective degradation of PAHs (Gryzenia *et al.*, 2009). For both PAHs and WO, Fenton treatment was

more efficient than persulfate oxidation which is in agreement with previous batch studies and conclusions made by many other authors (Ferrarese *et al.*, 2008; Usman *et al.*, 2011a; Usman *et al.*, 2011b; Usman *et al.*, 2011c; Yen *et al.*, 2011).

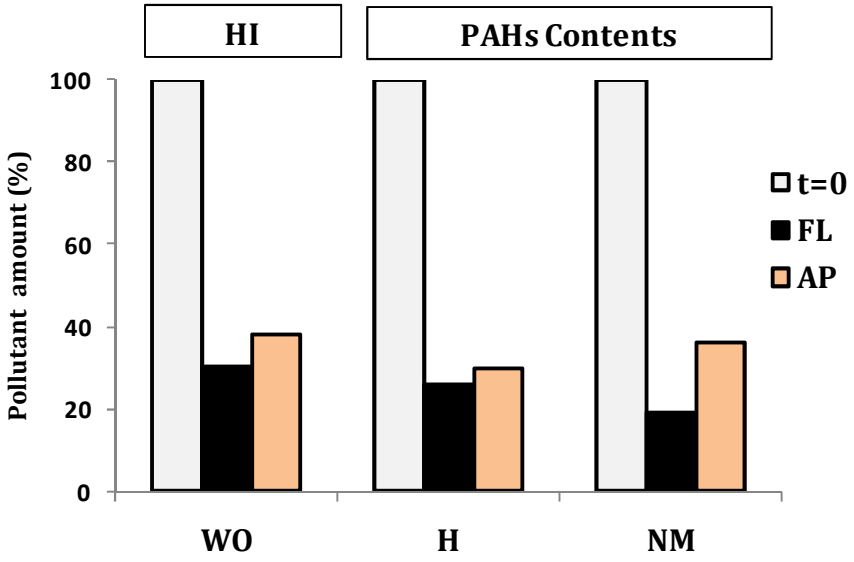

Fig. 2: Hydrocarbon contents (%) in weathered oil (WO), organic extract of H and NM soil, represented before (t=0) and after oxidation by Fenton-like (FL) and activated persulfate (AP). For WO, it is represented as hydrocarbon index (HI) measured by GC-FID while for H and NM soil extracts, it corresponds to PAHs contents measured by GC-MS.

3.3. µFTIR characterization

Investigations by µFTIR (Fig. 3) revealed that aliphatic bands are dominated in WO organic extract (CH_{ali} : 3000 – 2800 cm^{-1} and ΔCH_{ali} : 1470 – 1360 cm^{-1}) with a CH_3/CH_2 ratio values compatible with the predominance of iso and cyclo-alcanes (UCM). Only one weak oxygenated band (C=O : 1745 – 1705 cm^{-1}) appears in all samples. Initial EOM characteristics remain similar after treatment by both oxidants stating the absence of by-products as observed in previous batch study (Usman *et al.*, 2011a).

Moreover, initial EOM characteristics remain unchanged after FL oxidation for both H and NM organic extract (Fig. 3). The stability of the relative intensity of oxygenated bands (especially OH : 3700 – 3100 cm^{-1} and C=O : 1745 – 1705 cm^{-1}) suggests the absence of oxygenated by-products formation. Moreover, the similarity of aliphatic profiles (CH_{ali}: 3000 – 2800 cm^{-1} and ΔCH_{ali}: 1470 – 1360 cm^{-1}) and aromatic profiles (CH_{aro}: 3100 – 3000

cm^{-1}, C=C: 1620 – 1590 cm^{-1} and CH_{aro}: 900– 700 cm^{-1} reveals that no major molecular reorganization occurs. On the other hand, in case of AP oxidation, a small band was appeared in 1500-1700 cm^{-1} range of FTIR spectra for both H and NM extracts. It exhibits the formation of some oxygenated by-products by AP oxidation. Except of this oxygenated band, no significant reaction products were observed by both oxidants. Contrary to column, no by-products were observed in previous batch experiments by both oxidants (Usman *et al.*, 2011b; Usman *et al.*, 2011c). FTIR spectra suggest the complete degradation of hydrocarbons by FL oxidation and a slight formation of oxygenated by-products by AP oxidation.

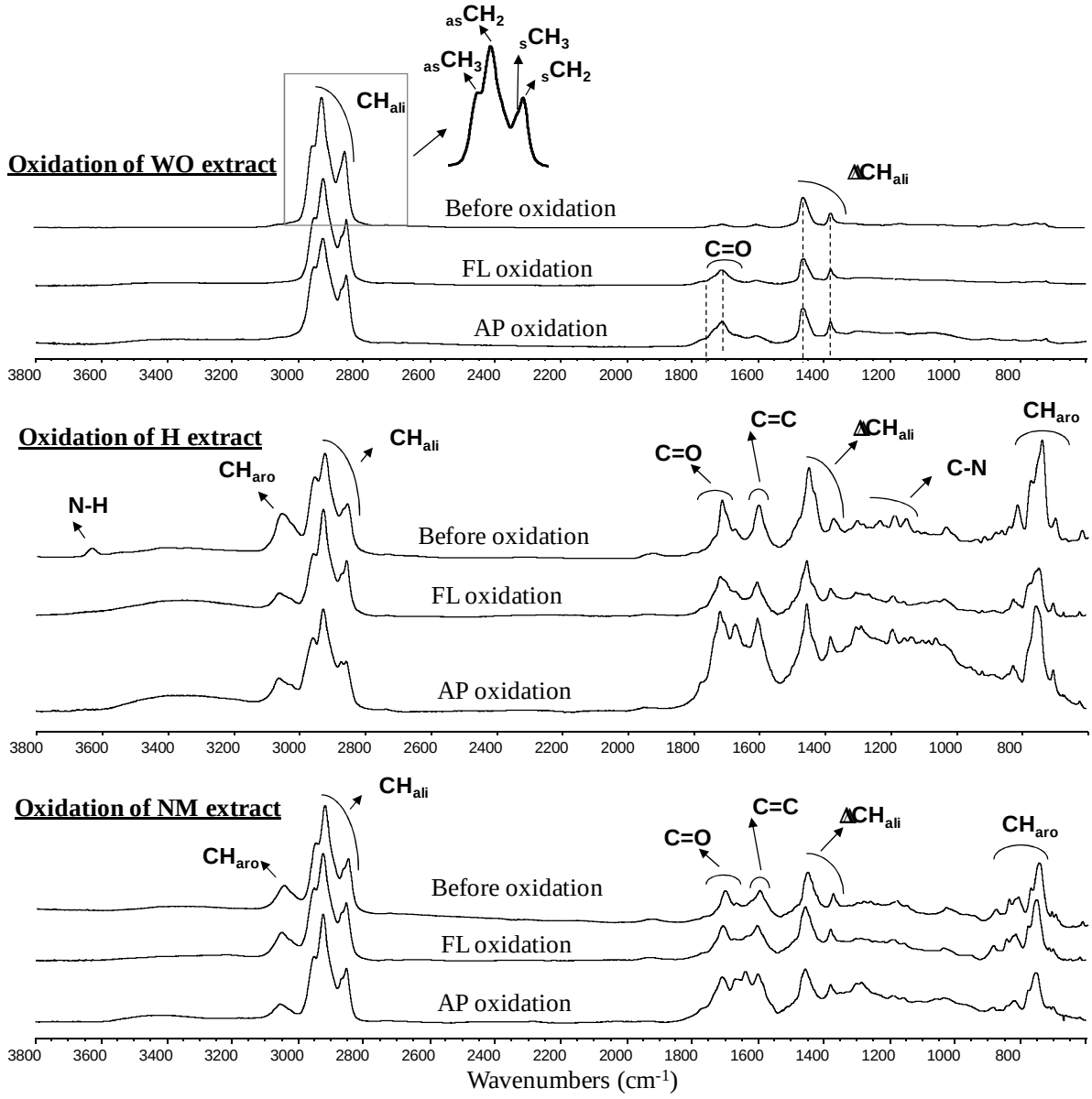

Figure 3: FTIR spectra of WO- weathered oil, organic extracts of H and NM soils before and after oxidation by Fenton-like (FL) and activated persulfate (AP).

4. Conclusion

Ability of magnetite-catalyzed Fenton and persulfate oxidation was represented in column experiments to degrade refractory oil residues (UCM, etc.) as well as PAHs. Achieved results confirm the results obtained in previous batch findings. Slight decrease in reactivity was observed in column experiments as compared to batch. Non-selective degradation was achieved by FL while AP showed less reactivity towards high molecular weight PAHs. Use of magnetite as iron catalyst in real soil column should be investigated.

Acknowledgements

The financial support of the HEC (Higher Education Commission of Pakistan) and GISFI (French Scientific Interest Group - Industrial Wasteland, www.gisfi.prd.fr) project is gratefully acknowledged.

CONCLUSIONS AND PERSPECTIVES

The formation of reactive iron minerals and their reactivity to catalyze chemical oxidation has been investigated in this work. Formation of magnetite and GR was quantified versus aging time (1h, 1day, 1 week and 1 month) and ferric substrate (F, G, L and H) in static batch conditions. Ferrihydrite was found as the most reactive to transform into magnetite. Large amounts of G and H were transformed into GR although they are known for their higher stability. Formation kinetics of GR was much higher than that of magnetite which could favor the formation of GR in environment. Additional experiments performed on three kinds of goethite (G1, G2 and G3) represented that the initiation of transformation reaction by Fe^{II} adsorption to singly coordinated sites through the formation of inner-sphere surface complexes seems to be the most plausible hypothesis. Surface characteristics of magnetite obtained from F, L and G were different so its reactivity could be different which will be addressed in further studies. Magnetite generated by biotic and abiotic ways was also different which could influence its reactivity. Moreover, use of ferrihydrite as starting substrate for transformations could serve as a novel way to prepare nano-magnetite which is highly stable.

The transformations of ferrihydrite rich sand (FRS) under flow through conditions (column experiments) produced small quantities of magnetite and goethite with large amount of untransformed F. Column experiments exhibit some constraints such as mobility of Fe^{II} solution, instability of GR during ***ex-situ*** analyses. Thus FRS transformations in specially designed column are in progress which would allow the ***in-situ*** analyses of product formed (Fig. 3.1). One side of this column is flat. In a lead box, this column is placed in such a way that its flat side is in front of MIMOS source which can move up and down. It will allow the ***in-situ*** analyses of iron products at different heights of column. In this way, after Fe^{II} injection in column, newly generated mixed Fe^{II}-Fe^{III} oxides could be analyzed without withdrawing the solid from column. Different mixing methods of reactants could also be tried in this column under saturated and unsaturated conditions.

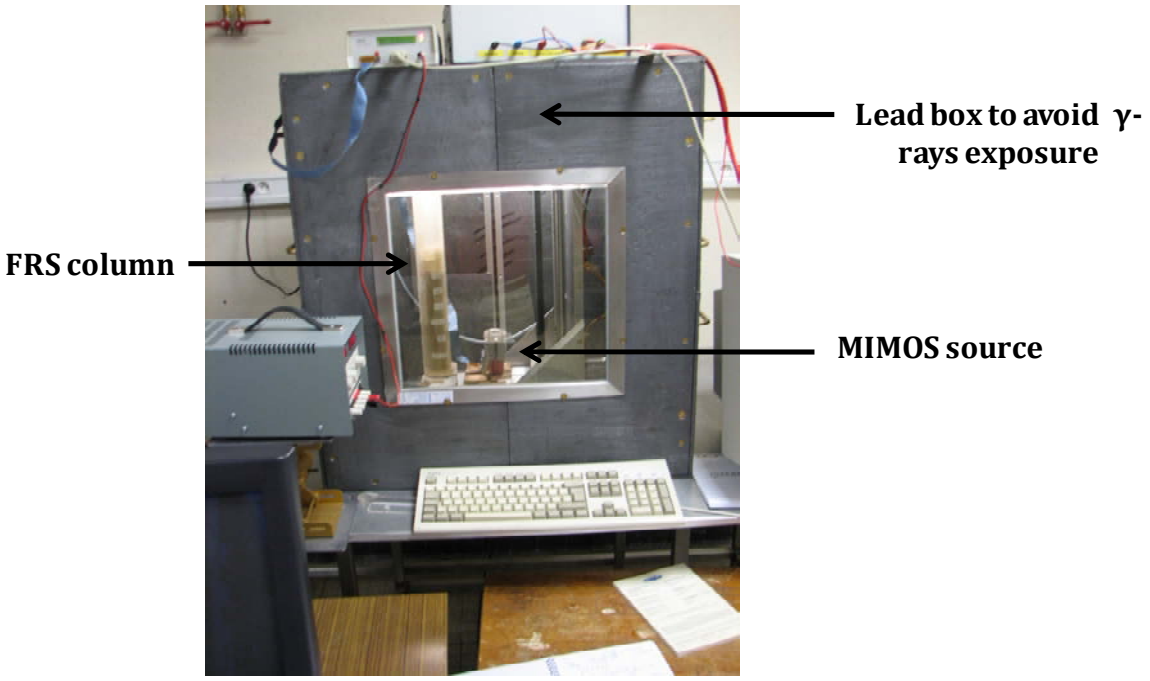

Fig. 3.1: In situ Mössbauer analysis of ferrihydrite rich sand (FRS) transformations in specially designed column.

Then, the reactivity of the magnetite synthesized from ferrihydrite in batch experiments was used to promote Fenton-like and persulfate oxidation for hydrocarbon remediation. Kinetic degradation of oil hydrocarbons as well as PAHs was investigated at circumneutral pH. Significant degradation of oil hydrocarbons present in weathered oil (extracted from an oil contaminated soil) as well as crude oil was achieved when oxidants were catalyzed by magnetite. Currently, many research organizations are working on soil rehabilitation projects by using bioremediation or excavation in oil contaminated sites of France. Magnetite catalyzed chemical oxidation could be a promising treatment for ex-situ application. Further experiments on field soils will allow a better understanding of real field application.

Magnetite was also found effective for the oxidation of two different PAHs-polluted soils if these soils were subjected to oxidation after a PAHs availability enhancement treatment. Oxidation experiments performed with soluble Fe^{II} as catalyst resulted in very low hydrocarbon degradation. Results of this study revealed the importance of the type of catalyst used (magnetite or soluble Fe^{II}), PAHs availability and soil matrix. These important factors

should be considered while designing an oxidation experiment. Magnetite was also found effective to catalyze chemical oxidation for degradation of both kinds of hydrocarbons spiked on sand in column experiments. PAHs availability was a crucial factor in aged contaminated soils which affected the oxidation efficiency which should be investigated in soils where contaminant availability is not an issue.

Results of this study suggest that magnetite can be used as iron source to activate both Fenton and persulfate oxidation at circumneutral pH. Magnetite catalyzed chemical oxidation could be a promising way as remediation treatment after soil excavation or for ***ex-situ*** applications.

Soil endogenous iron was unable to catalyze chemical oxidation stating the iron unavailability or lack of sufficient iron content in soil. Previous Mössbauer analysis conducted on soil NM showed the presence of magnetite (personal communication). Despite this magnetite presence, no natural activation of H_2O_2 or persulfate oxidation has been observed. So, the role of soil endogenous is difficult to be evidenced. Further experiments must be addressed to highlight the role of soil endogenous iron to promote chemical oxidation.

On the other hand, ***in situ*** mineralogical transformations of soil iron minerals to mixed Fe^{II}-Fe^{III} oxides (GR or magnetite) are questionable. Under static batch conditions, ferric minerals mixed with sand were completely transformed into Fe^{II}-Fe^{III} oxides but no transformation was achieved in two different natural soils. In fact, added Fe^{II} may be adsorbed or fixed on soil components such as clay and NOM. It may also undergo oxidation or precipitation in soil solution. Such transformation experiments are hard to investigate with surly zero results.

By using the findings of this research for ***in-situ*** applications, the most plausible way to promote chemical oxidation could be the injection of reactive iron minerals in soil system. However, injection of magnetite nano-particles in saturated and unsaturated porous media was never tested. In literature, injection of zero valent iron powder (ZVIP) is widely investigated especially in saturated zones such as aquifer to decontaminate ground water. One can imagine that magnetite nano-particles can be injected with the same manner as ZVIP. Use of magnetite would resolve the stability issue of catalysts. However, injection of iron particles (ZVIP or magnetite) in unsaturated zones such as vadose zone requires many investigations. The mobility, transport and fate of such particles should be addressed coupled to the modeling of reactive transport of particles. The reactivity, stability and eco-toxicity of magnetite particles

should also be tested in this context. Influence of this practice on soil characteristics, soil fertility and microbial population should also be explored. Influence of magnetite on hydraulic permeability of soil porous media must be studied. Its injection in saturated zone (aquifer) and unsaturated zone (vadose) should be investigated. This technique can be environmentally friendly and economically feasible in case of field application due to oxidation at soil natural conditions. The use of magnetite-catalyzed chemical oxidation could be considered as an innovative treatment for ***ex-situ*** or ***in-situ*** remediation of contaminated soil and groundwater.

References

Abdelmoula, M., Refait, P., Drissi, S.H., Mihe, J.P., Génin, J.M.R., (1996) Conversion electron Mössbauer spectroscopy and X-ray diffraction studies of the formation of carbonate-containing green rust one by corrosion of metallic iron in NaHCO3 and (NaHCO3 + NaCl) solutions. *Corrosion Science*, 38(4), 623-633.

Abdelmoula, M., Trolard, F., Bourrié, G., Génin, J.M.R., (1998) Evidence for the Fe(II)-Fe(III) Green Rust "Fougerite" Mineral Occurrence in a Hydromorphic Soil and Its Transformation with Depth. *Hyperfine Interactions*, 112(1), 235-238.

Ahmad, M., Teel, A.L., Watts, R.J., (2010) Persulfate activation by subsurface minerals. *Journal of Contaminant Hydrology*, 115(1-4), 34-45.

Aissa, R., Francois, M., Ruby, C., Fauth, F., Medjahdi, G., Abdelmoula, M., Génin, J.M., (2006) Formation and crystallographical structure of hydroxysulphate and hydroxycarbonate green rusts synthetised by coprecipitation. *Journal of Physics and Chemistry of Solids*, 67(5-6), 1016-1019.

Allen, S.A., Reardon, K.F., (2000) Remediation of contaminated soils by combined chemical and biological treatments. *Physical and Thermal Technologies: Remediation of Chlorinated and Recalcitrant Compounds*, 301-306.

Amellal, N., Portal, J.M., Berthelin, J., (2001) Effect of soil structure on the bioavailability of polycyclic aromatic hydrocarbons within aggregates of a contaminated soil. *Applied Geochemistry*, 16(14), 1611-1619.

Amonette, J.E., Workman, D.J., Kennedy, D.W., Fruchter, J.S., Gorby, Y.A., (2000) Dechlorination of carbon tetrachloride by Fe(II) associated with goethite. *Environmental Science and Technology*, 34(21), 4606-4613.

Andersson, B.E., Lundstedt, S., Tornberg, K., SchnÃ¼rer, Y., Ã–berg, L.G., Mattiasson, B., (2003) Incomplete degradation of polycyclic aromatic hydrocarbons in soil inoculated with wood-rotting fungi and their effect on the indigenous soil bacteria. *Environmental Toxicology and Chemistry*, 22(6), 1238-1243.

Anipsitakis, G.P., Dionysiou, D.D., (2004) Radical Generation by the Interaction of Transition Metals with Common Oxidants. *Environmental Science & Technology*, 38(13), 3705-3712.

Arden, T.V., (1950) The solubility products of ferrous and ferrosic hydroxides. *Journal of the Chemical Society (Resumed)*, 882-885.

Ardizzone, S., Formaro, L., (1983) Temperature induced phase transformation of metastable Fe(OH)3 in the presence of ferrous ions. *Materials Chemistry and Physics*, 8(2), 125-133.

Atlas, R.M., (1995) Petroleum biodegradation and oil spill bioremediation. *Marine Pollution Bulletin*, 31(4-12), 178-182.

Balazs, G., Cooper, J., Lewis, P., Adamson, M., (2002) Transition Metal Catalysts for the Ambient Temperature Destruction of Organic Wastes Using Peroxydisulfate. In: D.W. Tedder, F.G. Pohland (Eds.), *Emerging Technologies in Hazardous Waste Management 8* (Ed. by D.W. Tedder, F.G. Pohland), pp. 229-239. Springer US.

Barrón, V., Galvez, N., Hochella, M.F., Torrent, J., (1997) Epitaxial overgrowth of goethite on hematite synthesized in phosphate media; a scanning force and transmission electron microscopy study. *American Mineralogist*, 82(11-12), 1091-1100.

Belleville, P., Jolivet, J.-P., Tronc, E., Livage, J., (1992) Crystallization of ferric hydroxide into spinel by adsorption on colloidal magnetite. *Journal of Colloid and Interface Science*, 150(2), 453-460.

Benali, O., Abdelmoula, M., Refait, P., Génin, J.-M.R., (2001) Effect of orthophosphate on the oxidation products of Fe(II)-Fe(III) hydroxycarbonate: the transformation of green rust to ferrihydrite. *Geochimica et Cosmochimica acta*, 65(11), 1715-1726.

Benhabib, K., Faure, P., Sardin, M., Simonnot, M.-O., (2010) Characteristics of a solid coal tar sampled from a contaminated soil and of the organics transferred into water. *Fuel*, 89(2), 352-359.

Bernal, J.D., Dasgupta, D.R., Mackay, A.L., (1959) The oxides and hydroxides of iron and their structural inter-relationships. *Clay Minerals Bulletin*, 4(21), 15-30.

Berthelin, J., Ona-Nguema, G., Stemmler, S., Quantin, C., Abdelmoula, M., Jorand, F., (2006) Bioreduction of ferric species and biogenesis of green rusts in soils. *Comptes Rendus Geosciences*, 338(6-7), 447-455.

Biache, C., Ghislain, T., Faure, P., Mansuy-Huault, L., (2011) Low temperature oxidation of a coking plant soil organic matter and its major constituents: An experimental approach to simulate a long term evolution. *Journal of Hazardous Materials*, 188(1-3), 221-230.

Biache, C., Mansuy-Huault, L., Faure, P., Munier-Lamy, C., Leyval, C., (2008) Effects of thermal desorption on the composition of two coking plant soils: Impact on solvent extractable organic compounds and metal bioavailability. *Environmental Pollution*, 156(3), 671-677.

Biber, M.V., dos Santos Afonso, M., Stumm, W., (1994) The coordination chemistry of weathering: IV. Inhibition of the dissolution of oxide minerals. *Geochimica et Cosmochimica acta*, 58(9), 1999-2010.

Block, P.A., Brown, R.A., Robinson, D., (2004) Novel activation technologies for sodium persulfate in situ chemical oxidation. *Proceedings of the Fourth International Conference on Remediation Chlorinated Recalcitrant Compounds*.

Bogan, B.W., Trbovic, V., (2003) Effect of sequestration on PAH degradability with Fenton's reagent: roles of total organic carbon, humin, and soil porosity. *Journal of Hazardous Materials*, 100(1-3), 285-300.

Boily, J.-F., Nilsson, N., Persson, P., Sjöberg, S., (2000) Benzenecarboxylate Surface Complexation at the Goethite (α-FeOOH)/Water Interface: I. A Mechanistic Description of Pyromellitate Surface Complexes from the Combined Evidence of Infrared Spectroscopy, Potentiometry, Adsorption Data, and Surface Complexation Modeling. *Langmuir*, 16(13), 5719-5729.

Boopathy, R., (2000) Factors limiting bioremediation technologies. *Bioresource Technology*, 74(1), 63-67.

Borch, T., Masue, Y., Kukkadapu, R.K., Fendorf, S., (2006) Phosphate Imposed Limitations on Biological Reduction and Alteration of Ferrihydrite. *Environmental Science & Technology*, 41(1), 166-172.

Bossert, I.D., Bartha, R., (1986) Structure-biodegradability relationships of polycyclic aromatic hydrocarbons in soil. *Bulletin of Environmental Contamination and Toxicology*, 37(4), 490-495.

Brown, R.A., Robinson, D., (2004) Response to naturally occurring organic material: Permanganate vs. persulfate. In: *Proceedings of the Fourth International Conference on Remediation of Chlorinated and Recalcitrant Compounds, Monterey* (Ed. by A.R. Gavaskar, A.S.C. Chen). Battelle Press, Columbus, Ohio.

Buxton, G.V., Barlow, S., McGowan, S., Salmon, G.A., Williams, J.E., (1999) The reaction of the $SO3^{\cdot-}$ radical with Fe(II) in acidic aqueous solution - A pulse radiolysis study. *Physical Chemistry Chemical Physics*, 1(13), 3111-3115.

Buxton, G.V., Greenstock, C.L., Helman, W.P., Ross, A.B., (1988) Critical review of rate constants for reactions of hydrated electrons, hydrogen atoms and hydroxyl radicals in aqueous solution. *J. Phys. Chem. Ref. Data*, 17(2), 513-886.

Buxton, G.V., Malone, T.N., Salmon, G.A., (1997) Reaction of $SO4^{\bullet-}$ with Fe2+, Mn2+ and Cu2+ in aqueous solution. *Journal of the Chemical Society - Faraday Transactions*, 93(16), 2893-2897.

Cai, Q.-Y., Mo, C.-H., Wu, Q.-T., Zeng, Q.-Y., Katsoyiannis, A., Férard, J.-F., (2007) Bioremediation of polycyclic aromatic hydrocarbons (PAHs)-contaminated sewage sludge by different composting processes. *Journal of Hazardous Materials*, 142(1-2), 535-542.

Chaillan, F., Chaîneau, C.H., Point, V., Saliot, A., Oudot, J., (2006) Factors inhibiting bioremediation of soil contaminated with weathered oils and drill cuttings. *Environmental Pollution*, 144(1), 255-265.

Chaîneau, C.H., Yepremian, C., Vidalie, J.F., Ducreux, J., Ballerini, D., (2003) Bioremediation of a crude oil-polluted soil: Biodegradation, leaching and toxicity assessments. *Water, Air, and Soil Pollution*, 144(1-4), 419-440.

Chaudhuri, S.K., Lack, J.G., Coates, J.D., (2001) Biogenic Magnetite Formation through Anaerobic Biooxidation of Fe(II). *Applied and Environmental Microbiology*, 67(6), 2844-2848.

Christiansen, B.C., Balic-Zunic, T., Dideriksen, K., Stipp, S.L.S., (2009) Identification of green rust in groundwater. *Environmental Science and Technology*, 43(10), 3436-3441.

Cornell, R.M., Schwertmann, U., (1996) *The Iron Oxides: Structure, Properties, Reactions, Occurrence and Uses*. Wiley-VCH.

Cornell, R.M., Schwertmann, U., (2003) *The Iron Oxides: Structure, Properties, Reactions, Occurrence and Uses*. Wiley-VCH.

Crimi, M.L., Taylor, J., (2007) Experimental evaluation of catalyzed hydrogen peroxide and sodium persulfate for destruction of BTEX contaminants. *Soil and Sediment Contamination*, 16(1), 29-45.

Cronk, G., Cartwright, R., (2006) Optimization of a chemical oxidation treatment train process for groundwater remediation. *Proceedings of the Fifth International Conference on Remediation of Chlorinated and Recalcitrant Compounds*.

Cuypers, C., Grotenhuis, T., Joziasse, J., Rulkens, W., (2000) Rapid Persulfate Oxidation Predicts PAH Bioavailability in Soils and Sediments. *Environmental Science & Technology*, 34(10), 2057-2063.

Di Palma, L., (2005) In situ chemical oxidation of environments combined with hazardous materials. *Soil and Sediment Remediation: Mechanisms, Technologies and Applications*, 200-222.

Dixit, S., Hering, J.G., (2006) Sorption of Fe(II) and As(III) on goethite in single- and dual-sorbate systems. *Chemical Geology*, 228(1-3), 6-15.

Do, S.-H., Kwon, Y.-J., Kong, S.-H., (2010) Effect of metal oxides on the reactivity of persulfate/Fe(II) in the remediation of diesel-contaminated soil and sand. *Journal of Hazardous Materials*, 182(1-3), 933-936.

Eberson, L., (1987) *Electron Transfer Reactions in Organic Chemistry*. Springer-Verlag, Berlin.

Elsner, M., Schwarzenbach, R.P., Haderlein, S.B., (2003) Reactivity of Fe(II)-Bearing Minerals toward Reductive Transformation of Organic Contaminants. *Environmental Science & Technology*, 38(3), 799-807.

Elsner, M., Schwarzenbach, R.P., Haderlein, S.B., (2004) Reactivity of Fe(II)-Bearing Minerals toward Reductive Transformation of Organic Contaminants. *Environmental Science & Technology*, 38(3), 799-807.

Erbs, M., Hansen, H.C.B., Olsen, C.E., (1999) Reductive dechlorination of carbon tetrachloride using iron(II) iron(III) hydroxide sulfate (green rust). *Environmental Science and Technology*, 33(2), 307-311.

Farhataziz, T., Ross, A.B., (1977) Selected specific rates of reactions of transients in water and aqueous media III: hydroxyl radicals and their radical ions. National Standard Reference Data Series. US National Bureau of Standards, pp. 59.

Faure, P., Landais, P., Griffault, L., (1999) Behavior of organic matter from Callovian shales during low-temperature air oxidation. *Fuel*, 78(13), 1515-1525.

Fenton, H.J.H., (1894) Oxidation of tartaric acid in presence of iron. *Journal of the Chemical Society, Transactions*, 65, 899-910.

Ferguson, S.H., Woinarski, A.Z., Snape, I., Morris, C.E., Revill, A.T., (2004) A field trial of in situ chemical oxidation to remediate long-term diesel contaminated Antarctic soil. *Cold Regions Science and Technology*, 40(1-2), 47-60.

Ferrarese, E., Andreottola, G., Oprea, I.A., (2008) Remediation of PAH-contaminated sediments by chemical oxidation. *Journal of Hazardous Materials*, 152(1), 128-139.

Flotron, V., Delteil, C., Padellec, Y., Camel, V., (2005) Removal of sorbed polycyclic aromatic hydrocarbons from soil, sludge and sediment samples using the Fenton's reagent process. *Chemosphere*, 59(10), 1427-1437.

Franco, I., Contin, M., Bragato, G., De Nobili, M., (2004) Microbiological resilience of soils contaminated with crude oil. *Geoderma*, 121(1-2), 17-30.

Fredrickson, J.K., Zachara, J.M., Kennedy, D.W., Dong, H., Onstott, T.C., Hinman, N.W., Li, S.-m., (1998) Biogenic iron mineralization accompanying the dissimilatory reduction of hydrous ferric oxide by a groundwater bacterium. *Geochimica et Cosmochimica acta*, 62(19-20), 3239-3257.

Fredrickson, J.K., Zachara, J.M., Kennedy, D.W., Kukkadapu, R.K., McKinley, J.P., Heald, S.M., Liu, C., Plymale, A.E., (2004) Reduction of TcO4- by sediment-associated biogenic Fe(II). *Geochimica et Cosmochimica acta*, 68(15), 3171-3187.

Gaboriaud, F., Ehrhardt, J.-J., (2003) Effects of different crystal faces on the surface charge of colloidal goethite ([alpha]-FeOOH) particles: an experimental and modeling study. *Geochimica et Cosmochimica acta*, 67(5), 967-983.

Géhin, A., Ruby, C., Abdelmoula, M., Benali, O., Ghanbaja, J., Refait, P., Génin, J.-M.R., (2002) Synthesis of Fe(II-III) hydroxysulphate green rust by coprecipitation. *Solid State Sciences*, 4(1), 61-66.

Génin, J.-M.R., Bourrié, G., Trolard, F., Abdelmoula, M., Jaffrezic, A., Refait, P., Maitre, V., Humbert, B., Herbillon, A., (1998) Thermodynamic Equilibria in Aqueous Suspensions of Synthetic and Natural Fe(II)-Fe(III) Green Rusts: Occurrences of the Mineral in Hydromorphic Soils. *Environmental Science & Technology*, 32(8), 1058-1068.

Génin, J.-M.R., Ruby, C., Géhin, A., Refait, P., (2006a) Synthesis of green rusts by oxidation of Fe(OH)2, their products of oxidation and reduction of ferric oxyhydroxides; Eh-pH Pourbaix diagrams. *Comptes Rendus Geosciences*, 338(6-7), 433-446.

Génin, J.-M.R., Ruby, C., Upadhyay, C., (2006b) Structure and thermodynamics of ferrous, stoichiometric and ferric oxyhydroxycarbonate green rusts; redox flexibility and fougerite mineral. *Solid State Sciences*, 8(11), 1330-1343.

Génin, J.M.R., Olowe, A.A., Refait, P., Simon, L., (1996) On the stoichiometry and pourbaix diagram of Fe(II)-Fe(III) hydroxy-sulphate or sulphate-containing green rust 2: An electrochemical and Mössbauer spectroscopy study. *Corrosion Science*, 38(10), 1751-1762.

Ghislain, T., Faure, P., Biache, C., Michels, R., (2010) Low-Temperature, Mineral-Catalyzed Air Oxidation: A Possible New Pathway for PAH Stabilization in Sediments and Soils. *Environmental Science & Technology*, 44(22), 8547-8552.

Girard, A., Chaudron, G., (1935) Sur la constitution de la rouille. *Comptes Rendus de l' Academie des Sciences*, 200, 127-129.

Goi, A., Trapido, M., (2004) Degradation of polycyclic aromatic hydrocarbons in soil: The Fenton reagent versus ozonation. *Environmental Technology*, 25(2), 155-164.

Gorski, C.A., Nurmi, J.T., Tratnyek, P.G., Hofstetter, T.B., Scherer, M.M., (2009) Redox Behavior of Magnetite: Implications for Contaminant Reduction. *Environmental Science & Technology*, 44(1), 55-60.

Gorski, C.A., Scherer, M.M., (2009) Influence of Magnetite Stoichiometry on FeII Uptake and Nitrobenzene Reduction. *Environmental Science & Technology*, 43(10), 3675-3680.

Gorski, C.A., Scherer, M.M., (2010) Determination of nanoparticulate magnetite stoichiometry by Mossbauer spectroscopy, acidic dissolution, and powder X-ray diffraction: A critical review. *American Mineralogist*, 95(7), 1017-1026.

Gough, M.A., Rowland, S.J., (1990) Characterization of unresolved complex mixtures of hydrocarbons in petroleum. *Nature*, 344(6267), 648-650.

Gryzenia, J., Cassidy, D., Hampton, D., (2009) Production and accumulation of surfactants during the chemical oxidation of PAH in soil. *Chemosphere*, 77(4), 540-545.

Haapea, P., Tuhkanen, T., (2006) Integrated treatment of PAH contaminated soil by soil washing, ozonation and biological treatment. *Journal of Hazardous Materials*, 136(2), 244-250.

Haber, F., Weiss, J., (1934) The catalytic decomposition of hydrogen peroxide by iron salts. *Proc. R. Soc. London A*, 147, 332-351.

Hanna, K., (2007) Adsorption of aromatic carboxylate compounds on the surface of synthesized iron oxide-coated sands. *Applied Geochemistry*, 22(9), 2045-2053.

Hanna, K., Chiron, S., Oturan, M.A., (2005) Coupling enhanced water solubilization with cyclodextrin to indirect electrochemical treatment for pentachlorophenol contaminated soil remediation. *Water Research*, 39(12), 2763-2773.

Hanna, K., Kone, T., Medjahdi, G., (2008) Synthesis of the mixed oxides of iron and quartz and their catalytic activities for the Fenton-like oxidation. *Catalysis Communications*, 9(5), 955-959.

Hanna, K., Kone, T., Ruby, C., (2010a) Fenton-like oxidation and mineralization of phenol using synthetic Fe(II)-Fe(III) green rusts. *Environmental Science and Pollution Research*, 17(1), 124-134.

Hanna, K., Rusch, B., Lassabatere, L., Hofmann, A., Humbert, B., (2010b) Reactive transport of gentisic acid in a hematite-coated sand column: Experimental study and modeling. *Geochimica et Cosmochimica acta*, 74(12), 3351-3366.

Hansel, C.M., Benner, S.G., Fendorf, S., (2005) Competing Fe(II)-Induced Mineralization Pathways of Ferrihydrite. *Environmental Science & Technology*, 39(18), 7147-7153.

Hansen, H.C.B., (1989) Composition, stabilization, and light absorption of Fe(II)Fe(III) hydroxy-carbonate ("green rust'). *Clay Minerals*, 24(4), 663-669.

Hansen, H.C.B., Guldberg, S., Erbs, M., Bender Koch, C., (2001) Kinetics of nitrate reduction by green rusts--effects of interlayer anion and Fe(II):Fe(III) ratio. *Applied Clay Science*, 18(1-2), 81-91.

Hansen, H.C.B., Koch, C.B., (1998) Reduction of nitrate to ammonium by sulphate green rust: Activation energy and reaction mechanism. *Clay Minerals*, 33(1), 87-101.

Hansen, H.C.B., Koch, C.B., Nancke-Krogh, H., Borggaard, O.K., SÃ¸rensen, J., (1996) Abiotic nitrate reduction to ammonium: Key role of green rust. *Environmental Science and Technology*, 30(6), 2053-2056.

Harvey, R.G., (1997) *Polycyclic Aromatic Hydrocarbons*. Wiley-VCH.

Haselow, J.S., Siegrist, R.L., Crimi, M., Jarosch, T., (2003) Estimating the total oxidant demand for in situ chemical oxidation design. *Remediation Journal*, 13(4), 5-16.

Hayon, E., Treinin, A., Wilf, J., (1972) Electronic spectra, photochemistry, and autoxidation mechanism of the sulfite-bisulfite-pyrosulfite systems. The SO2-, SO3-, SO4-, and SO5- radicals. *Journal of the American Chemical Society*, 94(1), 47-57.

Henner, P., Schiavon, M., Morel, J.L., Lichtfouse, E., (1997) Polycyclic aromatic hydrocarbon (PAH) occurrence and remediation methods. *Analusis*, 25(9-10), M56-M59.

Hiemstra, T., Van Riemsdijk, W.H., (1996) A surface structural approach to ion adsorption: The charge distribution (CD) model. *Journal of Colloid and Interface Science*, 179(2), 488-508.

Hiemstra, T., van Riemsdijk, W.H., (2007) Adsorption and surface oxidation of Fe(II) on metal (hydr)oxides. *Geochimica et Cosmochimica acta*, 71(24), 5913-5933.

Hiemstra, T., Venema, P., Riemsdijk, W.H.V., (1996) Intrinsic Proton Affinity of Reactive Surface Groups of Metal (Hydr)oxides: The Bond Valence Principle. *Journal of Colloid and Interface Science*, 184(2), 680-692.

House, D.A., (1962) Kinetics and mechanism of oxidations by peroxydisulfate. *Chemical Reviews*, 62, 185-203.

Huang, C.P., Dong, C., Tang, Z., (1993) Advanced chemical oxidation: Its present role and potential future in hazardous waste treatment. *Waste Management*, 13(5-7), 361-377.

Huang, K.-C., Couttenye, R.A., Hoag, G.E., (2002) Kinetics of heat-assisted persulfate oxidation of methyl tert-butyl ether (MTBE). *Chemosphere*, 49(4), 413-420.

Huling, S.G., Arnold, R.G., Sierka, R.A., Miller, M.R., (1998) Measurement of hydroxyl radical activity in a soil slurry using the spin trap Î±-(4-pyridyl-1-oxide)-N-tert-butylnitrone. *Environmental Science and Technology*, 32(21), 3436-3441.

Huling, S.G., Pivetz, B.E., (2006) In-situ Chemical Oxidation (Ed. by O.o.R.a.D. U.S. Environmental Protection Agency, National Risk Management Research Laboratory, EPA/600/R-06/072).

Hwang, S., Cutright, T.J., (2003) Effect of expandable clays and cometabolism on PAH biodegradability. *Environmental Science and Pollution Research*, 10(5), 277-280.

Ishikawa, T., Kondo, Y., Yasukawa, A., Kandori, K., (1998) Formation of magnetite in the presence of ferric oxyhydroxides. *Corrosion Science*, 40(7), 1239-1251.

Ishikawa, T., Kumagai, M., Yasukawa, A., Kandori, K., Nakayama, T., Yuse, F., (2002) Influences of metal ions on the formation of [gamma]-FeOOH and magnetite rusts. *Corrosion Science*, 44(5), 1073-1086.

ITRC, (2005) Technical and Regulatory Guidance for In Situ Chemical Oxidation of Contaminated Soil and Groundwater. ITRC, ISCO Team, Washington, DC.

Jambor, J.L., Dutrizac, J.E., (1998) Occurrence and constitution of natural and synthetic ferrihydrite, a widespread iron oxyhydroxide. *Chemical Reviews*, 98(7), 2549-2585.

Jeon, B.-H., Dempsey, B.A., Burgos, W.D., (2003) Kinetics and Mechanisms for Reactions of Fe(II) with Iron(III) Oxides. *Environmental Science & Technology*, 37(15), 3309-3315.

Jolivet, J.P., Belleville, P., Tronc, E., Livage, J., (1992) Influence of Fe(II) on the formation of the spinel iron oxide in alkaline medium. *Clays & Clay Minerals*, 40(5), 531-539.

Jonsson, S., Persson, Y., Frankki, S., van Bavel, B., Lundstedt, S., Haglund, P., Tysklind, M., (2007) Degradation of polycyclic aromatic hydrocarbons (PAHs) in contaminated soils by Fenton's reagent: A multivariate evaluation of the importance of soil characteristics and PAH properties. *Journal of Hazardous Materials*, 149(1), 86-96.

Kahani, S.A., Jafari, M., (2009) A new method for preparation of magnetite from iron oxyhydroxide or iron oxide and ferrous salt in aqueous solution. *Journal of Magnetism and Magnetic Materials*, 321(13), 1951-1954.

Kanel, S.R., Neppolian, B., Choi, H., Yang, J.W., (2003) Heterogeneous catalytic oxidation of phenanthrene by hydrogen peroxide in soil slurry: Kinetics, mechanism, and implication. *Soil and Sediment Contamination*, 12(1), 101-117.

Kanel, S.R., Neppolian, B., Jung, H., Choi, H., (2004) Comparative removal of polycyclic aromatic hydrocarbons using iron oxide and hydrogen peroxide in soil slurries. *Environmental Engineering Science*, 21(6), 741-751.

Kawahara, F.K., Davila, B., Al-Abed, S.R., Vesper, S.J., Ireland, J.C., Rock, S., (1995) Polynuclear aromatic hydrocarbon (PAH) release from soil during treatment with Fenton's Reagent. *Chemosphere*, 31(9), 4131-4142.

Khan, A.I., O'Hare, D., (2002) Intercalation chemistry of layered double hydroxides: recent developments and applications. *Journal of Materials Chemistry*, 12(11), 3191-3198.

Killian, P.F., Bruell, C.J., Liang, C., Marley, M.C., (2007) Iron (II) Activated Persulfate Oxidation of MGP Contaminated Soil. *Soil and Sediment Contamination: An International Journal*, 16(6), 523-537.

Kiyama, M., (1974) Conditions for the formation of Fe3O4 by the air oxidation of Fe(OH)2 suspensions. *Bull. Chem. Soc. Jpn.*, 47(7), 1646-1650.

Klingelhöfer, G., Fegley Jr, B., Morris, R.V., Kankeleit, E., Held, P., Evlanov, E., Priloutskii, O., (1996) Mineralogical analysis of Martian soil and rock by a miniaturized backscattering Mössbauer spectrometer. *Planetary and Space Science*, 44(11 SPEC. ISS.), 1277-1288.

Kolthoff, I.M., Stenger, V.A., (1947) Volumetric analysis. *Titration Methods: Acid-Base, Precipitation, and Complex Reactions, Vol. II Second Revised Edition*.

Kone, T., Hanna, K., Abdelmoula, M., Ruby, C., Carteret, C., (2009) Reductive transformation and mineralization of an azo dye by hydroxysulphate green rust preceding oxidation using H2O2 at neutral pH. *Chemosphere*, 75(2), 212-219.

Kone, T., Hanna, K., Usman, M., (2011) Interactions of synthetic Fe(II)-Fe(III) green rusts with pentachlorophenol under various experimental conditions. *Colloids and Surfaces A: Physicochemical and Engineering Aspects*, 385(1-3), 152-158.

Kong, S.-H., Watts, R.J., Choi, J.-H., (1998a) Treatment of petroleum-contaminated soils using iron mineral catalyzed hydrogen peroxide. *Chemosphere*, 37(8), 1473-1482.

Kong, S.H., Watts, R.J., Choi, J.H., (1998b) Treatment of petroleum-contaminated soils using iron mineral catalyzed hydrogen peroxide. *Chemosphere*, 37(8), 1473-1482.

Kulik, N., Goi, A., Trapido, M., Tuhkanen, T., (2006) Degradation of polycyclic aromatic hydrocarbons by combined chemical pre-oxidation and bioremediation in creosote contaminated soil. *Journal of Environmental Management*, 78(4), 382-391.

Langwaldt, J.H., (2005) Stimulated in situ soil treatment: biodegradation coupled to Fenton'sreaction. *Soil and Sediment Remediation: Mechanisms, Technologies and Applications*, 223-247.

Larese-Casanova, P., Scherer, M.M., (2006) Fe(II) Sorption on Hematite: New Insights Based on Spectroscopic Measurements. *Environmental Science & Technology*, 41(2), 471-477.

Larese-Casanova, P., Scherer, M.M., (2008) Abiotic transformation of hexahydro-1,3,5-trinitro-1,3,5-triazine (RDX) by green rusts. *Environmental Science and Technology*, 42(11), 3975-3981.

Larsen, O., Postma, D., (2001) Kinetics of reductive bulk dissolution of lepidocrocite, ferrihydrite, and goethite. *Geochimica et Cosmochimica acta*, 65(9), 1367-1379.

Latimer, W.M., (1952) *Oxidation Potentials*. Prentice-Hall, Inc., Englewood Cliffs, NJ.

Legrini, O., Oliveros, E., Braun, A.M., (1993) Photochemical processes for water treatment. *Chemical Reviews*, 93(2), 671-698.

Liang, C., Bruell, C.J., Marley, M.C., Sperry, K.L., (2004) Persulfate oxidation for in situ remediation of TCE. II. Activated by chelated ferrous ion. *Chemosphere*, 55(9), 1225-1233.

Liang, C., Lee, I.L., Hsu, I.Y., Liang, C.-P., Lin, Y.-L., (2008) Persulfate oxidation of trichloroethylene with and without iron activation in porous media. *Chemosphere*, 70(3), 426-435.

Liang, C., Wang, Z.-S., Bruell, C.J., (2007) Influence of pH on persulfate oxidation of TCE at ambient temperatures. *Chemosphere*, 66(1), 106-113.

Liang, C.J., Bruell, C.J., Marley, M.C., Sperry, K.L., (2003) Thermally activated persulfate oxidation of trichloroethylene (TCE) and 1,1,1-trichloroethane (TCA) in aqueous systems and soil slurries. *Soil and Sediment Contamination*, 12(2), 207-228.

Liger, E., Charlet, L., Van Cappellen, P., (1999) Surface catalysis of uranium(VI) reduction by iron(II). *Geochimica et Cosmochimica acta*, 63(19-20), 2939-2955.

Lin, S.-S., Gurol, M.D., (1998a) Catalytic Decomposition of Hydrogen Peroxide on Iron Oxide: Kinetics, Mechanism, and Implications. *Environmental Science & Technology*, 32(10), 1417-1423.

Lin, S.S., Gurol, M.D., (1998b) Catalytic decomposition of hydrogen peroxide on iron oxide: Kinetics, mechanism, and implications. *Environmental Science and Technology*, 32(10), 1417-1423.

Liu, C., Kota, S., Zachara, J.M., Fredrickson, J.K., Brinkman, C.K., (2001) Kinetic Analysis of the Bacterial Reduction of Goethite. *Environmental Science & Technology*, 35(12), 2482-2490.

Liu, H., Guo, H., Li, P., Wei, Y., (2008) The transformation of ferrihydrite in the presence of trace Fe(II): The effect of the anionic media. *Journal of Solid State Chemistry*, 181(10), 2666-2671.

Liu, H., Li, P., Lu, B., Wei, Y., Sun, Y., (2009) Transformation of ferrihydrite in the presence or absence of trace Fe(II): The effect of preparation procedures of ferrihydrite. *Journal of Solid State Chemistry*, 182(7), 1767-1771.

Lu, M., Zhang, Z., Qiao, W., Guan, Y., Xiao, M., Peng, C., (2010a) Removal of residual contaminants in petroleum-contaminated soil by Fenton-like oxidation. *Journal of Hazardous Materials*, 179(1-3), 604-611.

Lu, M., Zhang, Z., Qiao, W., Wei, X., Guan, Y., Ma, Q., Guan, Y., (2010b) Remediation of petroleum-contaminated soil after composting by sequential treatment with Fenton-like oxidation and biodegradation. *Bioresource Technology*, 101(7), 2106-2113.

Lundstedt, S., Haglund, P., Öberg, L., (2003) Degradation and formation of polycyclic aromatic compounds during bioslurry treatment of an aged gasworks soil. *Environmental Toxicology and Chemistry*, 22(7), 1413-1420.

Lundstedt, S., Persson, Y., Öberg, L., (2006) Transformation of PAHs during ethanol-Fenton treatment of an aged gasworks' soil. *Chemosphere*, 65(8), 1288-1294.

Mackay, D., Shiu, W.Y., Ma, K.C., (1992) *Illustrated Handbook of Physical-chemical Properties and Environmental Fate for Organic Chemicals: Polynuclear Aromatic Hydrocarbons. Polychlorinated Dioxins, and Dibenzofurans*. Lewis Publisher, Chelsea, Michigan, USA.

Majzlan, J., Grevel, K.-D., Navrotsky, A., (2003) Thermodynamics of Fe oxides: Part II. Enthalpies of formation and relative stability of goethite ({alpha}-FeOOH), lepidocrocite ({gamma}-FeOOH), and maghemite ({gamma}-Fe2O3). *American Mineralogist*, 88(5-6), 855-859.

Manceau, A., (1995) The mechanism of anion adsorption on iron oxides: Evidence for the bonding of arsenate tetrahedra on free Fe(O, OH)6 edges. *Geochimica et Cosmochimica acta*, 59(17), 3647-3653.

Manceau, A., Gates, W.P., (1997) Surface structural model for ferrihydrite. *Clays and Clay Minerals*, 45(3), 448-460.

Manceau, A., Nagy, K.L., Spadini, L., Ragnarsdottir, K.V., (2000) Influence of Anionic Layer Structure of Fe-Oxyhydroxides on the Structure of Cd Surface Complexes. *Journal of Colloid and Interface Science*, 228(2), 306-316.

Mann, S., Sparks, N.H.C., Couling, S.B., Larcombe, M.C., Frankel, R.B., (1989) Crystallochemical characterization of magnetic spinels prepared from aqueous solution. *Journal of the Chemical Society, Faraday Transactions 1: Physical Chemistry in Condensed Phases*, 85(9), 3033-3044.

Martens, D.A., Frankenberger, W.T., (1995) Enhanced degradation of polycyclic aromatic hydrocarbons in soil treated with an advanced oxidative process - Fenton's reagent. *Journal of Soil Contamination*, 4(2), 175-190.

Mater, L., Rosa, E.V.C., Berto, J., Corrêa, A.X.R., Schwingel, P.R., Radetski, C.M., (2007) A simple methodology to evaluate influence of H2O2 and Fe2+ concentrations on the mineralization and biodegradability of organic compounds in water and soil contaminated with crude petroleum. *Journal of Hazardous Materials*, 149(2), 379-386.

Matta, R., Hanna, K., Chiron, S., (2007) Fenton-like oxidation of 2,4,6-trinitrotoluene using different iron minerals. *Science of The Total Environment*, 385(1-3), 242-251.

Matta, R., Hanna, K., Chiron, S., (2008) Oxidation of phenol by green rust and hydrogen peroxide at neutral pH. *Separation and Purification Technology*, 61(3), 442-446.

Minisci, F., Citterio, A., Giordano, C., (1983) Electron-transfer processes: peroxydisulfate, a useful and versatile reagent in organic chemistry. *Accounts of Chemical Research*, 16(1), 27-32.

Mora, V.C., Rosso, J.A., Carrillo Le Roux, G., Mártire, D.O., Gonzalez, M.C., (2009) Thermally activated peroxydisulfate in the presence of additives: A clean method for the degradation of pollutants. *Chemosphere*, 75(10), 1405-1409.

Murad, E., Johnston, J.H., (1984) *Mössbauer Spectroscopy Applied to Inorganic Chemistry*. Plenum, New York.

Myneni, S.C.B., Tokunaga, T.K., Brown, G.E., (1997) Abiotic Selenium Redox Transformations in the Presence of Fe(II,III) Oxides. *Science*, 278(5340), 1106-1109.

Nadim, F., Huang, K.C., Dahmani, A.M., (2006) Remediation of soil and ground water contaminated with PAH using heat and Fe(II)-EDTA catalyzed persulfate oxidation. *Water, Air, and Soil Pollution: Focus*, 6(1-2), 227-232.

Næs, K., Axelman, J., Näf, C., Broman, D., (1998) Role of soot carbon and other carbon matrices in the distribution of PAHs among particles, DOC, and the dissolved phase in the effluent and recipient waters of an aluminum reduction plant. *Environmental Science and Technology*, 32(12), 1786-1792.

Naille, S., Abdelmoula, M., Louber, D., Moulin, J.-P., Ruby, C., (2010) Reflexion Mössbauer analysis of the in situ oxidation products of hydroxycarbonate green rust. *Journal of Physics: Conference Series*, 217(1), 012084.

Nam, K., Rodriguez, W., Kukor, J.J., (2001) Enhanced degradation of polycyclic aromatic hydrocarbons by biodegradation combined with a modified Fenton reaction. *Chemosphere*, 45(1), 11-20.

Ndjou'ou, A.C., Cassidy, D., (2006) Surfactant production accompanying the modified Fenton oxidation of hydrocarbons in soil. *Chemosphere*, 65(9), 1610-1615.

Norman, R.O.C., (1979) Tilden Lecture. Applications of e.s.r. spectroscopy to kinetics and mechanism in organic chemistry. *Chemical Society Reviews*, 8(1), 1-27.

O'Loughlin, E.J., Burris, D.R., (2004) Reduction of halogenated ethanes by green rust. *Environmental Toxicology and Chemistry*, 23(1), 41-48.

O'Loughlin, E.J., Larese-Casanova, P., Scherer, M., Cook, R., (2007) Green rust formation from the bioreduction of γ-FeOOH (Lepidocrocite): Comparison of several Shewanella species. *Geomicrobiology Journal*, 24(3-4), 211-230.

O'Mahony, M.M., Dobson, A.D.W., Barnes, J.D., Singleton, I., (2006) The use of ozone in the remediation of polycyclic aromatic hydrocarbon contaminated soil. *Chemosphere*, 63(2), 307-314.

Oloughlin, E.J., Gorski, C.A., Scherer, M.M., Boyanov, M.I., Kemner, K.M., (2010) Effects of oxyanions, natural organic matter, and bacterial cell numbers on the bioreduction of lepidocrocite (γ-FeOOH) and the formation of secondary mineralization products. *Environmental Science and Technology*, 44(12), 4570-4576.

Olowe, A., Refait, P., Génin, J., (1990) Superparamagnetic behaviour of goethite prepared in sulphated medium. *Hyperfine Interactions*, 57(1), 2037-2043.

Olowe, A.A., Génin, J.M.R., (1991) The mechanism of oxidation of ferrous hydroxide in sulphated aqueous media: Importance of the initial ratio of the reactants. *Corrosion Science*, 32(9), 965-984.

Ona-Nguema, G., Abdelmoula, M., Jorand, F., Benali, O., Géhin, A., Block, J.C., Génin, J.M.R., (2002) Iron(II,III) hydroxycarbonate green rust formation and stabilization from lepidocrocite bioreduction. *Environmental Science and Technology*, 36(1), 16-20.

Ona-Nguema, G., Morin, G., Wang, Y., Menguy, N., Juillot, F., Olivi, L., Aquilanti, G., Abdelmoula, M., Ruby, C., Bargar, J.R., Guyot, F., Calas, G., Brown Jr, G.E., (2009) Arsenite sequestration at the surface of nano-Fe(OH)2, ferrous-carbonate hydroxide, and green-rust after bioreduction of arsenic-sorbed lepidocrocite by Shewanella putrefaciens. *Geochimica et Cosmochimica acta*, 73(5), 1359-1381.

Osgerby, I.T., (2006) ISCO Technology Overview: Do You Really Understand the Chemistry? In: E.J. Calabrese, P.T. Kostecki, J. Dragun, I.T. Osgerby (Eds.),

Contaminated Soils, Sediments and Water (Ed. by E.J. Calabrese, P.T. Kostecki, J. Dragun, I.T. Osgerby), pp. 287-308. Springer US.

Parkhurst, D.L., Appelo, C.A.J., (1999) User's guide to PHREEQC (Version 2) a computer program for speciation, batch-reaction, one-dimensional transport, and inverse geochemical calculations: U.S. Geological Survey Water-Resources Investigations Report pp. 99-4259.

Pedersen, H.D., Postma, D., Jakobsen, R., Larsen, O., (2005) Fast transformation of iron oxyhydroxides by the catalytic action of aqueous Fe(II). *Geochimica et Cosmochimica acta*, 69(16), 3967-3977.

Pennington, D.E., Haim, A., (1968) Stoichiometry and mechanism of the chromium(II)-peroxydisulfate reaction. *Journal of the American Chemical Society*, 90(14), 3700-3704.

Peulon, S., Antony, H., Legrand, L., Chausse, A., (2004) Thin layers of iron corrosion products electrochemically deposited on inert substrates: synthesis and behaviour. *Electrochimica Acta*, 49(17-18), 2891-2899.

Peyton, G.R., (1993) The free-radical chemistry of persulfate-based total organic carbon analyzers. *Marine Chemistry*, 41(1-3), 91-103.

Piskonen, R., Itävaara, M., (2004) Evaluation of chemical pretreatment of contaminated soil for improved PAH bioremediation. *Applied Microbiology and Biotechnology*, 65(5), 627-634.

Płaza, G., Nałęcz-Jawecki, G., Ulfig, K., Brigmon, R.L., (2005) The application of bioassays as indicators of petroleum-contaminated soil remediation. *Chemosphere*, 59(2), 289-296.

Postma, D., (1993) The reactivity of iron oxides in sediments: A kinetic approach. *Geochimica et Cosmochimica acta*, 57(21-22), 5027-5034.

Prélot, B., Villiéras, F., Pelletier, M., Gérard, G., Gaboriaud, F., Ehrhardt, J.-J., Perrone, J., Fedoroff, M., Jeanjean, J., Lefèvre, G., Mazerolles, L., Pastol, J.-L., Rouchaud, J.-C., Lindecker, C., (2003) Morphology and surface heterogeneities in synthetic goethites. *Journal of Colloid and Interface Science*, 261(2), 244-254.

Prince, R.C., (1993) Petroleum spill bioremediation in marine environments. *Critical Reviews in Microbiology*, 19(4), 217-242.

Rancourt, D.G., Ping, J.Y., (1991) Voigt-based methods for arbitrary-shape static hyperfine parameter distributions in Mössbauer spectroscopy. *Nuclear Instruments and Methods in Physics Research Section B: Beam Interactions with Materials and Atoms*, 58(1), 85-97.

Refait, P., Géhin, A., Abdelmoula, M., Génin, J.M.R., (2003) Coprecipitation thermodynamics of iron(II-III) hydroxysulphate green rust from Fe(II) and Fe(III) salts. *Corrosion Science*, 45(4), 659-676.

Refait, P., Génin, J.M.R., (1993) The oxidation of ferrous hydroxide in chloride-containing aqueous media and pourbaix diagrams of green rust one. *Corrosion Science*, 34(5), 797-819.

Refait, P.H., Abdelmoula, M., GÉnin, J.M.R., (1998) Mechanisms of formation and structure of green rust one in aqueous corrosion of iron in the presence of chloride ions. *Corrosion Science*, 40(9), 1547-1560.

Rivas, F.J., (2006) Polycyclic aromatic hydrocarbons sorbed on soils: A short review of chemical oxidation based treatments. *Journal of Hazardous Materials*, 138(2), 234-251.

Ruau, O., Landais, P., Gardette, J.L., (1997) Quantitative analysis of powdered organic matter by transmission infrared microspectroscopy using a diamond-window compression cell. *Fuel*, 76(7), 645-653.

Ruby, C., Aïssa, R., Géhin, A., Cortot, J., Abdelmoula, M., Génin, J.-M., (2006a) Green rusts synthesis by coprecipitation of FeII-FeIII ions and mass-balance diagram. *Comptes Rendus Geosciences*, 338(6-7), 420-432.

Ruby, C., Géhin, A., Abdelmoula, M., Génin, J.-M.R., Jolivet, J.-P., (2003) Coprecipitation of Fe(II) and Fe(III) cations in sulphated aqueous medium and formation of hydroxysulphate green rust. *Solid State Sciences*, 5(7), 1055-1062.

Ruby, C., Géhin, A., Aissa, R., Génin, J.M.R., (2006b) Mass-balance and Eh-pH diagrams of FeII-III green rust in aqueous sulphated solution. *Corrosion Science*, 48(11), 3824-3837.

Ruby, C., Usman, M., Naille, S., Hanna, K., Carteret, C., Mullet, M., François, M., Abdelmoula, M., (2010) Synthesis and transformation of iron-based layered double hydroxides. *Applied Clay Science*, 48(1-2), 195-202.

Rügge, K., Hofstetter, T.B., Haderlein, S.B., Bjerg, P.L., Knudsen, S., Zraunig, C., Mosbæk, H., Christensen, T.H., (1998) Characterization of Predominant Reductants in an Anaerobic Leachate-Contaminated Aquifer by Nitroaromatic Probe Compounds. *Environmental Science & Technology*, 32(1), 23-31.

Sahl, J., Munakata-Marr, J., (2006) The effects of in situ chemical oxidation on microbiological processes: A review. *Remediation Journal*, 16(3), 57-70.

Schwertmann, U., (1991) Solubility and dissolution of iron oxides. *Plant and Soil*, 130(1), 1-25.

Schwertmann, U., Cornell, R.M., (2000) *Iron Oxides in the Laboratory: Preparation and Characterization*. Wiley-VCH, New York.

Schwertmann, U., Fechter, H., (1994) The formation of green rust and its transformation to lepidocrocite. *Clay Minerals*, 29(1), 87-92.

Silva, Í.S., Santos, E.d.C.d., Menezes, C.R.d., Faria, A.F.d., Franciscon, E., Grossman, M., Durrant, L.R., (2009) Bioremediation of a polyaromatic hydrocarbon contaminated soil by native soil microbiota and bioaugmentation with isolated microbial consortia. *Bioresource Technology*, 100(20), 4669-4675.

Simon, L., François, M., Refait, P., Renaudin, G., Lelaurain, M., Génin, J.-M.R., (2003) Structure of the Fe(II-III) layered double hydroxysulphate green rust two from Rietveld analysis. *Solid State Sciences*, 5(2), 327-334.

Sirguey, C., Tereza de Souza e Silva, P., Schwartz, C., Simonnot, M.-O., (2008) Impact of chemical oxidation on soil quality. *Chemosphere*, 72(2), 282-289.

Spadini, L., Schindler, P.W., Charlet, L., Manceau, A., Vala Ragnarsdottir, K., (2003) Hydrous ferric oxide: evaluation of Cd-HFO surface complexation models combining CdK EXAFS data, potentiometric titration results, and surface site structures identified from mineralogical knowledge. *Journal of Colloid and Interface Science*, 266(1), 1-18.

Stampfl, P.P., (1969) Ein basisches eisen-II-III-karbonat in rost. *Corrosion Science*, 9(3), 185-187.

Stumm, W., Morgan, J.J., (1996) *Aquatic Chemistry: Chemical Equilibria and Rates in Natural Waters*. John Wiley and Sons, New York.

Stumm, W., Sulzberger, B., (1992) The cycling of iron in natural environments: Considerations based on laboratory studies of heterogeneous redox processes. *Geochimica et Cosmochimica acta*, 56(8), 3233-3257.

Sulzberger, B., Suter, D., Siffert, C., Banwart, S., Stumm, W., (1989) Dissolution of fe(iii)(hydr)oxides in natural waters; laboratory assessment on the kinetics controlled by surface coordination. *Marine Chemistry*, 28(1-3), 127-144.

Sun, H., Tateda, M., Ike, M., Fujita, M., (2003) Short- and long-term sorption/desorption of polycyclic aromatic hydrocarbons onto artificial solids: Effects of particle and pore sizes and organic matters. *Water Research*, 37(12), 2960-2968.

Tamaura, Y., (1985) Ferrite formation from the intermediate, green rust II, in the transformation reaction of ferric hydroxide oxide, .gamma.-FeO(OH), in aqueous suspension. *Inorganic Chemistry*, 24(25), 4363-4366.

Tamaura, Y., Buduan, P.V., Katsura, T., (1981) Studies on the oxidation of iron(II) ion during the formation of Fe3O4 and α-FeO(OH) by air oxidation of Fe[OH]2 suspensions. *Journal of the Chemical Society, Dalton Transactions*(9), 1807-1811.

Tamaura, Y., Ito, K., Katsura, T., (1983) Transformation of γ-FeO(OH) to Fe_3O_4 by adsorption of iron(II) ion on γ-FeO(OH). *Journal of the Chemical Society, Dalton Transactions*(2), 189-194.

Tamaura, Y., Yoshida, T., Katsura, T., (1984) The synthesis of green rust II(FeIIIu1-FeIIu2) and its spontaneous transformation into Fe3O4. *Bulletin of the Chemical Society of Japan*, 57(9), 2411-2416.

Tamura, H., Kawamura, S., Hagayama, M., (1980) Acceleration of the oxidation of Fe2+ ions by Fe(III)-oxyhydroxides. *Corrosion Science*, 20(8-9), 963-971.

Taylor, L.T., Jones, D.M., (2001) Bioremediation of coal tar PAH in soils using biodiesel. *Chemosphere*, 44(5), 1131-1136.

Thompson, S., Riggenbach, J., Brown, R.A., Hines, J., Haselow, J., (2006) Catalyzed persulfate remediation of chlorinated and recalcitrant compounds in soil. *Proceedings of the Fifth International Conference on Remediation of Chlorinated and Recalcitrant Compounds*.

Tobler, N.B., Hofstetter, T.B., Schwarzenbach, R.P., (2007) Assessing Iron-Mediated Oxidation of Toluene and Reduction of Nitroaromatic Contaminants in Anoxic Environments Using Compound-Specific Isotope Analysis. *Environmental Science & Technology*, 41(22), 7773-7780.

Torrent, J., Barron, V., Schwertmann, U., (1990) Phosphate adsorption and desorption by goethites differing in crystal morphology. *Soil Science Society of America Journal*, 54(4), 1007-1012.

Trolard, F., Génin, J.M.R., Abdelmoula, M., Bourrié, G., Humbert, B., Herbillon, A., (1997) Identification of a green rust mineral in a reductomorphic soil by Mossbauer and Raman spectroscopies. *Geochimica et Cosmochimica acta*, 61(5), 1107-1111.

Tronc, E., Belleville, P., Jolivet, J.P., Livage, J., (1992) Transformation of ferric hydroxide into spinel by FeII adsorption. *Langmuir*, 8(1), 313-319.

Tyre, B.W., Watts, R.J., Miller, G.C., (1991) Treatment of four biorefractory contaminants in soils using catalyzed hydrogen peroxide. *Journal of Environmental Quality*, 20(4), 832-838.

Usman, M., Faure, P., Hanna, K., Abdelmoula, M., Ruby, C., (2011a) Application of magnetite catalyzed chemical oxidation (Fenton-like and persulfate) for the remediation of oil hydrocarbon contamination. *Fuel*, (Accepted).

Usman, M., Faure, P., Ruby, C., Hanna, K., (2011b) Remediation of PAH-contaminated soils by magnetite catalyzed Fenton-like oxidation. *Applied Catalysis B: Environmental*, (Accepted).

Usman, M., Faure, P., Ruby, C., Hanna, K., (2011c) Application of magnetite-activated persulfate oxidation for the degradation of PAHs in contaminated soils. *Chemosphere*, (Accepted).

Valentine, R.L., Ann Wang, H.C., (1998) Iron oxide surface catalyzed oxidation of quinoline by hydrogen peroxide. *Journal of Environmental Engineering*, 124(1), 31-38.

Venema, P., Hiemstra, T., Weidler, P.G., van Riemsdijk, W.H., (1998) Intrinsic Proton Affinity of Reactive Surface Groups of Metal (Hydr)oxides: Application to Iron (Hydr)oxides. *Journal of Colloid and Interface Science*, 198(2), 282-295.

Viollier, E., Inglett, P.W., Hunter, K., Roychoudhury, A.N., Van Cappellen, P., (2000) The ferrozine method revisited: Fe(II)/Fe(III) determination in natural waters. *Applied Geochemistry*, 15(6), 785-790.

Voogt, F.C., Fujii, T., Smulders, P.J.M., Niesen, L., James, M.A., Hibma, T., (1999) NO_2-assisted molecular-beam epitaxy of Fe_3O_4, Fe_3-δO_4, and γ-Fe_2O_3 thin films on MgO(100). *Physical Review B*, 60(15), 11193-11206.

Walling, C., (1975) Fenton's reagent revisited. *Accounts of Chemical Research*, 8(4), 125-131.

Walling, C., Goosen, A., (1973) Mechanism of the ferric ion catalyzed decomposition of hydrogen peroxide. Effect of organic substrates. *Journal of the American Chemical Society*, 95(9), 2987-2991.

Wang, X., Bartha, R., (1990) Effects of bioremediation on residues, activity and toxicity in soil contaminated by fuel spills. *Soil Biology and Biochemistry*, 22(4), 501-505.

Watts, R.J., Bottenberg, B.C., Hess, T.F., Jensen, M.D., Teel, A.L., (1999a) Role of reductants in the enhanced desorption and transformation of chloroaliphatic compounds by modified Fenton's reactions. *Environmental Science and Technology*, 33(19), 3432-3437.

Watts, R.J., Dilly, S.E., (1996) Evaluation of iron catalysts for the Fenton-like remediation of diesel-contaminated soils. *Journal of Hazardous Materials*, 51(1-3), 209-224.

Watts, R.J., Stanton, P.C., Howsawkeng, J., Teel, A.L., (2002) Mineralization of a sorbed polycyclic aromatic hydrocarbon in two soils using catalyzed hydrogen peroxide. *Water Research*, 36(17), 4283-4292.

Watts, R.J., Teel, A.L., (2006) Treatment of contaminated soils and groundwater using ISCO. *Practice Periodical of Hazardous, Toxic, and Radioactive Waste Management*, 10(1), 2-9.

Watts, R.J., Udell, M.D., Kong, S., Leung, S.W., (1999b) Fenton-like soil remediation catalysed by naturally occurring iron minerals. *Environmental Engineering Science*, 16(1), 93-103.

Watts, R.J., Udell, M.D., Monsen, R.M., (1993) Use of iron minerals in optimizing the peroxide treatment of contaminated soils. *Water Environment Research*, 65(7), 839-844.

Waychunas, G.A., Rea, B.A., Fuller, C.C., Davis, J.A., (1993) Surface chemistry of ferrihydrite: Part 1. EXAFS studies of the geometry of coprecipitated and adsorbed arsenate. *Geochimica et Cosmochimica acta*, 57(10), 2251-2269.

Wild, S.R., Jones, K.C., (1995) Polynuclear aromatic hydrocarbons in the United Kingdom environment: A preliminary source inventory and budget. *Environmental Pollution*, 88(1), 91-108.

Wild, S.R., Obbard, J.P., Munn, C.I., Berrow, M.L., Jones, K.C., (1991) The long-term persistence of polynuclear aromatic hydrocarbons (PAHs) in an agricultural soil amended with metal-contaminated sewage sludges. *Science of The Total Environment*, 101(3), 235-253.

Williams, A.G.B., Scherer, M.M., (2004) Spectroscopic Evidence for Fe(II)-Fe(III) Electron Transfer at the Iron Oxide-Water Interface. *Environmental Science & Technology*, 38(18), 4782-4790.

Wilson, S.C., Jones, K.C., (1993) Bioremediation of soil contaminated with polynuclear aromatic hydrocarbons (PAHs): A review. *Environmental Pollution*, 81(3), 229-249.

Xue, X., Hanna, K., Abdelmoula, M., Deng, N., (2009a) Adsorption and oxidation of PCP on the surface of magnetite: Kinetic experiments and spectroscopic investigations. *Applied Catalysis B: Environmental*, 89(3-4), 432-440.

Xue, X., Hanna, K., Deng, N., (2009b) Fenton-like oxidation of Rhodamine B in the presence of two types of iron (II, III) oxide. *Journal of Hazardous Materials*, 166(1), 407-414.

Xue, X., Hanna, K., Despas, C., Wu, F., Deng, N., (2009c) Effect of chelating agent on the oxidation rate of PCP in the magnetite/H2O2 system at neutral pH. *Journal of Molecular Catalysis A: Chemical*, 311(1-2), 29-35.

Yan, J., Lei, M., Zhu, L., Anjum, M.N., Zou, J., Tang, H., (2010) Degradation of sulfamonomethoxine with Fe3O4 magnetic nanoparticles as heterogeneous activator of persulfate. *Journal of Hazardous Materials*, 186(2-3), 1398-1404.

Yan, J., Wang, L., Fu, P.P., Yu, H., (2004) Photomutagenicity of 16 polycyclic aromatic hydrocarbons from the US EPA priority pollutant list. *Mutation Research - Genetic Toxicology and Environmental Mutagenesis*, 557(1), 99-108.

Yang, L., Steefel, C.I., Marcus, M.A., Bargar, J.R., (2010) Kinetics of Fe(II)-Catalyzed Transformation of 6-line Ferrihydrite under Anaerobic Flow Conditions. *Environmental Science & Technology*, 44(14), 5469-5475.

Yap, C.L., Gan, S., Ng, H.K., (2011) Fenton based remediation of polycyclic aromatic hydrocarbons-contaminated soils. *Chemosphere*, 83(11), 1414-1430.

Yee, N., Shaw, S., Benning, L.G., Nguyen, T.H., (2006) The rate of ferrihydrite transformation to goethite via the Fe(II) pathway. *American Mineralogist*, 91(1), 92-96.

Yeh, C.K.J., Hsu, C.Y., Chiu, C.H., Huang, K.L., (2008) Reaction efficiencies and rate constants for the goethite-catalyzed Fenton-like reaction of NAPL-form aromatic hydrocarbons and chloroethylenes. *Journal of Hazardous Materials*, 151(2-3), 562-569.

Yen, C.-H., Chen, K.-F., Kao, C.-M., Liang, S.-H., Chen, T.-Y., (2011) Application of persulfate to remediate petroleum hydrocarbon-contaminated soil: Feasibility and comparison with common oxidants. *Journal of Hazardous Materials*, 186(2-3), 2097-2102.

Zachara, J.M., Kukkadapu, R.K., Fredrickson, J.K., Gorby, Y.A., Smith, S.C., (2002) Biomineralization of poorly crystalline Fe(III) oxides by dissimilatory metal reducing bacteria (DMRB). *Geomicrobiology Journal*, 19(2), 179-207.

Zegeye, A., Abdelmoula, M., Usman, M., Hanna, K., Ruby, C., (2011) In situ monitoring of lepidocrocite bioreduction and magnetite formation by reflection Mossbauer spectroscopy. *American Mineralogist*, 96(8-9), 1410-1413.

Zegeye, A., Mustin, C., Jorand, F., (2010) Bacterial and iron oxide aggregates mediate secondary iron mineral formation: green rust versus magnetite. *Geobiology*, 8(3), 209-222.

Zegeye, A., Ruby, C., Jorand, F., (2007) Kinetic and thermodynamic analysis during dissimilatory γ-FeOOH reduction: Formation of green rust 1 and magnetite. *Geomicrobiology Journal*, 24(1), 51-64.

ANNEXES

Annex No. 1

Synthesis and transformation of iron-based layered double hydroxides

Ruby, C., **Usman, M**., Naille, S., Hanna, K., Carteret, C., Mullet, M., François, M., Abdelmoula, M., (2010) Applied Clay Science 48, 195-202.

(This paper was reproduced with the permission of Elsevier.)

Annex No. 2

In situ monitoring of lepidocrocite bioreduction and magnetite formation by reflection Mossbauer spectroscopy

Zegeye, A., Abdelmoula, M., **Usman, M.,** Hanna, K., Ruby, C. (2011) American Mineralogist 96, 1410-1413.

(This paper was reproduced with the permission of American Mineralogist.)

Applied Clay Science 48 (2010) 195–202

Contents lists available at ScienceDirect

Applied Clay Science

journal homepage: www.elsevier.com/locate/clay

Synthesis and transformation of iron-based layered double hydroxides

C. Ruby [a,*], M. Usman [a], S. Naille [a], K. Hanna [a], C. Carteret [a], M. Mullet [a], M. François [b], M. Abdelmoula [a]

[a] Laboratoire de Chimie Physique et Microbiologie pour l'Environnement (LCPME), UMR7564 CNRS-Nancy Université, 405, Rue de Vandœuvre 54600 Villers-Lès-Nancy, France
[b] Institut Jean Lamour, Département P2M, Matériaux-Métallurgie-Nanosciences-Plasmas-Surfaces, UMR 7198-CNRS-Nancy-Université-UPV-Metz, Faculté des Sciences, BP 239, 54506 Villers-lès-Nancy, France

ARTICLE INFO

Article history:
Received 16 July 2009
Received in revised form 15 October 2009
Accepted 13 November 2009
Available online 26 November 2009

Keywords:
LDH
Green rust
Pyroaurite
Hydrotalcite
Fougerite
Mössbauer spectroscopy

ABSTRACT

Iron-based layered double hydroxides (LDHs) have the general formula $[M^{II}_{(1-x)}M^{III}_{x}(OH)_2]^{x+}\cdot[(x/n)\ A^{n-},\ m\ H_2O]^{x-}$ and contain a molar fraction of iron, i.e. Fe^{II} or Fe^{III} situated in the cationic layers, higher than 50%. LDHs containing Fe^{II} species are interesting materials for several applications such as the reduction of anionic pollutants or the degradation of organic pollutants. They are mostly prepared either by coprecipitation of dissolved species or by oxidation of hydroxylated Fe^{II} species. The synthesis routes were visualised in binary and ternary mass-balance diagrams. The LDH[Fe^{II}–Fe^{III}] particles were well crystallised hexagonal plates, the size of which diminishes rapidly when divalent or trivalent cations substitute ions. The LDH[Fe^{II}–Fe^{III}–CO_3] transformed into a mixture of magnetite Fe_3O_4 and siderite $FeCO_3$ in alkaline conditions, but the adsorption of silicate or phosphate anions on the lateral faces of the crystal prevented this decomposition. In oxic conditions, two mechanism of transformation were identified: (i) a fast *in situ* oxidation within the solid, (ii) dissolution–precipitation of the LDH forming ferric oxyhydroxides such as goethite (α-FeOOH).

© 2009 Elsevier B.V. All rights reserved.

1. Introduction

Mixed M^{II}–M^{III} layered double hydroxides (LDHs) are described by the general formula $[M^{II}_{(1-x)}M^{III}_{x}(OH)_2]^{x+}\cdot[(x/n)\ A^{n-},\ m\ H_2O]^{x-}$ where M^{II} and M^{III} are metal cations in the brucite-type layers Mg $(OH)_2$, A^{n-} are the intercalated anions and x is the molar fraction of the trivalent cation and also the electrostatic charge of both the brucite-type layers and the anionic interlayers. Most commonly, the values of x are found in the range of 0.2–0.33 (Khan and O'Hare, 2002). Recently, the interest for the synthesis and the characterisation of LDHs increased since these materials can be used for many potential applications. For example, LDHs are well known for their capacity to exchange various types of inorganic anions (Miyata, 1983; Khan and O'Hare, 2002). LDHs can easily incorporate organic and bioorganic molecules such as ascorbic acid (Aisawa et al., 2007), urease (Vial et al., 2008), DNA (Oh et al., 2006) and even ferritin (Clemente-León et al., 2008). A particular type of LDHs which contains only iron as a cation in the brucite-type layers is called Green Rust (GR), i.e. the LDH[Fe^{II}–Fe^{III}]. GR is an intermediate compound that forms during the Fe^{II} species oxidation in solution (Feitknecht and Keller, 1950). For example, carbonated GR was observed as a corrosion product in water drain by Stampfl (1969). In 1996, a natural sample found in a hydromorphic soil in the forest of Fougères (Brittany, France) was identified to be homologous to green rust by using Mössbauer and Raman spectrocopies (Trolard et al. 1997). This mineral was then named fougerite (IMA 2003-057). More recently, three new occurrences were found: one in coal mine drainage sediment in South Wales (Bearcock et al., 2006) and two others in Denmark (Christiansen et al., 2009). In this last study, an X-ray diffraction pattern that corresponds to synthetic carbonated GR was presented for the first time. The properties of GR, i.e. the LDH[Fe^{II}–Fe^{III}], were also studied because of its ability to reduce several anionic pollutants such as nitrate (Hansen, 2001), chromate (Loyaux-Lawniczak et al., 2000; Bond and Fendorf, 2003; Legrand et al., 2004) and seleniate (Refait et al., 2000, 2005a; Hayashi et al., 2009). Finally, GR was shown to promote the reduction/oxidation of an azo dye and therefore its removal from water (Kone et al., 2009) and the Fenton-like oxidation of phenol at neutral pH (Hanna et al., 2010).

In this paper, we will focus on the description of the synthesis routes and transformation of LDHs that contain a minimum of 50 % of iron atoms in the brucite-like layers, i.e. compound for which the ratio $n(Fe)/\{n(M^{II})+n(M^{III})\}$ is >50%. Similar to the terminology commonly used for metallic alloys, these compounds are called iron-based LDHs. The partial substitution of the Fe^{II} or Fe^{III} cations by other divalent or trivalent species lead to ternary systems such as LDH[{Fe^{II}–M^{II}}–Fe^{III}] or LDH[Fe^{II}–{Fe^{III}–M^{III}}. To our knowledge, three types of partial substitutions were studied: Fe^{II} by Ni^{II} (Refait and Génin, 1993; Refait et al., 2005b), Fe^{II} by Mg^{II} (Refait et al., 2001) and more recently Fe^{III} by Al^{III} (Ruby et al., 2008). Fully substituted compounds that correspond to the minerals pyroaurite $Mg_6Fe_2(OH)_{16}CO_3{,}4H_2O$ (Allmann, 1968) and reevesite $Ni_{18}Fe_6(OH)_{48}(CO_3)_3{,}12H_2O$, (De Waal and Viljoen, 1971) are not *strico sensu* iron-based LDHs, and the synthesis of such compounds will not be considered here. We will

* Corresponding author. Tel.: +33 3 83 68 52 53.
E-mail address: christian.ruby@lcpme.cnrs-nancy.fr (C. Ruby).

0169-1317/$ – see front matter © 2009 Elsevier B.V. All rights reserved.
doi:10.1016/j.clay.2009.11.017

report synthesis routes of iron-based LDH and transformation modes at both oxic and anoxic conditions.

2. Synthesis and characterisation

2.1. Formation paths: General description

2.1.1. M^{II}–M^{III} mass-balance diagram

The synthesis routes of iron-based LDHs can be illustrated in the mass-balance diagram presented in Fig. 1. Initially, this diagram was devised for interpreting pH titration curves obtained during the coprecipitation of Fe^{II} and Fe^{III} soluble species in sulphate solutions (Ruby et al., 2003) but it can easily be generalised to any type of divalent and trivalent cations. The ordinate $R = n(OH^-)/[n(M^{II}) + n(M^{III})]$ represents the number of hydroxyl species per mole of iron that are consumed during the precipitation of a given compound. The abscissa $x = n(M^{III})/[n(M^{II}) + n(M^{III})]$ indicates the molar fraction of trivalent cations. The position of the aqueous species M^{II}_{aq}, M^{III}_{aq} and solid compounds $M^{II}(OH)_2$, the LDH[M^{II}–M^{III}], the spinel $M^{II}M^{III}_2O_4$ and the oxyhydroxide $M^{III}OOH$ are indicated. The synthesis of LDHs is most commonly achieved by the addition of a basic solution to a solution of {M^{II}_{aq}, M^{III}_{aq}}. It corresponds to the vertical path [AD]. The major advantage of this method is that the value of x of the initial solution can be adjusted accurately in order to determine the flexibility of the M^{III} molar fraction.

LDHs may also contain a metal cation in two oxidation states M^{II} and M^{III} such as the 3d transition metals, i.e. Ti, V, Cr, Mn, Fe, Co and Ni. Such LDHs can be prepared by a precipitation/oxidation route (Fig. 1) in two steps: (i) A basic solution is added to a solution of M^{II} that precipitates to form either a suspension of solid $M^{II}(OH)_2$ or a {$M^{II}(OH)_2$, M^{II}_{aq}} mixture (path [BC]), (ii) the divalent species are then oxidised to form the LDH[M^{II}–M^{III}] (path CD). As it will be discussed in Section 2.2.2., the slope of line CD depends on the nature of the oxidant. The easiest way of oxidation is agitating the $M^{II}(OH)_2$ suspension in contact with air and controlling the redox potential E_h of the suspension to follow the oxidation steps. Other oxidants such as hydrogen peroxide H_2O_2, iodine I_2 or persulphate $S_2O_8^{2-}$ can also be used. The advantage is to know the oxidation state of the product by controlling the amount of added oxidant. The precipitation/oxidation pathway was used for the preparation of LDH[Fe^{II}–Fe^{III}] (Hansen, 2001; Génin et al., 2006a) and LDH[Co^{II}–Co^{III}] (Ma et al., 2008).

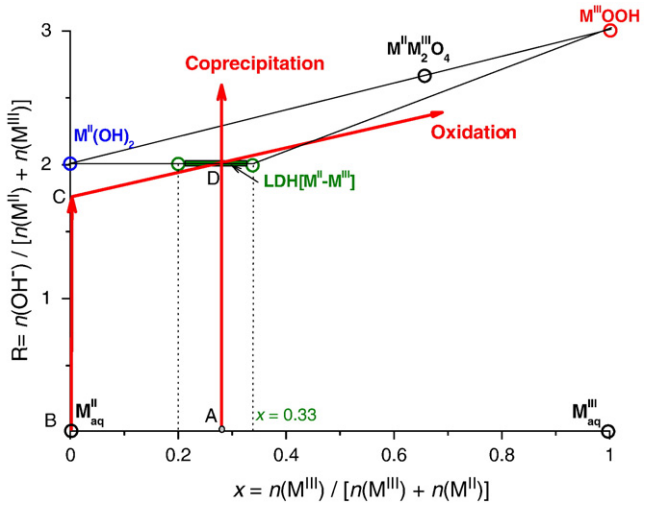

Fig. 1. M^{II}–M^{III} mass-balance diagram showing the coprecipitation and oxidation synthesis routes (adapted from Fig. 1 of Ruby et al., 2006b).

2.1.2. Formation of ternary LDH [Fe^{II}, {Fe^{III}, M^{III}}] and LDH[{Fe^{II}, M^{II}}, Fe^{III}]

Iron-based LDHs, with a partial substitution of the Fe^{III} or Fe^{II} are synthesised like the binary LDH[Fe^{II}–Fe^{III}], i.e. by coprecipitation or oxidation. Such syntheses can be represented in a ternary mass-balance diagram (Fig. 2). This representation was initially proposed to study the coprecipitation of [{Fe^{II}, {Fe^{III}, Al^{III}}}] mixtures in sulphate solution (Ruby et al., 2008). The diagram is an equilateral triangle and the composition of any point is easily obtained by plotting the perpendicular to the triangle sides as usually done when studying the phase diagram of ternary alloys (bottom of Fig. 2a). The number of moles of hydroxyl groups per mole of cations $R = n(OH^-)/n(M_{tot})$ necessary to form a given compound is situated on the perpendicular to the triangle base. The formation pathways of the M^{III}-substituted LDHs are presented in Fig. 2a. The domain of the ternary LDH[{Fe^{II}, M^{II}}, Fe^{III}] is situated in between the two segments corresponding to the LDH[Fe^{II}–Fe^{III}] and the LDH[Fe^{II}–M^{III}]. On Fig. 2b, the formation pathways of M^{II}-substituted LDHs are shown. The domain of the LDH [{Fe^{II}, M^{II}} Fe^{III}] is situated in between the segments corresponding to the LDH[Fe^{II}–Fe^{III}] and the LDH[{Fe^{II}, M^{II}}, Fe^{III}] with $x(M^{II}) = 0.5$. In both cases, the most trivial way to prepare such a compound is to prepare a mixture of soluble species, i.e. [{Fe^{II}, {Fe^{III}, M^{III}}] or [{Fe^{II}, M^{II}}, Fe^{III}] with the desired molar fractions, and to add a basic solution at a ratio $R = n(OH^-)/n(M_{tot})$ close to 2. This coprecipitation syntheses route corresponds to a vertical segment that starts into the composition domain of the ternary LDH and is situated perpendicularly to the triangle base. The LDH[{Fe^{II}, {Fe^{III}, M^{III}}] could also be obtained by partial oxidation of LDH[Fe^{II}–M^{III}] (Fig 4a), such a reaction has not yet been tested. In sulphate solution, the coprecipitation of the LDH[Fe^{II}–Al^{III}] leads unfortunately to an amorphous compound (Ruby et al., 2008) that is difficult to use as a starting product for an oxidation experiment. The oxidation path presented in Fig. 2b was used to prepare the LDH[{Fe^{II}, Ni^{II}}, Fe^{III}] (Refait and Génin, 1993). In these experiments, a mixture of soluble species {Fe^{II}_{aq}, Ni^{II}_{aq}}, *i.e.* point A, was precipitated to form a mixture of {$Fe(OH)_2$, $Ni(OH)_2$} in point B. In a second step, the Fe^{II} species were oxidised by air to form LDH[{Fe^{II}, Ni^{II}}, Fe^{III}] by following the path BC. During this oxidation, the quantity of Ni^{II} remained constant since Fe^{II} species were much more easily oxidised by dissolved O_2. A similar way of syntheses was used to prepare a fully substituted LDH(Co^{II}–Fe^{III}) by oxidation of LDH(Co^{II}–Fe^{II}) (Ma et al., 2007). Iodine I_2 was chosen as an oxidant because the standard redox potential of the I_2/I^- couple is situated in between the E^o values of the Fe^{II}/Fe^{III} and Co^{II}/Co^{III} couples. By this way, only the Fe^{II} species of the LDH(Co^{II}–Fe^{II}) were oxidised and a pure and well crystallised LDH(Co^{II}–Fe^{III}) was observed.

2.2. Synthesis of the LDH[Fe^{II}–Fe^{III}] (green rust)

2.2.1. Coprecipitation of soluble Fe^{II} and Fe^{III} species

The coprecipitation method was used to determine the flexibility of the x values of LDH[Fe^{II}–Fe^{III}–SO_4] (Ruby et al., 2003) and LDH[Fe^{II}–Fe^{III}–CO_3] (Ruby et al., 2006b). These experiments were conducted in a gas-tight reactor with continuous N_2 bubbling in aqueous solution in order to avoid the oxidation of ferrous ions Fe^{II}. A systematic study of the titration of Fe^{II} and Fe^{III} by NaOH in a sulphate solution showed that only LDH[Fe^{II}–Fe^{III}–SO_4] with a unique composition $x = 0.33$ was formed (Ruby et al., 2003). When the coprecipitation was realised at values of $x > 0.33$ or $x < 0.33$, {LDH[Fe^{II}–Fe^{III}–SO_4–$x = 0.33$], Fe_3O_4} and {LDH[Fe^{II}–Fe^{III}–SO_4-$x = 0.33$], $Fe(OH)_2$} mixtures were respectively formed. Nevertheless, the formation of a LDH[Fe^{II}–Fe^{III}–SO_4] with a ratio $x = 0.25$ was achieved by performing an anion exchange of LDH [Fe^{II}–Fe^{III}–Cl^-] precipitated at the same x value (Hansen et al., 2001). Some flexibility of the x values was also observed for LDH[Fe^{II}–Fe^{III}–CO_3] that can be prepared in the range $x \in [\sim 0.25, 0.33]$. For the preparation of the LDH[[Fe^{II}–Fe^{III}–CO_3] at $x = 0.25$, $FeCl_3$ and $FeCl_2$ salts had to be dissolved by the addition of a Na_2CO_3 solution. Indeed, if $Fe_2(SO_4)_3$ and $FeSO_4$ solutions were used, LDH[Fe^{II}–Fe^{III}–SO_4] was

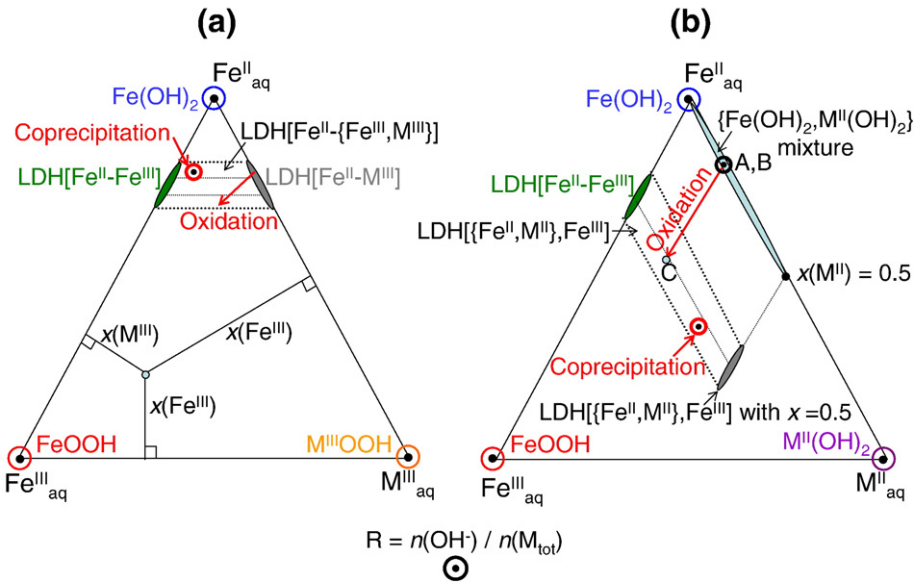

Fig. 2. Ternary mass-balance diagrams showing the domains and syntheses routes of M^{III} (a) and M^{II} (b) substituted iron-based LDHs.

formed before LDH[Fe^{II}–Fe^{III}–CO_3] and only the LDH[$x = 0.33$] was obtained.

2.2.2. Oxidation of $Fe(OH)_2$ and {$Fe(OH)_2$, Fe^{II}} mixture

Another easy way to prepare LDH[Fe^{II}–Fe^{III}] is oxidation by air of a suspension that contains $Fe(OH)_2$ precipitates. In sulphate and chloride solutions (Génin et al., 2006a), only suspensions containing a specific amount of soluble Fe^{II} species led to the formation of the pure LDH. For example in sulphate solution, this excess of Fe^{II}_{aq} is described by the following chemical reaction:

$$5Fe^{II}(OH)_2 + Fe^{2+}_{aq} + SO_4^{2-} + 1/2O_2 + H_2O \Leftrightarrow Fe^{II}_4Fe^{III}_2(OH)_{12}SO_4 \quad (1)$$

Therefore, the initial Fe^{II}_{aq} solution was partially precipitated by adding a NaOH solution with a ratio $r = n(OH^-)/n(Fe^{II})$ of exactly 5/3. If Fe^{II} species were precipitated with a ratio r equal to 2, pure $Fe(OH)_2$ was formed without any excess of Fe^{II}_{aq} and the oxidation yielded pure magnetite. For $5/3 < r < 2$, the formation of {LDH[Fe^{II}–Fe^{III}–SO_4], Fe_3O_4} mixtures was observed. Other experiments were carried out by using persulphate ions $S_2O_8^{2-}$ as oxidant (Ruby et al., 2006a). In this case, the oxidation of pure $Fe(OH)_2$ led to the formation of pure LDH [Fe^{II}–Fe^{III}] according to the following reaction:

$$5Fe^{II}(OH)_2 + S_2O_8^{2-} + 1/2O_2 + H_2O \Leftrightarrow Fe^{II}_4Fe^{III}_2(OH)_{12}SO_4 \quad (2)$$

The results with several oxidants (Ruby et al., 2006a) indicated that the thermodynamically favourable reactions were pH independent, as in the case of reactions (1) and (2). If the reduction of the oxidant corresponds to the general half reaction:

$$(Ox) + ne^- \Leftrightarrow (Red) + vOH^- \quad (3)$$

Preparing the LDH with a Fe^{III} molar fraction x requires a ratio $r = n(OH^-)/n(Fe^{II})$ of the initial solution (Ruby et al., 2006a):

$$r = 2 - (v/n)x \quad (4)$$

For example, for the redox couple O_2/OH^-, the half reaction is $O_2 + H_2O + 2e^- + 2\,OH^-$ and $(v/n) = 1$. For preparing LDH[Fe^{II}–Fe^{III}] at an x value of 1/3, an r value of 5/3 is obtained according to Eq. (4) which is in good agreement with the experimental observations.

2.2.3. Reactivity of Fe^{II} species with Fe^{III} oxyhydroxides

LDH[Fe^{II}–Fe^{III}] can also be formed by reaction of Fe^{II} species with Fe^{III} oxyhydroxides such as lepidocrocite γ-FeOOH (Tamaura, 1985) or ferrihydrite (Hansen, 2001). In these experiments, soluble Fe^{II} species were added to a suspension that contains the ferric oxyhydroxide at a pH close to 7. This pH allows a sufficient hydroxylation rate of the Fe^{II} species necessary to activate the reaction. LDH[Fe^{II}–Fe^{III}–SO_4] can also be prepared by fixing the hydroxylation rate $R = n(OH^-)/[n(Fe^{II}) + n(Fe^{III})]$ at exactly 7 with a basic solution such as NaOH (Ruby et al., 2003). This ratio corresponds to the formation of a mixture {FeOOH, 2 $Fe(OH)_2$} that was hypothesised to be the precursor of the formation of the LDH[Fe^{II}–Fe^{III}–SO_4]. A heterogeneous reaction at the surface of the ferric oxyhydroxide particles was described by Ruby et al. (2006b).

2.3. Characterisation of iron-based layered double hydroxides

2.3.1. Morphology of the crystals

Non-substituted LDH[Fe^{II}–Fe^{III}] prepared at room temperature either by coprecipitation or oxidation showed well-defined hexagonal plates with a lateral size D in the range of 100–500 nm and a thickness d of ~10–50 nm as observed by TEM (Fig. 3a). The ratio D/d was close to 10 for LDH[Fe^{II}–Fe^{III}–SO_4^{2-}] and close to 5 for LDH[Fe^{II}–Fe^{III}–CO_3^{2-}] (Ruby et al., 2006b). In this case, many LDH[Fe^{II}–Fe^{III}–CO_3^{2-}] crystals were seen with their basal plane situated perpendicularly to the TEM grid (Fig 3a). Diffraction of isolated crystals along the [001] zone axis was performed and allowed us to determine the parameter a of the hexagonal cell ($a \sim 3.2$ Å).

The substitution of the trivalent or the divalent cation by another cation rapidly decreased the crystal size (Fig. 3b, c). For example, the substitution of half of the Fe^{III} ions by Al^{III} in LDH[Fe^{II}–Fe^{III}–SO_4] decreased the lateral crystal size to ~10 nm (Fig. 3b). A more drastic effect was observed if the Fe^{II} species were fully substituted by Ni^{II} (Fig. 3c). In this case, the LDH consisted of nano-crystals and only heating in the range of 100 °C–180 °C formed larger crystals with a hexagonal shape (not shown). Note that heating to these temperatures decomposed iron-based LDH into {Fe_3O_4, $Fe(OH)_2$} or {Fe_3O_4, $FeCO_3$} mixtures. Therefore, heating is of no use for increasing the crystal size of iron-based LDHs.

2.3.2. Crystallographical structure

The structure of LDH[Fe^{II}–Fe^{III}–SO_4], LDH[Fe^{II}–Fe^{III}–Al^{III}–SO_4] and LDH[Fe^{II}–Fe^{III}–CO_3] were recently investigated by high resolution X-ray diffraction experiments performed at the European Synchrotron Radiation Facility (ESRF) (Aïssa et al., 2006; Ruby et al., 2008).

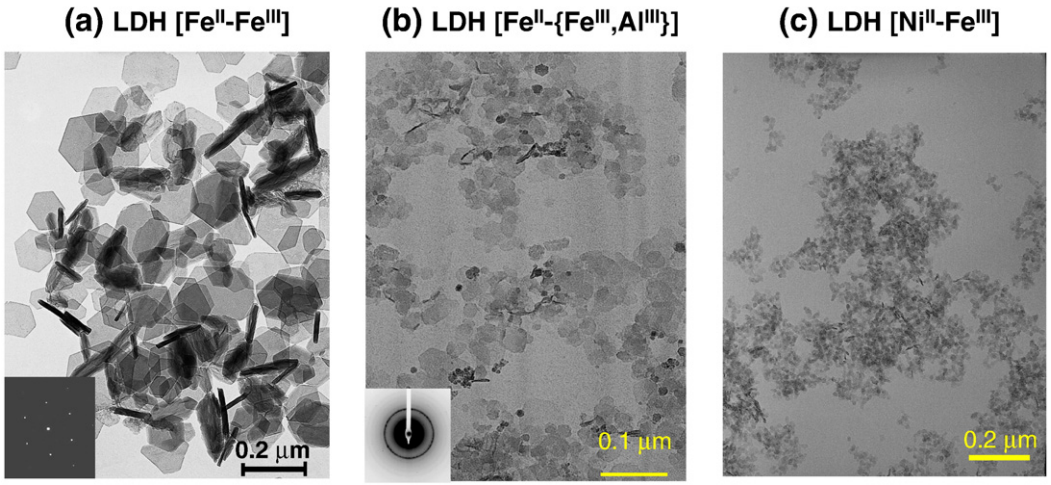

Fig. 3. Morphologies of iron-based LDHs crystals observed by transmission electron microscopy. Reprinted from Ruby et al. (2006b), with the permission of Masson Elsevier.

Diffractograms of the LDH[Fe^{II}–Fe^{III}–SO_4] and the LDH[Fe^{II}–Fe^{III}–CO_3] are presented in Fig. 4. The position of the reflection peaks showed that the two LDHs exhibited a quite different crystallographical structure that was determined with Rietveld refinements. The LDH [Fe^{II}–Fe^{III}–SO_4] crystallised in the hexagonal structure, space goup $P\bar{3}1m$, and the unit cell was characterised by the parameters $a = 5.50683(3)$ Å and $c = 10.9664(2)$ Å, where c is equal to the basal spacing d along the [001] axis. The LDH[Fe^{II}–Fe^{III}–CO_3] crystallised in the trigonal structure, space group $R\bar{3}m$, and the corresponding hexagonal triple cell was characterised by the parameters $a = 3.17588(2)$ Å and $c = 22.7123(3)$ Å; the basal spacing is now $d = c/3 = 7.57$ Å. The basal spacing d of the LDH[Fe^{II}–Fe^{III}–SO_4] was larger because it enclosed a double layer of oriented sulphate anions and water molecules (Ruby et al., 2008). Therefore, the structure of these two LDHs can be distinguished very easily by X-ray diffraction and were denominated by Bernal et al. (1959). Green rust 1 ($R\bar{3}m$) and green rust 2 ($P\bar{3}1m$). For instance, the position of the most intense (003) reflection peak of the LDH[Fe^{II}–Fe^{III}–CO_3] is situated at a much lower angle than the (0001) peak of LDH[Fe^{II}–Fe^{III}–SO_4] simply because of different basal spacing (Fig. 4).

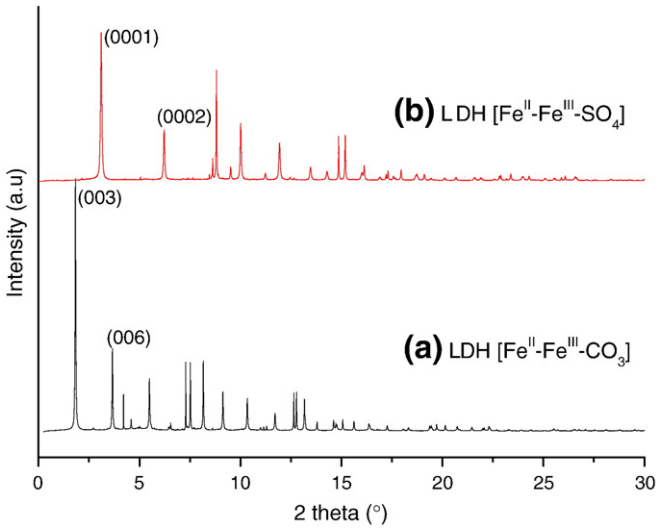

Fig. 4. High resolution X-ray diffraction patterns of hydroxysulphate recorded for a wavelength of the incident beam $\lambda = 0.35015$ Å (a) and hydroxycarbonate with $\lambda = 0.410792$ Å (b).

2.3.3. Mössbauer spectroscopy

^{57}Fe Mössbauer spectroscopy is a powerful technique for determining accurately the relative proportion of Fe^{II} and Fe^{III} species of iron-based LDHs. It is also very useful to detect the formation of iron containing by-products such as ferrous hydroxide $Fe(OH)_2$, siderite $FeCO_3$, magnetite Fe_3O_4 and the various ferric oxyhydroxides. This technique is only sensitive to the ^{57}Fe nucleus. For example, Mössbauer spectrum of the LDH[Fe^{II}–Fe^{III}–SO_4] recorded at 78 K is shown in Fig. 5a. It is characterised by a paramagnetic Fe^{II} doublet D_1 with a large quadrupole splitting $\Delta = 2.91$ mm s^{-1} and another Fe^{III} doublet D_2

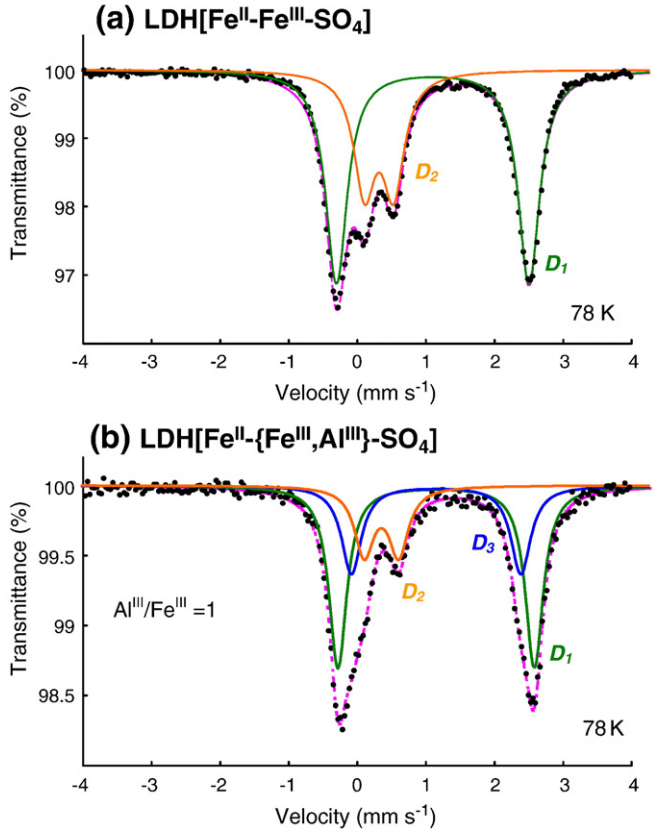

Fig. 5. Transmission Mössbauer spectra of hydroxysulphate (a) and Al^{III}–substituted hydroxysulphate (b). Reprinted from Ruby et al. (2006b), with the permission of Masson Elsevier.

with a much smaller quadrupole splitting $\Delta = 0.47\ mm\ s^{-1}$. The relative area of the doublet D_2 gives directly the value of the Fe^{III} molar fraction of the LDH; here $x = 34\%$. The substitution of the divalent or trivalent cations by other cations can also be followed indirectly with Mössbauer spectroscopy. For example, the spectrum of LDH[Fe^{II}–{Fe^{III}, Al^{III}}–SO_4] with a molar ratio $n(Al^{III})/n(Fe^{III})$ of 1 is presented in Fig. 5b. As expected, one observes a significant decrease of the relative area of doublet D_1 and the apparition of a new ferrous doublet D_3. The origin of doublet D_2 was attributed to Fe^{II} species having Al^{III} ions as first neighbours (Ruby et al., 2008).

3. Transformation of iron-based layered double hydroxides

3.1. Decomposition at anoxic condition

Iron-based LDHs may transform under anoxic conditions, particularly in basic solution. Two types of transformation were observed depending on the pH conditions (Ruby et al., 2003, 2006b). At room temperature, the LDH[Fe^{II}–Fe^{III}–SO_4] decomposed at pH ~ 11 according to the reaction:

$$Fe^{II}_4Fe^{III}_2(OH)_{12}SO_4 + 2OH^- \Leftrightarrow Fe^{II}Fe^{III}_2O_4 + 3Fe^{II}(OH)_2 + SO^{2-}_4 + 4H_2O \quad (5)$$

LDH[Fe^{II}–Fe^{III}–CO_3] transformed into magnetite and siderite at pH ~ 10 according to the reaction:

$$Fe^{II}_4Fe^{III}_2(OH)_{12}CO_3 + 2CO^{2-}_3 + 4H^+ \Leftrightarrow Fe^{II}Fe^{III}_2O_4 + 3Fe^{II}CO_3 + 8H_2O \quad (6)$$

LDH[Fe^{II}–Fe^{III}–SO_4] precipitated generally at a pH close to 7 both in the coprecipitation and the oxidation experiments and therefore reaction (5) can easily be avoided. On the contrary, LDH[Fe^{II}–Fe^{III}–CO_3] precipitated in alkaline solution at a pH between 8 and 10 and a partial transformation described in reaction (6) occurred within a few days. The introduction of very small amounts of phosphate or silicate anions prevented completely the decomposition of the LDH (Ruby et al., 2006b). This effect was demonstrated to be due to the adsorption of the phosphate species on the lateral faces of the LDH[Fe^{II}–Fe^{III}–CO_3] crystals (Bocher et al., 2004). This adsorption inhibits the release of the carbonate from the LDH structure.

3.2. Oxidation reactions

3.2.1. In-situ transformation within the solid

LDH[Fe^{II}–Fe^{III}] was oxidised *in situ* within the solid LDH[Fe^{II}–Fe^{III}] if either a strong oxidant such as H_2O_2 was used or if the oxidation was performed in a strongly aerated medium. At these conditions, the redox potential E_h measured in the suspension increased rapidly and oxidation was complete in approximately 1 h (Fig. 6a). If the starting material was LDH[Fe^{II}–Fe^{III}–CO_3), a continuous range of LDH related compounds with a variable composition of x was formed. The general chemical formula of these compounds was $Fe^{II}_{6(1-x)}Fe^{III}_{6x}O_{12}H_{2(7-3x)}CO_3$ with $x = [1/3–1]$ (Génin et al., 2006b). Reflexion Mössbauer spectra of the compounds at $x = 0.33$ and $x = 0.5$ are presented in Fig. 7. The two ferrous doublets D_1 and D_2 were attributed to Fe^{II} species having water molecules and carbonate species in their close neighbourhoods. A new doublet D_4 at x values higher than 0.33 (Fig. 7b) was attributed to Fe^{III} species in octahedral coordination with a partial deprotonation of the Fe–OH bonds. This hypothesis was confirmed by X-ray photoelectron spectroscopy by recording the O1s spectrum (Mullet et al., 2008). A progressive decrease of the OH^- component was observed when the ratio x increased (Fig. 8). This deprotonation process was also supported by X-ray diffraction patterns that exhibited a contraction of a few percentage of the crystallographical cell parameters and a progressive disordering of the

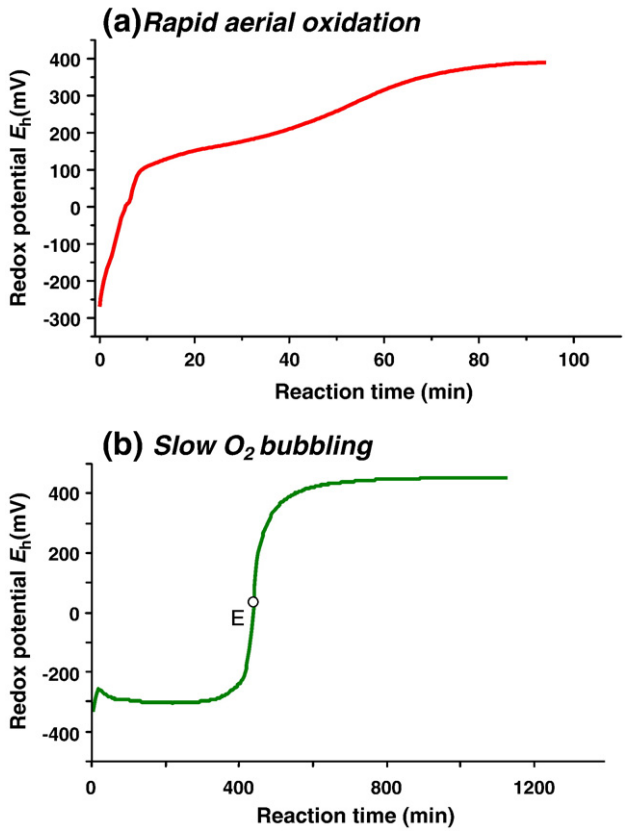

Fig. 6. Evolution of the redox potential measured inside the LDHs suspension during aerial oxidation of the iron-based LDHs.

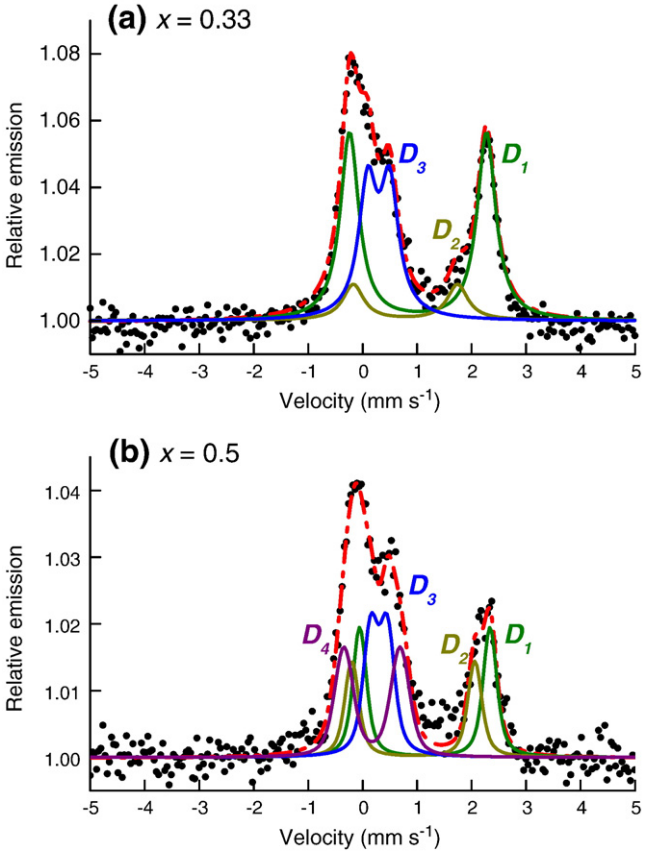

Fig. 7. Backscattered Mössbauer spectra of the hydroxycarbonate (a) and oxyhydroxicarbonate (b).

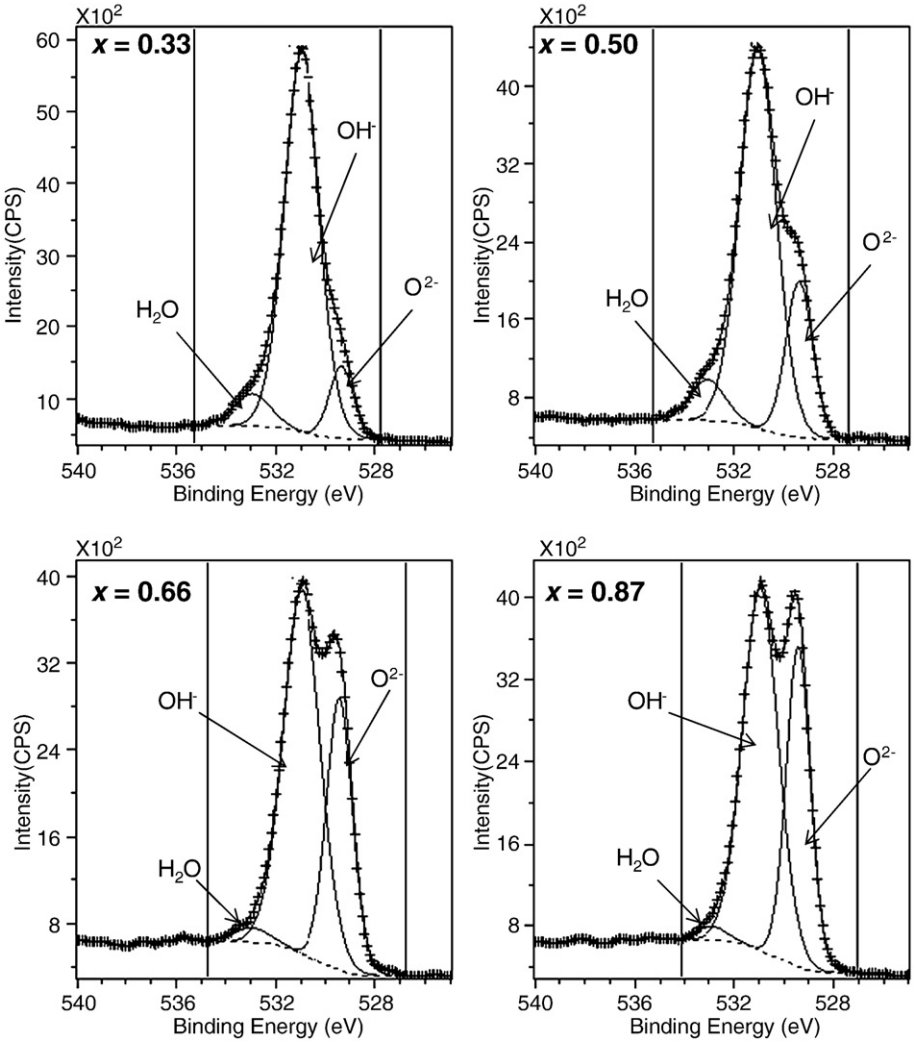

Fig. 8. O1s XPS spectra of the hydroxycarbonate (a) and oxyhydroxycarbonate (b,c &d).

structure. The hexagonal morphology of the crystals was conserved attesting that the oxidation occurred within the solid. The compound was therefore not longer *stricto sensu* a layered double hydroxide but rather a oxyhydroxycarbonate with a crystallographical structure strongly related to the initial LDH[Fe^{II}–Fe^{III}–CO_3] at $x = 0.33$.

3.2.2. Dissolution–precipitation mechanism

If the kinetics of the aerial oxidation of the LDH[Fe^{II}–Fe^{III}] was slower, the evolution of the redox potential (Fig. 6b) is changed differently in comparison with the one observed in Fig. 6a. Slow oxidation was achieved by bubbling small amount of O_2 into the suspension and the end of oxidation needed approximately 7 h. The curves presented initially a small hook followed by two plateaus separated by an equivalent point E. Point E corresponded to the end of the oxidation and its position is shifted on the right of the time scale if O_2 addition was reduced (not shown). In carbonate solutions, goethite α-FeOOH was the end-product of oxidation. On the contrary to Section 3.2.1, the crystallographical structure and morphology of goethite needles was different to the initial LDH. Therefore, the mechanism of formation was a dissolution–precipitation process. The presence of the first E_h plateau showed that a redox equilibrium existed between LDH[Fe^{II}–Fe^{III}–CO_3] and goethite. Therefore, a simple measure of the redox potential of the suspension was used to know which kind of oxidation mechanism was involved, i.e. *in situ* oxidation or dissolution–precipitation.

3.2.3. Reduction of pollutants by LDH(Fe^{II}–Fe^{III})

The studies concerning the reduction of pollutants by LDH(Fe^{II}–Fe^{III}) were initiated by Hansen et al. who showed that sulfated green rust was able to reduce either nitrite NO_2^- (Hansen et al., 1994) or nitrate NO_3^- (Hansen et al., 1996) into ammonium NH_4^+. A progressive transformation of LDH into magnetite Fe_3O_4 was observed due to a relatively slow kinetics. Further researches showed that LDH(Fe^{II}–Fe^{III}) can reduce many other oxoanions such as selenate $Se^{VI}O_4^{2-}$ into Se^{IV} and Se^0 (Myneni et al., 1997; Refait et al., 2000; Hayashi et al., 2009), chromate $Cr^{VI}O_4^{2-}$ into Cr^{III} (Loyaux-Lawniczak et al., 2000; Williams and Scherer, 2001; Bond and Fendorf, 2003; Legrand et al., 2004; Skovbjerg et al., 2006) and uranyl $U^{VI}O_4^{2-}$ into U^{IV} (O'Loughlin et al., 2003a). Interestingly, in the case of chromate reduction, the reaction leaded to the sequestration of the less toxic and less soluble Cr^{III} species into compounds such as Cr^{III} substituted magnetite (Bond and Fendorf, 2003) or goethite (Skovbjerg et al., 2006). Hansen group performed again a pioneer work concerning the reduction of chlorinated organic contaminants by sulphated green rust (Erbs et al., 1999) that was pursued by several authors (Lee and Batchelor, 2003; O'Loughlin et al., 2003b; Maithreepala and Doong, 2005; Choi and Lee, 2008). In comparison with others Fe^{II} containing minerals, e.g. magnetite, pyrite or iron-bearing philosilicates, LDH(Fe^{II}–Fe^{III}) was the most reactive compound (Lee and Batchelor, 2003). The reductive dechlorination was drastically accelerated when metallic species such as Cu^{II} or Ag^{I} ions were added into the suspension

(O'Loughlin et al., 2003b; Maithreepala and Doong, 2005; Choi and Lee, 2008). The key role of added metallic cations was explained by O'Loughlin et al. (2003b) and Suzuki et al. (2008) who clearly demonstrated that Cu^{II} and Ag^{I} species were transformed into Cu^{0} and Ag^{0}. These metals were proposed to be localised at the surface of the LDH(Fe^{II}–Fe^{III}) and allowed an acceleration of the reaction by acting as a galvanic couple with the iron species.

4. Conclusion

Iron-based layered double hydroxides LDHs[{Fe^{II}–M^{II}},{Fe^{III}–M^{III}}] that contain an iron molar fraction >50% were synthesised either by coprecipitation of dissolved cations or by the oxidation of M^{II} hydroxides. Non-substituted LDH[Fe^{II}–Fe^{III}], commonly called green rust, prepared at room temperature by both methods exhibited well crystallised hexagonal crystals. Partial substitution of Fe^{II} or Fe^{III} by other cations decreased crystal size. LDH[Fe^{II}–Fe^{III}–SO_4] contained a bi-layer of oriented sulphate anions and water molecules in the interlayer space. LDH[Fe^{II}–Fe^{III}–CO_3] contained only one layer of CO_3^{2-} and water molecules inside the interlayer space. Heating or alkaline conditions (pH>9) activated the decomposition of iron-based LDHs into biphasic mixtures. Adsorption of small quantities of phosphate or silicate anions on the lateral faces of the crystals slowed down this transformation in the case of LDH[Fe^{II}–Fe^{III}–CO_3]. At oxic conditions, fast reactions caused an *in situ* transformation of LDH that transforms into an oxyhydroxy-salt by deprotonation of hydroxyl groups. On the contrary to most of the other, iron-based LDHs had a flexibility of the *x* values in the range of 1/3–1. When oxidation was slower, the LDH was transformed into a ferric oxyhydroxide by a dissolution–precipitation mechanism. The structural characterisation of iron-based LDHs was investigated by several techniques such as high resolution X-ray diffraction, transmission electron microscopy and X-ray photoelectron and Mössbauer spectroscopies. Future works could be devoted to use iron-based LDHs for reducing anionic pollutants in conditions closer to field conditions, e.g. column reactors. Therefore the formation and reactivity of such compounds as coatings at the surface of minerals (*e.g.* quartz or clays) could be the subject of further studies.

Acknowledgments

The authors would like to thank Prof. Gerhard Lagaly (University of Kiel, Germany) for his remarks and corrections of the manuscript.

References

Aisawa, S., Higashiyama, N., Takahashi, S., Hirahara, H., Ikematsu, D., Kondo, H., Nakayama, H., Narita, E., 2007. Intercalation behavior of l-ascorbic acid into layered double hydroxides. Appl. Clay Sci. 35, 146–154.

Aïssa, R., Francois, M., Ruby, C., Fauth, F., Medjahdi, G., Abdelmoula, M., Génin, J.-M.R., 2006. Formation and crystallographical structure of hydroxysulphate and hydroxycarbonate green rusts synthetised by coprecipitation. J. Phys. Chem. Solids 67, 1016–1019.

Allmann, R., 1968. Crystal structure of pyroaurite. Acta Crystallogr., B Struct. Crystallogr. Cryst. Chem. 24, 972–977.

Bearcock, J.M., Perkins, W.T., Dinelli, E., Wade, S.C., 2006. Fe(II)/Fe(III) 'green rust' developed within ochreous coal mine drainage sediment in South Wales, UK. Mineral. Mag. 70, 731–741.

Bernal, J.D., Dasgupta, D., Mackay, A.L., 1959. The oxides and hydroxides of iron and their structural inter-relationships. Clay Miner. Bull. 4, 15–30.

Bocher, F., Géhin, A., Ruby, C., Ghanbaja, J., Abdelmoula, M., Génin, J.-M.R., 2004. Coprecipitation of Fe(II–III) hydroxycarbonate green rust stabilised by phosphate adsorption. Solid State Sci. 6, 117–124.

Bond, D.L., Fendorf, S., 2003. Kinetics and structural constraints of chromate reduction by green rusts. Environ. Sci. Technol. 37, 2750–2757.

Choi, J., Lee, W., 2008. Enhanced degradation of tetrachloroethylene by green rusts with platinum. Environ. Sci. Technol. 42, 3356–3362.

Christiansen, B.C., Balic-Zunic, T., Dideriksen, K., Stipp, S.L.S., 2009. Identification of green rust in groundwater. Environ. Sci. Technol. 43, 3436–3441.

Clemente-León, M., Coronado, E., Primo, V., Ribera, A., Soriano-Portillo, A., 2008. Hybrid magnetic materials formed by ferritin intercalated into a layered double hydroxide. Solid State Sci. 10, 1807–1813.

De Waal, S.A., Viljoen, E.A., 1971. Nickel minerals from Barberton, South Africa. IV. Reevesite, a member of the hydrotalcite group. Am. Mineral. 56, 1077–1081.

Erbs, M., Hansen, H.C.B., Olsen, C.E., 1999. Reductive dechlorination of carbon tetrachloride using iron(II)iron(III) hydroxide sulfate (green rust). Environ. Sci. Technol. 33, 307–311.

Feitknecht, W., Keller, G., 1950. Über die dunkelgrünen hydroxyverbindungen des eisens. Z. Anorg. Allg. Chem. 262, 61–68.

Génin, J.-M.R., Ruby, C., Géhin, A., Refait, P., 2006a. Synthesis of green rusts by oxidation of $Fe(OH)_2$, their products of oxidation and reduction of ferric oxyhydroxides; Eh–pH Pourbaix diagrams. C. R. Geosci. 338, 433–446.

Génin, J.-M.R., Ruby, C., Upadhyay, C., 2006b. Structure and thermodynamics of ferrous, stoichiometric and ferric oxyhydroxycarbonate green rusts; redox flexibility and fougerite mineral. Solid State Sci. 8, 1330–1343.

Hanna, K., Kone, T., Ruby, C., 2010. Fenton-like oxidation and mineralization of phenol using synthetic Fe(II)–Fe(III) green rusts. Environ. Sci. Pollut. Res. 17, 124–134.

Hansen, H.C.B., 2001. Environmental chemistry of iron(II)–iron(III) LDHs (green rusts). In: Rives, V. (Ed.), Layered Double Hydroxides: Present and Future. Nova Science Publishers, Huntington, N.Y., pp. 469–493.

Hansen, H.C.B., Borggaard, O.K., Sorensen, J., 1994. Evaluation of the free energy of formation of Fe(II)–Fe(III) hydroxide-sulfate (green rust) and its reduction of nitrite. Geochim. Cosmochim. Acta 58, 2599–2608.

Hansen, H.C.B., Koch, C.B., Nancke-Krogh, H., Borggaard, O.K., Sorensen, J., 1996. Abiotic nitrate reduction to ammonium: key role of green rust. Environ. Sci. Technol. 30, 2053–2056.

Hansen, H.C.B., Guldberg, S., Erbs, M., Koch, C.B., 2001. Kinetics of nitrate reduction by green rusts-effects of interlayer anion and Fe(II):Fe(III) ratio. Appl. Clay Sci. 18, 81–91.

Hayashi, H., Kanie, K., Shinoda, K., Muramatsu, A., Suzuki, S., Sasaki, H., 2009. pH-dependence of selenate removal from liquid phase by reductive Fe(II)–Fe(III) hydroxysulfate compound, green rust. Chemosphere 76, 638–643.

Khan, A.I., O'Hare, D., 2002. Intercalation chemistry of layered double hydroxides: recent developments and applications. J. Mater. Chem. 12, 3191–3198.

Kone, T., Hanna, K., Abdelmoula, M., Ruby, C., Carteret, C., 2009. Reductive transformation and mineralization of an azo dye by hydroxysulphate green rust preceding oxidation using H_2O_2 at neutral pH. Chemosphere 75, 212–219.

Lee, W., Batchelor, B., 2003. Reductive capacity of natural reductants. Environ. Sci. Technol. 37, 535–541.

Legrand, L., Figuigui, A.E., Mercier, F., Chausse, A., 2004. Reduction of aqueous chromate by Fe(II)/Fe(III) carbonate green rust: kinetic and mechanistic studies. Environ. Sci. Technol. 38, 4587–4595.

Loyaux-Lawniczak, S., Refait, Ph., Ehrhardt, J.-J., Lecomte, P., Génin, J.-M.R., 2000. Trapping of Cr by formation of ferrihydrite during reduction of chromate ions by Fe(II)–Fe(III) hydroxysalt green rusts. Environ. Sci. Technol. 34, 438–443.

Ma, R., Liu, Z., Takada, K., Iyi, N., Bando, Y., Sasaki, T., 2007. Synthesis and exfoliation of Co^{2+}–Fe^{3+} layered double hydroxides: an innovative topochemical approach. J. Am. Chem. Soc. 129, 5257–5263.

Ma, R., Takada, K., Fukuda, K., Iyi, N., Bando, Y., Sasaki, T., 2008. Topochemical synthesis of monometallic (Co^{2+}–Co^{3+}) layered double hydroxide and its exfoliation into positively charged $Co(OH)_2$ nanosheets. Angew. Chem. 120, 92–95.

Maithreepala, R.A., Doong, R.-A., 2005. Enhanced dechlorination of chlorinated methanes and ethenes by chloride green rust in the presence of copper(II). Environ. Sci. Technol. 39, 4082–4090.

Miyata, S., 1983. Anion-exchange properties of hydrotalcite-like compounds. Clays Clay Miner. 31, 305–311.

Mullet, M., Guillemin, Y., Ruby, C., 2008. Oxidation and deprotonation of synthetic FeII–FeIII (oxy)hydroxycarbonate Green Rust: an X-ray photoelectron study. J. Solid State Chem. 181, 81–89.

Myneni, S.C.B., Tokunaga, T.K., Brown Jr., G.E., 1997. Abiotic selenium redox transformations in the presence of Fe(II, III) oxides. Science 278, 1106–1109.

Oh, J.-M., Kwak, S.-Y., Choy, J.-H., 2006. Intracrystalline structure of DNA molecules stabilized in the layered double hydroxide. J. Phys. Chem. Solids 67, 1028–1031.

O'Loughlin, E.J., Kelly, S.D., Cook, R.E., Csencsits, R., Kemner, K.M., 2003a. Reduction of uranium(VI) by mixed iron(II)/iron(III) hydroxide (green rust): formation of UO_2 nanoparticles. Environ. Sci. Technol. 37, 721–727.

O'Loughlin, E.J., Kelly, S.D., Kemner, K.M., Csencsits, R., Cook, R.E., 2003b. Reduction of AgI, AuIII, CuII, and HgII by FeII/FeIII hydroxysulfate green rust. Chemosphere 53, 437–446.

Refait, P., Génin, J.-M.R., 1993. The oxidation of nickel(II)–iron(II) hydroxides in chloride-containing aqueous media. Corros. Sci. 34, 2059–2070.

Refait, P., Simon, L., Génin, J.-M.R., 2000. Reduction of SeO_4^{2-} anions and anoxic formation of iron(II)–iron(III) hydroxy-selenate green rust. Environ. Sci. Technol. 34, 819–825.

Refait, P., Abdelmoula, M., Trolard, F., Génin, J.-M.R., Bourrié, G., 2001. Mössbauer and XAS study of a green rust mineral; the partial substitution of Fe^{2+} by Mg^{2+}. Am. Mineral. 86, 731–739.

Refait, P., Abdelmoula, M., Simon, L., Génin, J.-M.R., 2005a. Mechanisms of formation and transformation of Ni–Fe layered double hydroxides in SO_3^{2-} and SO_4^{2-} containing aqueous solutions. J. Phys. Chem. Solids 66, 911–917.

Refait, Ph., Drissi, S.H., Abdelmoula, M., Jeannin, M., Reffass, M., Génin, J.-M.R., 2005b. Mechanisms of formation and transformation of Ni–Fe hydroxycarbonates. AIP Conference Proceedings, 765 (Industrial Applications of the Mössbauer Effect), pp. 79–84.

Ruby, C., Géhin, A., Abdelmoula, M., Génin, J.-M.R., Jolivet, J.-P., 2003. Coprecipitation of Fe(II) and Fe(III) cations in sulphated aqueous medium and formation of hydroxysulphate green rust. Solid State Sci. 5, 1055–1062.

Ruby, C., Géhin, A., Aïssa, R., Génin, J.-M.R., 2006a. Mass-balance and E_h–pH diagrams of Fe^{II}–^{III} green rust in aqueous sulphated solution. Corros. Sci. 48, 3824–3837.

Ruby, C., Aïssa, R., Géhin, A., Cortot, J., Abdelmoula, M., Génin, J.-M.R., 2006b. Green rusts synthesis by coprecipitation of Fe^{II}–Fe^{III} ions and mass-balance diagram. C. R. Geosci. 338, 420–432.

Ruby, C., Abdelmoula, M., Aïssa, R., Medjahdi, G., Brunelli, M., François, M., 2008. Aluminium substitution in iron(II–III)-layered double hydroxides: formation and cationic order. J. Solid State Chem. 181, 2285–2291.

Skovbjerg, L.L., Stipp, S.L.S., Utsunomiya, S., Ewing, R.C., 2006. The mechanisms of reduction of hexavalent chromium by green rust sodium sulphate: formation of Cr-goethite. Geochim. Cosmochim. Acta 70, 3582–3592.

Stampfl, P.P., 1969. Ein basiches eisen-II–III-karbonat in rost. Corros. Sci. 9, 185–187.

Suzuki, S., Shinoda, K., Sato, M., Fujimoto, S., Yamashita, M., Konishi, H., Doi, T., Kamimura, T., Inoue, K., Waseda, Y., 2008. Changes in chemical state and local structure of green rust by addition of copper sulphate ions. Corros. Sci. 50, 1761–1765.

Tamaura, Y., 1985. Ferrite formation from the intermediate, green rust II, in the transformation reaction of ferric hydroxide oxide, γ-FeO(OH), in aqueous suspension. Inorg. Chem. 24, 4363–4366.

Trolard, F., Génin, J.-M.R., Abdelmoula, M., Bourrié, G., Humbert, B., Herbillon, A., 1997. Identification of a green rust mineral in a reductomorphic soil by Mossbauer and Raman spectroscopies. Geochim. Cosmochim. Acta 61, 1107–1111.

Vial, S., Prevot, V., Leroux, F., Forano, C., 2008. Immobilization of urease in ZnAl Layered Double Hydroxides by soft chemistry routes. Microporous Mesoporous Mater. 107, 190–201.

Williams, A.G.B., Scherer, M.M., 2001. Kinetics of Cr(VI) reduction by carbonate green rust. Environ. Sci. Technol. 35, 3488–3494.

American Mineralogist, Volume 96, pages 1410–1413, 2011

LETTER

In situ monitoring of lepidocrocite bioreduction and magnetite formation by reflection Mössbauer spectroscopy

ASFAW ZEGEYE,* MUSTAPHA ABDELMOULA, MUHAMMAD USMAN, KHALIL HANNA, AND CHRISTIAN RUBY

Laboratoire de Chimie Physique et Microbiologie pour l'Environnement, LCPME, UMR 7564, Institut Jean Barriol, CNRS-Nancy Université, 405 rue de Vandoeuvre, 54600, Villers-lès-Nancy, France

ABSTRACT

The miniaturized Mössbauer spectrometer (MIMOS II) was used to monitor in situ the mineralogical transformation of lepidocrocite (γ-FeOOH) in a *Shewanella putrefaciens* culture under anaerobic conditions using methanoate as the electron source. Magnetite was the only biogenic mineral formed during the course of the incubation. The analysis of the biogenic mineral by transmission electron microscopy (TEM) revealed cubic-shaped crystals with a relatively homogeneous grain size of about 50 nm. After one day of incubation, the departure from stoichiometry, δ, of the biogenerated magnetite was very low (δ ~ 0.025) and rapidly reached values close to zero. Such low values of δ were not obtained for magnetite synthesized inorganically when Fe^{3+} in the form of γ-FeOOH was reacted with stoichiometric quantities of soluble Fe^{2+} and OH^-. The experimental setup used in this study could be replicated in field experiments when assessing the formation of magnetite in modern geological settings as its formation is suspected to be caused by a strong bacterial activity.

Keywords: MIMOS, magnetite, stoichiometry, biomineralization

INTRODUCTION

Magnetite, a mixed valence Fe(II–III) oxide ($Fe_{3-\delta}O_4$), is a commonly occurring mineral on Earth usually found in soils and sediments (Cornell and Schwertmann 1996). Under non-sulfidic reducing conditions, dissimilatory iron-reducing bacteria (DIRB) can play an important role in the biogeochemistry of iron by coupling the oxidation of an electron source (organic matter or H_2) to the external reduction of iron oxyhydroxides (Nealson and Saffarini 1994). Thus, Dos Santos and Stumm (1992) and Lovley et al. (1991) suggested that most of the Fe^{3+} reduction occurring in such environments is due to bacterial activity. Depending on the geochemical environments in which Fe^{3+} bioreduction takes place, DIRB activity can lead to diverse biogenic minerals such as magnetite, the discovery of which at a depth of 6.7 km below the surface has been used as a marker for DIRB activity (Gold 1992; Lovley et al. 1987). Moreover, the quantity of DIRB-induced extracellular magnetite per unit of biomass could be several thousand times more than magnetite formed by magnetotactic bacteria (Frankel 1987; Lovley 1991). Whereas many reports have focused on magnetite precipitated by magnetotactic bacteria (Kim et al. 2005; Kopp and Kirschvink 2008), very few reports (Gibbs-Eggar et al. 1999) have been able to demonstrate the unequivocal existence of extracellularly precipitated magnetite. This could be explained by the higher reactivity of magnetite formed by DIRB leading to the paucity of magnetite in the natural environment (Kukkadapu et al. 2005; Li et al. 2009). Indeed, the reactivity and stability of magnetite is dictated partly by its stoichiometry defined by $x = Fe^{3+}/\{Fe^{2+} + Fe^{3+}\}$ where $0.67 \leq x \leq 1$, with stoichiometric magnetite ($x = 0.67$ or $\delta = 0$) being the most reactive composition (Cutting et al. 2010; Gorski and Scherer 2009). It was shown that stoichiometric magnetite had a lower reduction potential than that of non-stoichiometric magnetite, consistent with higher reactivity toward pollutants such as nitrobenzene compounds (Gorski et al. 2010).

Numerous laboratory studies have pointed out that geochemical parameters such as the nature of the iron oxide, the concentration of dissolved Fe^{2+}, the bacteria/iron oxide ratio, and the physiochemical characteristics of the culture media could have an impact on the subsequent mineralization of magnetite (Fredrickson et al. 1998; Roh et al. 2003; Zachara et al. 1998; Zegeye et al. 2010). These studies mainly focused on gaining a better understanding of the bioreduction processes by characterizing the secondary mineral. While the stoichiometry of the magnetite as a secondary mineral has widely been investigated at the end of the bioreduction reaction (Kukkadapu et al. 2005; Li et al. 2009), the evolution of the stoichiometry of magnetite during its formation has not yet been fully studied. Indeed, to understand the stability of a biogenic magnetite and its persistence in soils and sediments a thorough investigation of the evolution of its stoichiometry during bioreduction is needed.

EXPERIMENTAL METHODS

Bioreduction experiments

To investigate the fluctuation of magnetite stoichiometry during iron bioreduction, we examined microbially induced lepidocrocite reduction using *Shewanella putrefaciens* CIP 8040, a facultative DIRB. The lepidocrocite was prepared by aerobic oxidation of $FeCl_2$ in sodium hydroxide solution (Schwertmann and Cornell 2000). An anaerobic cell suspension (10^6 CFU mL^{-1}) was used to inoculate a non-growth-supporting medium containing sodium methanoate (1 *mM*) as the electron source and lepidocrocite (3 *mM*) as the electron acceptor under strict anaerobic conditions as described in a recent study (Zegeye et al. 2007). The control experiment was cell-free and otherwise identical to the biotic sample.

* E-mail: asfaw.zegeye@lcpme.cnrs-nancy.fr

Reflection Mössbauer spectroscopy and transmission electron microscopy (TEM)

The precipitation of biogenic magnetite was monitored in situ by using a miniaturized Mössbauer spectrometer (MIMOS), designed for Mars missions (Klingelhöfer et al. 2003), and adapted to laboratory measurements (Fig. 1, supplementary data[1]). The MIMOS works in back-scattering geometry, without sample preparation and/or thickness matrix effect correction, and thereby differs from transmission Mössbauer spectroscopy. Re-emitted backscattered γ-rays (14.4 keV) were selected by four Si-PIN-diodes detectors. Center shifts, *CS*, were reported with respect to that of α-Fe at room temperature. Mössbauer spectra were computer-fitted (recoil software, Ottawa University) with a sum of Lorentzian shape lines, which excludes a particle size distribution model. The relative areas of iron fitted in different sites have not been calibrated by the recoilless fraction, due to its relatively small contribution (Eeckhout and De Grave 2003; Sawatzky et al. 1969).

TEM observations and selected area electron diffraction (SAED) were carried out using a Philips CM20 TEM (200 kV) at the end of the incubation period (i.e., 26 days). One drop of the suspension was laid on an amorphous carbon-coated grid and loaded into the analysis holder of the microscope under 10^{-8} Torr vacuum.

Results and discussion

The lepidocrocite and magnetite spectra displayed a doublet and two sextets, respectively (Fig. 1), with Mössbauer hyperfine parameters (Table 1, supplementary data[1]) similar to those published in the literature (Da Costa et al. 1998; De Grave et al. 2002). For stoichiometric magnetite, Fe_3O_4, the outer sextet, S_A, corresponds to $^{Tet}Fe^{3+}$ ions in the tetrahedral A-sites, whereas the inner sextet S_B corresponds to the $^{Oct}Fe^{2+}$ and the $^{Oct}Fe^{3+}$ ions present in the octahedral B-sites. In fact, due to very fast electron hopping between the $^{Oct}Fe^{2+}$ and the $^{Oct}Fe^{3+}$ ions at temperatures above the Verwey transition (121 K), the sextet S_B observed by Mössbauer spectroscopy is integrated into a peak representing an average valence of $^{Oct}Fe^{2.5+}$ ions. The analysis of Mössbauer spectra showed that magnetite precipitated as the only biogenic mineral and indicated that 6% of the initial lepidocrocite remained at the end of the incubation period (Fig. 1f, d = 26). During magnetite formation, no intermediate mineral, such as green rust, was observed, which indicates that the solution was supersaturated with respect to magnetite (Fig. 1). In contrast, no lepidocrocite transformation was detected at any time during the control experiment (data not shown), thereby indicating that the MIMOS can be used to assess mineralogical transformation ensuing from bacterial activity.

TEM images of the secondary mineral revealed aggregates of magnetite crystals with only slight differences in size and morphology (Fig. 2a). The particles consisted of cubic-shaped crystals with a relatively homogeneous grain size of ~50 nm. The grain size measured in this study was in the upper range of the usual grain size observed for bio-induced magnetite (10–120 nm) and therefore would not display superparamagnetism (Li et al. 2009; Vali et al. 2004). The *d*-spacings calculated from SAED (Table 2, supplementary data) were characteristic of magnetite and confirmed its presence as the sole secondary mineral (Fig. 2b).

An interesting observation in this study was the evolution of magnetite stoichiometry during the bioreduction process. The general formula of magnetite is

$$^{Tet}Fe^{3+}[^{Oct}Fe^{2+}_{(1-3\delta)}Fe^{3+}_{(1+2\delta)}V_\delta]O_4,\ (0 \le \delta \le 1/3),$$

where "V" denotes the cations vacancies accounting for charge balance. For non-stoichiometric magnetite ($0 < \delta \le 1/3$), a first fraction of the $^{Oct}Fe^{3+}$ species participates in the electron hopping and a second fraction screens the lack of charge of the cations vacancy (Coey et al. 1971; Ramdani et al. 1987; Voogt et al. 1999). To distinguish between the two $^{Oct}Fe^{3+}$ species, the formula of non-stoichiometric magnetite can be rewritten as $^{Tet}Fe^{3+}[^{Oct}\{Fe^{2+}_{(1-3\delta)}Fe^{3+}_{(1-3\delta)}\}Fe^{3+}_{5\delta}V_\delta]O_4$. The Mössbauer spectrum of $Fe_{3-\delta}O_4$ at room temperature consists of three sextets: (1) S_{B1} corresponding to the $^{Oct}Fe^{2.5+}$ ions, (2) S_{B2} associated to the $^{Oct}Fe^{3+}$, (3) S_A corresponding to the $^{Tet}Fe^{3+}$ ions (Vandenberghe et al. 2000). However, the hyperfine parameters of sextets S_A and S_{B2} are very close to each other and the spectrum of a non-stoichiometric magnetite can be fitted with only two sextets (Gorski and Scherer 2010; Voogt et al. 1999), the outer sextet corresponding to the superposition of sextets S_A and S_{B2} and the inner sextet representing S_{B1}. The ratio between the relative area (*RA*) of the sextets $\beta = RA\ (S_A + S_{B2})/RA\ (S_{B1})$ is therefore $(1 + 5\delta)/(2 - 6\delta)$ and the vacancy degree can be deduced as $\delta = (2\beta - 1)/(6\beta + 5)$. From the experimental values of β, the vacancy parameter δ of magnetite was calculated as a function of the incubation time (Fig. 3). The initial magnetite formed after one day of incubation has a very slight departure from stoichiometry $\delta \sim 0.025$, and a value very close to $\delta \sim 0$ was reached after 5 days. After 7 days, a magnetite with an apparent excess of Fe^{2+} corresponding to a negative value $\delta \sim -0.02 \pm 0.01$ was measured. Despite the fact that biogenic magnetite that

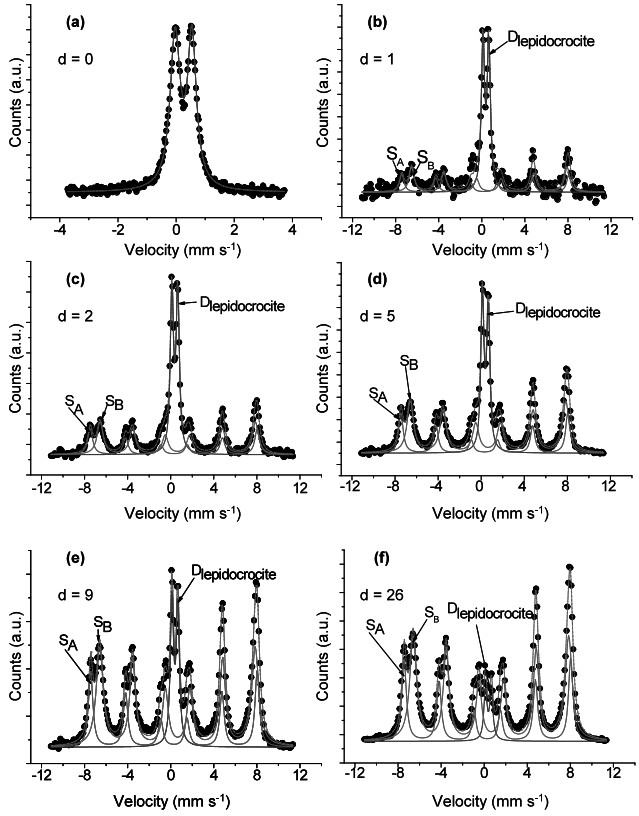

Figure 1. Mössbauer spectra of solid compounds obtained at different incubation times. (**a**) Initial mineral, (**b**) 1 day, (**c**) 2 days, (**d**) 5 days, (**e**) 9 days, and (**f**) 26 days. The hyperfine parameters collected at room temperature are shown in Table 1 (supplementary data).

[1] Deposit item AM-11-040, Supplementary Tables and Figure. Deposit items are available two ways: For a paper copy contact the Business Office of the Mineralogical Society of America (see inside front cover of recent issue) for price information. For an electronic copy visit the MSA web site at http://www.minsocam.org, go to the *American Mineralogist* Contents, find the table of contents for the specific volume/issue wanted, and then click on the deposit link there.

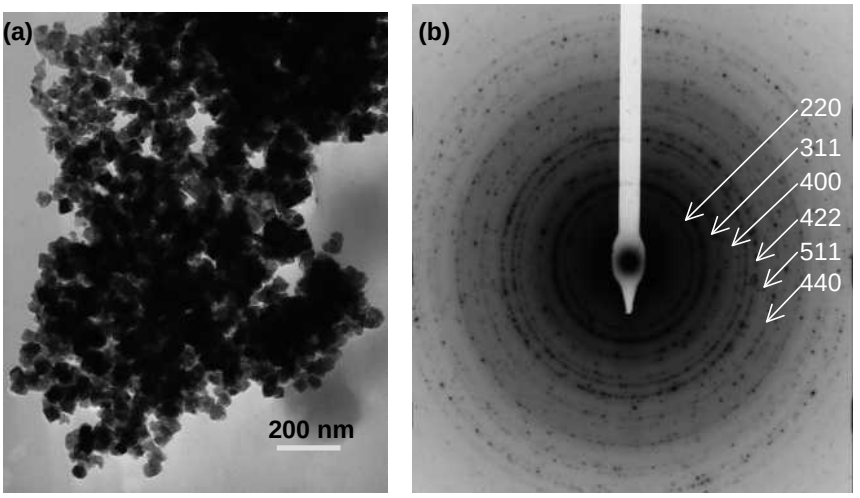

FIGURE 2. (**a**) TEM image of mineral formed after 26 days of incubation whose structure is determinate by the SAED analysis (**b**).

were precipitated in *Shewanella* cultures and contained a slight excess of Fe^{2+} ions in their structure have already been reported in previous research (Kukkadapu et al. 2005; Li et al. 2009), the negative departure from stoichiometry measured in this study was very close to the experimental error. It is therefore difficult to unambiguously conclude that a negative value of δ would be characteristic of a transient state of magnetite during the bio-reduction process. Finally, the product obtained after 26 days of incubation was a stoichiometric magnetite Fe_3O_4. For comparison, an abiotic experiment was conducted by adding soluble Fe^{2+} ions to a suspension of lepidocrocite at a fixed value of the ferric molar fraction $x = 0.67$ to form a stoichiometric magnetite according to the following reaction:

$$2\ \gamma\text{-}Fe^{3+}OOH + Fe^{2+} + 2\ OH^- = Fe^{2+}Fe^{3+}_2O_4 + 2\ H_2O \qquad (1)$$

The precipitation of magnetite was achieved by adding to this initial suspension a basic solution of NaOH with an OH^-/Fe^{3+} molar ratio of 1. The suspension was agitated for an hour and aged in a static condition for 26 days. The vacancy parameter of this abiotic magnetite was measured for three aging times, i.e., 1 h, 1 day, and 26 days (Fig. 3) by recording the corresponding Mössbauer spectra. About 75% of the lepidocrocite was transformed into a quasi-stoichiometric magnetite after 1 h of aging. After both 1 day and 26 days of aging time, the rest of lepidocrocite was transformed into a magnetite with a vacancy parameter close to $\delta \approx 0.05$.

The Fe^{2+}-Fe^{3+} mass-balance diagram previously described by Ruby et al. (2006) presents the domain of composition $x = Fe^{3+}/[Fe^{2+} + Fe^{3+}]$ corresponding to the vacancy parameter δ of the biotic and abiotic magnetite synthesized in this study ($x = \{2 + 2\delta\}/\{3 - \delta\}$). The value of x for each incubation time is determined by the following formula:

$$x = RA\ (\gamma\text{-FeOOH}) + RA\ (Fe_{3-\delta}O_4)\ \{2 + 2\delta\}/\{3 - \delta\} \qquad (2)$$

where *RA* (γ-FeOOH) and *RA* ($Fe_{3-\delta}O_4$) are the relative areas of the lepidocrocite and magnetite components of the Mössbauer spectra (Table 1, supplementary data), respectively. The values of x for several incubation times are presented at the bottom right of Figure 4. It decreases gradually between $x = 0.84$ and $x = 0.68$ for incubation times varying between 1 day and 26 days, respectively. The composition of the suspension is, therefore, favorable to the formation of a magnetite having relatively high departure from the stoichiometric value $x = 0.67$. However, in both experiments, the departure from stoichiometry was relatively limited if it is compared to the global domain of composition of magnetite, a solid solution that is bounded by $x = 0.67$ for Fe_3O_4 and $x = 1$ for maghemite γ-Fe_2O_3. Nevertheless, magnetite was formed with a composition very close to $^{Tet}Fe^{3+}[^{Oct}Fe^{2+}Fe^{3+}]O_4$ ($\sim 0.65 \leq x \leq \sim 0.69$) during the entirety of the bioreduction experiment. Because DIRB reduce the Fe^{3+} oxide into Fe^{2+} in a progressive manner, one would expect that x would decrease gradually from $x = 1$ to $x = 0.67$. However, the local biological conditions favor the formation of a mixture of lepidocrocite and stoichiometric magnetite rather than a non-stoichiometric magnetite, which would become stoichiometric during the course of the reduction along the reaction path A_1B (Fig. 4). Such a stoichiometric magnetite was not obtained during the abiotic experiment despite the fact that stoichiometric conditions were imposed. Reaction 1 corresponding to the segment A_2B was, therefore, not fully accomplished and a small part of the soluble Fe^{2+} ions that was present in the initial solution did not incorporate in the final solid product, i.e., $Fe_{2.95}O_4$, leading to a non-stoichiometric magnetite. Similarly, Gorski and Scherer (2009, 2010) pointed out that excessive washing of a stoichiometric magnetite caused the magnetite to become oxidized due to Fe^{2+} dissolution. We, therefore, speculate that an excess of Fe^{2+} (more than what is needed for stoichiometric magnetite) in the synthesis solution is needed to maintain the stoichiometry of the abiotic magnetite. On the other hand, DIRB were able to maintain a flux of Fe^{2+} to sustain the stoichiometry of the biogenic magnetite.

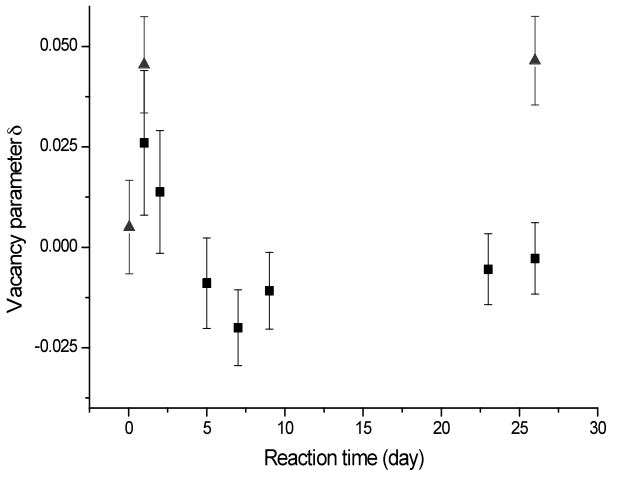

FIGURE 3. Vacancy parameter δ of magnetite calculated as a function of the incubation time. Square = biogenic magnetite, triangle = abiotic magnetite.

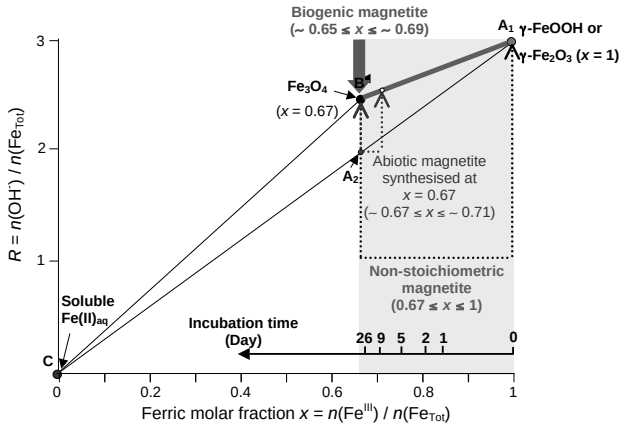

FIGURE 4. Fe^{2+}-Fe^{3+} mass-balance diagram showing the composition domain of biotic and abiotic magnetite and the ferric molar fraction *x* of the suspension at different incubation time (right bottom).

To our knowledge this is the first study reporting the in situ monitoring of a biogenic magnetite ($Fe_{3-\delta}O_4$) stoichiometry during its formation. The relative proportion of the two sextets S_A and S_B of the Mössbauer spectrum of the magnetite were used to determine the eventual departure from stoichiometry δ. The resulting magnetite was stoichiometric with δ = 0. The paucity of bacterially induced magnetite in the environment could be explained by their reactivity, which is related to their stoichiometry. Recently, the MIMOS apparatus was used to study in situ the mineralogical transformation of Fe-containing compounds in hydromorphic soils (Feder et al. 2005). Therefore, the experimental approach used in the present study could be applied in field experiments to assess in situ the formation of biogenic magnetite in modern geological settings where its formation is suspected to be caused by a strong bacterial activity.

ACKNOWLEDGMENTS

The authors thank the Agence Nationale de la Recherche (ANR) and Agence de la Maîtrise de l'Energie (ADEME) for financial support (program Ecotech 2009, CERVEAU NP, décision attributive d'aide no. 0994C0103). We thank the Lorraine Region for financing of the MIMOS apparatus (CPER 2005–2009). The authors acknowledge J. Ghanbaja (Nancy Université) for the TEM analyses.

REFERENCES CITED

Coey, J.M.D., Morrish, A.H., and Sawatzky, G.A. (1971) Mössbauer study of conduction in magnetite. Journal de Physique, C1-271–C1-273.

Cornell, R.M. and Schwertmann, U. (1996) The Iron Oxides: structure, properties, reactions, occurrences and uses, 573 p. VCH, Weinheim, Germany.

Cutting, R.S., Coker, S.V., Telling, N.D., Kimber, R.L., Pearce, C.I., Ellis, B.L., Lawson, R.S., van Der Laan, G., Pattrick, R.A.D., Vaughan, D.J., Arenholz, E., and Lloyd, J.R. (2010) Optimizing Cr(VI) and TC(VII) remediation through nanoscale biomineral engineering. Environmental Science and Technology, 44, 2577–2584.

Da Costa, G.M., De Grave, E., and Vanderberghe, R.E. (1998) Mössbauer studies of magnetite and Al-substituted maghemites. Hyperfine Interaction, 117, 207–243.

De Grave, E., Barrero, C.A., Da Costa, G.M., Vanderberghe, R.E., and Van San, E. (2002) Mössbauer spectra α- and γ-polymorphs of FeOOH and Fe_2O_3: effects of poor crystallinity and of Al-for-Fe substitution. Clay Minerals, 37, 591–606.

Dos Santos, A.M. and Stumm, W. (1992) Reductive dissolution of iron (III) (hydr)oxides by hydrogen sulfide. Langmuir, 8, 1671–1675.

Eeckhout, S.G. and De Grave, E. (2003) Evaluation of ferrous and ferric Mössbauer fractions. Part II. Physics and Chemistry of Minerals, 30, 142–146.

Feder, F., Trolard, F., Klingelhöfer, G., and Bourrié, G. (2005) In situ Mössbauer spectroscopy: evidence for green rust (fougerite) in a gleysol and its transformation with time and depth. Geochimica et Cosmochimica Acta, 69, 4463–4483.

Frankel, R.B. (1987) Anaerobes pumping iron. Nature, 330, 208–208.

Fredrickson, J.K., Zachara, J.M., Kennedy, D.W., Dong, H., Onstott, T.C., Hinman, N.W., and Li, S.-M. (1998) Biogenic iron mineralization accompanying the dissimilatory reduction of hydrous ferric oxide by a groundwater bacterium. Geochimica et Cosmochimica Acta, 62, 3239–3257.

Gibbs-Eggar, Z., Jude, B., Dominik, J., Loiseau, J.L., and Oldfield, F. (1999) Possible evidence for dissimilatrory bacterial magnetite dominating the magnetite properties of recent lake sediments. Earth and Planetary Science Letters, 168, 1–6.

Gold, T. (1992) The deep, hot biosphere. Proceedings of the National Academy of Science, 89, 6045–6049.

Gorski, C. and Scherer, M.M. (2009) Influence of magnetite stoichiometry on Fe^{II} uptake and nitrobenzene reduction. Environmental Science and Technology, 43, 3675–3680.

——— (2010) Determination of nanoparticulate magnetite stoichiometry by Mössbauer spectroscopy, acidic dissolution, and powder X-ray diffraction: A critical review. American Mineralogist, 95, 1017–1026.

Gorski, C., Nurmi, J.T., Tratnyek, P.G., Hofstetter, B., and Scherer, M.M. (2010) Redox behaviour of magnetite: implication for contaminant reduction. Environmental Science and Technology, 44, 55–60.

Kim, D.K., Kodama, K.P., and Moeller, R.E. (2005) Bacterial magnetite produced in water column dominates lake sediment mineral magnetism: Lake Ely, USA. Geophysical Journal International, 163, 26–37.

Klingelhöfer, G., Morris, R.V., Bernhardt, B., Rodionov, D., De Souza, P.A., Squyres, S.W., Foh, J., Kankeleit, E., Bonnes, U., Geller, R., and others. (2003) Athena MIMOS II Mössbauer spectrometer investigation. Journal of Geophysical Research-Planets, 108, 8067.

Kopp, R.E. and Kirschvink, J.L. (2008) The identification and biogeochemical interpretation of fossil magnetotactic bacteria. Earth Science Review, 86, 42–61.

Kukkadapu, R.K., Zachara, J.M., Fredrickson, J.K., Kennedy, D.W., Dohnalkova, A.C., and McCready, D.E. (2005) Ferrous hydroxycarbonate is a stable transformation product of biogenic magnetite. American Mineralogist, 90, 510–515.

Li, Y.L., Pfiffner, S.M., Dyar, M.D., Vali, H., Konhauser, K., Cole, D.R., Rondinone, A.J., and Phelps, T.J. (2009) Degeneration of biogenic superparamagnetic magnetite. Geobiology, 7, 25–34.

Lovley, D.R. (1991) Magnetite formation during microbial iron reduction. In R.B. Frankel, and R.P. Blakemore, Eds., Iron Biominerals, p. 155–166. Plenum, New York.

Lovley, D.R., Stolz, J.F., Nord, G.L., and Phillips, E.J.P. (1987) Anaerobic production of magnetite by a dissimilatory iron-reducing microrganism. Nature, 330, 252–54.

Lovley, D.R., Phillips, E.J.P., and Lonergan, D.J. (1991) Enzymatic versus nonenzymatic mechanisms for Fe(III) reduction in aquatic sediments. Environmental Science and Technology, 25, 1062–1067.

Nealson, K.H. and Saffarini, D. (1994) Iron and manganese in anaerobic respiration: environmental significance, physiology, and regulation. Annual Review of Microbiology, 48, 311–43.

Ramdani, A., Steinmetz, J., Gleitzer, C., Coey, J.M.D., and Friedt, J.M. (1987) Perturbation de l'échange électronique rapide par les lacunes cationiques dans $Fe_{3-x}O_4$ (x<0,09). Journal of Physics and Chemistry of Solids, 48, 217–228.

Roh, Y., Zhang, C.L., Vali, H., Lauf, R.J., Zhou, J., and Phelps, T.J. (2003) Biogeochemical and environmental factors in Fe biomineraliztion: magnetite and siderite formation. Clays and Clay Minerals, 51, 83–95.

Ruby, C., Rabha, A., Gehin, A., Cortot, J., Abdelmoula, M., and Genin, J.M. (2006) Green rusts synthesis by coprecipitation of Fe^{II}-Fe^{III} ions and mass balance diagram. Comptes Rendus Geosciences, 338, 420–432.

Schwertmann, U. and Cornell, R.M. (2000) Iron Oxide in the Laboratory: Preparation and characterization. Wiley-VCH, New York.

Sawatzky, G.A., Van der Woude, F., and Morrish, A.H. (1969) Recoiless-fraction ratios for Fe^{57} in octahedral and tetrahedral sites of a spinel and a garnet. Physical Review, 183, 383–386.

Vali, H., Kleiss, B., Li, Y.-L., Sears, S.K., Kim, S.S., Kirschvink, L., and Zang, C.L. (2004) Formation of tabular single-domain magnetite induced by geobacter metallireducens GS-15. Proceedings of the National Academy of Science, 10, 16121–16126.

Vandenberghe, R.E., Barrero, C.A., Da Costa, G.M., Van San, E., and De Grave, E. (2000) Mössbauer characterization of iron oxides and (oxy)hydroxides: the present state of the art. Hyperfine Interactions, 126, 247–259.

Voogt, T., Fujii, T., Smulders, P.J.M., Niesen, L., James, M.A., and Hibma, T. (1999) NO_2-assisted molecular-beam epitaxy of Fe_3O_4, $Fe_{3-\delta}O_4$, and γ-Fe_2O_3 thin films on MgO (100). Physical Review B, 60, 11193–11206.

Zachara, J.M., Li, S.-M., Kennedy, D.W., Smith, S.C., and Gassman, P.L. (1998) Bacterial reduction of crystalline Fe^{3+} oxides in single phase suspensions and subsurface materials. American Mineralogist, 83, 1426–43.

Zegeye, A., Ruby, C., and Jorand, F. (2007) Kinetic and thermodynamic analysis during dissimilatory γ-FeOOH reduction: formation of green rust 1 and magnetite. Geomicrobiology Journal, 24, 51–64.

Zegeye, A., Mustin, C., and Jorand, F. (2010) Bacterial and iron aggregates mediate secondary iron mineral formation: green rust versus magnetite. Geobiology, 8, 209–222.

MANUSCRIPT RECEIVED JANUARY 25, 2011
MANUSCRIPT ACCEPTED APRIL 8, 2011
MANUSCRIPT HANDLED BY IAN SWAINSON